

Advanced Magnetic Resonance  
Spectroscopic techniques for Neurometabolic  
Profiling of Multiple Sclerosis

by

Oun Al-iedani

A thesis submitted to the University of Newcastle in fulfilment  
of the requirements for the degree of

Doctor of Philosophy

in

Magnetic Resonance in Medicine

Faculty of Health and Medicine

University of Newcastle

August 2019

*To my late parents, Issa, Khadeeja and my spiritual mother Fatima*

## ABSTRACT

Multiple sclerosis (MS) is an immune-mediated neuronal disorder in which inflammatory cells attack the myelin of the central nervous system, leading to varying extents of neuroaxonal injury, demyelination and gliosis by affecting both the brain and spinal cord. In the last few decades, conventional MRI techniques, sensitive at detecting MS plaques in the brain and spinal cord, have been the main imaging tool for diagnosis and on-going monitoring for MS pathology, reflecting inflammatory activity via T2 lesions and brain damage via atrophy measurements. However, MRI features of MS are not specific to its pathological substrates which contribute to the development of permanent disability. Presently, MRI is not able to quantify the damage in normal appearing white matter and has technical limitations in detecting and quantifying damage to grey matter. Also, the clinical manifestations of MS plaques in different anatomical locations such as spinal cord and optic nerves are variable.

A non-invasive, advanced MR technique of one-dimensional (1D) magnetic resonance spectroscopy (H-MRS) is capable of exploring the metabolic alterations of the MS brain in relatively small volumes of interest. This has the potential to provide molecular biomarkers for early detection and to monitor disease progression of the MS brain. This technique may allow better understanding of the pathophysiology of symptoms and aid in the development of new treatments.

In this thesis, the diurnal stability and long-term repeatability and reliability of *in-vitro* and *in-vivo* measurements at 3 Tesla have been investigated to prove the validity of H-MRS technique in clinical settings. This study demonstrates the stability of neurometabolite levels in longitudinal studies (over extended periods of time) and the reliable detection and distinction of neurometabolites between healthy controls (HCs) and MS patients. The findings of the study showed H-MRS is reliable and had minimal diurnal variations.

Disease modifying therapies (DMT) for multiple sclerosis treatment were deemed vital to understand the underlying pathology resulting in disease progression and therefore assist in developing new meaningful imaging biomarkers to evaluate the clinical efficacy of treatment radiologically. Few studies have used 1D H-MRS to monitor the response to DMT in relapsing-remitting MS (RRMS) and to assess if immunomodulatory therapies can reverse or prevent the progression of neuronal injury. Dimethyl fumarate (DMF), an oral DMT for MS, displays anti-oxidative properties, thought to be via modulation of glutathione (GSH).

A longitudinal study was designed to evaluate the impact of DMF treatment longitudinally over 24 months (five time points) on hippocampal neurometabolites in RRMS patients using single voxel 1D H-MRS techniques at short TE and 3T. This study showed that cross-sectional analysis confirmed the importance of hippocampal NAA and increase in myo-inositol as indicators of axonal loss and gliosis in RRMS cohort compared to HCs. This study also showed that DMF treatment may impact on hippocampal metabolism, specifically GSH levels, which supports its assumed anti-oxidant mode of action, resulting in an anti-inflammatory effect in the MS brain following DMF treatment. This study is the first to illustrate a change in hippocampal metabolism associated with the onset of treatment with DMF in RRMS patients.

This thesis also investigated the impact of DMF treatment on the pre-frontal cortex (PFC) and posterior cingulate gyrus (PCG) metabolic profiles at pre- and post-treatment onset at four time points using 1D H-MRS technique. The correlation between brain metabolites and severity of clinical and neuropsychological symptoms were analysed at three time points at baseline, 12 and 24 months following the initiation of DMF treatment in the regions responsible for cognitive functioning; PFC and PCG. This study showed significant cross-sectional reductions in N-acetylaspartate (NAA) in PFC and PCG and increase in PFC tCho in RRMS cohort compared to HCs. DMF treatment showed the mean NAA levels in PFC and PCG were altered significantly over the 24-month treatment period, but stabilised and didn't significantly change

between 1st and 2nd year of treatment. This study demonstrated that 1D H-MRS is a sensitive marker of disease activity with several metabolites correlating with clinical parameters, but also capable to detect a treatment effects prior to volumetric change. This study suggested that PCG and PFC regions may be sensitive to the progression of clinical and cognitive disabilities of MS patients and may play an important role in monitoring cognitive performance.

Injectable DMTs (interferon and glatiramer acetate) as well as oral DMTs (fingolimod and DMF) have not only shown the reduction of relapse rate and T2 lesion load but also brain atrophy, which seems to be related to long term disease on disability. Additionally, the efficacy of these DMTs have also been evaluated using 1D H-MRS methods in a cross-sectional fashion. This study is the first *in-vivo* investigation of the impact of these treatments on the hippocampus, PFC and PCG metabolism in RRMS patients. RRMS patients, on therapy for a minimum of 6 months, with no new clinical symptoms or change in their disability status in the last 6 months were included in the study. This study also established the association between clinical symptoms in MS patients especially cognitive function and neurometabolites as well as volumetric changes. We also confirmed the importance of NAA and myo-inositol (m-Ins) as indicators of axonal loss and gliosis. This study demonstrated hippocampal metabolic correlation with memory, disability scale and TARCS; PCG with memory, CSF volume and TARCS; while PFC metabolites correlated with attention, depression and anxiety. The cross-sectional nature of our findings warrants longitudinal investigations to further clarify clinical effects of fingolimod and injectables, and to determine associations between hippocampus, PFC and PCG metabolic levels and treatment efficacy.

Clinically, three-dimensional magnetic resonance spectroscopic imaging (3D MRSI) is more suitable than single voxel method due to the former's ability to obtain important metabolic information with extended brain coverage. This thesis investigated the performance of fast MRSI techniques at short TE and 3T, using LASER sequence

with adiabatic gradient-offset independent adiabaticity wideband pulse (GOIA-W)[16,4]. This fast MRSI techniques coupled with tissue segmentation of the brain were used to identify neurometabolic differences in normal appearing white matter (NAWM) and white matter lesions (WML) of RRMS patients compared to age and sex-matched HCs. This study used a novel post-processing analysis pipeline and three binary support vector machine (SVM) classification that allowed individual small voxel analysis to demonstrate true nature of NAWM and WML and distinguish tissue types. Our findings of significant changes in NAWM and more so in WML of MS patients compared with healthy voxels using spiral 3D MRSI indicates that the metabolic abnormalities (reduced NAA and increased m-Ins) in RRMS are associated with a gradual loss of axonal integrity and astrogliosis in white matter. This study demonstrates the benefit of MRSI in evaluating MS neurometabolic changes in damaged NAWM. SVM of MRSI data in the MS brain may be suited for clinical monitoring and progression of MS patients.

## **Statement of Originality**

I hereby certify that the work embodied in the thesis is my own work, conducted under normal supervision. The thesis contains no material which has been accepted, or is being examined, for the award of any other degree or diploma in any university or other tertiary institution and, to the best of my knowledge and belief, contains no material previously published or written by another person, except where due reference has been made. I give consent to the final version of my thesis being made available worldwide when deposited in the University's Digital Repository, subject to the provisions of the Copyright Act 1968 and any approved embargo.

Oun Al-iedani

30/08/2019

## **Thesis by publication**

I hereby certify that this thesis includes published and non-published papers. I have included as part of the thesis a written declaration from each co-author, endorsed in writing by the Faculty Assistant Dean (Research Training), attesting to my contribution to any jointly authored papers.

By signing below, I confirm that Oun Al-iedani contributed analysis and writing to the paper/publication included in Chapter 3.

**Jameen Arm**

Date : 10/08/19

By signing below, I confirm that Oun Al-iedani contributed analysis and writing to the paper/publication included in Chapter 7.

**Neda Gholizadeh**

Date :16 /08/19

By signing below, I confirm that Oun Al-iedani contributed analysis and writing to the paper/publication included in Chapter 7.

**Ovidiu Andronesi**

Date :25 /08/19

By signing below, I confirm that Oun Al-iedani contributed analysis and writing to the paper/publication included in Chapter 7.

**Scott Quadrelli**

Date : 10/08/19

By signing below, I confirm that Oun Al-iedani contributed analysis and writing to the paper/publication included in Chapter 3, 4 and 7.

**Rodney Lea**

Date : 07/08/19

By signing below, I confirm that Oun Al-iedani contributed analysis and writing to the papers/publications included in Chapters 2, 3, 4, 5, 6, and 7.

**Karen Ribbons**

Date :19 /08/19

By signing below, I confirm that Oun Al-iedani contributed analysis and writing to the papers/publications included in Chapters 2, 3, 4, 5, 6, and 7.

**Jeannette Lechner-Scott**

Date : 09/08/19

By signing below, I confirm that Oun Al-iedani contributed analysis and writing to the papers/publications included in Chapters 2, 3, 4, 5, 6, and 7.

**Saadallah Ramadan**

Date : 07/08/19

Faculty of Health and Medicine Assistant Dean Research Training

**Lesley MacDonald-Wicks**

Date : 28/08/19

## **Acknowledgements**

First and foremost, I would like to express my utmost gratitude to my supervisor, Associate Professor Saad Ramadan for continued guidance, encouragement and support during my PhD study. He continually and genuinely conveyed a spirit of adventure with regards to the research progress, scholarships, manuscripts and this thesis. I could not have imagined having a better supervisor for my PhD studies.

My sincerest thanks to my co-supervisor Dr Karen Ribbons who taught me new things in relation to writing, planning, design and critical thinking, in addition to recruitment of MS patients and healthy controls. We had many hours of discussions during my PhD journey where we discussed many challenging topics. I also thank her for dedicating many hours to review my written manuscripts after she left HMRI.

My very special thanks go out to Prof Jeannette Lechner-Scott. Without her motivation and encouragement, I would not have considered a graduate career specializing in multiple sclerosis (MS). In spite of her heavy clinical workload at different clinics, she was always there to support and give advice and review manuscripts. I doubt that I will ever be able to convey my full appreciation.

I must acknowledge A Prof Rod Lea for his ongoing advice on the statistical aspects of my project. I learned many things from Rod, and I hope we will work more in the future. I also acknowledge senior radiographers Kate Skehan, Shiami Luchow and Kristen Fisher for their assistance, company and scanning of my study subjects.

I also acknowledge Neda Gholizadeh, Dr. Scott Quadrelli, Jameen Arm for reviewing papers and intellectual contribution. Nicole Lingard for the ethics governance and Dr. Peter Lau for radiological advice. All the above provided me with advice at times of critical need, which helped enrich the experience.

I recognize that this research would not have been possible without the financial assistance of Iraqi government, HMRI pilot grant for scan funding, University of Newcastle and scholarship from MS Research Group (Prof Jeanette Lechner-Scott).

Last but not the least, I would like to thank my family for the support they provided me through my entire life and I must acknowledge their continual support in the challenging times in my PhD journey and can rejoice my accomplishment with them.

## **Table of Contents**

<b>Chapter 1 : Introduction.....</b>	<b>39</b>
<b>1.1 What is multiple sclerosis? .....</b>	<b>39</b>
<b>1.2 Classification of MS types .....</b>	<b>40</b>
<b>1.3 Pathophysiology of MS .....</b>	<b>41</b>
<b>1.4 Management of MS.....</b>	<b>42</b>
<b>1.5 MS diagnosis and clinical management .....</b>	<b>42</b>
<b>1.6 Limitation of conventional MRI methods .....</b>	<b>43</b>
<b>1.7 Advanced MR techniques.....</b>	<b>44</b>
<b>1.8 Biochemical profiling using MRS.....</b>	<b>45</b>
<b>1.9 Significance of current research project.....</b>	<b>49</b>
<b>Chapter 2 : Fast Magnetic Resonance Spectroscopic Imaging Techniques in Human Brain- Applications in Multiple Sclerosis.....</b>	<b>53</b>
<b>ABSTRACT .....</b>	<b>53</b>
<b>2.1 Introduction .....</b>	<b>53</b>
2.1.1 MRS and MRSI .....	53
2.1.2 Multiple Sclerosis (MS) .....	55
<b>2.2 Data Acquisition Techniques .....</b>	<b>56</b>
2.2.1 Single-voxel techniques.....	56

2.2.2 Conventional multi-voxel techniques.....	58
<b>2.3 Parallel imaging.....</b>	<b>59</b>
<b>2.4 Fast multi-voxel techniques.....</b>	<b>60</b>
2.4.1 Spiral MRSI.....	61
2.4.2 Turbo spectroscopic imaging (turbo-MRSI) .....	63
2.4.3 Echo-planar spectroscopic imaging (EPSI).....	65
<b>2.5 Comparison of MRSI techniques .....</b>	<b>70</b>
<b>2.6 MRSI in Multiple Sclerosis .....</b>	<b>72</b>
<b>2.7 Concluding remarks and summary.....</b>	<b>78</b>
<b>Chapter 3 : Diurnal Stability and Long-Term Repeatability of Neurometabolites Using Single Voxel 1H Magnetic Resonance Spectroscopy .....</b>	<b>80</b>
<b>ABSTRACT .....</b>	<b>80</b>
<b>3.1 Introduction.....</b>	<b>81</b>
<b>3.2 Materials and methods .....</b>	<b>82</b>
3.2.1 Participants .....	82
3.2.2 Study design .....	82
3.2.3 MRI acquisition and structural assessments.....	83
3.2.4 H-MRS acquisition, post-processing and analysis .....	84
3.2.5 Statistical analysis .....	85
<b>3.3 Results .....</b>	<b>86</b>

3.3.1 In-vitro .....	87
3.3.2 In-vivo .....	87
<b>3.4 Discussion.....</b>	<b>91</b>
<b>3.5 Conclusion.....</b>	<b>94</b>
<b>Chapter 4 : A longitudinal, observational study of the effect of dimethyl fumarate on hippocampal metabolites in RRMS using 1H-MR spectroscopy .....</b>	<b>95</b>
<b>ABSTRACT .....</b>	<b>95</b>
<b>4.1 Introduction.....</b>	<b>96</b>
<b>4.2 Methods.....</b>	<b>96</b>
4.2.1 Patients and Healthy Control Subjects .....	96
4.2.2 Study design .....	97
4.2.3 MRI Acquisition and Structural assessments .....	97
4.2.4 H-MRS Acquisition, Post-Processing and Analyses.....	98
4.2.5 Clinical Assessments.....	99
4.2.6 Statistical Analysis .....	100
<b>4.3 Results .....</b>	<b>101</b>
4.3.1 Participant demographics and characteristics.....	101
4.3.2 Morphology (whole brain and voxel characteristics).....	102
4.3.3 MR Spectroscopy .....	103
4.3.4 Correlation of metabolites with clinical and volumetric measures .....	105

<b>4.4 Discussion.....</b>	<b>106</b>
<b>4.5 Conclusion.....</b>	<b>110</b>
<b>Chapter 5 : Effect of dimethyl fumarate (Tecfidera) on microstructure and biochemistry in the brain of MS patients .....</b>	<b>112</b>
<b>ABSTRACT .....</b>	<b>112</b>
<b>5.1 Introduction.....</b>	<b>113</b>
<b>5.2 Methods.....</b>	<b>115</b>
5.2.1 Patients and Healthy Control Subjects .....	115
5.2.2 Study design .....	115
5.2.3 Binary mask for the voxel segmentation .....	115
5.2.4 MRI Acquisition and Structural assessments .....	116
5.2.5 H-MRS Acquisition, Post-Processing and Analyses .....	118
5.2.6 Clinical Assessments.....	120
5.2.7 Statistical Analysis .....	121
<b>5.3 Results .....</b>	<b>121</b>
5.3.1 Participant demographics and characteristics.....	121
5.3.2 Morphology (whole brain and voxel characteristics).....	123
5.3.3 MR Spectroscopy .....	126
5.3.4 Correlation of PFC metabolites with clinical and volumetric measures ..	130
5.3.5 Correlation of PCG metabolites with clinical and volumetric measures .	132

<b>5.4 Discussion.....</b>	<b>134</b>
<b>5.5 Conclusion.....</b>	<b>141</b>
<b>Chapter 6 : Cross sectional evaluation of neurometabolic alterations in RRMS with fingolimod and injectable treatment using advanced MRS .....</b>	<b>143</b>
<b>ABSTRACT .....</b>	<b>143</b>
<b>6.1 Introduction.....</b>	<b>144</b>
<b>6.2 Methods.....</b>	<b>149</b>
6.2.1 Patients and Healthy Control Subjects .....	149
6.2.2 Study design .....	149
6.2.3 Binary mask for the voxel segmentation.....	150
6.2.4 MRI acquisition and structural assessments.....	151
6.2.5 H-MRS Acquisition, Post-Processing and Analyses.....	153
6.2.6 Clinical Assessments.....	156
6.2.7 Statistical Analysis .....	157
<b>6.3 Results .....</b>	<b>158</b>
6.3.1 Participant demographics and characteristics.....	158
6.3.2 Morphology (whole brain and MRS voxel characteristics) .....	159
6.3.3 MR Spectroscopy .....	161
6.3.4 Correlation of hippocampal metabolites with clinical and volumetric measures .....	166
6.3.5 Correlation of PCG metabolites with clinical measures.....	168

6.3.6 Correlation of PFC metabolites with clinical measures .....	169
<b>6.4 Discussion.....</b>	<b>171</b>
<b>6.5 Conclusion.....</b>	<b>178</b>
<b>Chapter 7 : Spiral-MRSI and tissue segmentation of normal-appearing white matter and white matter lesions in relapsing remitting Multiple Sclerosis patients .....</b>	<b>179</b>
<b>ABSTRACT .....</b>	<b>179</b>
<b>7.1 Introduction.....</b>	<b>180</b>
<b>7.2 Methods.....</b>	<b>183</b>
7.2.1 Patients and Healthy Control Subjects .....	183
7.2.2 MRI protocol and Structural assessments .....	183
7.2.3 Validation of MRSI voxel coordinates in vitro and in vivo .....	184
7.2.4 Binary mask for the segmentation of MRSI VOI.....	185
7.2.6 White matter lesion quantification .....	186
7.2.7 Brain volume quantification .....	187
7.2.8 Magnetic resonance spectroscopic imaging .....	187
7.2.9 Post-processing and statistical analysis .....	188
<b>7.3 Results .....</b>	<b>189</b>
7.3.1 Participant demographics and characteristics.....	189
7.3.2 Morphology (whole brain and voxel characteristics).....	191
7.3.3 Magnetic resonance spectroscopic imaging .....	193

<b>7.4 Discussion.....</b>	<b>198</b>
<b>7.5 Conclusion.....</b>	<b>204</b>
<b>Chapter 8 : Summary and future work .....</b>	<b>205</b>
<b>    Future work and recommendations .....</b>	<b>205</b>
<b>Bibliography.....</b>	<b>211</b>

## List of Figures

- Figure 1-1 Normal neuron with a Myelin vs Demyelination in MS with damaged Myelin. [https://www.researchgate.net/publication/230554483\\_Multiple\\_Sclerosis](https://www.researchgate.net/publication/230554483_Multiple_Sclerosis) ..... 39
- Figure 1-2. Common initial symptoms of MS. (National Multiple Sclerosis Society, Multiple Sclerosis: <https://www.nationalMSSociety.org/PRC>)..... 40
- Figure 1-3. The course of MS is highly varied and heterogeneous. The disease is characterized initially by episodes of reversible clinically isolated neurological deficits, which is often followed by progressive neurological deterioration over time. Activity is defined as the presence of clinical relapse or presence of new plaques over time either on T2 scan or T1 contrast enhanced MRI scans <sup>6</sup>. ..... 41
- Figure 1-4. Standardized brain MRI protocol to evaluate patients in whom multiple sclerosis is clinically suspected. a. Axial T1-weighted pre-contrast, b. Proton Density weighted and c. T2-weighted sequences, followed by d. Sagittal post-contrast T2-weighted fluid-attenuated inversion recovery (FLAIR), e. Axial post-contrast T2-FLAIR and f. Axial post-contrast T1-weighted sequences<sup>16</sup>. ..... 43
- Figure 1-5. DTI images represents (a) MD, describes the total amount of diffusion in a given voxel. (b) FA, the degree of anisotropy in a given voxel and therefore the strength of the directional diffusion, value from 0 (isotropy) to 1 (anisotropy). (c) AD, diffusion along the principle axis of diffusion ellipsoid. (d) RD, average diffusion along the two minor axes<sup>23</sup> ..... 44
- Figure 1-6. The neurometabolic changes of the MS..... 47
- Figure 2-1. Two single-voxel localisation methods: (a) the PRESS sequence; (b) the STEAM sequence. Note that the three orthogonal slice-selective gradient pulses are indicated by black, green and red colours in the schematic representation. Reproduced with permission from <sup>80</sup>..... 57
- Figure 2-2. Signal obtained from prefrontal cortex (PFC) of voxel size (1.5cm<sup>3</sup>) from a healthy subject: (a) at short TE and (b) at long TE using PRESS approach on a 3T scanner (Prisma, Siemens, Erlangen)..... 58
- Figure 2-3. MRSI data acquired from a 3-year-old girl with an idiopathic developmental delay. Data was acquired using a 2D PRESS-MRSI at 3T (TE: 135ms) in the axial plane with voxel size of 1.5cm<sup>3</sup>. Reproduced with permission from <sup>80</sup> ..... 59
- Figure 2-4. Illustrates the data spectroscopy and mapping of brain metabolite of conventional MRSI methods (top line) compared with SENSE-MRSI acquisition methods (bottom line) of (a) voxel in tumorous tissue and (b) healthy tissue; with an acquisition time of (14.02min) and (3.37min) respectively, and acquisition data

parameter (TE/TR: 228/1500ms), slice thickness (20 mm) and FOV (220mm). Reproduced with permission from <sup>96</sup> .....	60
Figure 2-5. (a) In a spiral MRSI, two time-varying readout gradients are administered in the data acquisition period with oscillating spiral trajectories. (b) Outlines the projection of a k-space trajectory along the $k_f$ axis. The spiral trajectories originate from the $(k_x, k_y)$ plane and repeatedly run a path through the $k_x, k_y, k_f$ spaces with multiple and simultaneous spiral trajectories increasing volumetric acquisition around the $k_f$ axis. Reproduced with permission from <sup>80, 102</sup> .....	61
Figure 2-6. Displays the spectral data from three slices using a spiral MRSI technique at 3T (TE/TR: 144ms/2s, FOV: 8x9x6cm) using a 32-channel phased array head coil. Reproduced with permission from <sup>104</sup> .....	63
Figure 2-7. Readout strategy for Turbo-MRSI sequence using spin-echo imaging per excitation preceded by water and lipid suppression (CHESS and outer-volume suppression (OVS)). Reproduced with permission from <sup>80</sup> .....	64
Figure 2-8. (a) EPSI sequences are applied to encode localised spectra with a single readout gradient. (b) k-space trajectories of echo-planar spectroscopic imaging indicate data acquisition in one TR of the pulse sequence during spectral encoding. Reproduced with permission from <sup>80</sup> .....	65
Figure 2-9. Whole brain mapping and a spectrum of major metabolites, mean water-reference spectroscopic imaging (SI H <sub>2</sub> O Reference) using EPSI at 3T from a healthy subject (TE/TR=70/1710ms), total acquisition time (26 min), k-space points (50x50x18), FOV (28x28x18cm <sup>3</sup> ) and voxel volume (0.31cm <sup>3</sup> ). Reproduced with permission from <sup>94</sup> .....	67
Figure 2-10. Illustrates the comparison between two fast MRSI sequences at 3T: (a) the 3D-EPSI and (b) GRAPPA-EPSI sequences, to show the whole brain mapping of metabolites with interleaved water reference acquisition (SI H <sub>2</sub> O Reference) from a healthy normal subject at intermediate TE (70ms). Reproduced with permission from <sup>130</sup> .....	69
Figure 2-11. Shows the spectra of voxels in (a) GM and (b) WM of healthy and PPMS subjects: (c, d) acquired from healthy subject in GM and WM, respectively and (e, f): acquired from GM and WM regions of a PPMS patient, respectively. Experimental parameters: TE/TR=135ms/1500ms, FOV (16x16cm <sup>2</sup> , yellow border) and VOI(8x8x2cm <sup>3</sup> , white border). Reproduced with permission from <sup>141</sup> .....	74
Figure 2-12. Spectroscopic data from a typical SPMS brain from three separate regions: [1] MS lesion, [2] CGM and [3] NAWM. The voxels are represented by the numbers and red spots. Experimental parameters: 3D-EPSI (TE/TR=144/2000ms), acquisition time (20min), FOV (24x24x8 cm <sup>3</sup> ) and slice thickness (4mm) at 1.5T. Reproduced with permission from <sup>49</sup> .....	75

Figure 3-1. Graphical representation of <i>in-vitro</i> study design for diurnal effect (A) and repeatability (B) and <i>in-vivo</i> study design for diurnal variability (C) and repeatability (D) study where, time of day defined as T1 =0700, T2=1200 and T3=1700 and S1 represents the first four sessions, S2 represents the last four sessions after one-month break. ....	83
Figure 3-2. Positioning of the PCG voxel in three planes. T1-weighted MR images from healthy participant in axial, sagittal and coronal planes demonstrating the PCG voxel size and position (white box). ....	85
Figure 3-3. H-MRS spectra of <i>in-vivo</i> and <i>in-vitro</i> . LCModel fitting output of typical H-MRS spectra of <i>in-vivo</i> (left) data acquired from PCG and <i>in-vitro</i> (right) at 3T and a TE value of 30 ms. Cr, creatine; PCr, phosphocreatine; Glx, glutamate+glutamine; m-Ins, myo-inositol; GPC, glycerophosphocholine; PCh, phosphocholine; GSH, glutathione; Asp, aspartate; NAA, N-acetylaspartate; Lac, lactate; MM, macromolecular; Lip, lipid. ....	86
Figure 3-4. Intra/inter-session CVs from <i>in-vitro</i> H-MRS data using repeatability approach. ....	87
Figure 3-5. <i>In-vivo</i> diurnal variations of GPC and Glx metabolite ratios for PCG brain region. *: $p < 0.05$ , **: $p < 0.01$ . ....	88
Figure 3-6. Intra/inter-subject repeatability CV <sub>cor</sub> from <i>in-vivo</i> H-MRS data. ....	89
Figure 4-1. T1-weighted MR images from a multiple sclerosis patient in coronal, sagittal and axial planes demonstrating the hippocampal voxel size and position (white box). ....	98
Figure 4-2. LCModel fitting output of typical H-MRS spectra of <i>in-vivo</i> (left) data acquired from hippocampus and <i>in-vitro</i> (right) at 3T and a TE value of 30ms. Cr: creatine; PCr: phosphocreatine; Glx: glutamate+glutamine; mI: myo-inositol; GPC: glycerophosphocholine; PCh: phosphocholine; GSH: glutathione; NAA: N-acetylaspartate. ....	99
Figure 4-3. Neurometabolites levels (NAA, m-Ins) in RRMS compared to HCs at baseline and 2yrs follow up:with significant difference to total creatine (tCr) for healthy controls (HCs) and relapsing-remitting multiple sclerosis (RRMS) pre and post onset of treatment with DMF. T0: baseline; T1: 1 month of treatment; ↑: the time at which the therapeutic dose level was reached; T6: 6 months of treatment; T12: 12 months of treatment; T24: 24 months of treatment; m-Ins: myo-inositol; NAA: N-acetylaspartate. ....	104
Figure 4-4. Pre and post treatment with dimethyl fumarate (DMF) effect on ratio of glutathione (GSH) to total creatine (tCr) levels in relapsing-remitting multiple sclerosis (RRMS) with healthy controls (HCs) as a reference line. T0: baseline; T1: 1 month of treatment; T6: 6 months of treatment; T12: 12 months of treatment; T24: 24 months of treatment. ....	105

Figure 5-1. Reconstructed MRS voxels displayed as a mask overlying the T2-FLAIR images from a RRMS patient showing lesion map (red colour pixels), (A) PCG mask, (B) PFC mask and (C) lesion map on global white matter. The results of partial volume segmentation using FSL FAST produced (D) WM mask, (E) GM mask, and (F) CSF mask. ....	116
Figure 5-2. Brain tissue volume, normalised for subject head size, was estimated with SIENAX. Final SIENAX segmentation results of whole brain (top row) and peripheral cortex masked segmentation (bottom row). ....	117
Figure 5-3. T1-weighted MR images in coronal, sagittal and axial planes demonstrating the (A) PCG and (B) PFC voxels size and position (white box).....	118
Figure 5-4. Samples of <i>in-vivo</i> MR spectra from PFC (top) and PCG (bottom) regions analysed by LCModel indicating the major brain metabolites at 3T and short TE (30ms).....	119
Figure 5-5. PFC neurometabolite/tCr ratio in HCs and RRMS pre and post inception of DMF treatment. ....	127
Figure 5-6. PCG neurometabolite / tCr ratio in HCs and RRMS pre and post inception of DMF treatment. ....	129
Figure 6-1. Reconstructed MRS voxels displayed as a mask overlying the T2 FLAIR images and lesion map (red colour), (A) PCG mask, (B) PFC mask and (C) hippocampal mask. The results of partial volume segmentation using FSL FAST, (D) WM mask, (E) GM mask, and (F) CSF mask.....	151
Figure 6-2. Brain tissue volume, normalised for subject head size, was estimated with SIENAX. Final SIENAX segmentation results of whole brain (top row) and peripheral cortex masked segmentation (bottom row). ....	152
Figure 6-3. T1-weighted MR images in coronal, sagittal and axial planes demonstrating the PCG (A), PFC (B) and hippocampal (C) voxels sizes and positions (white box). ....	153
Figure 6-4. Samples of <i>in-vivo</i> MR spectra levels from HCs (left) and MS patients (right) for (A) hippocampal, (B) PCG and (C) PFC regions analysed by LCModel indicating the major set of brain metabolites at 3T and short TE. ....	155
Figure 6-5. Hippocampal neurometabolite/tCr ratio (tNAA and Glx) in HCs and RRMS fingolimod and injectables (INJ: GA+interferon) disease modifying therapies.....	163
Figure 6-6. PCG neurometabolite/tCr ratio (tNAA and Cr) in HCs and RRMS fingolimod and injectable treatments (INJ: GA+interferon). ....	163
Figure 6-7. PFC neurometabolite / tCr ratio (NAA and m-Ins) in HCs and RRMS fingolimod and injectable (INJ: GA+interferon) disease modifying therapies. ....	164

Figure 6-8. Comparison the levels neurometabolite/tCr ratio (tNAA) in HCs and RRMS fingolimod (Gilenya) in three regions hippocampal (HIPPO), PCG and PFC.  $**p \leq 0.001$  RRMS (fingolimod group) vs HCs at baseline. .... 164

Figure 6-9. Comparison of the neurometabolite/tCr ratio (tNAA, NAA, Glx, Glu and m-Ins) in HCs and total RRMS in three regions of hippocampal (HIPPO), PCG and PFC.  $*p \leq 0.01$ ,  $**p \leq 0.001$  RRMS vs HCs at baseline. .... 165

Figure 7-1 A. MRSI VOI (inner white box) and voxel location of interest (blue box) in an ACR phantom, B. In vivo MRSI multi-voxel VOI, voxel of interest location and corresponding spectrum. .... 184

Figure 7-2. Pipeline of volumetric brain tissue segmentation from MRI and MRSI data.  
A. A binary mask of a MRSI single slice VOI (8x10 cm<sup>2</sup>) was created using the SPM toolbox. B. partial volume masks for each tissue type were created using FSL FAST. C. Partial volume segmentation of the lesion filled T1-MPRAGE structural images. D. Tissue segmentation of MRSI VOI (CSF, GM and WM) and lesion segmentation overlaid on the T2-FLAIR image. .... 186

Figure 7-3. FOV (yellow box) and VOI (white box) positions in axial, sagittal and coronal MPRAGE planes with voxel size (red box, 10×10×10) mm<sup>3</sup>. .... 188

Figure 7-4. MRSI grid and tissue segmentation overlaid on the T2-FLAIR in MS brain slice. MRI color code: yellow indicates NAWM, red indicates WM lesions, grey indicates GM. .... 193

Figure 7-5. The LCModel fitting output of neurometabolites acquired from one MRSI voxel at similar voxel and slice position. Panel A: Healthy control, Panel B: MS brain .... 195

Figure 7-6. Box plot of statistically significant differences in the neurometabolic ratios (NAA/tCr, m-Ins/tCr, Glx/tCr and (m-Ins+Gly)/tCr) in three different tissues for WML, NAWM-MS and HC voxels. .... 195

Figure 7-7. A. Box plot of significant differences in the neurometabolic ratios (NAA/tCr and m-Ins/tCr) for MS lesion voxels, NAWM-MS and HC voxels in four slices within large VOI (320 cm<sup>3</sup>). The statistically significant difference considered as  $p < 0.05$  between the two groups. B. The receiver operating characteristic (ROC) curves of three SVM classification (HCs vs NAWM, NAWM vs WML, HCs vs WML) using a leave-one-out cross-validation technique for major neurometabolites/tCr ratios yielding statistically significant differences between models. .... 197

Figure 8-1. Mapping of NAA concentrations in single slice and multi-slice using fast MRSI based representation of data, overlaid with structural image. .... 209

Figure 8-2. Sample of the mapping 3 DMRs, located at deep cortical white matter in posterior parietal lobes at post-central gyrus, for neurometabolites in the RRMS

brain using fast MRSI technique. A DMR represents 3 or more adjacent voxels having statistically significant metabolic differences between RRMS and HCs.  
..... 210

## List of Tables

Table 2-1. Brain metabolite concentration and acquisition time of various MRSI techniques. ....	70
Table 2-2. Brain metabolite concentrations obtained in fast MRSI techniques. ....	71
Table 2-3. Brain metabolite concentration were acquired for MS patients and HCs by applying PRESS-MRSI and fast MRSI methods. *Tacq: acquisition time.....	76
Table 3-1. Descriptive statistics and repeatability data for <i>in-vivo</i> neurometabolites/tCr ratios from six participants. ....	89
Table 3-2. Variances and reliability of major neurometabolites data from healthy participants in PCG.....	90
Table 4-1. Cross sectional analysis of mean demographic scores and disease-related variables for MS and HCs groups at baseline and 2 years. ....	101
Table 4-2. Mean values of spectroscopic voxel segmentation and volume of brain fractions for RRMS patients compared to HCs showing treatment effect across time points. ....	103
Table 4-3. Spearman’s correlation between neurometabolites ratios and cognitive functions in RRMS across 24 month study period. Only statistically significant changes are listed.....	106
Table 5-1. Cross-sectional analysis of mean demographic scores and disease-related variables for MS and HCs groups at baseline and 2 years. ....	122
Table 5-2. Mean values of spectroscopic voxel segmentation of PFC region and volume of brain fractions for RRMS patients compared to HCs showing treatment effect across time points. ....	124
Table 5-3 Mean values of spectroscopic voxel segmentation of PCG region and volume of brain fractions for RRMS patients compared to HCs showing treatment effect across time points. ....	125
Table 5-4. Mean values of neurometabolite/tCr of PFC region in HCs and RRMS pre and post inception of DMF treatment, showing treatment effect across time points. ....	127
Table 5-5 Mean values of neurometabolite/tCr of PCG region in HCs and RRMS pre and post inception of DMF treatment, showing treatment effect across time points. ....	129
Table 5-6. Spearman’s correlation between PFC neurometabolites ratios and cognitive functions in RRMS across 24 month study period. Only statistically significant changes are listed.....	131

Table 5-7 Spearman’s correlation between PCG neurometabolites ratios and cognitive functions in RRMS across 24 month study period. Only statistically significant changes are listed.....	133
Table 6-1. Dosing summaries for fingolimod or injectable disease therapies compounds of RRMS patients. ....	150
Table 6-2. Cross-sectional analysis of mean demographic scores and disease–related variables for RRMS (fingolimod and injectables) and HCs groups at baseline.	158
Table 6-3. Mean values of spectroscopic voxel segmentation of hippocampal, PCG and PFC regions and volume of brain fractions for RRMS patients compared to age and sex-matched HCs at baseline. ....	160
Table 6-4. Mean values of brain-metabolite/tCr of hippocampal, PCG and PFC regions in HCs and RRMS (fingolimod and injectable cohorts). * $p \leq 0.05$ ; ** $p \leq 0.01$ RRMS vs HCs at baseline. ....	166
Table 6-5. Spearman’s correlation between hippocampal neurometabolite ratios and cognitive functions and volumetric measures in RRMS (fingolimod cohort) at baseline. Only statistically significant changes are listed. ....	167
Table 6-6. Spearman’s correlation between PCG neurometabolites ratios and cognitive functions in RRMS (fingolimod cohort) at baseline. Only statistically significant changes are listed.....	169
Table 6-7. Spearman’s correlations between PFC neurometabolite ratios and cognitive functions in RRMS (fingolimod cohort) at baseline. Only statistically significant changes are listed.....	170
Table 7-1. Cross-sectional analysis of mean demographic scores and disease-related variables for MS and HCs groups at baseline. ....	190
Table 7-2. Top: Mean values of tissue segmentation within MRSI VOI and whole brain for RRMS patients and HCs. * Statistical significance ( $p < 0.05$ ). Bottom: Mean values of MRSI voxels volume fractions within WML and NAWM voxels of RRMS patients compared to HCs.* Statistical significance ( $p < 0.05$ ).....	192
Table 7-3. Summary of statistically significant differences in the metabolic ratios of three different tissues types from MRSI data; NAWM and WML for RRMS group compared to WM for HCs. Gly: glycine. * Statistical significance ( $p < 0.05$ ). ..	196

## List of Publications in this thesis

- **Chapter 2**

**O. Al-iedani**, J. Lechner-Scott, K. Ribbons, S. Ramadan, “Fast magnetic resonance spectroscopic imaging techniques in human brain-applications in multiple sclerosis”, *Journal of Biomedical Science*, 2017; 24:17.

- **Chapter 3**

**O. Al-iedani**, J. Arm, K. Ribbons, R. Lea, J. Lechner-Scott, S. Ramadan, “Diurnal stability and long-term repeatability of neurometabolites using single voxel 1H magnetic resonance spectroscopy”, *European journal of radiology*, 2018; 107-113.

- **Chapter 4**

**O. Al-iedani**, K. Ribbons, R. Lea, S. Ramadan, J. Lechner-Scott, “A Longitudinal, Observational Study of the Effect of Dimethyl Fumarate on Hippocampal Metabolites in RRMS using 1H-MR Spectroscopy”, *J Biomedical Sci*, 2018; 4:16.

- **Chapter 7**

**O. Al-iedani**, K. Ribbons, N. Golizadeh, J. Lechner-Scott, S. Quadrelli, R. Lea, O. Andronesi, S. Ramadan. “Spiral-MRSI and tissue segmentation of normal-appearing white matter and white matter lesions in relapsing remitting Multiple Sclerosis patients”, *Magnetic Resonance Imaging Journal* (Accepted).

## **Additional publications co-authored during candidature**

- N. Gholizadeh, P. B. Greer, J. Simpson, Caixia Fu, **O. Al-iedani**, P. Lau, A. Heerschap, S. Ramadan, “Supervised risk predictor of central gland lesions in prostate cancer using <sup>1</sup>H magnetic resonance spectroscopic imaging with gradient offset independent adiabaticity pulses”, J Magn Reson Imaging. doi:10.1002/jmri.26803.
- S. Quadrelli, K. Ribbons, J. Arm, **O. Al-iedani**, J. Lechner-Scott, R. Lea, S. Ramadan, “2D in-vivo L-COSY spectroscopy identifies neurometabolite alterations in treated multiple sclerosis”, Therapeutic Advances in Neurological Disorders, 2019.
- J. Arm, **O. Al-iedani**, R. Lea, J. Lechner-Scott, S. Ramadan, “Diurnal variability of cerebral metabolites in healthy human brain with 2D localized correlation spectroscopy (2D L-COSY)” , Therapeutic Advances in Neurological Disorders, Journal of magnetic resonance imaging : JMRI 2019.
- J. Arm, **O. Al-iedani**, S. Quadrelli, K. Ribbons, R. Lea, J. Lechner-Scott, S. Ramadan, “ Reliability of neurometabolite detection with two-dimensional localized correlation spectroscopy at 3T” , Journal of magnetic resonance imaging : JMRI 2018;48:1559-1569.

## List of Presentations

- **O. Al-iedani**, K. Ribbons, J. Lechner-Scott, S. Quadrelli, R. Lea, O. Andronesi, S. Ramadan. “Spiral-MRSI and tissue segmentation of normal-appearing white matter and white matter lesion load in relapsing remitting Multiple Sclerosis patients”, Montreal, Canada, (2019).
- **O. Al-iedani**, K. Ribbons, R. Lea, S. Ramadan, J. Lechner-Scott. “The effect of Dimethyl fumarate treatment on neuro-metabolite levels in relapsing-remitting multiple sclerosis using <sup>1</sup>H-MR spectroscopy”, The Australian Society for Medical Research (ASMR), Newcastle, Australia, (2019).
- A. Alshehri, **O. Al-iedani**, N. Golizadeh, R. Lea, J. Lechner-Scott, S. Ramadan. “Identify clinical differences between early relapsing-remitting Multiple Sclerosis and Healthy Controls using advanced Diffusion Tensor Imaging technique”, The Australian Society for Medical Research (ASMR), Newcastle, Australia, (2019).
- N. Gholizadeh, P. B. Greer, J. Simpson, **O. Al-iedani**, P. Lau, A. Heerschap, S. Ramadan, “Supervised risk predictor of central gland lesions in prostate cancer using GOIA-sLASER <sup>1</sup>H MRSI”, Annual Meeting ESMRMB, Rotterdam, Netherlands, (2019).
- N. Gholizadeh, P. B. Greer, J. Simpson, **O. Al-iedani**, P. Lau, A. Heerschap, S. Ramadan, “Supervised machine learning of prostate cancer in the peripheral zone using multiparametric MRI”, Annual Meeting ISMRM-ESMRMB, Montreal, Canada, (2019).
- S. Quadrelli, K. Ribbons, R. Lea, J. Arm, **O. Al-iedani**, S. Ramadan, J. Lechner-Scott. “Can MR spectroscopy predict multiple sclerosis and its clinical symptoms”, European Committee for Treatment and Research in Multiple Sclerosis (ECTRIMS), Berlin, Germany, (2018).

- **O. Al-iedani**, K. Ribbons, N. Gholizadeh, O. Andronesi, J. Lechner-Scott, R. Lea, S. Ramadan. “Evaluation of metabolic alterations in the MS brain using fast Spiral MRSI and machine learning”, Pan-Asian Committee for Treatment and Research in Multiple Sclerosis (PACTRIMS), Australia, (2018).
- **O. Al-iedani**, K. Ribbons, R. Lea, S. Ramadan, J. Lechner-Scott. “The effect of Dimethyl fumarate treatment on hippocampal metabolites in RRMS using 1H-MR spectroscopy”, European Committee for Treatment and Research in Multiple Sclerosis (ECTRIMS), Paris, France, (2017).
- K. Ribbons, J. Arm, R. Lea, S. Ramadan, **O. Al-iedani**, J. Lechner-Scott. “Metabolites in the posterior cingulate cortex are correlated to clinical symptoms in relapsing remitting multiple sclerosis”, European Committee for Treatment and Research in Multiple Sclerosis (ECTRIMS), Paris, France, (2017).
- **O. Al-iedani**, K. Ribbons, J. Arm, J. Lechner-Scott, S. Ramadan. “Diurnal effects on brain MRI volume and 1D MR neurospectroscopy” , The Australia and New Zealand society for Magnetic Resonance conference, Kingscliff, NSW, Australia, (2017).
- **O. Al-iedani**, K. Ribbons, R. Lea, J. Lechner-Scott, O. Andronesi, S. Ramadan. “Mapping Differential Metabolic Regions in the MS brain using fast Spiral MRSI”, The Australia and New Zealand society for Magnetic Resonance conference, Kingscliff, NSW, Australia, (2017).
- K. Ribbons, J. Arm, R. Lea, S. Ramadan, **O. Al-iedani**, J. Lechner-Scott. “Metabolites in the posterior cingulate cortex are correlated to clinical symptoms in relapsing remitting multiple sclerosis”, The MS Research Australia Progress in MS Research Conference (MSRA), Sydney, Australia, (2017).

- **O. Al-iedani**, K. Ribbons, R. Lea, S. Ramadan, J. Lechner-Scott. “The effect of Dimethyl fumarate treatment on hippocampal metabolites in RRMS using 1H-MR spectroscopy”, The MS Research Australia Progress in MS Research Conference (MSRA), Sydney, Australia, (2017).
- **O. Al-iedani**, K. Ribbons, J. Arm, J. Lechner-Scott, S. Ramadan. “Diurnal effects on brain MRI volume and 1D MR neurospectroscopy”, International Society for Magnetic Resonance in Medicine (ISMRM), Honolulu, USA, (2017).
- S. Luchow, S. Quadrelli, J. Arm, **O. Al-iedani**, K. Skehan, K. Fisher, B. Schmitt, B. Marechal, S. Ramadan. “Fully automated morphometric brain volume extraction vs FreeSurfer”, International Society for Magnetic Resonance in Medicine (ISMRM), Honolulu, USA, (2017).
- **O. Al-iedani**, K. Ribbons, J. Lechner-Scott, S. Ramadan. “Detection of Biochemical Alterations in RRMS patients by 1D MR Spectroscopy”, The Australian Society for Medical Research (ASMR), Newcastle, Australia, (2016)
- K. Ribbons, S. Quadrelli, J. Lechner-Scott, **O. Al-iedani**, J. Arm , C. Mountford, S. Ramadan. “2D MR spectroscopy can identify molecules differentiating MS from healthy controls”, European Committee for Treatment and Research in Multiple Sclerosis (ECTRIMS), Barcelona, SPAIN, (2015)

## List of Abbreviations

1D	One Dimensional
2D	Two Dimensional
3D	Three Dimensional
AD	Axial Diffusivity
ARCS	Audio Recorded Cognitive Screen
ARR	Annualised Relapse Rate
AUC	Area Under Curve
CHESS	Chemical Shift Selective Suppression Pulses
Cho	Choline
CNS	Central Nervous System
Cr	Creatine
CRLB	Cramer-Rao lower bound
CSF	cerebrospinal fluid
CSI	Chemical Shift Imaging
CV	Coefficient of Variation
DASS-21	Depression Anxiety Stress Scale
DMF	Dimethyl Fumarate

DMT	Disease modifying therapies
DTI	Diffusion Tensor Imaging
EDSS	expanded disability status scale
EPI	Echo Planar Imaging
EPSI	Echo Planar Spectroscopic Imaging
FA	Fractional Anisotropy
fMRI	functional MRI
FOV	Field of View
FSL	FMRIB Software Library
GA	glatiramer acetate (GA)
GABA	$\Gamma$ -Aminobutyric Acid
Gln	Glutamine
Glu	Glutamate
Glx	Glutamine+Glutamate
GM	Grey Matter
GPC	Glycerophosphocholine
GOIA	Gradient-Modulated Offset-Independent Adiabatic
GRAPPA	Generalised Autocalibrating Partially Parallel Acquisitions

GSH	Glutathione
IFN- $\beta$	Interferon
JPRESS	J-Resolved Spectroscopy
LCmodel	Linear Combination of model spectra
MD	Mean Diffusivity
MEGA	Mescher-Garwood
m-Ins	Myo-Inositol
MFIS	Modified Fatigue Impact Scale
MPRAGE	Magnetization-Prepared RAPid Gradient Echo
MRI	Magnetic Resonance Imaging
MRS	Magnetic Resonance Spectroscopy
MRSI	Magnetic Resonance Spectroscopic Imaging
MS	Multiple Sclerosis
MSSS	Multiple Sclerosis Severity Score
NAA	N-Acetylaspartate
NAWA	Normal Appearing White Matter
OVS	Outer Volume Suppression

PBVC	Percentage Brain Volume Change
PCG	Posterior Cingulate Gyrus
PEPSI	Proton Echo-Planar Spectroscopic Imaging
PFC	pre-frontal cortex
PPMS	Primary Progressive Multiple Sclerosis
PRESS	Point RESolved Spectroscopy
PSF	Point Spread Function
RD	Radial Diffusivity
RF	Radio Frequency
ROC	Receiver Operator Characteristic
ROI	Region of Interest
RRMS	Relapsing-Remitting Multiple Sclerosis
SDMT	Symbol Digit Modalities Test
SENSE	SENSitivity Encoding
SIENAX	Structural Image Evaluation with Normalisation of Atrophy cross-sectional
sLASER	Semi-Localized Adiabatic Selective Refocusing
SMASH	SiMultaneous Acquisition of Spatial Harmonics

SNR	Signal-To-Noise Ratio
SPM	Statistical Parametric Mapping
SPMS	Secondary Progressive Multiple Sclerosis
STEAM	Stimulated Echo Acquisition Mode
SVM	Support Vector Machine
SVS	Single Voxel Spectroscopy
T2-FLAIR	T2-weighted Fluid-Attenuated Inversion Recovery
tCho	Total Choline
TE	Echo Time
tCr	Total Creatine
TM	Mixing Time
tNAA	total N-acetylaspartate
TR	Repetition Time
VOI	Volume of Interest
WM	White Matter
WML	White Matter Lesion

## Symbols

$\%$	Per cent
$\gamma$	Gyromagnetic ratio
$B_0$	Main static magnetic field
$B_1$	Applied magnetic field
cm	Centimeter
G	Gradient strength
Hz	Hertz
$M_0$	Equilibrium magnetization
mm	Millimeter
ms	Millisecond
T	Tesla
$T-1$	Longitudinal relaxation time constant
$T-2$	Transverse relaxation time constant
TE	Echo time
TR	Repetition time

# Chapter 1 : Introduction

## 1.1 What is multiple sclerosis?

Multiple sclerosis (MS) is an immune-mediated neuronal disorder in which inflammatory cells attack the myelin of the central nervous system (CNS) (Figure 1-1), leading to varying extents of neuroaxonal injury, demyelination and gliosis by affecting both the brain and spinal cord<sup>1</sup>. It is the second most common disabling neurological disease in young people, affecting people predominantly in their productive years (20-45 years)<sup>2</sup>. There are approximately 2.5 million people in the world with MS and 23,000 people in Australia.

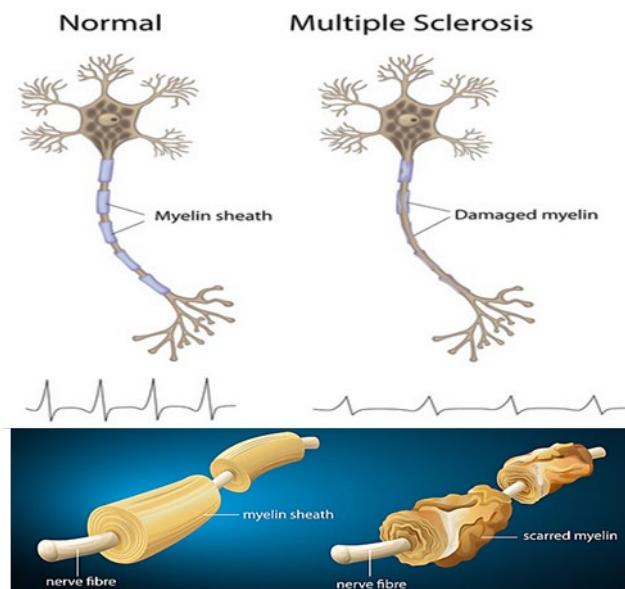


Figure 1-1 Normal neuron with a Myelin vs Demyelination in MS with damaged Myelin. [https://www.researchgate.net/publication/230554483\\_Multiple\\_Sclerosis](https://www.researchgate.net/publication/230554483_Multiple_Sclerosis)

MS patients experience widely varying signs and symptoms that depend on the extent and location of the nerve damage and are related and interdependent Figure 1-2. One untreated symptom may trigger a host of additional symptoms and strongly impact a patient's quality of life.

Typically, symptoms of MS are based on the location of the plaque and most patients initially experience exacerbations and remissions due to inflammation and recovery with remyelination which in the later stages is exhausted and then leads to persistent symptoms. Common initial symptoms of MS include optic neuritis, sensory disturbances and weakness<sup>3</sup>.

During the disease course, most patients will experience mobility impairment (80%) and fatigue (70%)<sup>4</sup> but also cognitive, sexual as well as bowel and bladder dysfunction and loss of coordination<sup>5</sup>.

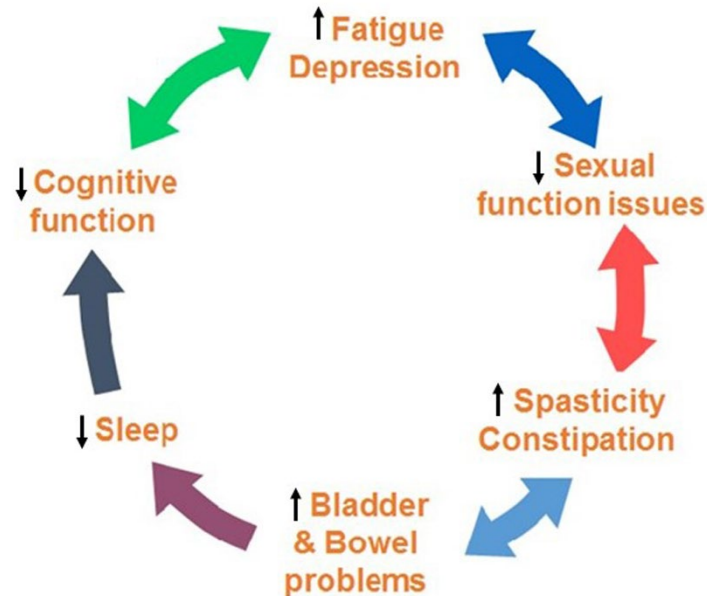


Figure 1-2. Common initial symptoms of MS. ([National Multiple Sclerosis Society, Multiple Sclerosis: https://www.nationalMSSociety.org/PRC](https://www.nationalMSSociety.org/PRC)).

## 1.2 Classification of MS types

Relapsing-remitting MS (RRMS) accounts for 85% of MS patients. RRMS is a sequence of remission phases (stability) and relapse or exacerbation<sup>1</sup>. Chronic progressive MS is divided into primary progressive MS (PPMS), secondary progressive MS (SPMS) and progressive relapsing (PRMS) (Figure 1-3). However, the new classification by Lublin<sup>6</sup> aims to distinguish progressive disease according to their clinical and MRI activity. Around two-thirds of patients diagnosed with RRMS may develop into SPMS which can be defined as an initial period of relapsing-remitting and gradual neurological worsening of disease. PPMS is defined by slowly progressing disability from onset, characterised by localised subpial inflammation without blood brain barrier disruption<sup>7</sup>.

Clinically isolated syndrome	Not active
	Active*
Relapsing -remitting disease	Not active
	Active*
*Activity = clinical relapses and/or MRI (gadolinium-enhancing MRI lesion; new/enlarging T2 lesions)	
Primary progressive (progressive accumulation of disability from onset)	Active* and with progressive
progressive disease	Active* but without progressive
Secondary progressive (progressive accumulation of disability after an initial relapsing course)	Not active and without progression (stable disease)
*Activity = clinical relapses and/or MRI (gadolinium-enhancing MRI lesion; new/enlarging T2 lesions)	
"Progression measured by clinical evaluation at least once yearly.	

Figure 1-3. The course of MS is highly varied and heterogeneous. The disease is characterized initially by episodes of reversible clinically isolated neurological deficits, which is often followed by progressive neurological deterioration over time. Activity is defined as the presence of clinical relapse or presence of new plaques over time either on T2 scan or T1 contrast enhanced MRI scans <sup>6</sup>.

### 1.3 Pathophysiology of MS

The exact pathophysiological mechanism of this neuro-degenerative disorder and loss of function is still not clear, although there are great advances in the scope of treatment for MS. Genetic predisposition and activation of the immune system by environmental factors are thought to initiate the disease<sup>8</sup>. Most regions identified in large genome wide associated studies indicate T cell activation as the major factor in developing the disease <sup>9</sup>. The combination of lower genetic tolerance to environmental factors like Epstein-Barr virus (EBV), HIV-6 (Herpesvirus 6), HRTLV and Chlamydia Pneumoniae as well as UV exposure, diet and smoking most likely trigger the onset of disease<sup>10</sup>.

## 1.4 Management of MS

Management of MS patients is divided into prophylactic immunomodulatory therapy and symptom management (spasticity, bladder dysfunction, fatigue, depression, anxiety, etc.). Disease modifying therapy can reduce the relapse rate and delay progression of disability. It consists of short and long-term treatments<sup>11</sup>.

Relapses are usually treated acutely with high dose intravenous methylprednisolone (MP) (500-1000 mg) over 3-5 days. The long term treatment attempts to suppress the autoprolieration of immune cells. There are currently 11 MS treatments approved by the TGA, all demonstrating evidence of slowing the progression of disability in patients. For example, ABC (Avonex, Betaferon and Copaxone) treatments in most countries are considered first line treatment and are applied as subcutaneous or intramuscular injections<sup>12</sup>. Recently, oral treatments like Fingolimod (Gilenya), Teriflunomide (Aubagio) and dimethyl fumarate (Tecfidera) have been introduced, all acting on reducing the circulating lymphocyte count<sup>12</sup>. More potent therapies such as Natalizumab (Tysabri) and Alemtuzumab (Lemtrada) are applied as infusions and carry a high risk of secondary infections or autoimmune diseases. Treatment effect is usually monitored by assessing annualised relapse rate (ARR) and change in expanded disability status scale (EDSS) as well as activity on MRI<sup>13</sup>.

## 1.5 MS diagnosis and clinical management

The diagnosis of MS is based on the medical history of recurrent episodes of neurological dysfunction and a set of diagnostic tools including MRI, evoked potentials and lumbar puncture. Assessing nerve function with evoked potentials is based on measuring conduction speed of the brain's response to visual, auditory, and sensory stimuli. Typically, demyelinated fibres show a delayed response<sup>14</sup>. A lumbar puncture is done to exclude infectious causes and to demonstrate inflammation in the cerebrospinal fluid (CSF) (i.e. revealing the number of oligoclonal banding ) that is restricted to the CNS and not in the periphery<sup>3</sup>. MRI has become one of the most valuable modalities of medical imaging methods due to its ability to provide excellent tissue contrast and it is a non-invasive technique. Conventional MRI includes T1 with and without gadolinium to assess if there is a breakdown of the blood brain barrier and T2-FLAIR sequences to assess the lesion load. Additionally, proton density and T2 demonstrates the location of periventricular MS lesions indicating excess of water and inflammation (Figure 1-4.) Recently, the emphasis on MRI in the diagnostic process has been growing and has

reached a stage where it can be used alone for diagnosis. The disease pathology is mainly focal loss of myelin from inflammation.

These focal inflammatory white matter lesions ('plaques') best seen on FLAIR, characterise primary demyelination whereas "black holes" on T1 demonstrate the variable extent of axonal loss and reactive gliosis<sup>15</sup>.

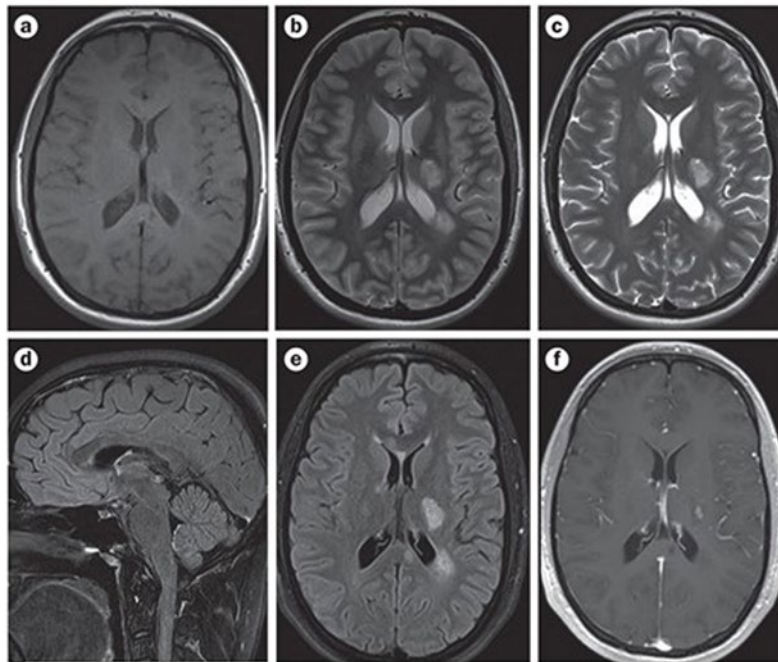


Figure 1-4. Standardized brain MRI protocol to evaluate patients in whom multiple sclerosis is clinically suspected. a. Axial T1-weighted pre-contrast, b. Proton Density weighted and c. T2-weighted sequences, followed by d. Sagittal post-contrast T2-weighted fluid-attenuated inversion recovery (FLAIR), e. Axial post-contrast T2-FLAIR and f. Axial post-contrast T1-weighted sequences<sup>16</sup>.

## 1.6 Limitation of conventional MRI methods

Patients diagnosed with MS using T2 lesion load on MRI to fulfil McDonald criteria<sup>17</sup>, will often have to undergo additional testing for verification of diagnosis. Routine MRI is not specific for MS and only detects about 60% of new forming lesions<sup>18</sup>. Also, MRI findings do not correlate well with EDSS<sup>19</sup>. Additionally, routine MRI techniques are insensitive to axonal loss, gliosis and demyelination processes. In absence of any better option, MRI is used not only for diagnosis but also for clinical management and as a therapeutic decision-making tool. Therefore, monitoring disease activity on annual imaging is considered best practice. Advanced MR techniques are indicated to extend the sensitivity and specificity of detection of ongoing activity of MS.

## 1.7 Advanced MR techniques

Selected major advanced MRI techniques include diffusion tensor imaging (DTI), functional MRI (fMRI) and MR spectroscopy (MRS). DTI measures the random translational diffusion of water molecules in brain tissue. It is a non-invasive method, with unparalleled sensitivity to water movements within the architecture of the tissues. It uses existing MRI technology and requires no new equipment, contrast agents or chemical tracers. The four most informative DTI measures are fractional anisotropy (FA), mean diffusivity (MD), radial diffusivity (RD) and axial diffusivity (AD) as shown in Figure 1-5. FA indicates the relative presence of a preferred direction of diffusion and ranges between 0 and 1. MD indicates the extent to which water is able to freely diffuse, and reflects the overall presence of barriers to diffusion. RD and AD reflect the ability of water molecules to diffuse along and perpendicular to the main direction of diffusion. In presence of demyelination, increased RD is often detected<sup>20, 21</sup>. AD and RD, are markers of the integrity of axons and myelin, respectively, while MD is a scalar quantity used to measure overall diffusion within a voxel, that is representative of axonal and myelin loss<sup>21</sup>. Decrease in FA is reflective of tissue damage such as demyelination<sup>22</sup>.

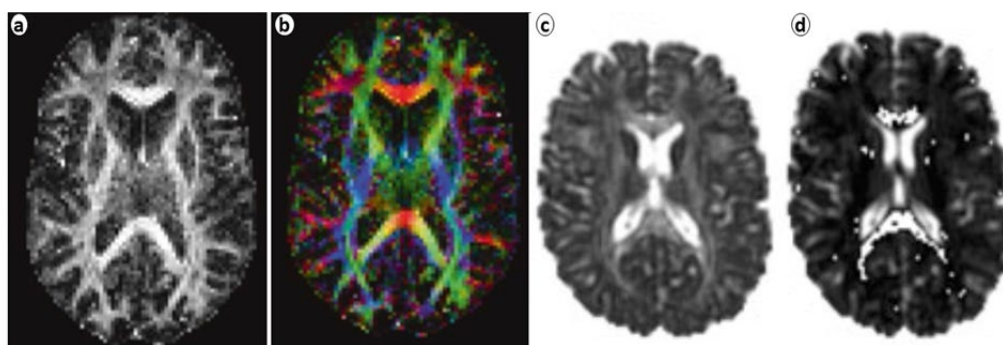


Figure 1-5. DTI images represents (a) MD, describes the total amount of diffusion in a given voxel. (b) FA, the degree of anisotropy in a given voxel and therefore the strength of the directional diffusion, value from 0 (isotropy) to 1 (anisotropy). (c) AD, diffusion along the principle axis of diffusion ellipsoid. (d) RD, average diffusion along the two minor axes<sup>23</sup>.

Another non-invasive technique, fMRI, uses the blood oxygenation level dependent (BOLD) signal to localise neuronal activity. This technique is able to assess the abnormal pattern of brain activation and function that results from disease progression. The main target of fMRI in all MS studies rely on functional reorganisation process (i.e. brain plasticity

phenomenon) in recovery symptoms during the progression of MS<sup>24</sup>. Mostly, this process leads to increase in the magnitude or extent of brain activity compared to healthy control at a specific task performance. Further, this process was detected within different brain functions such as motor, cognitive and visual systems<sup>25</sup>. Previous fMRI studies confirmed that increased reorganization process was correlated with tissue damage at early stage of the disease. In contrast, during disease progression the brain of MS patients showed decrease in activation due to the overall tissue damage becoming too significant for compensation<sup>26</sup>. Finally, the advanced technique of MRS has the unique potential to capture biochemical changes in the brain before morphological and atrophic changes, as described below.

## 1.8 Biochemical profiling using MRS

MRS is a non-invasive technique used to identify and quantify metabolites *in-vivo*, giving chemical information rather than anatomical information, as in MR imaging.

The measurements are collected from a localised voxel in a specific region of the brain; therefore, location of the voxel has major implications. There are substantial differences in neurometabolites in grey compared to white matter, and also in lesions compared to normal appearing white matter (NAWM)<sup>27-29</sup>. In clinical practice, MRS techniques have been used to evaluate the neurometabolic changes of the MS brain (Figure 1-6) to allow the following to be identified:

<b>Metabolite</b>	<b>Description</b>
N-acetylaspartate (NAA)	Predominantly present in cell bodies and acts as a neuronal marker. In MS, reduction in NAA level reflects axonal degeneration and as an indicator of axonal loss in early stages of the relapsing form. MRS studies have shown decrease in NAA in MS lesions and normal appearing white matter further supporting the importance of NAA as disease marker <sup>30</sup> .
Creatine+Phosphocreatine (tCr)	Creatine (Cr) and phosphocreatine (PCr) play an essential role in the storage and transmission of phosphate-bound energy in the form of adenosine triphosphate (ATP).

Cho and choline-containing compounds	In MS, an indicator of brain tissue damage or diffuse axonal injury is likely to result in the degradation of membrane constituents by releasing choline into interstitial space. Usually grouped within the B-complex vitamins and present in the synaptic ends of cholinergic neurons and cell membranes, and part of lipid metabolism <sup>30</sup> .
m-Ins	Acts as glial cell marker in brain tissue, increased myo-inositol has been related to higher metabolic rate and increased glial activity in MS lesions, NAWM, thalamus and cortical grey matter <sup>31</sup> .
Macromolecules (MM)	In various pathologies, including MS, the presence of mobile lipids or pathologically altered macromolecules may provide useful additional diagnostic information. The increasing lipid/MM signal might be due to breaking down of myelin layers.
Glutamate (Glu)+glutamine (Gln) (Glx)	Glutamate is a major excitatory neurotransmitter, which is predictive of poor outcome when elevated <sup>32</sup> . <i>In-vivo</i> glutamate toxicity in MS correlated with reduction of NAA, cerebral volume decline and decay of functional performances measured by Paced Auditory Serial Addition Test-3 (PASAT) and Gln is a regulator of Glu metabolism.
Gamma-aminobutyric acid (GABA)	GABA is a major inhibitory transmitter which plays an important role in MS progression. Abnormalities in GABA concentrations have been associated with neurodegenerative disease processes. It has been shown that GABA is reduced by MS onset <sup>33</sup> and that some drugs might be able to modulate its concentration. Monitoring GABA <i>in-vivo</i> in a timely manner has the potential to evaluate the level of treatment efficacy in MS patients <sup>34</sup> .

Phenylalanine (Phe)	Increased by 37% in repetitive head injury, Phe plays an important role in influencing mood in a way that leads to depression and anxiety. As depression and anxiety are symptoms occurring in over 50% of patients with MS and have a significant impact on cognition, quantifying Phe is essential in monitoring MS progression <sup>35</sup> .
Fucose (Fuc)	Fucosylation increases with inflammation <sup>36</sup> . Fucosylation of brain glycoconjugates has been shown to be crucial for neuronal plasticity.

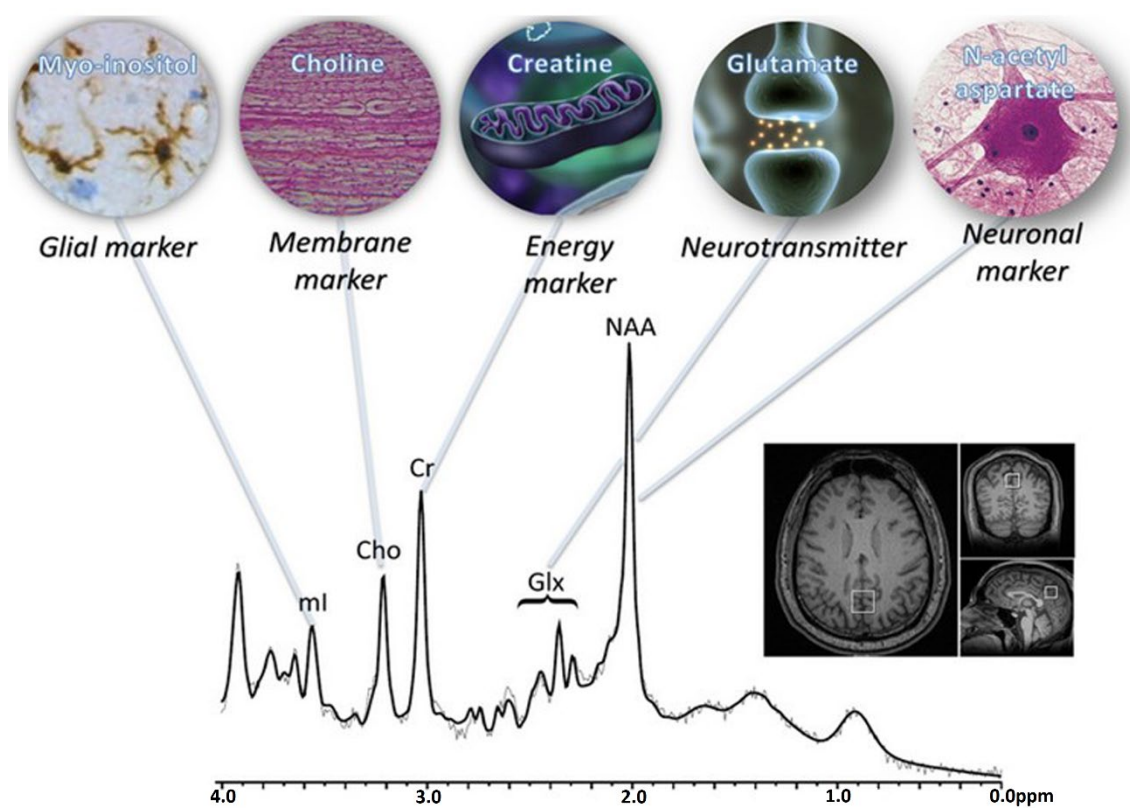


Figure 1-6. The neurometabolic changes of the MS.

Novel MR methods such as single voxel (SV) H-MRS<sup>37</sup> and multi-voxel MRS imaging (MRSI)<sup>38</sup> can differentiate the pathological processes within MS lesions as well as in NAWM. SV methods such as STimulated Echo Acquisition Method (STEAM) and Point RESolved Spectroscopy (PRESS) are typically used to excite a specific region of interest (ROI) within the brain. MRS was the first unconventional MR method to prove neurometabolic abnormalities related to pathological processes of the disease, particularly in MS which has the potential to improve the specificity of the diagnosis and aid clinical management<sup>39,40</sup>. Figure 1-6 shows a typical single voxel spectrum from a brain.

MRSI is a multivoxel method, covering a larger area of the brain compared to the single region in the SV method. Clinically, MRSI is more suitable due to its ability to obtain important metabolic information with extended spatial coverage, which will reflect better on overall disease activity. Several reports have shown that using MRS methods coupled with tissue segmentation can evaluate spectroscopic changes of brain metabolites within white matter lesions (WML), NAWM and grey matter (GM) in the hippocampus as well as other brain regions in MS patients<sup>41-46</sup>. Most conventional two-dimensional (2D) and three-dimensional (3D) MRSI in the above studies, used PRESS for localization which suffers from suboptimal data quality, limited spatial coverage and resolution, long acquisition times and localization artefacts. However, in spite of the encouraging results of MRSI applications, the real challenge is to perform metabolic mapping of the majority of the brain, with high spatial resolution, improved localisation and short acquisition times.

Methodological improvements have been achieved to enable fast MRSI acquisition. Interestingly, a few studies have applied fast 3D MRSI methods to cover large regions of the MS brain and to evaluate brain-metabolites in WML, NAWM and cortical GM. These fast MRSI studies mostly used echo planar spectroscopic imaging (EPSI)<sup>47-50</sup>, a technically demanding sequence with specialised acquisition and processing requirements, with suboptimal point spread function behaviour. In order to apply a clinically useful technique, time efficient MRSI methods that use spiral techniques is used in this proposal to map metabolites in the majority of the brain, for MS clinical management purposes. Spiral MRSI sequences will be used to demonstrate differences between MS patients and healthy controls by measuring the biochemical profiles and generating a metabolite distribution map of the whole brain.

## 1.9 Significance of current research project

MS is a heterogeneous disease with a multitude of pathophysiological mechanisms, most of which are poorly understood. Although myelin and axonal loss can be considered as structural, chemical events that contribute to this are rather elusive. In this study, we developed advanced MRS techniques for monitoring and evaluating the treatment response in MS patients. These MRI techniques will have tremendous potential for clinical use as quantitative imaging based surrogate biomarker to understanding disease pathology. Initially, we applied a single voxel MRS method to investigate the metabolic concentration changes longitudinally in hippocampal, pre-frontal cortex (PFC) and posterior cingulate gyrus (PCG) regions of relapsing-remitting MS (RRMS) patients. We also evaluated the effect of disease modifying agents on neurometabolites. Understanding the limitations of the single voxel technique, we developed a whole brain fast MRS technique (FAST MRSI) to extend the coverage to include the entire brain in a single short data acquisition without compromising the spatial resolution. As part of this, we developed a novel post processing pipeline method, (multivoxel segmentation technique) to segment the whole brain into smaller components with each component representing a wealth of biochemical information from areas as small as  $1\text{cm}^3$ . With FAST MRSI and multivoxel segmentation methods, we were able to map the metabolic profile of RRMS patients for the whole brain classifying various tissue types (white/grey matter & CSF), lesion characteristics and normal appearing brain tissues.

The first part of the study began looking at the validity of single voxel method MRS technique. We designed this study to evaluate the diurnal stability and long-term repeatability and reliability of one-dimensional (1D) proton magnetic resonance spectroscopy (H-MRS) *in-vitro* and *in-vivo* at a 3T human MR system. Both intra-subject (within subject) and inter-subject (between subjects) variability of neurometabolites were measured over short and long-term intervals. This aspect will be an important factor in longitudinal studies in chronic conditions, attempting to quantify changes in metabolites over extended periods of time. In this study, spectral diurnal and repeatability measures were initially obtained from a standard brain phantom followed by evaluating the diurnal variability, long-term repeatability and reliability of localised 1D H-MRS of neurometabolites in 10 healthy participants. The findings of the study showed 1D H-MRS is reliable and had minimal diurnal variations as shown by Al-iedani et al<sup>51</sup>.

In the second study, we focussed on investigating 20 relapsing-remitting MS (RRMS) patients, compared to age and sex-matched HCs to assess the metabolic impact of DMF treatment longitudinally over 24 months. We also highlighted the importance of MRS technique in the cross-sectional evaluation of metabolic concentration changes in hippocampal, PFC and PCG regions. Associations of the neuro metabolic changes related to clinical symptoms were also assessed. This study demonstrated that glutathione (GSH) levels in RRMS group significantly increased following DMF (Tecfidera) treatment in the hippocampus. This was published in *Journal of Biomedical Sciences*<sup>52</sup>.

In the third study, we again focussed on a larger sample size of 98 relapsing-remitting MS (RRMS) patients, compared to age and sex-matched HCs to assess the metabolic impact of DMTs (Fingolimod and injectable treatments). We investigated the importance of MRS technique in the cross-sectional evaluation of metabolic concentration changes in hippocampal, PFC and PCG regions. Associations of the neurometabolic changes related to clinical symptoms were also assessed. This study demonstrated that neurometabolites in our RRMS group significantly changed compared to HCs. This was presented as a poster at *ECTRIMS and AMSR conferences*.

In the last part of our project, we employed the novel FAST MRSI technique and multi-voxel segmentation method to map the neurometabolic profiles of 16 RRMS patients and 9 HCs. We applied 3D spiral MRSI with LASER sequence with GOIA-W (16,4) RF pulses to evaluate the performance of fast spiral MRSI technique, coupled with tissue segmentation of the majority of the brain to identify neurochemical differences in NAWM and WML of stable RRMS patients. The difference in large spectroscopic data sets in the entire VOI was evaluated with support vector machine method with multi-models of MS and HCs. Correlation of whole brain metabolic changes and their relationship to clinical signs of disability (i.e. cognitive functions, fatigue and mood) were also assessed. The results of the study revealed that there is significant difference in neurometabolites in NAWM as well as lesions in RRMS compared to HCs. The findings of this study has been submitted to the *Journal of Magnetic Resonance in Medicine* and was presented as an oral presentation at (*ISMRM*) conference<sup>53</sup> and as an e-poster at (*PACTRIMS*) conference<sup>54</sup>.

The structure of this thesis is as follows:

**Chapter 2. Fast Magnetic Resonance Spectroscopic Imaging Techniques in Human Brain-Applications in Multiple Sclerosis**, introduces the underlying principles of MRS and the different MRSI techniques are compared, focussing on recent advances in high-speed MRSI methods. MS was used as an example pathology in a clinical setting where MRSI techniques was applied to map brain metabolic changes in different areas of the brain and at different disease stages to evaluate the potential use of the technique as a tool in disease diagnosis and clinical management.

**Chapter 3. Diurnal Stability and Long-Term Repeatability of Neurometabolites Using Single Voxel 1H Magnetic Resonance Spectroscopy** presents the diurnal variability, long-term repeatability and reliability of localised 1D H-MRS quantification of posterior cingulate gyrus metabolites in phantom and healthy participants on a 3T clinical MR system.

**Chapter 4: Longitudinal, observational study of the effect of dimethyl fumarate on hippocampal metabolites in RRMS using <sup>1</sup>H-MR spectroscopy**, applied the first study using H-MRS to investigate the longitudinal metabolic changes in the hippocampus of RRMS patients following initiation of dimethyl fumarate treatment. The association of hippocampal neurometabolite changes in RRMS with severity of clinical and neuropsychological symptoms were also explored.

**Chapter 5. The effect of Dimethyl fumarate treatment on pre-frontal cortex and posterior cingulate gyrus metabolite levels in RRMS using H-MRS** presents the non-invasive H-MRS method to evaluate the pre-frontal cortex and posterior cingulate gyrus neurometabolite changes in RRMS patients compared to healthy controls pre and post dimethyl fumarate treatment over two years.

Chapter 6. **Cross sectional evaluation of neurometabolic alterations in RRMS with fingolimod and injectable treatment using advanced MRS**, presents the non-invasive H-MRS method to evaluate neurometabolite profile changes of RRMS patients compared with healthy controls, to evaluate the treatment of Fingolimod and injectable on the hippocampal, pre-frontal cortex and posterior cingulate gyrus metabolism in RRMS patients. Neurometabolite levels and volumetric MRI data were also correlated with clinical assessment parameters of MS patients with different treatments.

Chapter 7. **Spiral-MRSI and tissue segmentation of normal-appearing white matter and white matter lesions in relapsing remitting multiple sclerosis patients**, presents the performance of fast spiral MRSI techniques coupled with tissue segmentation of the majority of the brain to identify neurometabolic differences in NAWM and WML of stable RRMS patients compared to age and sex-matched HCs. The support vector machines (SMV) was also applied to investigate the differences in large spectroscopic data sets in the entire volume of interest (VOI) with multi-models of MS and HCs.

Chapter 8. **Summarizes this thesis and discusses future work.**

# **Chapter 2 : Fast Magnetic Resonance Spectroscopic Imaging Techniques in Human Brain- Applications in Multiple Sclerosis**

Oun Al-iedani, Jeannette Lechner-Scott, Karen Ribbons and Saadallah Ramadan

## **ABSTRACT**

Multi-voxel magnetic resonance spectroscopic imaging (MRSI) is an important imaging tool that combines imaging and spectroscopic techniques. MRSI of the human brain has been beneficially applied to different clinical applications in neurology, particularly in neuro-oncology but also in multiple sclerosis, stroke and epilepsy. However, a major challenge in conventional MRSI is the longer acquisition time required for adequate signal to be collected. Fast MRSI of the brain *in-vivo* is an alternative approach to reduce scanning time and make MRSI more clinically suitable.

Fast MRSI can be categorised into spiral, echo-planar, parallel and turbo imaging techniques, each with its own strengths. After a brief introduction on the basics of non-invasive examination (H- MRS) and localization technique principles, different fast MRSI techniques will be discussed from their initial development to the recent innovations with particular emphasis on their capacity to record neurochemical changes in the brain in a variety of pathologies.

The clinical applications of the whole brain fast spectroscopic techniques can assist in the assessment of neurochemical changes in the human brain and help in understanding the roles they play in disease. To illustrate the usefulness of these techniques in the clinical context, MRSI applications in multiple sclerosis was reviewed. The available up to date and relevant literature is discussed and an outline of future research is presented.

## **2.1 Introduction**

### **2.1.1 MRS and MRSI**

Magnetic resonance spectroscopy (MRS) is a technique used to identify and quantify metabolites *in-vivo*, giving chemical and quantitative information rather than anatomical information as in routine MR imaging. MRS interrogates a three-dimensional volume of tissue within the body positioned in a MR scanner, to produce a “spectrum” of information about

existing chemicals and their relative concentrations. Most applications and technical developments of MRS have focussed on the human brain in clinical studies and for increased understanding of the pathology in Parkinson's disease <sup>55</sup>, Alzheimer's disease <sup>56</sup>, stroke <sup>57</sup> and multiple sclerosis (MS) <sup>58, 59</sup>. MR spectra can be acquired from many chemical elements. However, proton (<sup>1</sup>H) spectroscopy provides a large sensitivity advantage over other nuclei used in MRS (e.g. <sup>31</sup>P and <sup>13</sup>C). This is because it has the greatest gyromagnetic ratio ( $\gamma$ ) of non-radioactive nuclei and a high natural abundance. This sensitivity is further enhanced compared to other nuclei, due to propitious metabolite relaxation times and several essential brain metabolites having multiple protons.

In 1985, Bottomley et al, used a slice-selective spin-echo excitation and frequency-selected water suppression (at 1.5 tesla (T)) to obtain the first spatially localised human brain spectrum, at a time when spatial localisation and spectral resolution were limited <sup>60</sup>. Many spatial localisation techniques were developed in the 1980s, when the technology was in its elementary stages and faced many difficulties in implementation and efficiency. Presently, the two most basic and common techniques used in spectroscopy are Stimulate Echo Acquisition Mode (STEAM) <sup>61, 62</sup> and Point RESolved Spectroscopy (PRESS), <sup>63, 64</sup> which are based on three slice-selective pulses applied in orthogonal planes.

MRSI can also be used in an MR scanner to fully cover an organ, e.g. brain, by giving a spectroscopic signature from each part of this organ. It is a method used to collect spectroscopic data and spatial distribution of metabolites using multiple-voxel locations within a single measurement. Multi-voxel spectroscopy (2 or 3 dimensional (2D or 3D)) plays a particularly prominent role, not only in increasing the spatial coverage, but also in improving the efficiency of data collection. Major disadvantages of the technique are long acquisition times, lack of adequate signal-to-noise ratio (SNR), insufficient water and lipid suppression and limited spatial coverage. These limitations pose major constraints to the usefulness of this technique. Despite these disadvantages, MRSI has the potential to play a significant role to assist in clinical diagnosis and treatment planning. Many different MRSI acquisition methods have been developed, including conventional and fast MRSI methods, each of which has its own advantages and disadvantages.

MRSI was initially conceptually proposed and implemented in a phantom with varying phosphorus chemical shift composition by Brown et al. in 1982 <sup>65</sup>. The method used a sequence of radiofrequency (RF) pulses and magnetic field gradients to measure chemical shift

distribution across a rectangular grid. Simple Fourier transformation was applied to recover the original chemical shift distribution. The first *in-vivo* application was carried out on a human forearm on a 1.5T magnet by Pykett et al. <sup>66</sup>.

### 2.1.2 Multiple Sclerosis (MS)

MS is an immune-mediated neuronal disorder in which inflammatory cells attack the myelin of the central nervous system (CNS), leading to varying extents of neuroaxonal injury, demyelination and gliosis by affecting both the brain and spinal cord <sup>67,68</sup>. Typically, symptoms of MS are based on the location of the plaque and most patients experience initially exacerbations and remissions due to inflammation and recovery with remyelination which, in the later stages, is exhausted and then leads to persistent symptoms. Clinically, MS can be classified into: (a) relapsing-remitting MS (RRMS) that accounts for 85% of MS patients, and is characterised with remission phases (stability) and relapse or exacerbation <sup>1</sup>, (b) chronic progressive MS is divided into primary progressive MS (PPMS), secondary progressive MS (SPMS) and progressive relapsing (PRMS). However, the new classification by Lublin <sup>6</sup> aims to characterise progressive disease according to its clinical and MRI activity. PPMS is defined by slowly progressing disability from onset, characterised by localised subpial inflammation without blood brain barrier disruption <sup>7</sup>. The diagnosis and management of MS is increasingly reliant on non-invasive MR modality. Indeed, the current diagnostic criteria for MS <sup>17</sup> includes specific MR imaging features which provides evidence of dissemination in space and time of brain and spinal cord lesions. Recent guidelines regarding the frequency of MRI studies and evaluations <sup>69</sup> suggest that MR imaging should be undertaken between every 6 months to 2 years for all RRMS patients, to monitor new and enhancing lesions, and contribute to the medical management of the relapsing form of the disease. However, in contrast there are no current reliable markers to evaluate therapeutic efficacy in the progressive forms of MS, which has been a major obstacle in the development of new disease-modifying therapies.

H-MRS might add to the specificity of diagnosis and clinical management by the potential identification of new disease biomarkers <sup>39,40</sup>. H-MRS provides a unique potential to evaluate biochemical alteration in MS. In light of this, neurochemical changes of the brain are related to the metabolite concentration levels. For instance, a reduction of N-acetylaspartate (NAA) level, which is an amino acid derivative and has a high concentration in the brain, reflects axonal degeneration or loss. <sup>39,70</sup> Increased Creatine (Cr) level is known to play an important role in regulation of cellular energy metabolism and can indicate gliosis <sup>71</sup>. Furthermore,

increased resonance intensity of Choline (Cho) indicates an altered turnover of cell membrane's steady state. Alteration in myo-inositol (m-Ins) concentration can indicate increased glial cell activity or changes in the inflammatory cells <sup>72</sup>.

Although existing MR protocols used in MS focus on changes in white matter lesions, it is evident that there is a disparity between lesion load and clinical disability <sup>73</sup> and current MR protocols have limited sensitivity in detecting changes in grey matter. This leaves neuroradiologists with the dilemma on how to best accurately evaluate pathological changes occurring across the entire MS brain <sup>74</sup>.

Several studies have used single-voxel spectroscopy (SVS) methods to evaluate spectroscopic changes of brain metabolites and their ratios in several ROIs including normal appearing white matter (NAWM) and (grey matter) GM, <sup>41, 42</sup> looking at whole brain NAA (WBNA) <sup>75</sup> at different fields strengths (1.5-3T) and echo times (TE) (20-70ms) <sup>76</sup>. These techniques have successfully collected data from a limited region of the brain, within acceptable acquisition times. The challenge for these methods is to be able to perform a metabolic mapping of the whole brain, with high spatial resolution and short TE in order to estimate neurochemical changes within larger brain regions in one session. The potential usefulness of these techniques in a clinical setting is also dependent on the acquisition time for the MRS or MRSI protocol. If the intention is to run these novel MR metrics in parallel to the standard MS MR protocols, acquisition times and quantification procedures need to be optimised to make this application feasible.

## **Scope of the review**

In this article, the underlying principles of MRS will be described and the different MRSI techniques will be compared, focussing on recent advances in high-speed MRSI methods. MS will be used as the example pathology in a clinical setting, where MRSI techniques are applied to map brain metabolic changes in different areas of the brain and at different disease stages to evaluate the potential use of the technique as a tool in disease diagnosis and clinical management.

## **2.2 Data Acquisition Techniques**

### **2.2.1 Single-voxel techniques**

In general, the spatial coverage of MRS falls into two categories, either localised SVS or multi-voxel MRSI <sup>77</sup>. The performance of these techniques is based on a slice-selective

excitation of RF pulses in variant forms, combined with magnetic-field gradients. The primary principle of SVS is that it sequentially excites three orthogonal slices, whose intersection defines the volume of interest (VOI). Then the generated echo signal is accumulated so that only the signal from the voxel, where all three slices intersect survives. To ensure signal fidelity, signal from outside the VOI can be eliminated by dephasing crusher gradients and phase cycling of RF pulses <sup>78</sup>. In SVS techniques, STEAM or PRESS are typically used to excite the VOI within the brain as a standard method of clinical imaging <sup>79</sup>. Figure 2-1 shows that single-voxel localisation methods collect signals from a rectangular region of interest (ROI). PRESS (Figure 2-1a) uses a double echo technique; where the procedure consists of an initial 90° RF pulse applied with an x-gradient to excite a slice followed by second and third 180° RF pulses applied with two other gradient pulses along y and z planes, respectively. Also, appropriate spoiler gradients along all gradient channels are used to dephase undesired coherence. In STEAM (Figure 2-1b) three 90° RF pulses are used in order to obtain the stimulated echo. Accompanying this operation, a large spoiler gradient pulse is employed to dephase other created signals during the mixing time (TM). A second 90° RF pulse is applied after half of TE from the first 90° RF pulse. In order to eliminate any undesired signals, spoiler gradients need to be carefully applied during TE on all gradient channels.

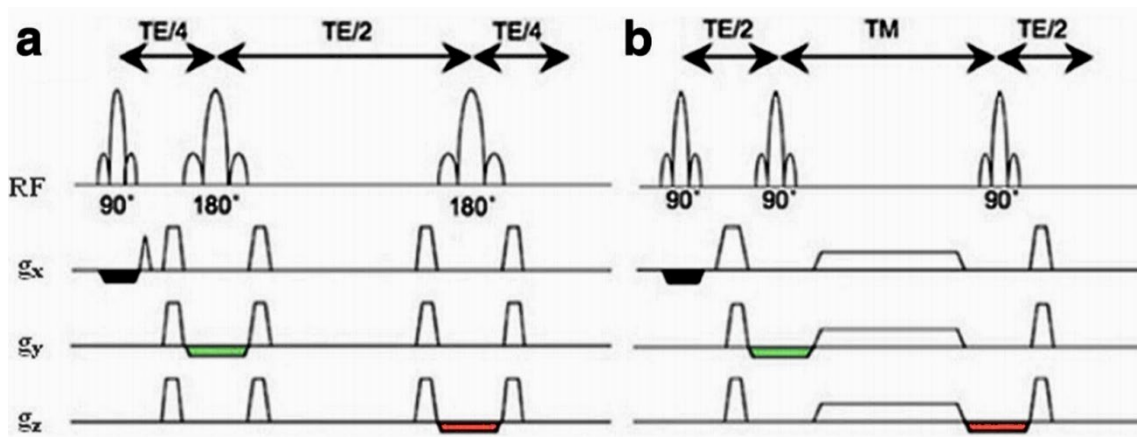


Figure 2-1. Two single-voxel localisation methods: (a) the PRESS sequence; (b) the STEAM sequence. Note that the three orthogonal slice-selective gradient pulses are indicated by black, green and red colours in the schematic representation. Reproduced with permission from <sup>80</sup>.

To determine which sequence is selected depends on the specialty that is required by an application. STEAM uses symmetric RF pulses and optimised gradient waveforms to minimise TE, so it is applicable to instances that require short TE values for the retention of metabolites with short T2. PRESS accommodates the requirements for studies that have a preference for longer TE and it comes with higher signal yield due to the 180° RF pulses used <sup>62, 81</sup>. PRESS

can still be used in cases where T2 is long and T2\* (T2 with static magnetic field (Bo) inhomogeneity contributions) is short. Figure 2-2 shows typical single-voxel spectra acquired on a 3T Prisma scanner (Siemens, Erlangen) at different TE value.

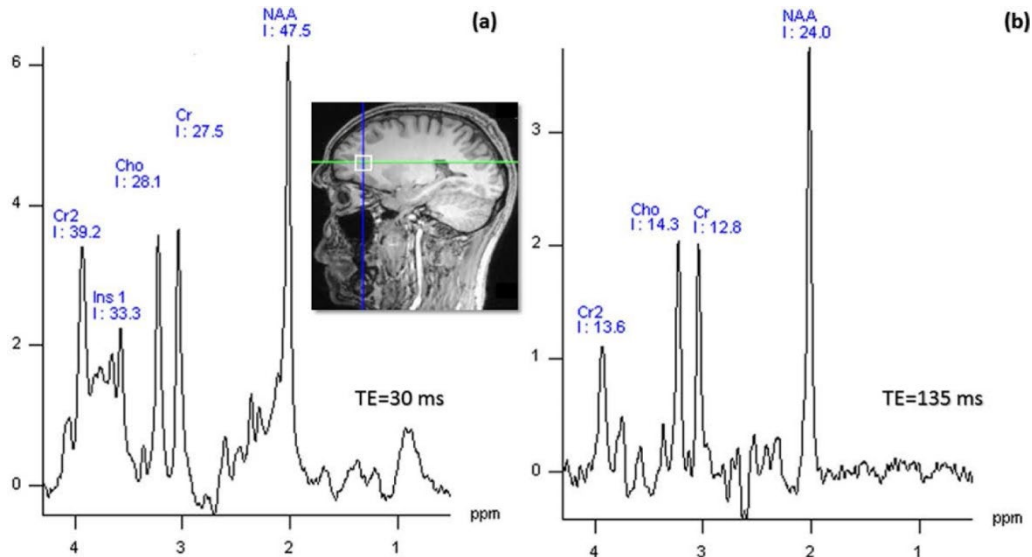


Figure 2-2. Signal obtained from prefrontal cortex (PFC) of voxel size ( $1.5\text{cm}^3$ ) from a healthy subject: (a) at short TE and (b) at long TE using PRESS approach on a 3T scanner (Prisma, Siemens, Erlangen).

## 2.2.2 Conventional multi-voxel techniques

Single-voxel techniques are invariably used in clinical settings, however, SVS techniques are restricted by their limited coverage and coarse spatial resolution. These constraints can be overcome by MRSI techniques<sup>65</sup>. For more global coverage, MRSI can also be extended to 3D-MRSI<sup>82-84</sup>.

The conventional 2D- and 3D-MRSI studies of the human brain, which are usually based on PRESS sequence, have numerous challenges which include long acquisition times, low SNR and extra-voxel contamination. Scan time is proportional to number of phase-encoding steps, repetition time (TR) and number of averages<sup>62, 80, 85</sup>. Although PRESS-MRSI was designed for routine scanners, the scan times were still too long for clinical applications especially in 3D mode<sup>86</sup>. In addition to long scanning time, the homogeneity of magnetic field becomes an important issue especially when PRESS-MRSI is used to map the whole brain. For the latter issue, for example, higher order shimming was developed to improve the field homogeneity for larger volumes<sup>87</sup>. Other MRSI techniques have been expanded upon in other studies<sup>85</sup>. Figure 2-3 shows an example of 2D PRESS-MRSI data at 3T<sup>80</sup>.

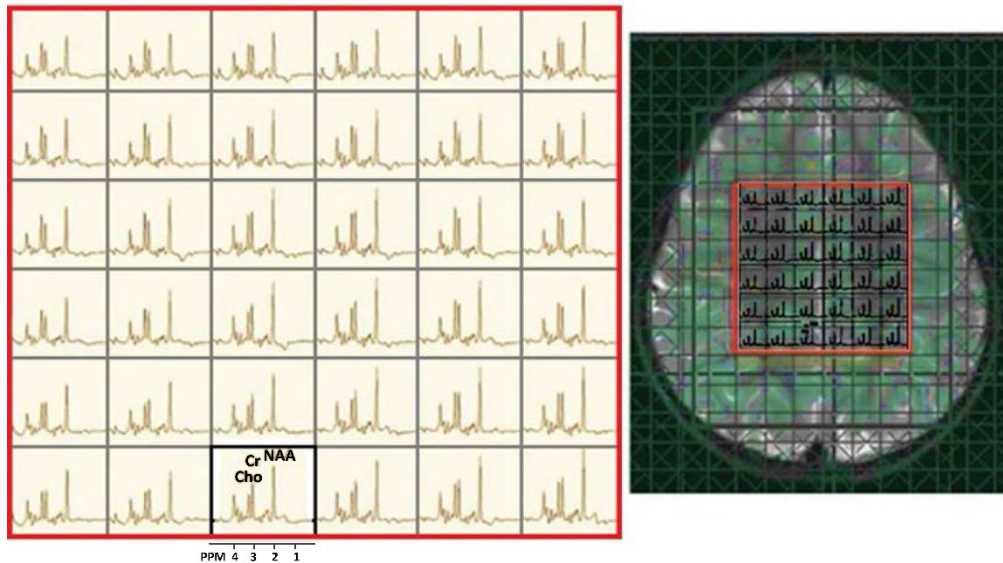


Figure 2-3. MRSI data acquired from a 3-year-old girl with an idiopathic developmental delay. Data was acquired using a 2D PRESS-MRSI at 3T (TE: 135ms) in the axial plane with voxel size of  $1.5\text{cm}^3$ . Reproduced with permission from <sup>80</sup>.

To overcome the above challenges, fast MRSI techniques were introduced as an improved alternative to facilitate implementation of this technique in the clinic, and to eliminate challenges associated with conventional MRSI techniques.

### 2.3 Parallel imaging

Parallel imaging techniques, such as sensitivity encoding (SENSE) <sup>88</sup>, simultaneous acquisition of spatial harmonics (SMASH) <sup>89</sup> and generalised auto-calibrating partial parallel acquisition (GRAPPA) <sup>90</sup>, have been introduced and commonly used to accelerate MRI techniques and can also be applied to improve the temporal performance of conventional MRSI <sup>91-93</sup>. In parallel imaging, signal sensitivity and spatial encoding can be improved by using multiple receiver coils, whereby the number of needed k-space lines decreases with considerable acceleration in the image acquisition.

For SENSE-MRSI, the principal balance between acceleration of spatial encoding and noise amplification is an essential requirement due to two factors; the reduced number of phase-encoding steps, and the acceleration factor (R). It has been proposed that low SNR can be improved in parallel imaging by increasing the number of coil elements <sup>94</sup>. For example, the performance of SENSE based 2D-MRSI can be improved using an 8-12 channel-coil <sup>93</sup>, and SENSE based 3D-MRSI using a 32 channel coils <sup>95</sup>. An important additional advantage of parallel imaging techniques is their compatibility with fast MRSI approaches discussed below.

Figure 2-4 shows an example of a SENSE-MRSI data with an acquisition time of only 3.37min

96

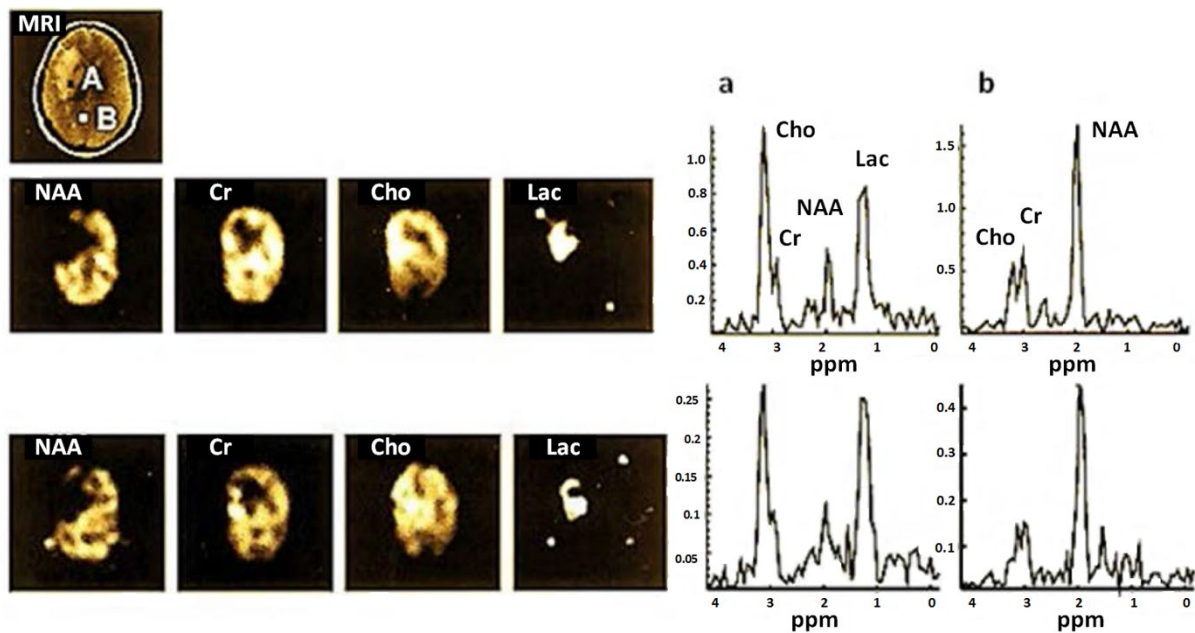


Figure 2-4. Illustrates the data spectroscopy and mapping of brain metabolite of conventional MRSI methods (top line) compared with SENSE-MRSI acquisition methods (bottom line) of (a) voxel in tumorous tissue and (b) healthy tissue; with an acquisition time of (14.02min) and (3.37min) respectively, and acquisition data parameter (TE/TR: 228/1500ms), slice thickness (20 mm) and FOV (220mm). Reproduced with permission from <sup>96</sup>.

## 2.4 Fast multi-voxel techniques

In order to study the whole brain, there must be a decrease in the scanning time to avoid motion sensitivity. MRSI methods can be accelerated using time-varying gradients during the readout of spectroscopic imaging data <sup>97-100</sup>. Efficient spatial and spectral k-space sampling with time-varying gradients is a mechanism that can be used to address time limitations. The majority of k-space trajectories that are widely used in spectroscopic imaging are echo-planar and spiral trajectories <sup>101-103</sup>. Recent developments in the gradients hardware design made it possible to traverse the k-space within a shorter period of time within each repetition <sup>104</sup>. For this reason, spiral imaging has shown to be useful in specific applications such as cardiovascular and functional brain imaging applications <sup>105</sup>.

A number of fast MRSI acquisition techniques designed to collect k-space data in three spatial dimensions have been reviewed elsewhere <sup>94, 106</sup>. Their main aim is not only to reduce

acquisition time but also to minimise voxel signal contamination and improve metabolite mapping of the whole brain <sup>107</sup>.

Many different strategies for fast MRSI have been used to gain high spatial resolution and to improve the time efficiency of MRSI experiments. The most common and effective of these approaches applied to the human brain are briefly described in this article.

### 2.4.1 Spiral MRSI

Spiral MRSI is a fast spectroscopic imaging technique that traverses k-space by spiral trajectories. Oscillating readout gradients are applied in a spectroscopic imaging sequence in two spatial dimensions during the data acquisition. These gradient waveforms ( $G_x$ ,  $G_y$ ) rapidly traverse spiral trajectories in two directions of k-space ( $k_x$ ,  $k_y$ ). These trajectories can be fully or partially covered within one TR as shown in Figure 2-5.

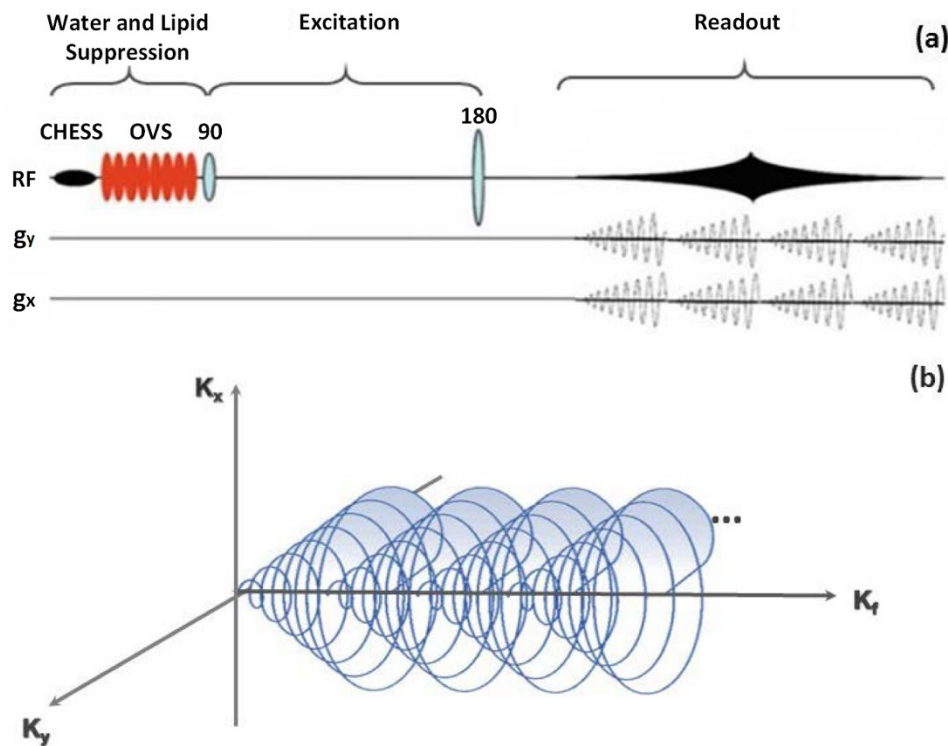


Figure 2-5. (a) In a spiral MRSI, two time-varying readout gradients are administered in the data acquisition period with oscillating spiral trajectories. (b) Outlines the projection of a k-space trajectory along the  $k_f$  axis. The spiral trajectories originate from the  $(k_x, k_y)$  plane and repeatedly run a path through the  $k_x$ ,  $k_y$ ,  $k_f$  spaces with multiple and simultaneous spiral trajectories increasing volumetric acquisition around the  $k_f$  axis. Reproduced with permission from <sup>80, 102</sup>.

Due to this ability, a sequence with spiral trajectory has a much quicker acquisition time compared to conventional MRSI methods<sup>104</sup>. This single-shot spiral-imaging technique sets a remarkable new standard for fast spectroscopic imaging.

Spiral MRSI was originally introduced by Adalsteinsson et al.<sup>102</sup> to evaluate the neurochemical change of metabolites in GM in patients with SPMS<sup>58</sup>. However, this technique has limitations in certain clinical applications (i.e. increased blurring and hardware limitation), and thus never became a widely used tool despite its advantages.

Data sampled in spiral spectroscopic imaging sequences are usually non-uniform, and thus acquired data has to be re-gridded to reconstruct the data onto a Cartesian k-space, where Fourier transformation can be applied<sup>103, 105</sup>. Due to the data collection being completely symmetric and sampled around the centre of k-space, several artefacts that are influenced by external variables such as motion or other instabilities are reduced<sup>108</sup>. As a result, spiral MRSI offers shorter imaging time, higher spatial resolution, improved point spread function (PSF) and SNR.

Spiral spectroscopic imaging can be readily and effectively combined with other imaging-based techniques such as parallel imaging methods leading to Mayer et al. proposing their accelerated version of this technique for human brain at 3T<sup>109</sup>.

Recent work focussed on improving localisation and spectral quality of spiral MRSI<sup>110-112</sup>. These developments will have significant clinical impact on the study of human brain. Despite spiral MRSI having several 'theoretical' benefits, its major drawback is the high strain on gradient hardware as a result of its demanding trajectory design<sup>104</sup>. An example of the clinical application of the spiral MRSI at 3T, with a data-acquisition time of 13.5 minutes is shown in Figure 2-6.

SENSE-based spiral MRSI<sup>109</sup> has been applied to address the challenges associated with clinical application, for example volumetric coverage and evaluation of the neurochemical change of the whole human brain<sup>113</sup>.

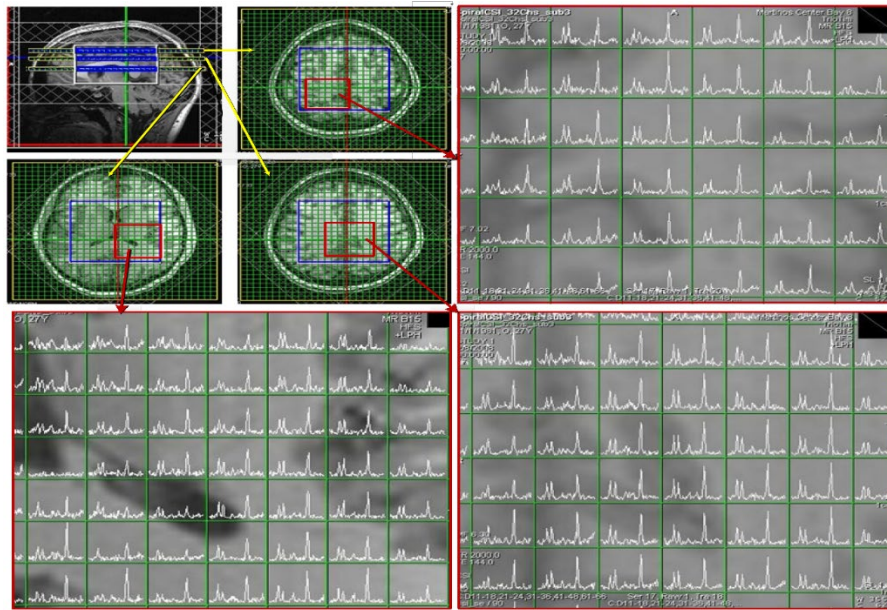


Figure 2-6. Displays the spectral data from three slices using a spiral MRSI technique at 3T (TE/TR: 144ms/2s, FOV: 8x9x6cm) using a 32-channel phased array head coil. Reproduced with permission from <sup>104</sup>.

#### 2.4.2 Turbo spectroscopic imaging (turbo-MRSI)

MRSI can also be accelerated by multiple-echo refocussing which is analogous to turbo-spin-echo imaging as seen in Figure 2-7. Determining the efficiency of this data collection strategy is largely dependent on rapid acquisition time and spatial resolution without signal loss of brain metabolites <sup>114</sup>. Turbo-MRSI techniques have proven successful in the past in detecting major brain metabolites such as NAA, Cho and Cr within an acceptable acquisition duration at 1.5T <sup>115</sup>. Stengel et al. has succeeded in reducing the acquisition time to 6 minutes by using turbo-MRSI with four phase encodes per TR to study stroke patients <sup>116</sup>.

Even though turbo-MRSI techniques have successfully mapped and assessed uncoupled brain metabolite distributions with long TE, mapping of coupled resonance metabolites (e.g. glutamine+glutamate (Glx)) proved to be a challenge. Fortunately, Yahya et al. <sup>117</sup> proposed modifications that allow the quantitation of Glx at TE of 100ms and 170ms in addition to halving acquisition time.

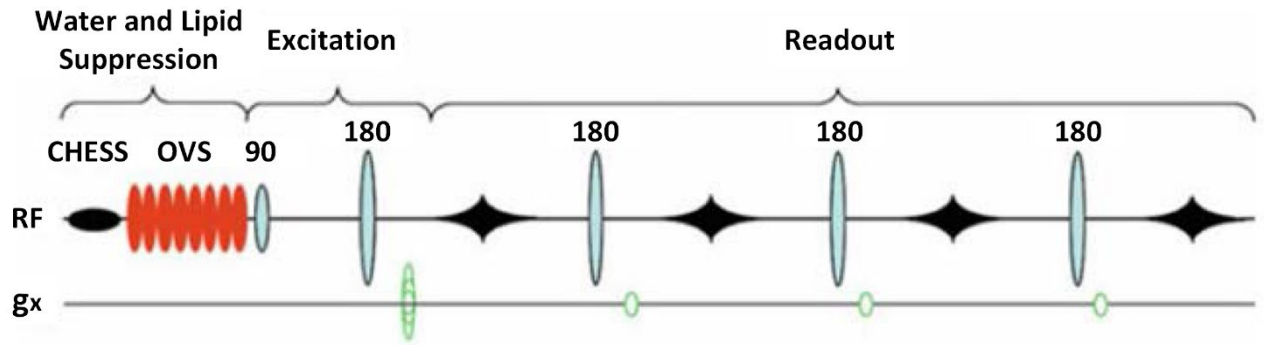


Figure 2-7. Readout strategy for Turbo-MRSI sequence using spin-echo imaging per excitation preceded by water and lipid suppression (CHESS and outer-volume suppression (OVS)). Reproduced with permission from <sup>80</sup>.

Turbo-MRSI can be combined with parallel imaging techniques such as SENSE to improve acquisition rate to obtain higher resolution (high sensitivity). Dydak et al. was able to design a turbo-SENSE-MRSI sequence that uses an echo train length of four to acquire spectroscopic data within two to three minutes and reduced acquisition times by about eight folds compared to conventional MRSI techniques <sup>96</sup>.

Due to combining multiple-echo MRSI methods with parallel imaging techniques, high a spatial resolutions MRSI has become clinically feasible. Many challenging clinical applications have been achieved through the use of the turbo-SENSE-MRSI technique <sup>118</sup> involving high spatial encoding train (i.e. long multiple-echoes train) which is only feasible at 3T. For instance, acquisition times are significantly reduced (~1 min) to obtain brain metabolites ratios Cho/NAA and Cr/NAA with a TE of 144ms, even though SNR is reduced because of the longer echo train. In addition to these clinical successes, turbo-MRSI techniques <sup>119</sup> have made it possible to evaluate brain metabolite levels within the pons, accumulating spectroscopic data within very short periods of time (1min 20sec) using long TE (288ms) at 1.5T.

The advent of the turbo-MRSI technique has made faster data acquisition possible, although with a major drawback of lowering spectral resolution, due to the short time between consecutive refocusing pulses <sup>116, 119</sup>. The second disadvantage is the drop in SNR as a consequence of the increase in spatial encoding trains of more than two, as the spatial encoding maintains a balance between the output of acquisition scan time and SNR <sup>96, 118</sup>.

### 2.4.3 Echo-planar spectroscopic imaging (EPSI)

The introduction of echo-planar imaging (EPI) originally proposed by Mansfield<sup>120</sup> has facilitated the development of EPSI on conventional clinical MRI scanners. The latter technique made the mapping of spatial metabolite distributions in the brain possible, accelerating spectral data acquisition compared to conventional MRSI, therefore creating an exceptionally fast imaging technique. New improvements to the readout frame of EPI techniques meant that an oscillating readout gradient can be reproducibly used in EPSI. EPSI encoding method that uses multiple-slice or PRESS excitation in 2D or 3D-MRSI<sup>121, 122</sup> has become the method of choice. These improvements have led to the advent of EPSI to change how MRSI is applied in the clinical setting.

In the last decade, EPSI was widely used to acquire MRSI data in a shorter scanning time by encoding spatial and spectral dimensions in a single readout gradient (Figure 2-8a). This fact is based on rapid k-space sampling per excitation that allows planar data collection on rectilinear trajectories (Figure 2-8b).

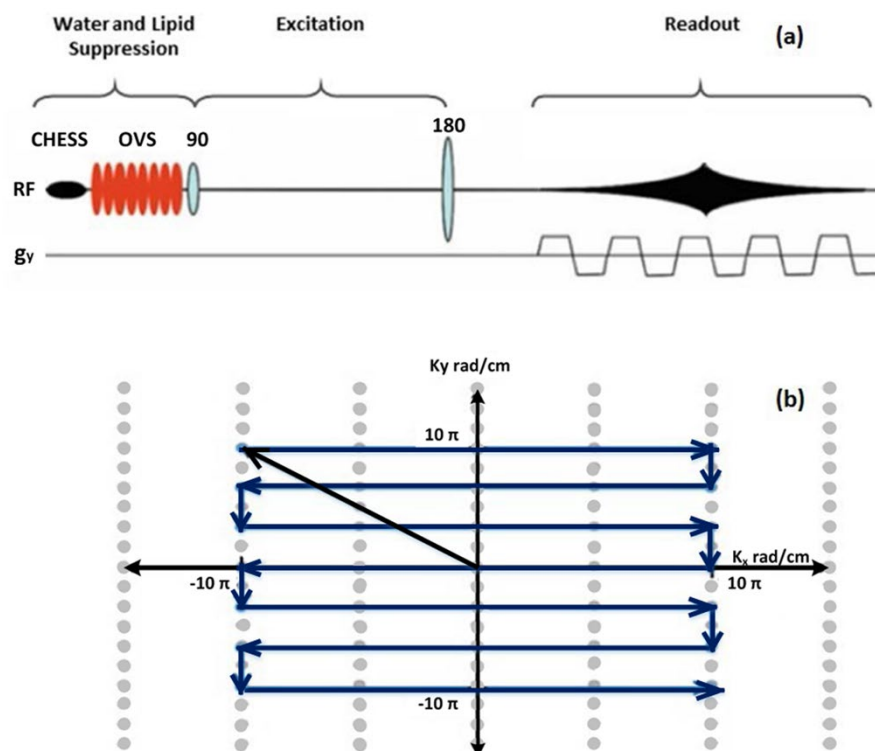


Figure 2-8. (a) EPSI sequences are applied to encode localised spectra with a single readout gradient. (b) k-space trajectories of echo-planar spectroscopic imaging indicate data acquisition in one TR of the pulse sequence during spectral encoding. Reproduced with permission from 80.

Echo-planar encoding has proved particularly useful in H-MRSI applications. Its application has improved performance in covering large volumes due to its improved spatial and temporal resolution, compared to typical conventional phase encoded MRSI.

The spectroscopic images for distribution of the major metabolites in the human brain were first obtained with 3D-EPSI technique by Posse et al. <sup>121</sup> and later with fully automated analysis by Ebel et al. <sup>122</sup>. A comparison between EPSI and conventional MRSI spectra indicate a similarity in SNR per unit volume and unit time <sup>106, 123</sup>. However, an outstanding feature of the two-dimensional EPSI method <sup>101</sup> is the improvement of spatial resolution and SNR for a number of metabolites at short TE (13ms) and acquisition time (64s). In addition to evaluating and detecting the three major metabolite maps (NAA, Cho, Cr), 2D-EPSI was also applied to measure the changes in brain lactate at long TE (272ms) and 1.5Tesla <sup>124</sup>.

3D-EPSI was implemented by Maudsley et al. <sup>125</sup> in mapping the distributions of the three major metabolites (NAA, Cho, Cr) over a wide region of the human brain at intermediate TE (70ms) where metabolite ratios and average metabolite values in GM and white matter (WM) were clinically determined on a 3T MRI scanner. MRSI data processing was carried out by a fully automated processing approach (Metabolite Imaging and Data Analysis System (MIDAS)) <sup>126</sup>. Metabolite maps obtained from volumetric EPSI technique with an acquisition time of 26 min are shown in Figure 2-9.



Figure 2-9. Whole brain mapping and a spectrum of major metabolites, mean water-reference spectroscopic imaging (SI H<sub>2</sub>O Reference) using EPSI at 3T from a healthy subject (TE/TR=70/1710ms), total acquisition time (26 min), k-space points (50x50x18), FOV (28x28x18cm<sup>3</sup>) and voxel volume (0.31cm<sup>3</sup>). Reproduced with permission from <sup>94</sup>.

New EPSI methods were developed where the quantity of k-space lines is reduced. When 2D-spatial selective RF (2DRF) are incorporated within EPSI sequences, a new type of 2DRF-EPSI is obtained <sup>127</sup>. 2DRF-EPSI addresses the poor image quality that results from artefacts and low spatial resolution, by shortening echo-train length, and doubling the spatial resolution along the direction of phase-encoding.

The implementation of EPSI techniques at high field (3 to 7T) has enabled not only to linearly gain SNR per unit volume and time but has also allowed for the evaluation of J-coupled metabolites such as glutamate (Glu) and glutamine (Gln) <sup>94</sup>. 3D-EPSI was successfully applied to assess the concentrations of major metabolites, including J-coupled, at 4T and 3T in GM and WM <sup>99</sup> of healthy volunteers. This is an important development as it has greatly increased the spectral resolution and SNR associated with shortened experimental time (<10min) and has thus sparked interest in clinical studies of MS and stroke for the potential benefits of this methodology <sup>99</sup>.

Short TE EPSI was recently introduced by Ding et al. <sup>128</sup> to evaluate the neurochemical variation of major metabolites as well as Glx and m-Ins in conjunction with parallel imaging acquisition. NAA, tCr, Cho, Glx and m-Ins were found to have different mapping concentrations in WM and GM in comparison with other short TE (15ms) studies <sup>95</sup>. Mapping of whole brain metabolites was also achieved by the implementation of 3D-EPSI at short TE

(20ms)<sup>129</sup>. An improvement in short TE EPSI applications with high spatial resolution and improved SNR by increasing spatial sensitivity using multiple coils<sup>130, 131</sup>.

The significant development of advanced gradient hardware has resulted in the emergence of a new EPSI method that focuses on high spatial resolutions with a large coverage of the human brain at 3T. The flyback 3D-EPSI technique<sup>86</sup> was presented to improve the spatial resolution and SNR for different metabolites (NAA, Cr, Cho and lactate). Zierhut et al. employed flyback EPSI for a detailed analysis of the data from a human glioma patient with an acquisition time of less than 9.5min, with a spatial resolution of 1cc<sup>86</sup>.

The developments in whole brain coverage have shown that the efficiency of spatial and spectral encoding can be improved by applying volumetric EPSI techniques. However, these improvements are still limited by long acquisition times, which are considered to be a crucial factor in many clinical studies<sup>47</sup>. The first modification to enhance the acceleration of data collection was the use of SENSE-EPSI. This strategy combined the spatial and spectral encoding capabilities and has been investigated by Lin et al.<sup>132</sup> to obtain major brain metabolites maps. In this particular study, the data acquisition time was halved to 32s for 32×32 image matrix with high spatial-temporal resolution, using SENSE acceleration factor of two. However, SNR declines with faster acceleration, which can affect the usefulness of these techniques clinically. 3D-EPSI and 2D-SENSE<sup>95</sup> are combined to acquire higher spatial resolution data that covers the whole brain in a shorter acquisition time (1min) for 32×32×8 spatial matrix and TE (15ms) at high field (3T).

Another method that can be used to map metabolite distribution in the whole brain is the 3D GRAPPA-EPSI techniques<sup>133</sup>. The spectral quality, brain metabolite concentrations and SNR values from 3D GRAPPA-EPSI were obtained with an acceleration factor of 1.5 which shows similar results to the 3D-EPSI technique<sup>133</sup>. Reduction of SNR has become a major challenge for implementing 2D GRAPPA-EPSI<sup>134</sup> techniques with a 32 channel coil array<sup>99</sup>, which improves SNR values due to the large numbers of small sized coils<sup>135</sup>. In addition to this, 2D GRAPPA-EPSI allows for the mapping of most metabolites within a much shorter time.

Dydak et al. incorporated the MEscher-GARwood (MEGA) editing scheme<sup>136</sup> within the EPSI technique<sup>137, 138</sup> for mapping of the main inhibitory neurotransmitter  $\gamma$ -aminobutyric acid (GABA) levels. The MEGA-EPSI method can perform data acquisition of GABA level activity

in less than 10 minutes in a 2D slice. The short acquisition time and high sensitivity of the 2D MEGA-EPSI lead to the creation of 3D MEGA-EPSI technique due to its increased spatial resolution with an acquisition times of 17 minutes for eight slices at 3T, which is a major improvement compared to other techniques <sup>139</sup>.

Recently, image quality and brain metabolites concentrations have been studied by applying a commonly reduced k-space strategy at 3T. For this purpose, the GRAPPA-EPSI technique was introduced by Sabati et al. <sup>130</sup> to improve the spectral quality associated with accelerated acquisition of volumetric EPSI data. This has resulted in an experimental time of 16 minutes at the expense of SNR values <sup>86</sup>. The results obtained from 3D-EPSI techniques are compared to the GRAPPA-EPSI technique in Figure 2-10.

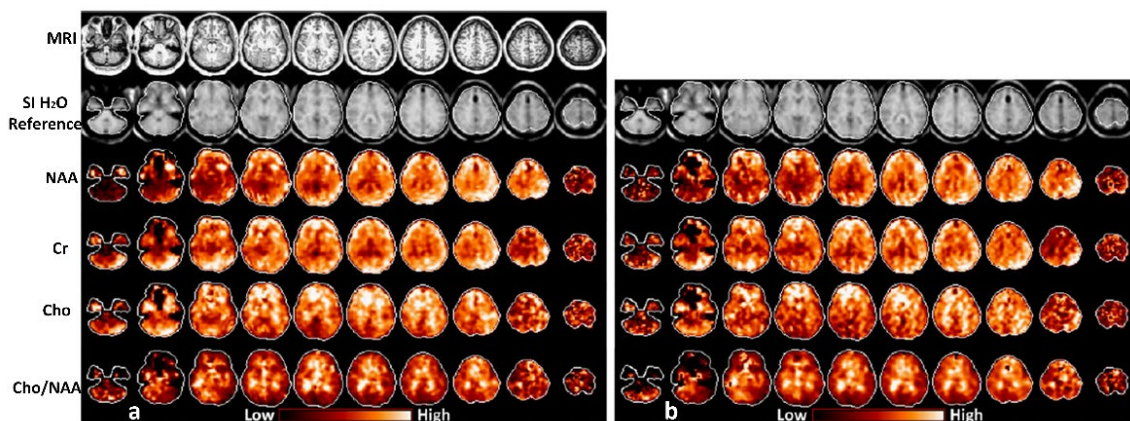


Figure 2-10. Illustrates the comparison between two fast MRSI sequences at 3T: (a) the 3D-EPSI and (b) GRAPPA-EPSI sequences, to show the whole brain mapping of metabolites with interleaved water reference acquisition (SI H<sub>2</sub>O Reference) from a healthy normal subject at intermediate TE (70ms). Reproduced with permission from <sup>130</sup>.

A further benefit to the EPSI technique is its flexibility to adapt to a wide range of techniques to improve speed of data collection in certain specialised areas across a wide-range of MRSI and MRI techniques, including: Flyback, GRAPPA, and SENSE in 2D and 3D modes that would otherwise be relying on slow conventional MRSI methods.

Some disadvantages regarding EPSI need to be mentioned. The speed of data collection is the root cause for EPSI's major technical problems with the gradient system, especially when recording data with disequilibrium of positive and negative gradient lobes <sup>85</sup>. This leads to further contraction of spectral bandwidth which poses a problem considering EPSI has less SNR than traditional phase-encoded MRSI. Therefore, multiple averages are required to improve SNR. Regardless, when the above challenges are suitably addressed, EPSI can be considered one of the best techniques for whole brain 3D-MRSI <sup>122</sup>.

## 2.5 Comparison of MRSI techniques

Advances on MRSI techniques have focussed on either improving the temporal resolution or investigating the relationship between spatial resolution and SNR. To achieve these aims, work has been carried out to improve the MRSI techniques and increase spatial coverage e.g. 2D-3D MRSI.

Detecting various brain metabolites *in-vivo*, using different parameters for 3D PRESS-MRSI<sup>83, 86</sup> showed variable NAA concentrations in different acquisitions at 3T. Recently, the 3D PRESS-MRSI has been improved by using 4 slices in PRESS box and outer volume suppression pulses to cover the whole brain with an acquisition time of 9 minutes, leading to spectral data of NAA, Cho and Cr<sup>84</sup>. Multiple 2D-MRSI has significant improvements for spatial resolution, SNR and whole brain metabolite mapping at long TE<sup>140</sup>.

A summary of the results of various MRSI methods are shown in Table 2-1. Data shown represents measured metabolites from HCs using PRESS-MRSI with different parameters.

Table 2-1. Brain metabolite concentration and acquisition time of various MRSI techniques.

Methods	TE/TR (ms)	Metabolite(mM)	Tacq (min)*	Brain region/ FOV/ voxel size/B <sub>0</sub> (Tesla)	Ref.
3D PRESS-MRSI	144/1100	NAA: 10.1±0.64	21.12	Centre of brain/ 12x12x8 cm <sup>3</sup> /1 cm <sup>3</sup> /3T	86
3D PRESS-MRSI	144/1100	NAA: 6.9±1.3, Cho: 6.5±1.4 Cr: 6.1±1.2	17	Not reported/ 12x12x8 and 16x16x8 cm <sup>3</sup> /1 cm <sup>3</sup> /3T	83
3D PRESS-MRSI	144/1100	Cho/NAA:(0.51-0.54)	21.12	Not reported/ 12x12x8 cm <sup>3</sup> / 1 cm <sup>3</sup> /3T	92
Multiple 2D-MRSI	144/ 2300	NAA:2.5±4.47, Cho:2.94±9.71, Cr:7.3±4.09	26	Whole brain scans/ Not reported	140
2D-MRSI	135/1500	MS patients: NAA:9.48±0.73  Controls: NAA:11.58±0.37	NR**	WM and GM/ 16x16 cm <sup>2</sup> / 2 cm <sup>3</sup> /1.5T	141

3D PRESS-MRSI with OVS	144/1500	Cho/Cr :1.24 NAA/Cr:1.94	9	Whole brain/ 16x16x16, 18x18x16 cm <sup>3</sup> /1 cm <sup>3</sup> /3T	84
---------------------------	----------	-----------------------------	---	---	----

\*Tacq: acquisition time.

\*\*NR: Not reported.

Improvements in spatial coverage and temporal resolution have been achieved by using novel MRSI techniques as shown in Table 2-2. High speed EPSI was used at short TE (15 ms) to find out that in HCs Glu (12.8±1.5 mM) in GM is of a significantly higher concentration than in WM (7.0±1.1 mM) and also higher than other brain metabolites like NAA (8.6±0.7 mM) and m-Ins (6.3±0.7 mM) in GM in HCs<sup>99</sup>. These improvements in temporal resolution due to GRAPPA enabled by higher number of coil elements (32 channel)<sup>134</sup> make this technique suitable for clinical studies with acceptable acquisition times. Whole brain has also been studied by using EPSI techniques at short TE (17.6ms) to measure the brain metabolites in both GM and WM of brain. The results showed that the value of NAA concentration is higher in the parietal lobes in GM (12.05±0.47 mM) than in WM (8.74±0.34 mM)<sup>128</sup>.

Whole brain was also studied by GRAPPA-EPSI short TE technique, where NAA (15.36±2.62), m-Ins (6.11±1.14), tCr (11.97±1.67) and Glx (18.40±3.19) mM were found to be more abundant in GM than WM<sup>134</sup>. In addition, GRAPPA-EPSI sequence at TE of 70ms<sup>130</sup> found that WM NAA concentration (595±37.9) to be higher than Cr (346±23.9) and Cho (100±9.7) in institutional units (IU) for HCs. A summary of fast MRSI studies in human brain and their results are shown in Table 2-2.

Table 2-2. Brain metabolite concentrations obtained in fast MRSI techniques.

Methods	TE/TR (ms)	Metabolite (mM)	Tacq (min)	Brain region/ FOV/ voxel size/ Cohort/ Bo(Tesla)	Ref
EPSI	18/1550	GM in frontal lobe left: NAA:11.10±0.32, tCho:2.04±0.16, Glx:10.22±0.53 WM in frontal lobe left: NAA:9.51±0.27, tCho:1.95±0.16, Glx:6.43±0.34	16	whole brain/ 28x28x18 cm <sup>3</sup> /1 cm <sup>3</sup> / 20 HCs/ 3T	128
EPSI with OVS	15/2000	GM: NAA: 8.6±0.7, Glu:12.8±1.5, tCho:1.4±0.2.	8.5	WM and GM/ 26 cm/ 1 cm <sup>3</sup> / 9 HCs/ 3T	99

		WM:NAA:7.2±0.7, Glu:7.0±1.1, tCho:1.4±0.2			
3D GRAPPA-EPSI	70/1710	*NAA: 595±37.9, Cr: 346±23.9 Cho: 100±9.7	16	Whole brain/ 28x28x18 cm <sup>3</sup> / 0.31 cm <sup>3</sup> / 25 patients with mild traumatic brain injuries(mTBI) & 25 HCs/ 3T	130
GRAPPA-EPSI	15/2000	GM: NAA:15.36±2.62, Glx:18.40±3.19, Cho:3.19±0.58 WM: NAA: 14.46±1.79, Glx: 11.01±3.20, Cho:3.19±0.45	1.5	WM and GM/ 24 cm/ 0.85 cm <sup>3</sup> / 5 HCs/ 3T	134
3D SENSE-EPSI	15/2000	NAA:9.5±4.3, Cho:1.4±0.9, Glu:8.8±5.2, Cr:7.2±2.8	8.5	WM and GM/ 24x24x10 cm/ 0.7 cm <sup>3</sup> / HCs/ 3T	95
3D EPSI-MRSI	70/1710	**GM: NAA:4948±75, Cr: 3461±53, Cho: 544±13 in Occipital WM:NAA:5165±81, Cr: 3048±48, Cho: 671±12 in Occipital	NA	WM and GM/ 28x28x18 cm <sup>3</sup> / 0.31 cm <sup>3</sup> / 88 HCs/ 3T	125
3D PRESS-MRSI	144/1500	Concentration for age groups(25-32 ) NAA/Cr:1.8 in Frontal lobe NAA/Cr : 1.9 in Occipital lobe	13	Whole brain/ 32 cm /1 cm <sup>3</sup> / 8 HCs/ 1.5T	107

\*Mean metabolite concentrations averaged over all voxels of WM brain tissue in parietal lobe.

\*\*Average metabolite values in IU.

## 2.6 MRSI in Multiple Sclerosis

MRSI was applied to MS patients at 1.5T with long TE values <sup>142-145</sup> and at 2T with short TE values <sup>146</sup>. Some studies focussed on lesions compared to NAWM and GM <sup>68</sup>. Other studies compared distinct different clinical groups such as RRMS <sup>46, 147</sup>, SPMS and PPMS <sup>148, 149</sup>.

Conventional MRSI techniques have identified changes in metabolite concentration in limited regions within NAWM or GM affected by the disease process <sup>45, 150, 151</sup>. For this purpose, Tiberio et al. used 3D PRESS-MRSI at TE of 30ms and 1.5T. Statistically significant metabolic differences between RRMS patients and HCs were found in NAWM total NAA and cortical grey matter (CGM) Glx and Cho <sup>45</sup>. This technique was also used at TE of 40ms and 3T by Ratiney et al. <sup>152</sup> to investigate m-Ins concentration level in normal appearing white and grey matter (NAGM). m-Ins concentration was significantly increased in both NAWM and NAGM of MS patients compared to control subjects. Changes in the above metabolites have been associated with clinical impairment and/or neuronal dysfunction in MS patients.

In another study, RRMS patients and age-matched controls were recruited to investigate abnormal metabolic changes in GM and WM by using conventional 3D-MRSI techniques at 3T<sup>46</sup>. With an MRSI scan lasting 34min, it was found that the concentrations of Cr, Cho and m-Ins in WM of RRMS group were higher ( $p \leq 0.01$ ) compared to controls and WM NAA was lower ( $p = 0.07$ ). NAA reduction reflects neuronal and glial loss or impairment at early stage of RRMS, whereas brain inflammation leads to increase of m-Ins and Cr concentration levels due to intense gliosis. Additionally, increase in Cho levels is usually associated with abnormal membrane turnover from myelin breakdown.

Suhy et al.<sup>149</sup> found that NAA was reduced in RRMS and PPMS from NAWM compared to HCs WM. Similarly, the normalized value of brain metabolites in NAWM of RRMS and PPMS patients shows that there is a significant decrease in NAA/Cr ratio ( $p = 0.027$ ). These results were achieved by applying a 2D PRESS-MRSI at long TE (135ms) at 1.5T in RRMS and PPMS groups. However, by applying a 2D PRESS-MRSI at TE (135ms) at 3T no statistically significant difference of absolute concentrations of Cr, NAA and NAA/Cr ratio was found in NAWM between RRMS vs control group<sup>43</sup>, but significant reduction was found for NAA/Cr ( $p < 0.0003$  and  $p < 0.001$ ) in SPMS compared to RRMS and control groups. The above work suggested reduction in NAA and NAA/Cr as potential indicators for irreversible damage in MS. NAA Reduction is usually associated with neuroaxonal injury. Astrocytic proliferation reflects increased levels of Cr. NAA and NAA/Cr are constantly reported with lower level values from NAWM and lesion of MS patients. Recently, Khan et al. showed that tNAA/tCr ( $1.88 \pm 0.19$  mM,  $p < 0.05$ ) has strong and statistically significant inverse correlation with total disability score in a group of 39 RRMS patients<sup>153</sup>.

Spectroscopic data from early RRMS in NAWM, CGM and lesions have been reported by Kapeller et al.<sup>38</sup>. This study focussed primarily on quantifying the concentration of the NAA, Cr and m-Ins using PRESS-MRSI technique at short TE (30ms). Lower NAA concentration ( $p < 0.01$ ) was found in RRMS in CGM and NAWM compared to controls. Shorter TE is more sensitive to coupled metabolites than longer TE spectroscopy.

A PPMS group was studied by Sijens et al. at long TE (135ms) by using 2D PRESS-MRSI<sup>141</sup>. Results from the brain metabolic maps from PPMS patients confirmed that Cr levels were elevated, whereas NAA and Cho concentrations were decreased in WM more than in GM in PPMS compared with controls. The bigger decrease of NAA and Cho in WM is expected as a

result of the larger presence of myelin in WM than in GM <sup>141</sup>. Figure 2-11 depicts brain sample spectral data from PPMS patients and controls in GM and WM <sup>141</sup>.

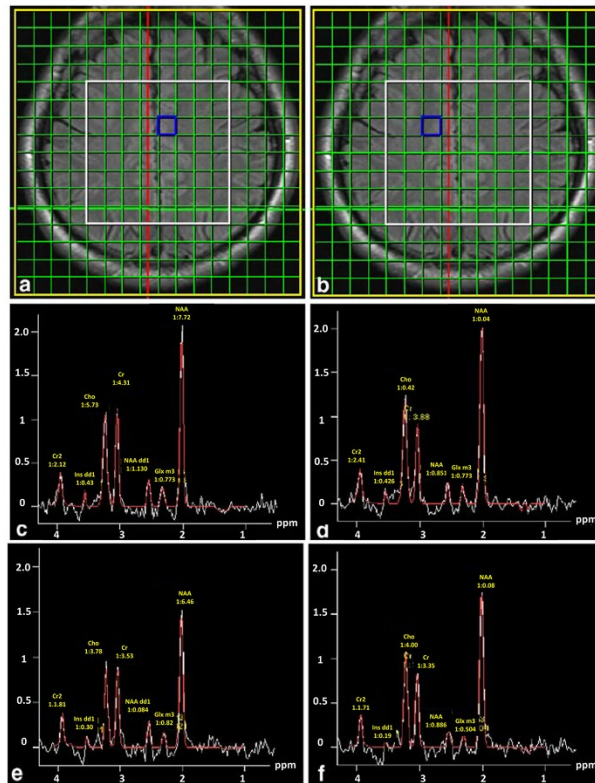


Figure 2-11. Shows the spectra of voxels in (a) GM and (b) WM of healthy and PPMS subjects: (c, d) acquired from healthy subject in GM and WM, respectively and (e, f): acquired from GM and WM regions of a PPMS patient, respectively. Experimental parameters: TE/TR=135ms/1500ms, FOV (16x16cm<sup>2</sup>, yellow border) and VOI(8x8x2cm<sup>3</sup>, white border). Reproduced with permission from <sup>141</sup>.

Recently, *in-vivo* proton MRSI technique at long TE (135ms) and 3T has been reported by Rahimian et al. <sup>44</sup> not only to measure brain metabolite concentration of NAA, Cho and Cr, NAA/Cr and NAA/Cho in RRMS and PPMS groups but also to differentiate between MS subtypes. Comparing the results obtained shows that there was a significant increase in Cr concentration in non-enhancing lesions of RRMS patients compared to the PPMS patients (p=0.008) whilst the concentration of NAA/Cr was significantly reduced (p=0.03) in PPMS compared with RRMS. However, there was no statistically significant difference in concentrations of Cho, NAA and NAA/Cho between the two groups.

EPSI allowed detection of neuro-metabolites in the visual tract WM of MS patients <sup>59</sup>. In this study, EPSI was used to study neurochemical changes at 1.5T associated with visually evoked potential (VEP) abnormalities. It was found that the average value of NAA is

significantly lower ( $p \leq 0.05$ ) in the abnormal VEP group than in the normal VEP group. 3D-MRSI was implemented using EPSI techniques at 1.5T<sup>49</sup> to measure the major metabolite ratios in control and MS cohorts from two ROIs: supratentorial brain and central brain. This study was performed at long TE (144ms) on three subtypes of MS: RRMS, PPMS and SPMS, where it was found that NAA/Cr ratio was significantly decreased ( $p < 0.01$ ) for all MS cohorts compared to HCs in both ROI. Sample spectroscopic data from SPMS patients are shown in Figure 2-12.

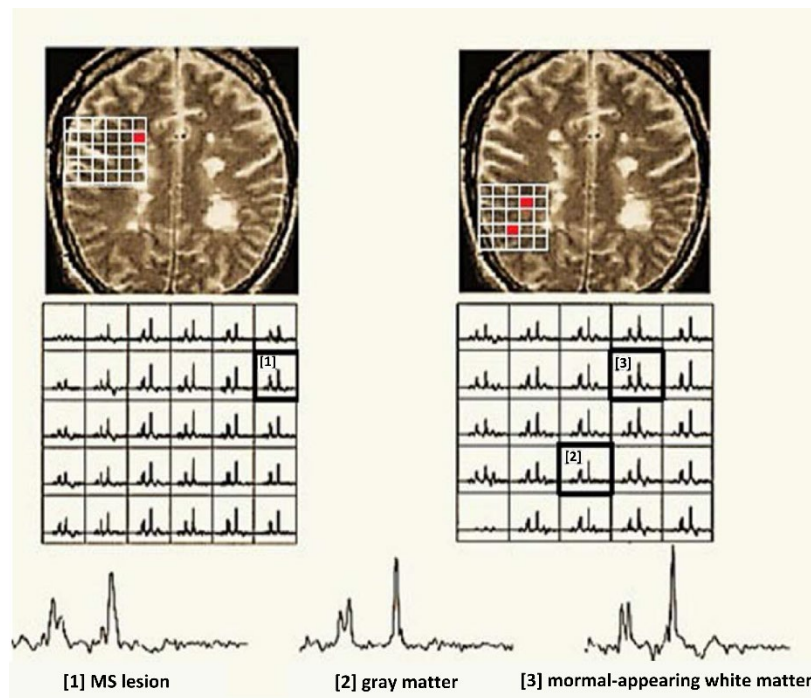


Figure 2-12. Spectroscopic data from a typical SPMS brain from three separate regions: [1] MS lesion, [2] CGM and [3] NAWM. The voxels are represented by the numbers and red spots. Experimental parameters: 3D-EPSI (TE/TR=144/2000ms), acquisition time (20min), FOV (24x24x8 cm<sup>3</sup>) and slice thickness (4mm) at 1.5T. Reproduced with permission from<sup>49</sup>.

The multi-slice EPSI technique was introduced by Mathiesen et al.<sup>47</sup> as a response to the limitations of VOI in conventional MRS techniques. The introduction of this technique made it possible to measure brain metabolites in specific regions such as MS lesions, NAWM, CGM and to estimate WB (whole brain) NAA which is generally considered an indicator of disease progression and treatment efficiency. Decreases in global ratios (NAA/Cr and Cho/Cr) were noticed for early MS patients compared with healthy subjects, however, no statistically significant differences were noticed in NAA/Cr between these two groups<sup>47</sup>.

Due to the capabilities of multi-slice EPSI technique to cover larger regions of the brain, it has been employed to evaluate the global brain NAA/Cr ratio, which might be a good indicator

for progression and cognitive decline in MS<sup>50</sup>. Thus, measuring NAA/Cr ratio in WM and GM within scan times of 20min and TE of 144ms, provided multi-slice EPSI a particular clinical utility. Similarly, reduction of NAA in GM of RRMS and SPMS groups was demonstrated by using a volumetric spiral MRSI technique<sup>58</sup> at a low static field of 1.5T. A study by De Stefano et al. confirmed that brain MR spectroscopic data has a significant role in detecting neuroaxonal damage caused by MS disease with decreased NAA/Cr ratio<sup>154</sup> due to the consistent finding of decrease NAA signal being linked to axonal damage. Moreover, acute lesions were found to have high Glu levels; which might suggest a connection between the axonal injury in active lesions and Glu excitotoxicity<sup>154</sup>. Donadieu et al. used fast 3D-EPSI (TE: 20ms) at 3T to acquire spectral maps of the complete brain of MS patients (N=19) and compared them to age and gender matched HCs<sup>155</sup>. Their findings indicated a reduction in NAA and Glx (-15% and -20%) in GM, while m-Ins was increased in WM of the MS group (+22%). A summary of the results of MRSI methods are shown in Table 2-3.

Table 2-3. Brain metabolite concentration were acquired for MS patients and HCs by applying PRESS-MRSI and fast MRSI methods. \*Tacq: acquisition time.

Methods	TE/TR (ms)	Metabolite (mM)	Tacq* (min)	Brain region/ FOV/voxel size/Cohort/Bo(Tesla)	Ref
2D-MRSI	30/3000	CGM: Controls, tNAA: 8.3±1.0, Cr: 5.9 ±0.8 RRMS, tNAA: ↓, Cr: ↓	29	NAWM, CGM/ 30 cm/2.34 mL/ 16 RRMS, 12 HCs/1.5T	38
2D-MRSI	135/1800	Controls, NAA/Cr: 2.22±0.19 RRMS, NAA/Cr: ↓ PPMS, NAA/Cr: ↓	13	WM, NAWM/ 21×21 cm/ 2.4 cm <sup>3</sup> / 15 PPMS, 13 RRMS & 20 HCs/ 1.5T.	149
PRESS-MRSI	30/3000	NAWM: Controls, tNAA: 8.82, Cr: 4.87 RRMS, tNAA: ↓, Cr : ↓		NAWM, CGM/ 30x30 cm/ 2.3 mL/ 25 RRMS, 28 HCs/ 1.5T	150
2D-MRSI	135/1500	GM: Controls, NAA:10.63±0.6, Cr:6.13±0.31 PPMS, NAA: ↓, Cr: ↓ WM: Controls, NAA:11.48±0.37, Cr: 5.35±0.45 PPMS, NAA: ↓, Cr: ↓	7	WM and GM/ 16 x16 cm <sup>2</sup> / 2 cm <sup>3</sup> / 4 PPMS & 4 HCs/ 1.5T	141
PRESS-MRSI	30/3000	NAWM: Controls, tNAA: 9.18±0.6 RRMS, tNAA: ↓	NA	NWWM and CGM/ 30x30 cm/ 20 RRMS, 10 HCs /1.5T	45

		CGM: Controls, tNAA: 9.28±1.02 RRMS, tNAA: ↓			
3D-MRSI	70/1710	GM: Controls, NAA:8.5±0.6, Cr: 6.8±0.6 RRMS, NAA: ↑, Cr: ↑ WM: Controls, NAA:7.9±0.6, Cr: 4.9±0.2 RRMS, NAA: ↓, Cr: ↑	34	WM and GM/ 16x16 cm/ 0.75 cm <sup>3</sup> , 18 RRMS, 10 HCs/ 3T	46
MRSI	135/1000	RRMS, NAA: 8.45±0.88, Cr: 5.2±0.73 PPMS, NAA: ↓, Cr: ↑	45	MS lesion for RRMS & PPMS/ 16x16/ 1.2 cm <sup>3</sup> / 15 RRMS, 15 PPMS/ 3T	44
2D PRESS-MRSI	135/1500	NAWM: Controls, NAA: 12.3±0.4, Cr: 8.4±0.4 RRMS, NAA: ↑, Cr: ↑ SPMS, NAA: ↓, Cr: ↓	15	Fronto-parietal WM/ 16x16 cm/1 cm <sup>3</sup> / 27 RRMS, 10 SPMS & 8 HCs/ 3T	43
EPSI	272/4000	Normal VEP, NAA: 7692±632 Abnormal VEP NAA: ↓	9	Mid-thalamus / 24 cm/ 9 MS with abnormal VEP& 8 MS normal VEP/ 1.5T	59
3D-EPSI	144/2000	Central brain: Controls, NAA/Cr: 1.963±0.167 MS patients, NAA/Cr: ↓	20	Corpus callosum, STB/ 24x24x16 cm/ 1 cm <sup>3</sup> / 9 RRMS, 21 SPMS, 18 PPMS & 10 HCs/ 1.5T	49
EPSI	144/4300	NAA/Cr: 1.55±0.1 from RRMS	20	Whole brain/ not reported /1 cm <sup>3</sup> , 20 RRMS & 75 HCs/ 1.5T	50
Spiral-MRSI	144/2000	WM: Controls, NAA: 159 A.U. (mean conc.) RRMS, NAA: ↓ SPMS, NAA: ↓	15	NAWM, GM in supratentorial brain/ 24 cm/ 1.2 mL/ 5 RRMS, 5 SPMS & 9 HCs/ 1.5T	58
EPSI	144/4300	Controls, NAA/Cr: 1.5±0.09 MS patients, NAA/Cr: ↑	20	Whole brain/ not reported/ 1 cm <sup>3</sup> , 18 RRMS & 18 HCs/ 1.5T	47
3D-EPSI	20/1720	GM: Controls, NAA: 10±0.85, Glx: 6.5±1.1 MS patients, NAA: ↓, Glx: ↓	17.48	Whole brain/ 28x28x18 cm/ 1 cm <sup>3</sup> , 19 RRMS & 19 HCs / 3T	155

## **Reproducibility of MRSI of MS patients**

Reproducibility of fast MRSI techniques has not been evaluated. It is important that MRSI techniques have good reproducibility and recent studies have shown good correlation between time points. Mostert et al. tested MRSI reproducibility with stable MS patients 4 week apart and found good short term reproducibility of NAA/Cr measurement <sup>156</sup>. Vafaeyan et al. also validated the reproducibility of NAA/Cr and NAA/Cho in MS as they found high correlation of these ratios at different time points <sup>157</sup>.

## **2.7 Concluding remarks and summary**

In recent years, the evolution of MR technologies have led to developments of brain H-MRS and clinical MR imaging procedures which enabled the collection of morphometric and biochemical information in a single imaging session. There are a variety of H-MRS techniques that are used to detect and evaluate the biochemical changes of the whole brain, where whole brain coverage requires improving spatial resolution and SNR. Fast MRSI is more suited to a clinical setting, mainly due to faster acquisition time, improved SNR and spatial resolution.

The short acquisition time of fast MRSI requires advanced and robust design in the hardware and software systems to improve and modify sequences for these techniques, making them more adaptable, especially when there is a need to combine them with other acceleration techniques by either increasing field strength or modifying coil design.

EPSI has brought about revolutionary improvement in the technological capacity of MRSI, compared to conventional MRSI methods. This development has improved the time efficiency of data collection and enhanced the recording of the brain metabolite distribution. Data acquisition has seen the biggest improvement, with speeds more than two to three times faster than that of traditional MRSI methods. This has provided the opportunity for clinical research to be done on the whole brain with acquisition times of less than 16min.

This article has shown the benefits and ability of the EPSI to adapt to a diverse range of techniques such as flyback-EPSI, MEGA-EPSI, GRAPPA-EPSI, SENSE-EPSI H-MRSI techniques and 2D and 3D echo-planar techniques. This also enables the detection of J-coupled brain metabolites like GABA, Glu, Gln and m-Ins. Moreover, it can be concluded that the echo-planar imaging sequence has proven to be a successful and accelerated technique in clinical

studies not only in multiple sclerosis<sup>58</sup> but also in Parkinson's disease<sup>55</sup>, Alzheimer's disease<sup>56</sup> and stroke<sup>57</sup>.

*In-vivo* spectroscopy has the potential to play an important role in biomarker discovery and disease activity prediction in MS. MRSI studies confirmed that NAA/Cr can distinguish MS from HCs independent from the ROI. NAA can also be a potential marker of neuronal function in NAWM, CGM for different clinical groups identifying the progressive stage of the disease. Longitudinal studies with techniques applicable in clinical setting are required to determine if MRSI can close the gap in MRI imaging by defining the disease course for the individual patient. The larger ROI afforded by MRSI compared to conventional MRS has provided evaluations of neurometabolite changes to be assessed across a much larger area, thereby assessing whole brain pathological changes occurring in MS. The improvements in achieving shorter acquisition times for MRSI now provide a greater likelihood of clinical application of these techniques.

### **Ethics approval and consent to participate**

“Not applicable” (The present paper is a review article and thus it does not involve performing research on human subjects, but it describes published data).

### **Competing interests**

OA and KR declare that they are no competing interests. JLS has accepted travel compensation from Novartis, Biogen and Merck Serono. Her institution receives the honoraria for talks and advisory board commitment and also clinic support as well as research grants from Bayer Health Care, Biogen, CSL, Genzyme Sanofi, Merck, Novartis and TEVA.

### **Funding**

SR received research funding from Hunter Medical Research Institute.

### **Author's contributions**

OA has been involved in writing, compiling and revising the manuscript critically to suit publication standards. JLS, KR and SR contributed significantly on revising, literature and critical suggestions to reshape the manuscript. All authors read and approved the final version of manuscript.

# Chapter 3 : Diurnal Stability and Long-Term Repeatability of Neurometabolites Using Single Voxel 1H Magnetic Resonance Spectroscopy

O. Al-iedani, J. Arm, K. Ribbons, R. Lea, J. Lechner-Scott, S. Ramadan

## ABSTRACT

**Purpose:** This study was designed to evaluate the diurnal stability and long-term repeatability and reliability of one-dimensional (1D) hydrogen magnetic resonance spectroscopy (H-MRS) *in-vitro* and *in-vivo* at 3T.

**Material and method:** A standard brain phantom was used for *in-vitro* study. *In-vivo* diurnal evaluation involved ten healthy subjects, while repeatability study involved six subjects. MRS was acquired from posterior cingulate gyrus (PCG) and processed with LCModel. Diurnal effects were assessed with repeated measures ANOVAs, repeatability was evaluated using coefficient of variation (CV), while reliability was assessed with standard error measurement (SEM) and intra-class correlation coefficient (ICC).

**Results:** Diurnal metabolic changes *in-vitro* were non-significant. The intra/inter-*in-vitro* CVs for the major metabolites; N-acetylaspartate (NAA), creatine (Cr), myo-inositol (m-Ins), glutamate+glutamine (Glx) and total choline (tCho) were 1–3%/2–6%, respectively. Statistically significant *in-vivo* diurnal effects were only seen for glycerophosphocholine (GPC, +10%,  $F= 10.6$ ,  $p= 0.001$ ) and Glx (+6%,  $F= 5.1$ ,  $p= 0.018$ ). The intra/inter-subject CVs for the major metabolites ranged from 2–5%/ 5–9%, respectively. The major metabolites displayed ICC ranging from 0.5–0.7 and low SEM (0.001–0.078) reflecting high reliability in detecting neurometabolites. The inter-week interval for *in-vivo* measurements had minimal effect on metabolite ratios ( $F= 1.4$ ,  $p= 0.09$ ).

**Conclusion:** *In-vitro* MRS showed no diurnal effects and minimal variation in metabolite levels. Most PCG metabolites are not altered diurnally. The low *in-vivo* variability of metabolite concentration supports the use of localised MRS on clinical 3T scanners for reliable neurometabolic profiling of the brain.

### 3.1 Introduction

Non-invasive techniques such as H Magnetic Resonance Spectroscopy (H-MRS) have the potential to provide neurometabolite profiles *in-vivo* that can add specificity to diagnostic and clinical management in a wide range of neurological diseases <sup>39</sup>. For instance, in multiple sclerosis patients, a reduction of N-acetylaspartate (NAA) and glutathione (GSH) levels has been associated with axonal damage and oxidative stress, respectively <sup>39, 158</sup>, while increased total creatine (tCr), total choline (tCho) and myo-inositol (m-Ins) concentrations have been used as markers of altered turnover of cell membranes and increased glial cell activity <sup>159</sup>.

The H-MRS technique is a reliable and reproducible method that has been successfully used to detect neurometabolites alteration in multiple brain regions, but limited studies have measured variability of these neurometabolites in intra-subject (within subject) and inter-subject (between subjects) settings, over short and long-term intervals (repeatability). This aspect will be an important factor in longitudinal studies in chronic conditions, attempting to quantify changes in metabolites over extended periods of time. One possible factor of intra-individual variation in metabolite profile over time that needs to be considered is a potential diurnal effect (time of day). There are limited studies to date that have investigated physiological factors, such as hydration status and diurnal effects by quantitative H-MRS techniques <sup>160-162</sup>. One study has demonstrated that the diurnal variability of gamma-aminobutyric acid (GABA) in healthy subjects was not significantly affected, using quantitative edited MRS at 3T in visual and sensorimotor cortices <sup>162</sup>. Others showed that the physiological diurnal effects on NAA might significantly influence measurements in the striatum region <sup>161</sup>, while no diurnal metabolic effect was observed in the anterior cingulate cortex <sup>160</sup>.

For any H-MRS technique to be valuable for clinical studies, it has to be repeatable over time with acceptable intra-subject variability and needs to be reproducible reliably in short and long term studies <sup>163, 164</sup>. Previous reproducibility studies *in-vivo* showed that MRS techniques are reliable in detecting neurometabolites changes at 1.5T <sup>165, 166</sup> and 3T <sup>164, 167, 168</sup> with improved reproducibility coefficient of variation for intra/inter-subject assessments. Nonetheless, most of the previous studies were performed over 1–6 week periods to assess the reliability of measurements in different brain regions <sup>169, 170</sup>. However, for such techniques to have applicability in chronic disease longer test-retest evaluations are warranted to enable assessments of disease progression and long term medical management to be investigated.

In the current study, spectral diurnal and repeatability measures were obtained from a standard brain phantom. Additionally, the diurnal variability, long-term repeatability and reliability of localised 1D H-MRS quantification of PCG metabolites in healthy participants was performed on a 3T clinical system.

## **3.2 Materials and methods**

### **3.2.1 Participants**

Ten participants, 5 males and 5 females ( $36.1 \pm 7.7$  years), with no history of neurological conditions, were recruited from the Hunter Medical Research Institute (HMRI) research register. All participants complied to the study inclusion criteria, which included passing an MRI safety clearance as well as being able to comply with all study procedures. Institutional Review Board (IRB) approval was obtained from the Hunter New England Local Health District Human Research Ethics Committee, with written informed consent obtained from all participants prior to undertaking any study-related procedures. To limit the impact of other potential physiological factors, subjects were also instructed to abstain from any supplements, coffee, and rigorous exercise prior to each MRS/MRI scan.

### **3.2.2 Study design**

#### *In-vitro*

To identify intra/inter-session variations due to scanner performance such as frequency drift, RF fluctuations and shim, *in-vitro* diurnal and repeatability measurements were carried out on a spherical GE spectroscopic phantom fitted with a temperature gauge <sup>165</sup> (Braino) containing brain metabolites at physiological pH and concentrations: NAA(12.5 mM), creatine hydrate (Cr, 10 mM), choline chloride (Cho, 3 mM), m-Ins (7.5 mM), L-glutamic acid (Glu, 12.5 mM), DL-lactic acid (Lac, 5 mM), sodium azide (0.1%), potassium phosphate monobasic (KH<sub>2</sub>PO<sub>4</sub>, 50 mM), sodium hydroxide (NaOH, 56 mM) and 1 ml/l Gd-DPTA (Magnevist).

To measure *in-vitro* diurnal effect, Braino was scanned 3 times daily for five days (Figure 3-1A). To measure intra-session variability, the phantom was scanned ten times in succession without being removed from the scanner in a single session. For inter-session variability, the phantom was scanned three times each week (Figure 3-1B). All phantom measurements were performed at the same time of the day to avoid any potential confounders. Prior to each measurement and after positioning, the phantom was allowed to equilibrate in the isocentre of

the magnet for five minutes, in order to achieve thermal stability as well as to avoid any random fluid movements.

### *In-vivo*

The *in-vivo* diurnal stability study involved all ten healthy subjects, 5 males and 5 females (36.1±7.7 years). Participants underwent three MRS time point measurements, scanned over a 10-hour period at 0700(T1), 1200 (T2) and 1700 (T3) on the same day within a week (Figure 3-1C). For repeatability study, six healthy subjects, 3 males and 3 females (38.1±4 years), as sub-group of the above ten subjects, underwent eight weekly MRS sessions, over the course of three months with an inter-session delay of one month after the first four sessions (Figure 3-1D). S1 represents the first four sessions and S2 represents the last four sessions after one-month break. Weekly sessions were performed on the same day and at the same time to reduce diurnal effects <sup>162</sup>.

<b>A</b> <i>In vitro</i> diurnal					<b>B</b> <i>In vitro</i> repeatability											
Period	No. of scans	Time of day			Intra-Sessions 10 times in single session without removing the scanner table											
		T1	T2	T3	Inter-Sessions				Break=1 month							
5 days	15	5	5	5	W 1	W 2	W 3	W 4		W 9	W 10	W 11	W 12			
Total	15 Sessions			No. of scans				12 Sessions				12 Sessions				
					3	3	3	3	3	3	3	3	3			
					Total				12 Sessions				Total			
					12 Sessions				12 Sessions				12 Sessions			

<b>C</b> <i>In vivo</i> diurnal					<b>D</b> <i>In vivo</i> repeatability											
Sex	HCs No.	Time of day			S1											
		T1	T2	T3	S1				Break=1 month	S2						
Female	5	5	5	5	W 1	W 2	W 3	W 4		W 9	W 10	W 11	W 12			
Male	5	5	5	5	3	3	3	3		3	3	3	3			
Total	10	30 Sessions			Total				24 Sessions				24 Sessions			
					3	3	3	3	3	3	3	3				
					Total				24 Sessions				Total			
					24 Sessions				24 Sessions				24 Sessions			

Figure 3-1. Graphical representation of *in-vitro* study design for diurnal effect (A) and repeatability (B) and *in-vivo* study design for diurnal variability (C) and repeatability (D) study where, time of day defined as T1 =0700, T2=1200 and T3=1700 and S1 represents the first four sessions, S2 represents the last four sessions after one-month break.

### 3.2.3 MRI acquisition and structural assessments

All MRI/MRS scans were undertaken on a 3T Prisma (Siemens Healthineers, Erlangen, Germany) MRI scanner equipped with a Siemens 64-channel head and neck receiver coil located at the HMRI Imaging Center. The auto-align localiser option was activated for all measurements to achieve reproducibility for both structural as well as MRS voxel placements

<sup>171</sup>.

Experimental parameters of the three-dimensional isotropic T1-weighted Magnetization-Prepared RApid Gradient Echo (MPRAGE) were as follows; sagittal orientation, TR/TE/TI= 2000/3.5/1100 ms, 7° flip angle, field of view (FOV)= 256x256 mm, pixel size= 1x1x1 mm<sup>3</sup>, NEX= 4 and acquisition time = 5 minutes. Sagittal MPRAGE was reconstructed online into 1mm coronal and axial slices to guide voxel positioning.

Reproducibility of voxel re-positioning at repeated scans was optimised at three levels. Firstly, head tilt angle (head to feet direction) for each participant was manually measured, after fixing it at patient comfort level, at the very first session and subsequently the same tilt angle was followed for the seven scanning sessions. Secondly, a rigorous three-point anatomical check (three corners of MRS voxel in relation to the anatomy of splenium of corpus callosum) was performed. Finally, the spectroscopic voxel was segmented to obtain cerebrospinal fluid (CSF), grey matter (GM) and white matter (WM) using SPM12<sup>172</sup>. The latter step was performed off-line after data collection, which aimed to improve accuracy in the MRS voxel re-positioning during longitudinal assessments.

### **3.2.4 H-MRS acquisition, post-processing and analysis**

H-MRS data was acquired using a Point RESolved Spectroscopy (PRESS) sequence at short echo time, acquired from the region of interest (ROI), as shown in Figure 3-2. The following parameters were used: TR/TE= 2000/30ms, PCG voxel size= 30x30x30 mm<sup>3</sup>, averages= 96, vector size= 1024 points, preparation scans= 4, RF offset frequency= 3.2 ppm and water suppression was enabled<sup>173</sup>. Water reference was also acquired (4 averages) from the same voxel position and size after disabling RF part of water suppression module. Automatic shimming followed by manual shimming was performed for every single measurement for phantom and *in-vivo* experiments to improve field homogeneity.

H-MRS data was exported offline and analysed with LCModel using a basis set specifically for 3T and TE= 30ms with water normalization. Concentrations of the brain metabolites were expressed as a ratio to total creatine (Cr+PCr= tCr) with only Cramer-Rao lower bound (CRLB (%SD)) less than or equal 20% accepted.

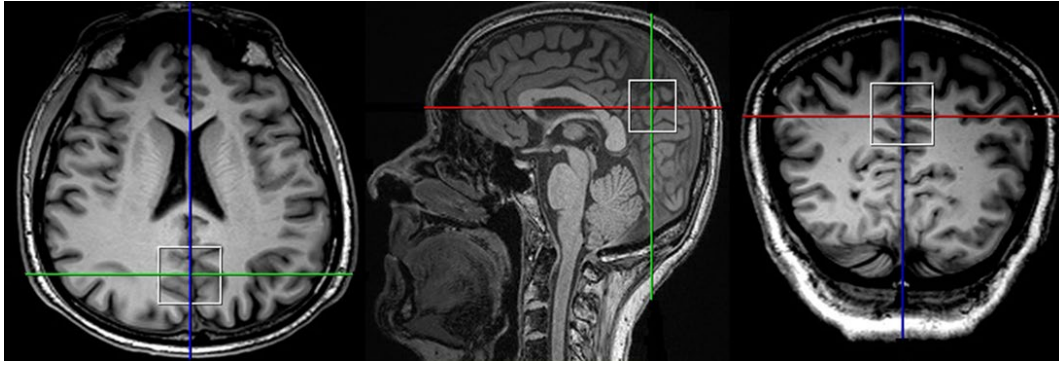


Figure 3-2. Positioning of the PCG voxel in three planes. T1-weighted MR images from healthy participant in axial, sagittal and coronal planes demonstrating the PCG voxel size and position (white box).

### 3.2.5 Statistical analysis

Diurnal stability of H-MRS of major brain metabolites (NAA, Cr, tCho, m-Ins, GSH and glutamate+glutamine (Glx)) was assessed using SPSS repeated measures ANOVAs (post-hoc Bonferroni adjustment)<sup>174</sup>. One MRS data point (T3, female) was excluded due to poor quality shim. To investigate *in-vivo* temporal stability for long-term repeatability descriptive and reliability analyses were implemented as follows: mean and standard deviations of spectroscopic measurements were reported for three groups of sessions; the first four sessions, the last four sessions and all eight sessions. Furthermore, repeatability was measured by calculating coefficient of variance (CV) in both intra/inter-subjects for each neurometabolite.

Due to small sample size and to avoid a biased estimator of the standard population coefficient of variation, a corrected coefficient of variation (CV<sub>cor</sub>) was used throughout this work and was calculated using the following formula:

$$CV_{cor} = \left(1 + \frac{1}{4N}\right) CV$$

where CV is standard deviation/mean and N is the sample size. The CV mentioned in the rest of the text refers to CV<sub>cor</sub> and is expressed in percentage (%).

Intra-subject CV was computed from the eight repeated MR sessions while inter-subject CV was calculated using the average variance of the repeated measurements for eight sessions. ANOVA (analysis of variance) of the repeated measurements was used to identify any differences between first and last four sessions. Furthermore, variance components for between subjects ( $\sigma^2_b$ ), within subjects ( $\sigma^2_w$ ), and residual errors ( $\sigma^2_r$ ) were computed simultaneously using a two-way linear mixed effects model applying restricted maximum likelihood (REML) estimation, whereby each metabolite was considered dependant variable and subject identity

and time points were covariates. Intra-class correlation coefficient (ICC) is the most conservative estimator of reliability of test-retest measurement, along with standard error measurement (SEM) for accurate measure of intra-subject variability. ICC and SEM were estimated using the variance components as described elsewhere<sup>175, 176</sup>:

$$ICC = \frac{\sigma^2_b}{\sigma^2_b + \sigma^2_w + \sigma^2_r}$$

$$SEM = \sqrt{\sigma^2_w + \sigma^2_r} \times \sqrt{1 - \alpha}$$

Where  $\sigma^2_b$  is between subject variance,  $\sigma^2_w$  is within subject variance,  $\sigma^2_r$  is residual error variance and  $\alpha$  is Cronbach Alpha, obtained from reliability analysis for each metabolite. ICC < 0.4 indicated poor reliability,  $0.4 \leq ICC < 0.75$  indicated fair to good reliability, and  $ICC \geq 0.75$  indicated excellent reliability<sup>177</sup>.

### 3.3 Results

All of the ten participants met all the enrollment criteria and successfully completed diurnal scans sessions. From these ten individuals, six participants also completed all of the long-term repeatability scanning sessions. The quality of spectra for each spectrum for *in-vitro* (phantom) and *in-vivo* was determined by full width at half maximum (FWHM) of the magnitude water signal that ranged from 3.5–6 Hz (mean: 4.75Hz) and 12–18 Hz (mean: 15 Hz), respectively. *In-vivo* and *in-vitro* sample spectra analyzed by LCModel are shown in Figure 3-3.

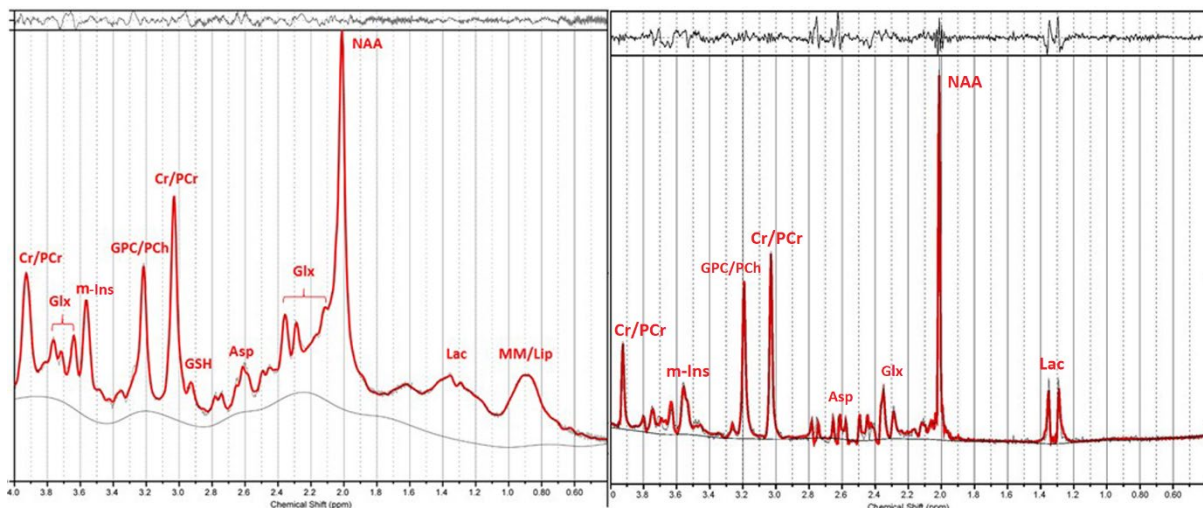


Figure 3-3. H-MRS spectra of *in-vivo* and *in-vitro*. LCModel fitting output of typical H-MRS spectra of *in-vivo* (left) data acquired from PCG and *in-vitro* (right) at 3T and a TE value of 30 ms. Cr, creatine; PCr, phosphocreatine; Glx, glutamate+glutamine; m-Ins, myo-inositol; GPC,

glycerophosphocholine; PCh, phosphocholine; GSH, glutathione; Asp, aspartate; NAA, N-acetylaspartate; Lac, lactate; MM, macromolecular; Lip, lipid.

### 3.3.1 In-vitro

Repeated measures ANOVAs showed no statistically significant changes in metabolite levels at all time points ( $F= 3.2, p> 0.09$ ). The findings of repeatability of intra/inter-session from phantom experiments corresponding to metabolites measurement are shown in Figure 3-4. The intra-session CV (range: 1–3%) of metabolite concentrations was smaller than inter-session CV (range: 2–6%) for major metabolites (NAA, Cr, m-Ins, Glx and tCho). The repeated measures of ANOVA showed no statistically significant changes between the first (S1) and last (S2) four sessions ( $F= 5.62, p> 0.08$ ) in long-term repeatability.

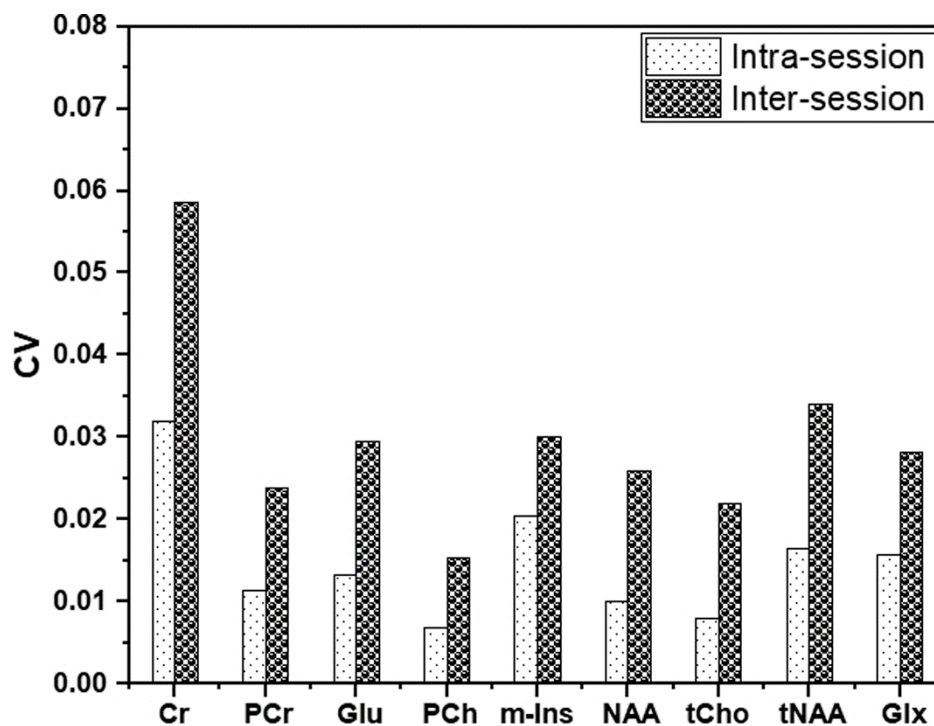


Figure 3-4. Intra/inter-session CVs from *in-vitro* H-MRS data using repeatability approach.

### 3.3.2 In-vivo

#### *Diurnal variability*

Using single voxel 1D H-MRS, repeated measures ANOVAs for tCr ratios of all analysed metabolites showed statistically significant diurnal effects only for glycerophosphocholine (GPC,  $F= 10.6, p= 0.001$ ) and Glx, ( $F= 5.1, p= 0.018$ ). Post hoc tests revealed that there was a statistically significant increase of +10% in GPC levels from the T1 to T2 time points ( $0.17\pm 0.03$  vs  $0.19\pm 0.02, p= 0.006$ ) and a decrease of -5% from the T2 to

T3 time points ( $0.19\pm 0.02$  vs  $0.18\pm 0.022$ ,  $p= 0.02$ ). For Glx, an increase of +6% from the T1 to T3 time points was observed ( $1.23\pm 0.06$  vs  $1.314\pm 0.1$ ,  $p= 0.04$ ) (Figure 3-5). Furthermore, sex did not impact on neurometabolite levels ( $F= 2.78$ ,  $p= 0.4$ ). Statistical analysis of the MRS voxel tissue composition for the diurnal study showed mean values of GM, WM and CSF fractions as  $0.49\pm 0.03$ ,  $0.43\pm 0.05$  and  $0.08\pm 0.01$ , respectively, with no statistically significant difference over the 10-hour period ( $p> 0.1$ ).

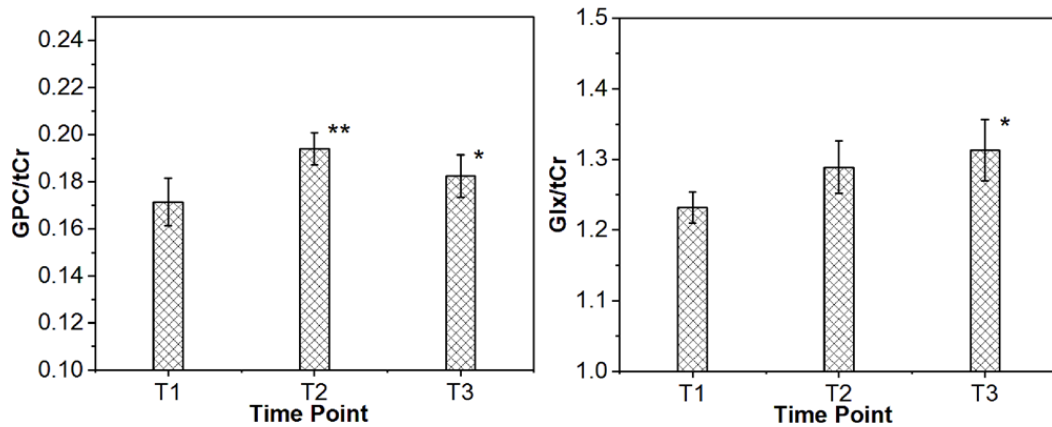


Figure 3-5. *In-vivo* diurnal variations of GPC and Glx metabolite ratios for PCG brain region. \*:  $p< 0.05$ , \*\*:  $p< 0.01$ .

#### *Intra/Inter-subject variability (repeatability)*

Segmentation of MRS voxel tissue composition showed mean values of GM, WM and CSF for the eight long-term repeatability sessions, which were  $0.49\pm 0.01$ ,  $0.41\pm 0.01$  and  $0.10\pm 0.02$  respectively, and there was also no statistically significant difference noted in the voxel tissue composition during the three month period.

To explore the temporal intra-subject variability of repeated MRS measurements over time, CVs of spectroscopy profiles from each subject for each session were computed and averaged (all eight sessions) to obtain the intra-subject CVs of the six subjects. The smallest CV in intra-subject variability was found for NAA (2.6%). Other results for four major metabolites (Cr, m-Ins, Glx and tCho) ranged from 3.5–5%; while, GSH and GPC has the highest CVs ranging between (6–10%).

Inter-subject variability was measured by averaging the CVs of each metabolites derived from each session (all 8 sessions). Similar to intra-subject variability, the lowest and highest inter-subject CVs were obtained from NAA (5.7%) and GPC (%14), respectively. Furthermore, the variability of Cr, Glx, m-Ins and tCho between subjects ranged from 6.5–8.5% (Table 3-1).

Reported relaxation times (T1 and T2) of brain metabolites *in-vivo* at 3T show that negligible corrections to MRS quantification is required.<sup>178</sup> *In-vivo* metabolites measurement repeatability results of intra/inter-subject study are shown in Figure 3-6.

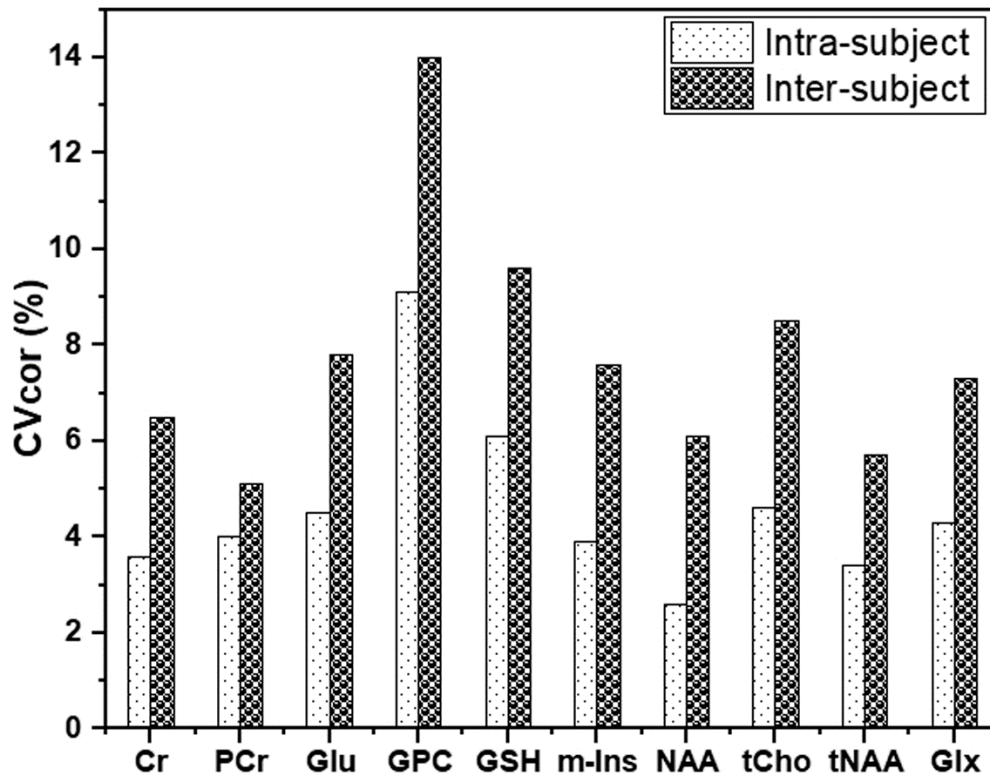


Figure 3-6. Intra/inter-subject repeatability CVcor from *in-vivo* H-MRS data.

Table 3-1. Descriptive statistics and repeatability data for *in-vivo* neurometabolites/tCr ratios from six participants.

Metabolite	Intra-subject			Inter-subject		
	Mean	SD	CVcor %	Mean	SD	CVcor %
Cr	0.43	0.02	3.6	0.44	0.01	6.5
PCr	0.57	0.02	4	0.56	0.01	5.1
Glu	1.15	0.04	4.5	1.06	0.02	7.8
GPC	0.22	0.01	9.1	0.19	0.01	14
GSH	0.19	0.01	6.1	0.21	0.00	9.6
m-Ins	0.87	0.02	3.9	0.82	0.00	7.6
NAA	1.45	0.04	2.6	1.38	0.02	6.1
tCho	0.23	0.01	4.6	0.20	0.00	8.5
tNAA	1.59	0.06	3.4	1.53	0.03	5.7
Glx	1.29	0.04	4.3	1.25	0.01	7.3

<b>MRI</b>						
CSF	0.12	0.06	8	0.09	0.01	10
GM	0.49	0.02	2	0.50	0.01	3
WM	0.39	0.06	4	0.41	0.02	5

Abbreviations: CV, coefficient of variation; Cr, creatine; PCr, creatine phosphate; Glu, glutamate; GPC, glycerophosphocholine; GSH, glutathione; m-Ins, myo-inositol; NAA, N-acetylaspartate; tCho, total choline; Glx, glutamate+glutamine; tCr, total creatine; CSF, cerebrospinal fluid; GM, grey matter; WM, white matter.

### *Test-retest Reliability*

To establish the absolute test-retest reliability of quantifying MRS profiles from the PCG brain region using H-MRS techniques, neurometabolite levels were examined by using ICC and SEM over eight sessions in six subjects. Using linear mixed effects model, calculation of variance within subjects, between subjects and residual errors are shown in Table 3-2. Furthermore, the ICC results indicated more robust estimation of reliability by including the residual errors. The ICC results for four major metabolites (NAA, m-Ins, Cr and Glx) ranged from (0.55–0.7); while, GSH and GPC had the smallest ICC (0.45). Along with CV and SEM, ICC values yielded much better accuracy in this test-retest study by comparing ratios between subject variability to the total variance, accounting for inherent errors associated with repeated measurements.

Table 3-2. Variances and reliability of major neurometabolites data from healthy participants in PCG.

<b>Metabolites</b>	<b>Variance</b>			<b>ICC</b>	<b>SEM</b>
	<b>Between subjects</b>	<b>within subjects</b>	<b>Residual error</b>		
Cr	6.677E-04	0.000E+00	4.914E-04	0.576	0.034
GPC	1.779E-04	0.000E+00	2.248E-04	0.442	0.003
GSH	2.580E-04	4.776E-08	3.067E-04	0.457	0.006
m-Ins	7.909E-04	2.780E-04	2.579E-04	0.596	0.032
NAA	5.205E-05	0.000E+00	2.383E-05	0.686	0.001
tCho	5.100E-04	3.992E-09	5.216E-04	0.510	0.005
tNAA	1.445E-03	8.801E-09	8.049E-04	0.642	0.047
Glx	3.088E-03	8.353E-07	2.342E-03	0.569	0.078

ICC, intra-class correlation coefficient; SEM, standard error measurement; tNAA, total N-acetylaspartate. Note: all abbreviations are as those in Table 3-1.

#### *Longitudinal repeatability sessions (inter-session variability)*

Temporal changes in longitudinal reproducibility sessions (8 sessions) was performed by establishing two sub inter-sessions with one-month break. Inter-session variability was measured by averaging the neurometabolites levels obtained from S1 and S2. No marked change in the mean neurometabolites levels between S1 and S2 was detected. Statistical analysis, using student t-test, indicated that there was no significant difference in CV between these two sessions for any of the metabolites ( $p > 0.08$ ).

### **3.4 Discussion**

As expected, the effect of time of day on H-MRS phantom measurement was not significant, in agreement with Soreni et al.<sup>161</sup>. Our repeatability results were in agreement with other studies<sup>165</sup>, which showed that inter-session CV values were higher than those obtained for intra-session CV values, in spite of the fact that the intra-day phantom measurements were carried out without moving the table.

Intra/inter-CV values of NAA *in-vitro* ( $\leq 2.5\%$ ) were much lower than CV values reported in earlier studies<sup>165</sup>. While Cr showed high intra/inter-CV values *in-vitro* ( $< 6\%$ ), all other metabolites showed lower Intra/inter-CV values ( $\leq 3.5\%$ ).

In our cohort of ten healthy participants, the diurnal variability of PCG neurometabolite H-MRS profiles was evaluated (single voxel, PRESS, TE: 30 ms) at 3T. Significant *in-vivo* diurnal effects on Glx and GPC levels were observed. However, there was no significant interaction between other major neurometabolites levels (NAA, Cr, m-Ins and Cho) and intra-subject variability. Furthermore, the degree of variability was +6% from T1 to T3 for Glx and +10% from T1 to T2 for GPC. It is interesting to note that variability of Glx and GPC are higher than other metabolites<sup>160</sup> which might be due to their active role in the major metabolic pathways in the brain. It is also possible that the variation could be attributed to levels of hydration, diet and increased demand in cognitive processing<sup>179</sup>. Similarly, a previous physiological variability study confirmed our findings, that the majority of neurometabolites levels were not affected by the time of day<sup>160</sup>.

In contrast, diurnal physiological variability study by Soreni et al.<sup>161</sup> demonstrated significant diurnal effects on NAA/Cr ratio ( $p = 0.012$ ) in the striatum region. Insignificant

GABA diurnal variations in the visual and sensorimotor cortex <sup>162</sup>, suggest that diurnal factors can be ignored in this brain region. It is important to note the metabolite levels differ in different parts of the brain <sup>180</sup> and this could be a reason for not detecting any changes in their study.

In addition to diurnal effects, the impact of voxel repositioning was studied previously <sup>160, 161</sup> as another source of variability in MRS measurements. These studies suggested that voxel repositioning effects in healthy subjects are not critical even though MRS data was acquired from relatively small voxels (4.5 cm<sup>3</sup> and 6 cm<sup>3</sup>). In the current study, MRS data was acquired from a 27 cm<sup>3</sup> PCG voxel size at 3T. The PCG region was chosen due to its technical feasibility (minimal motion, good shim, high signal to noise ratio) <sup>36</sup>, its correlation with mood processing (motor cortex) and cognitive performances <sup>181</sup> and its significant importance is an ongoing investigations in our group. It did not show any detectable variability due to voxel repositioning. Furthermore, segmentation of the PCG voxels at 3 time points for each subject showed that tissue fractions are not significantly different between different times of day, suggesting the voxel repositioning can be achieved reliably and reproducibly.

For voxel positioning effect in repeatability study, tissue segmentation within voxel was performed as additional independent estimator for inter-subject variance, where inter-subject CV values of CSF, GM and WM were higher than intra-subject. Additionally, tissue segmentation results revealed there was insignificant differences (0.1–0.2%) between sessions; leading to the conclusion that the error from tissue type variations has minimal effect on metabolic concentrations. Alternatively, automated voxel positioning as described in <sup>182</sup> can provide an acceptable level of voxel repositioning.

In our cohort of six healthy participants, we evaluated the reliability of 1D H-MRS in detecting and quantification of brain metabolites at PCG in six healthy participants, with a longitudinal approach for repeatability using Fourier transform processing techniques.

The findings of long-term repeatability approach showed that the intra/inter-subjects CV values, for the majority of PCG metabolites, are relatively low compared to previous repeatability and reproducibility studies, performed at 1.5T and 4T, applied to different brain regions <sup>169, 183</sup>. These differences in intra/inter-variability estimates may reflect difference in voxel size and location, acquisition sequences, quantitation methods and post-processing protocols <sup>176</sup>.

As expected, most of the single and multi-voxel repeatability studies reported <sup>128, 165, 184, 185</sup>, show that inter-subject CV values were higher than intra-subject CV values. The *in-vivo*

variability could be related to individual biological and regional variations, physiological fluctuations and movement during data acquisition in addition to other intra-subject variabilities<sup>166, 170</sup>. Higher inter-subject CV values during long-term repeatability studies could also be partially attributed to small fluctuations in longitudinal hardware performance such as RF power and B1/B0 inhomogeneities, which are evident and unavoidable.

Intra/inter-subject CV values of NAA *in-vivo* ( $\leq 6\%$ ) were much lower than CV values reported in earlier studies<sup>169, 183, 186</sup> that used the same acquisition parameters. While GPC showed high intra/inter-subject CV values *in-vivo* ( $< 14\%$ ), m-Ins and Glx demonstrated lower and similar CV values ( $7.6\%$ ) for intra/inter-subject CV in *in-vivo* study. Identical and similar CV values for m-Ins and Glx were previously reported by Ding et al.<sup>128</sup> and Wijtenburg et al.<sup>187</sup>, even though different acquisition and quantitation methods were used (EPSI and STEAM) at 3T.

Our inter-subject CV values ( $\leq 8\%$ ) of selected PCG metabolites (NAA, tNAA, tCho and m-Ins) were slightly higher than corresponding CV values ( $\leq 5\%$ ) reported by Terpstra et al. (2016) who used semi-LASER to acquire PCG spectral data at 3T from six healthy participants over a one-month period<sup>167</sup>. Compared to Wijtenburg et al. PCG repeatability study CV values ( $\leq 7.5\%$ ), that used short TE STEAM sequence (6.5 ms) at 3T<sup>187</sup>, our inter-subject CV values were slightly higher ( $3.5\%$ ). This is probably due to the improved signal to noise ratio at the reduced TE duration. Additionally, better inter-subjects PCG CV values were obtained ( $\leq 9.5\%$ ) for low concentration metabolites (e.g. GSH) compared to Terpstra et al.<sup>167</sup> ( $\leq 12\%$ ) and Wijtenburg et al.<sup>187</sup> ( $\leq 8.6\%$ ) studies.

We hypothesized that the introduction of a one-month delay after the first four sessions would impact CV values for the last four sessions. Although CV values for the final weeks varied slightly, this change was insignificant. This is in line with other MRS studies confirming that the interval between MRS experiments has a negligible effect<sup>175, 188, 189</sup>. It is reassuring to note that the CV values of the PCG metabolites ( $5\text{--}14\%$ ) fall within the wider range of relative neurometabolite changes in other neurological and psychiatric disorders<sup>190, 191</sup>. These neurometabolites can be consistently measured in relation to small changes in concentration, which suggests that short TE H-MRS can be employed in longitudinal studies in several chronic neurological diseases including multiple sclerosis.

The reliability of quantifying PCG neurometabolite levels using H-MRS techniques was assessed using ICC and SEM. The ICC value indicated conservative estimates for relative

reliability of a test from variances between subjects, and SEM values gives an absolute index of reliability in terms of within subject variation from multiple measurements<sup>192, 193</sup>.

The major *in-vivo* neurometabolites (NAA, m-Ins, Cr and Glx) showed very good ICC ( $\geq 0.6$ , Range: 0.6–0.7) in this study. *In-vivo* NAA showed consistently highest ICC (0.7), which is similar to PCG ICC results reported by Wijtenburg et al using STEAM sequence at 3T<sup>187</sup>. Furthermore, NAA ICC showed comparable results to other studies (0.6 and 0.83) that used different MRS methods at 3T<sup>128, 176</sup>. Glx and m-Ins also gave high ICC values ( $\sim 0.6$ ) in this study, which was previously shown by Gasparovic et al.<sup>176</sup>. GSH, however, due to its lower concentration, yielded the smallest ICC value (0.46) which is similar to that reported in a previous study (0.5)<sup>187</sup>.

The low ICC value for lower concentrations metabolites is primarily a result of high residual error ( $\sigma^2r$ ) or random noise relative to inter-subject errors ( $\sigma^2b$ ). In principle, the inter-subject variance is attributed to real differences in metabolic concentrations among the participants<sup>164, 189</sup>. It is then reasonable to expect low ICC for lower concentration metabolites when higher random noise is unavoidable, as evident in other studies<sup>164</sup>.

Despite the fact that every effort was made to reduce limitations in our study, subject movement during data acquisition and intrinsic variabilities were difficult to control and accounted for. This study is also limited by the low number of subjects and repetitions as well as equipment fluctuation.

### **3.5 Conclusion**

Our results support that H-MRS is a reliable tool for the detection of neurometabolites in the brain and has validity in longitudinal studies. The findings of this study demonstrated high repeatability and reliability of detection of PCG metabolites on standard clinical 3T, which were substantially improved compared to previous reproducibility studies. Additionally, the introduction of interval delay between MRS sessions has minimal impact on PCG metabolites levels.

## Chapter 4 : A longitudinal, observational study of the effect of dimethyl fumarate on hippocampal metabolites in RRMS using 1H-MR spectroscopy

O.Al-iedani, K. Ribbons, R. Lea, S. Ramadan, J. Lechner-Scott

### ABSTRACT

**Background:** Dimethyl fumarate (DMF), an oral disease modifying treatment for multiple sclerosis (MS), displays anti-oxidative properties, thought to be via modulation of glutathione (GSH). However, to date, the effect of DMF on the metabolic profile of MS brains has not been evaluated. The aim of this study was to measure cross-sectional changes in hippocampal neurometabolites in relapsing-remitting MS (RRMS) patients, compared to healthy controls (HCs) and then evaluate the metabolic impact of DMF treatment longitudinally over 24 months.

**Methods:** H-MRS was undertaken on 20 RRMS patients prior to and up to 24 months post-inception of DMF treatment and 20 age sex-matched HCs. Spectroscopic data was acquired from the hippocampus using single voxel spectroscopy (6.75mL, PRESS, TE 30ms) at 3T.

**Results:** We identified a significant reduction in hippocampal N-acetylaspartate (NAA, -13%,  $p= 0.0001$ ) and increased myo-inositol (m-Ins, +9%,  $p= 0.02$ ) in RRMS patients, before starting DMF, compared to HCs. Following treatment onset, GSH levels differed significantly over 24 months in the RRMS group ( $F= 3.5$ ,  $p< 0.05$ ). There was a reduction in GSH from baseline to 1 month of treatment ( $p= 0.014$ ). This reduction remained statistically significant after 6 months of treatment ( $p= 0.04$ ), but slightly increased after 12 and 24 months of treatment ( $p= 0.15$  and  $0.18$ , respectively), approaching levels seen in HCs.

**Conclusions:** The trend for the rebound effect of GSH following 24 months of DMF treatment, is suggestive of recovery from the inflammatory event and is the first demonstration of an anti-oxidative effect in the MS brain following DMF treatment.

## 4.1 Introduction

The mode of action of Dimethyl fumarate (DMF)<sup>194</sup> in multiple sclerosis (MS) is thought to be partly due to its anti-oxidative properties, through modulation of systemic glutathione (GSH) activation, thereby attenuating oxidative stress and cellular loss in active MS<sup>195</sup>. To date, the impact of DMF on metabolic changes and oxidative status in the MS brain has not been extensively investigated.

The development of novel and non-invasive MR techniques such as H-MRS, enable monitoring of a number of chemical entities in the MS brain to be explored, including GSH<sup>39, 159</sup>. Srinivasan et al.<sup>196</sup> demonstrated GSH levels to be significantly higher in grey matter (GM) compared to white matter (WM) in healthy controls (HCs) and reported a significant reduction in GM GSH in relapsing-remitting MS (RRMS). Also, regions of higher oxidative stress, within the WM T2 lesions in RRMS, have shown a depletion in GSH compared to normal appearing white matter<sup>197</sup>. In fronto-parietal regions of secondary progressive MS (SPMS) patients, GSH levels are reduced compared to that measured in HCs<sup>198, 199</sup>. Other studies confirmed lower GSH concentrations not only in SPMS, but also in the total fronto-parietal regions of primary progressive MS patients. Moreover, there was a positive association between the levels of GSH in this region with cognitive function, including memory and processing speed<sup>200</sup>.

In the current study, we applied H-MRS to investigate longitudinal metabolic changes in the hippocampus of RRMS patients following initiation of DMF treatment. We also explored if hippocampal neurometabolite changes in RRMS were associated with severity of clinical and neuropsychological symptoms.

## 4.2 Methods

### 4.2.1 Patients and Healthy Control Subjects

Twenty patients with confirmed RRMS, in accordance with the McDonald criteria<sup>17</sup>, aged between 20 to 55 years, who were considered eligible to commence DMF treatment by their treating neurologist, were included in this study. HCs (N=20) were age ( $\pm 2$  years) and sex-matched to the RRMS cohort. Out of the remaining 20 RRMS patients, 7 could not be evaluate at 2 years due to various reasons such as pregnancy, having stopped DMF due to side effects or patient's choice.

All patients were recruited from the John Hunter Hospital, Newcastle, Australia, MS outpatient clinic. Age and sex-matched HCs were derived from the Hunter Medical Research Institute (HMRI) research register and needed to comply to the study inclusion criteria, which included passing an MRI safety clearance, as well as being able to comply with all study procedures. Institutional Review Board approval was obtained from the Hunter New England Local Health District Human Research Ethics Committee, with written informed consent obtained from all subjects prior to undertaking any study-related procedures. All scans were conducted between December 2015 and March 2018.

#### **4.2.2 Study design**

In the RRMS cohort, an open-label longitudinal observational study was conducted to evaluate the impact of DMF treatment on the hippocampal metabolite profile. We also conducted cross-sectional evaluation prior to and at 24 months post DMF treatment inception, between RRMS patients and HCs. MRI/MRS data was acquired from the RRMS cohort at five different time points; Baseline (T0, pre-DMF onset), 1 month (T1), 6 months (T6), 12 months (T12) and 24 months (T24) post inception of DMF treatment onset. HCs were scanned at baseline and 24 months. DMF dosing was escalated over the first month of treatment, to achieve a therapeutic dose of 480 mg/day according the following regime: 120 mg/day week 1, 240 mg /day week 2, 360 mg/day week 3 and 480 mg/day from week 4 onwards.

#### **4.2.3 MRI Acquisition and Structural assessments**

All MRI/MRS scans were undertaken on a 3T Prisma (Siemens Healthineers, Erlangen, Germany) MRI scanner equipped with a 64-channel head and neck coil located at the HMRI, Newcastle, NSW, Australia. Experimental parameters of the three-dimensional isotropic T1-weighted Magnetization-Prepared Rapid Gradient Echo (MPRAGE) were as follows; sagittal orientation, TR/TE/TI=2000/3.5/1100 ms, 7° flip angle, field of view (FOV)=256x256 mm, pixel size =1x1x1 mm<sup>3</sup>, NEX=4 and acquisition time =5 minutes. Three-dimensional T2 FLuid-Attenuated Inversion Recovery (T2-FLAIR) sequence, TR/TE/TI =5000/386/1800ms, 12° flip angle, FOV=256x256 mm, pixel size=1x1x1 mm<sup>3</sup>, echo train duration=858ms, NEX=1 and acquisition time=4 minutes.

Quantification of hyperintense WM lesions were performed using T2-FLAIR data, where total lesion volumes were derived using the SPM platform. Annualised atrophy changes in percentage brain volume change (PBVC) for 13 RRMS patients in (Baseline, T12 and T24) were assessed using SIENA <sup>201</sup>.

SPM<sup>202</sup> was used to segment the spectroscopic voxel into cerebrospinal fluid (CSF), GM and WM. For accuracy in the MRS voxel re-positioning, during longitudinal re-assessment, MPRAGE data was reconstructed into 1mm coronal and axial slices on the scanner. Lesions within the MRS voxel were segmented using the lesion growth algorithm described by Quadrelli et al<sup>203</sup>.

#### 4.2.4 H-MRS Acquisition, Post-Processing and Analyses

One-dimensional (1D) <sup>1</sup>H hippocampal MRS was applied using a Point RESolved Spectroscopy (PRESS) sequence at short echo time, acquired from the region of interest (ROI), as shown in Figure 4-1.

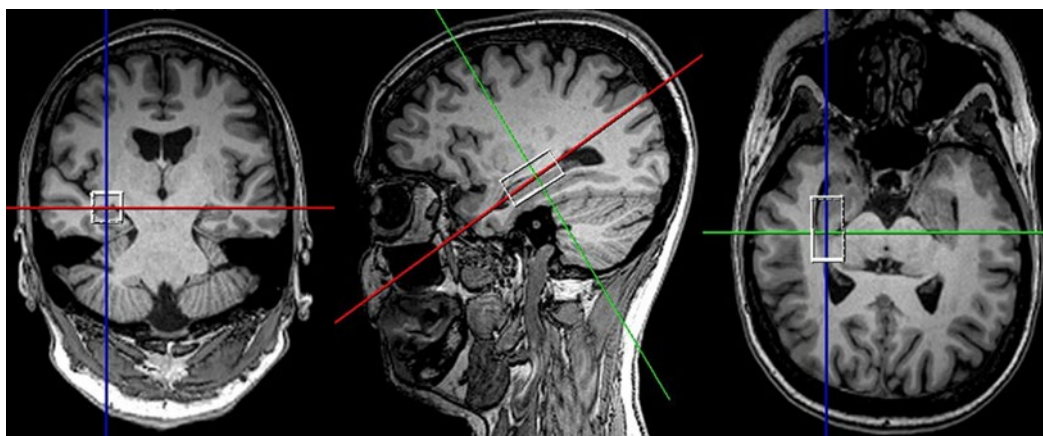


Figure 4-1. T1-weighted MR images from a multiple sclerosis patient in coronal, sagittal and axial planes demonstrating the hippocampal voxel size and position (white box).

The following parameters were used: TR/TE=2000/30ms, hippocampal voxel size =30x15x15 mm<sup>3</sup>, averages = 96, vector size =1024 points, preparation scans =4, RF offset frequency =3.2 ppm and water suppression was enabled. Water reference was also acquired (4 averages) from the same voxel position and size after disabling RF part of water suppression module.

Although non-edited MRS is less commonly used than J-edited MEGA-PRESS sequences<sup>204</sup> for detection of low concentration metabolites such as GSH, others have shown that non-edited MRS can be used to measure GSH reliably<sup>187, 205</sup>. We validated non-edited MRS (TE=30ms) by acquiring MRS data from two phosphate-buffered GSH phantoms (3 and 6 mM, pH=7.4) and fitting them using automated linear combination of model spectra (LCModel, v6.2-2B)<sup>206</sup> software package. Both phantoms contained equal amounts of NAA (12.5mM), creatine (Cr) (10mM) and choline (Cho) (3mM). LCModel fitting yielded the

correct ratios of GSH/Cr in both phantoms. Samples of *in-vivo* MR spectra from hippocampus and *in-vitro* MRS data analysed by LCModel are shown in Figure 4-2.

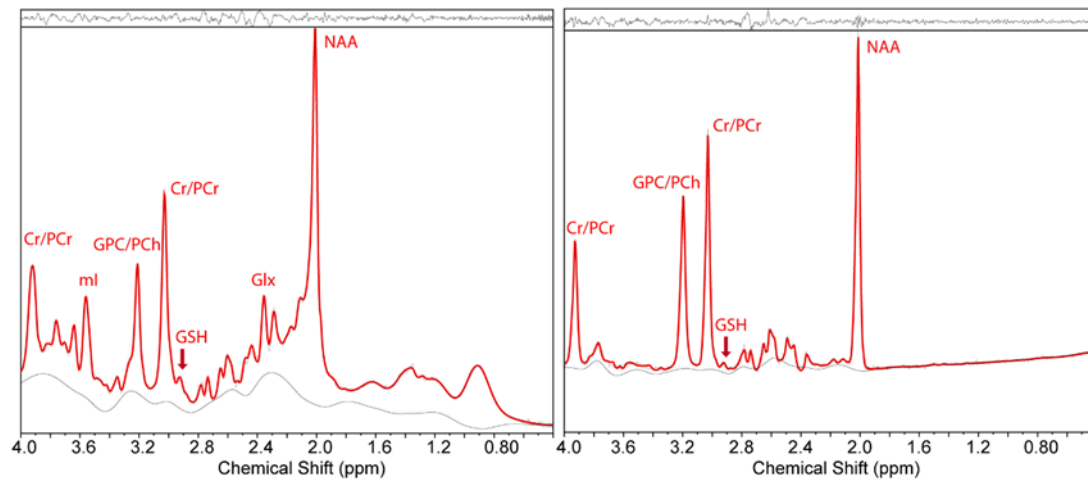


Figure 4-2. LCModel fitting output of typical H-MRS spectra of *in-vivo* (left) data acquired from hippocampus and *in-vitro* (right) at 3T and a TE value of 30ms. Cr: creatine; PCr: phosphocreatine; Glx: glutamate+glutamine; ml: myo-inositol; GPC: glycerophosphocholine; PCh: phosphocholine; GSH: glutathione; NAA: N-acetylaspartate.

Single voxel 1D MRS was transferred offline and analysed with LCModel using a basis set specifically designed for 3T and TE=30ms with water normalization. This technique allowed the estimation of overlapping resonant metabolites such as glutamine+glutamate (Glx) at short TE. A water reference scan was used for eddy-current correction as well as partial volume correction in LCModel by adjusting ‘WCONC’ parameter based on percentages of WM, GM and CSF as described in the LCModel manual. Concentrations of the brain metabolites were expressed as a ratio with respect to total creatine (Cr+phosphocreatine (PCr) = tCr) with Cramer-Rao lower bound (CRLB (SD %)) less than or equal 20% accepted.

#### Quality Control

Maintenance of quality control for MRI and MRS data was carried out by weekly scanning of the American College of Radiologists (ACR) phantom and spherical GE spectroscopic phantom<sup>165</sup> containing stable brain metabolites at physiological pH and concentrations.

#### 4.2.5 Clinical Assessments

Disability status was evaluated in the RRMS group, prior to and at 12 and 24 months following the inception of DMF treatment, by applying the Expanded Disability Severity Scale (EDSS). All EDSS evaluations were performed by a neurologist who had undertaken appropriate neuro status certification training. The Multiple Sclerosis Severity Score (MSSS)

was calculated using the EDSS and duration of disease for each patient according to the algorithms provided by Roxburgh et al.<sup>207</sup>.

Similarly, all study participants (RRMS and HCs) were assessed for cognitive performance at baseline, 12 and 24 months using the Audio Recorded Cognitive Screen (ARCS), which is a valid and reliable instrument for administering neuropsychological tests of cognitive function to unsupervised individuals<sup>13</sup>. The ARCS assesses performance in the domains of memory, verbal fluency, language (object naming), visuospatial function and attention with elements from each domain score, then used to derive an overall 'global' cognitive performance score. The Symbol Digit Modalities Test (SDMT) was undertaken concurrently as a measure of attention and information processing speed presented in the visual modality.

The mental health status of participants was assessed using the short version of the Depression Anxiety Stress Scale (DASS-21)<sup>208</sup>. Higher scores were indicative of higher levels of depression, stress and anxiety. All scores, derived from the 21-point scale, were multiplied by 2 to enable comparison to the full 42-point scale DASS and determine clinical cut offs for symptom severity.

Fatigue status was determined using the Modified Fatigue Impact Scale (MFIS), a modified form of the Fatigue Impact Scale<sup>209</sup>. The questionnaire was based on items derived from interviews with MS patients concerning how fatigue impacts in their lives. This instrument provided an assessment of the effects of fatigue in terms of physical and cognitive functioning.

#### **4.2.6 Statistical Analysis**

To investigate the significant difference between MS and HCs groups, T-tests were applied using SPSS, for independent and paired sample analyses. Major brain metabolites (NAA, Cr, total choline (tCho), m-Ins, GSH and Glx) were analysed from MS patients and HCs at different time points. The level of significant change in metabolite levels associated with onset of DMF treatment was assessed using repeated measures ANOVA, adjusted for appropriate covariates, followed by post hoc testing using Least Significant Difference (LSD). Additionally, correlation between clinical symptoms and metabolite levels was performed using the correlation coefficient for non-parametric correlations (Spearman's rho).

## 4.3 Results

### 4.3.1 Participant demographics and characteristics

All of the 20 recruited RRMS patients met the enrollment criteria. Patients were predominantly female, early in their disease course with mild disability (EDSS  $2\pm 0.18$ ) (Table 1). Cross-sectional evaluation showed significant differences in severity of mood symptoms, fatigue status and cognition impairment in the RRMS patients compared to age and sex-matched HCs at baseline and at two years (Table 1). There were no significant changes in levels of clinical symptoms for HCs during the 24-months period (baseline and 24 month) (Table 1). Reliable data were obtained from HCs and MS participants at each time point. Additionally, using repeated measures of ANOVA, longitudinal analysis (treatment effect) showed no statistical change was observed in the level of any clinical symptoms, EDSS, MSSS and disease duration for DMF treatment for 13 RRMS patients at three time points (T0, T12 and T24) over the two years ( $p > 0.4$ ,  $F < 0.7$ ). We observed no statistical changes in the level of severity of disability at DMF treatment onset and at the 24 months post-DMF treatment.

Table 4-1. Cross sectional analysis of mean demographic scores and disease-related variables for MS and HCs groups at baseline and 2 years.

Characteristics	Baseline			2 yrs follow up		
	HCs(N=20)	MS(N=20)	<i>p</i> -value	HCs(N=13)	MS(N=13)	<i>p</i> -value
Sex (% female)	80%	80%	0.884	85%	85%	0.684
Age	35±1.62	35±1.64	0.921	37±1.62	37±1.64	0.721
Disease Duration (yrs)	-	5±1.3	-	-	6±1.50	-
EDSS	-	2±0.18	-	-	2±0.41	-
MSSS	-	3.75±0.4	-	-	3±0.71	-
Total ARCS	93±2.84	82±3.44	0.015	95±4.05	83±5.33	0.096
Memory	92±2.78	87±4.74	0.346	96±2.34	83±7.94	0.173
Fluency	92±4.02	81±3.44	0.053	92±5.72	84±5.84	0.333
Visuospatial	100±0.6	102±0.92	0.040	100±1.54	101±1.01	0.211
Language	92±4.16	81±4.43	0.066	94±6.12	80±3.83	0.066
Attention	101±2.43	91±3.42	0.015	101±2.37	97±4.62	0.437

SDMT	63±3.27	52±2.51	0.010	64±2.49	53±3.47	0.020
DASS-21	10±1.76	36±5.95	0.000	8±1.67	23±4.57	0.006
Stress	6±1.29	17±2.54	0.001	5±0.82	15±2.71	0.003
Anxiety	2±0.53	10±2.07	0.000	1±0.41	5±1.27	0.004
Depression	2±0.34	10±1.94	0.000	2±0.97	6±1.81	0.044
MFIS	12.95±2.48	37.4±3.87	0.000	12±4.44	29±4.47	0.010
Physical fatigue	5±1.06	18.1±2.03	0.000	5±2.27	13.1±2.36	0.021
Cognitive fatigue	7.9±1.64	19.32±2.06	0.000	7±2.27	16±2.34	0.008

Data are expressed as mean values ± SEM. MFIS: Modified Fatigue Impact Scale; SDMT: symbol digit modalities test; DASS-21: depression anxiety stress scales; EDSS: expanded disability status scale; MSSS: multiple sclerosis severity score; ARCS: audio recorded cognitive screen.

#### 4.3.2 Morphology (whole brain and voxel characteristics)

There was a significant variation in the MRS voxel composition (GM, WM and CSF fractions) between HCs and MS patients using cross-sectional analysis, with a significant reduction in the WM fraction within the hippocampal voxel in the RRMS cohort at baseline (pre-DMF onset) compared to the HC group. We observed no significant difference at 24 months follow up post-DMF treatment start in voxel composition between HCs and MS patients. In addition, we saw no significant change in the total brain volume between the RRMS cohort and HCs at baseline and also at 2yrs (Table 2). Interestingly, within the RRMS cohort, longitudinal analysis showed the onset of DMF treatment had a significant impact on the WM voxel composition ( $F=2.65$ ,  $p=0.04$ ) up to 24 months post-treatment. We saw no significant change in the whole brain T2-FLAIR lesion load, during the 24-month DMF treatment period ( $F=1.24$ ,  $p=0.12$ ) (Table 2). There was no morphological changes during the 24-months DMF treatment period.

Annualised atrophy changes of PBVC were analysed for 13 RRMS patients at three time periods (T0 vs T12, T12 vs T24 and T0 vs T24), yielding  $-0.35±0.14$ ,  $-0.40±0.12$  and  $-0.55±0.19$ , respectively. No substantial change was observed in the average annualised rate of brain volume loss between 1<sup>st</sup> and 2<sup>nd</sup> year of treatment with DMF. PBVC which was analysed for the matched 13 HCs for only one time period (T0 vs T24), yielding  $(-0.19±0.11)$  significantly lower atrophy rate than that observed in the patient cohort.

Table 4-2. Mean values of spectroscopic voxel segmentation and volume of brain fractions for RRMS patients compared to HCs showing treatment effect across time points.

	Regions	HCs	MS baseline	T1	T6	T12	T24	HCs(2yrs)	F	<i>p</i>	
Sample size		N=20					N=13				
MRS voxel	CSF%	3.2±0.008	4.7±0.006	3.8±0.005	3.8±0.005	3.5±0.004	3.9±0.006	4.4±0.019	1.33	0.272	
	GM%	40±0.009	46±0.025	47.8±0.006	47.6±0.007	45±0.02	46.5±0.008 <sup>b</sup>	40.1±0.02	2.00	0.101	
	WM%	55.7±0.011	46±0.024 <sup>a</sup>	48±0.007	48±0.008	51±0.022	49.6±0.01	55.4±0.045	2.65	0.040	
	LV (mm <sup>3</sup> )	-	0.011±0.005	0.030±0.012	0.024±0.01	0.016±0.009	0.023±0.006	-	1.82	0.152	
Whole brain (mm <sup>3</sup> )	WBV	1623.3±27.4	1603.7±14.3	-	-	-	1601.2±16.5	1621.6±24.1	-	-	
	T2 lesion volume	-	4.9±0.9	4.83±0.88	4.82±0.98	4.7±0.98	4.7±0.98	-	1.24	0.120	

**a:**  $p \leq 0.001$  MS vs HCs at baseline, **b:**  $p \leq 0.01$  MS vs HCs at 2 year follow up. CSF: cerebrospinal fluid; LV(mm<sup>3</sup>): lesion volume within MRS voxel; GM: grey matter; MRS: magnetic resonance spectroscopy; T1:1 month of treatment; T6: 6 months of treatment; T12: 12 months of treatment; T24: 24 months of treatment; WM: white matter; WBV: whole brain volume.

### 4.3.3 MR Spectroscopy

Using single voxel 1D MRS, cross-sectional analysis identified a statistically significant reduction in hippocampal NAA (-13%,  $p=0.0001$ ) and increase in m-Ins (+9%,  $p=0.02$ ) in the total RRMS cohort at baseline, compared to HCs (Figure 4-3). In contrast, we did not observe any significant difference in the level of hippocampal Glx, Cr, tCho or GSH between the RRMS group at baseline compared to HCs (data not shown). When assessing only the cohort that was followed up (N=13), cross-sectional analysis showed no statistical significance ( $p>0.05$ ) in hippocampal metabolites (NAA, Glx, Cr, tCho, m-Ins and GSH) between the RRMS cohort (N=13) and matched HCs (N=13) at the 24 month time point. No statistically significant difference was observed in MRS data between HCs at baseline compared to HCs at 2yrs and between MS at baseline compared to MS at 2yrs.

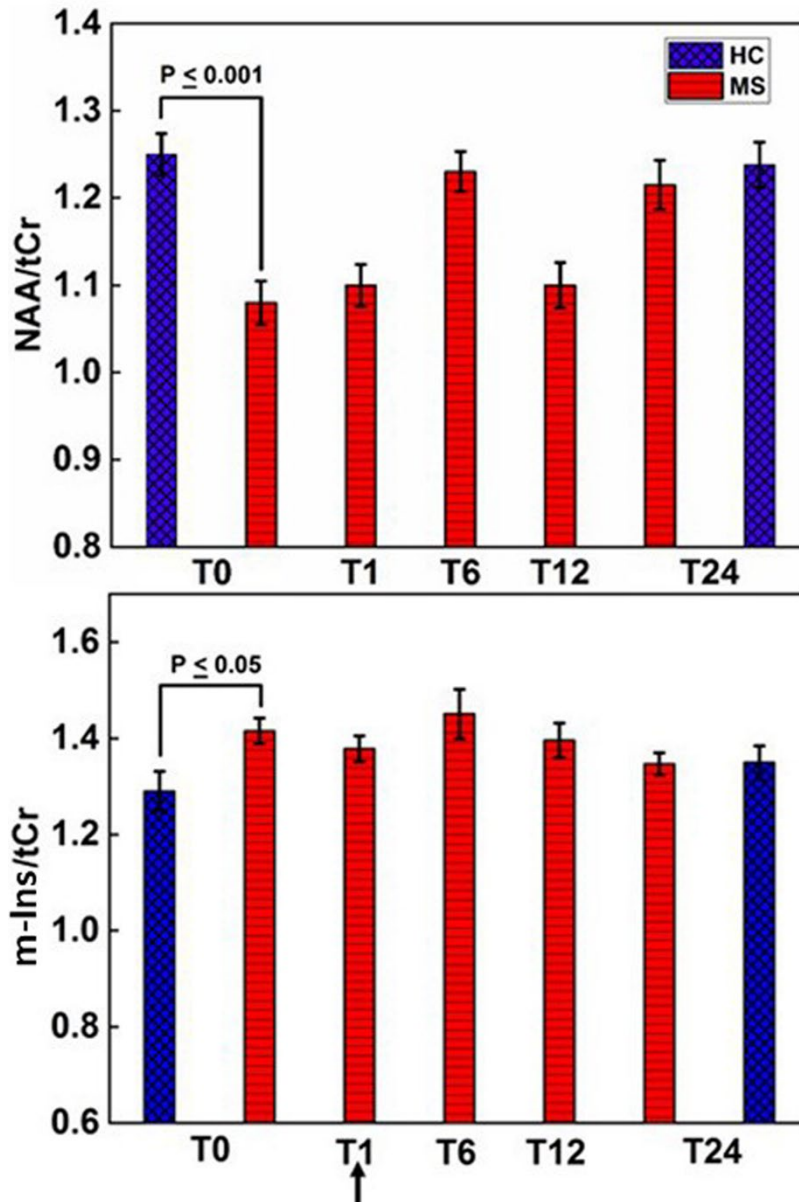


Figure 4-3. Neurometabolites levels (NAA, m-Ins) in RRMS compared to HCs at baseline and 2yrs follow up:with significant difference to total creatine (tCr) for healthy controls (HCs) and relapsing-remitting multiple sclerosis (RRMS) pre and post onset of treatment with DMF. T0: baseline; T1: 1 month of treatment; ↑: the time at which the therapeutic dose level was reached; T6: 6 months of treatment; T12: 12 months of treatment; T24: 24 months of treatment; m-Ins: myo-inositol; NAA: N-acetylaspartate.

Longitudinal analysis showed the onset of treatment with DMF did not significantly impact on the levels of hippocampal NAA, m-Ins, Glx, tCho or Cr in the RRMS group. However, as the DMF treatment progressed, the mean hippocampal GSH levels were altered significantly over the 24-month treatment period ( $F=3.5, p<0.03$ ) (Figure 4-4). Post hoc tests revealed that there was a statistically significant reduction of -28% in GSH levels from the baseline pre-treatment time point to T1 ( $0.6\pm0.061$  vs  $0.43\pm0.039, p=0.014$ ). This reduction remained

statistically significant at T6 ( $0.45 \pm 0.03$ ,  $p=0.035$ ), but slightly increased at T12 ( $0.48 \pm 0.045$ ,  $p=0.15$ ) and T24 ( $0.49 \pm 0.029$ ,  $p=0.18$ ) to approach levels seen in the HC group.

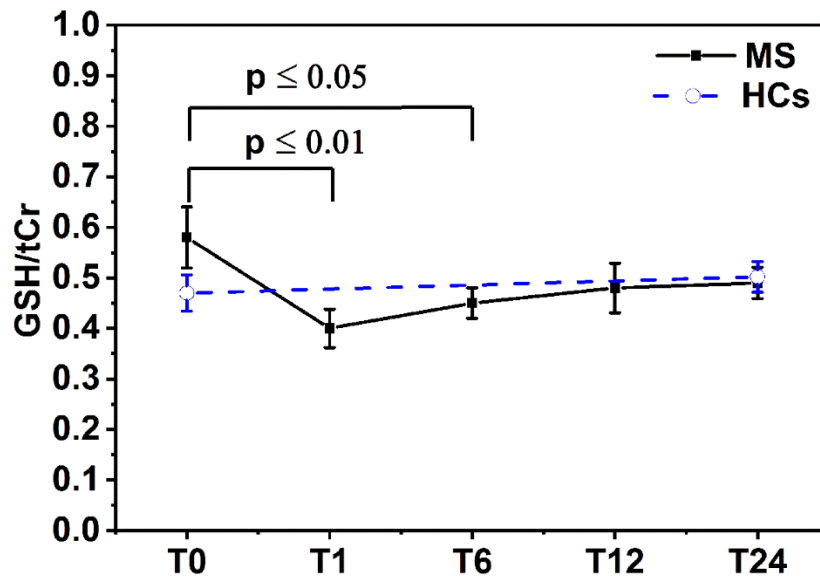


Figure 4-4. Pre and post treatment with dimethyl fumarate (DMF) effect on ratio of glutathione (GSH) to total creatine (tCr) levels in relapsing-remitting multiple sclerosis (RRMS) with healthy controls (HCs) as a reference line. T0: baseline; T1: 1 month of treatment; T6: 6 months of treatment; T12: 12 months of treatment; T24: 24 months of treatment.

#### 4.3.4 Correlation of metabolites with clinical and volumetric measures

We investigated associations between clinical symptoms and hippocampal metabolite levels at the baseline, 12-month and 24-month post-DMF treatment onset. The clinical symptoms that showed the strongest associations with hippocampal metabolite levels were related to mood status at T12 and T24 (Table 3). There was a positive correlation between the levels of hippocampal tCho, m-Ins and Cr with the overall severity of mood symptoms (total DASS-21 scores), as well as the levels for each domain, depression, anxiety and stress (Table 3), while Glx levels showed an association with anxiety levels. The cognitive domains evaluated by the ARCS displayed associations with hippocampal NAA only at T24, while processing speed and attention, determined by the SDMT, were negatively correlated with hippocampal m-Ins at T12. Other clinical symptoms that showed the associations with hippocampal metabolite levels were related to disability status, MSSS score, at baseline and T24 (Table 3). There was a positive correlation between the levels of hippocampal Glx and NAA with the MSSS score at baseline (Table 3), while Glx levels showed an association with duration of disease at baseline and T24.

There was evidence for hippocampal axonal integrity (NAA/tCr) to be negatively correlated with voxel CSF ( $r=-0.47$ ) as well as whole brain lesion volume score ( $r=-0.66$ ) at T12 and positively correlated with total brain volume ( $r=0.65$  and  $0.68$ ) at baseline and T12.

Table 4-3. Spearman's correlation between neurometabolites ratios and cognitive functions in RRMS across 24 month study period. Only statistically significant changes are listed.

Time points	Metabolite/tCr	Clinical parameters				
T0	Glx	EDSS	MSSS	D D	WM	
		-0.593*	0.663*	-0.754**	-0.577*	
	NAA		MSSS	WBV	WM	
			0.637*	0.657*	-0.654*	
T12	m-Ins	SDMT	DASS-21	Depression	Anxiety	Stress
		-0.551*	0.695**	0.634**	0.687**	0.549*
	tCho		DASS-21	Depression	Anxiety	Stress
			0.554*	0.543*	0.647*	0.540*
	Glx				Anxiety	
					0.499*	
T24	Cr		DASS-21	Depression		Stress
			0.691*	0.639*		0.631*
	m-Ins			D D		
				0.595*		
	Glx			D D		
				-0.572*		
	NAA	TARCS	Attention			
		0.624*	0.626*			

\*  $p \leq 0.05$ ; \*\*  $p \leq 0.01$ . Cr: creatine; DASS-21: depression anxiety stress scales; D D: disease duration; EDSS: expanded disability status scale; Glx: glutamate+glutamine; NAA: N-acetylaspartate; m-Ins: myo-inositol; MSSS: multiple sclerosis severity score; SDMT: symbol digit modalities test; TARCS: total audio recorded cognitive screen; tCho: total choline; T0: baseline; T12: 12 months of treatment; T24: 24 months of treatment; WBV: whole brain volume; WM: white matter.

#### 4.4 Discussion

Our cohort of 20 RRMS patients was clinically stable while undergoing treatment with DMF. The hippocampus is involved in learning and memory function and has the highest degree of neuroplasticity in the brain, with regional neurogenesis occurring throughout adult

life. In MS, changes in hippocampal proliferation, lesion load, volume and connectivity have been associated with alterations in cognitive and mood function in the EAE mouse model of MS<sup>210</sup> and in MS patients<sup>211</sup>. Despite their relatively short disease duration and low disability score, our RRMS cohort displayed cognitive impairment, evidenced by poorer visuospatial, fluency and attention scores, as well as lower overall performance scores on the ARCS than the HCs. Similarly, the RRMS cohort had worse attention and processing speeds in comparison to HCs, resulting in lower SDMT scores. Our study demonstrated no statistical change in the level of clinical symptoms, EDSS, MSSS for the study periods (T0-T12 and T12-T24) while being treated with DMF over the two years. These results cannot be interpreted as supportive of predicting reduction of progression of disability later on. However, the protective value of treatment on disability may be evident when evaluated over a longer period of time.

In spite of the fact that the whole brain lesion load was low in our patient group, our findings indicated a reduction in total brain volume and partial GM volume within the hippocampal voxel, compared to healthy controls in cross-sectional and longitudinal studies. Reduction in brain volumes have been correlated to an increase risk of disease progression rates and decrease of treatment effect in MS<sup>212</sup>.

Previous literature<sup>213</sup> reported a faster rate of atrophy in MS patients (0.5–1.35% per year) compared to age-matched HCs (0.1–0.3% per year), which is consistent with our annual PBVC value of -0.4 and -0.55 for RRMS cohort and -0.19 for HCs group over 2 years. Therefore, the average annualised rate of brain volume loss over 2 years while receiving treatment with DMF, might suggest an effect of DMF on brain volume, which was described in the pivotal trials<sup>214</sup>. A lower rate of brain volume loss has been associated with benefit on disease progression in MS<sup>215</sup>.

Using single voxel MRS, we confirmed the importance of NAA and m-Ins as indicators of axonal loss and gliosis<sup>216</sup>. We found a significant reduction in hippocampal NAA and an increase in m-Ins in RRMS in comparison to age and sex-matched healthy individuals in the cross-sectional analyses. Furthermore, these changes were associated with morphological changes within the brain including increased CSF volume, total brain volume loss and T2 lesion volume. The use of NAA as a marker of neuronal integrity was further supported by the reduction in NAA levels associated with an 18% lower white matter content in the hippocampal voxel compared to that seen in the same region in healthy controls. Indeed, others have shown an increase in white matter NAA content following treatment with MS disease-modifying therapy<sup>217</sup>. Reduced level of NAA in the grey matter of MS patients has also been recently

demonstrated<sup>155</sup> further supporting the importance of NAA as disease marker. Increased levels of m-Ins have been detected by others in the CSF from MS patients<sup>218</sup> and also in the T1-weighted hypo-intense chronic MS lesions<sup>219</sup>, the latter thought to be associated with astrogliosis around the lesion<sup>68</sup>.

Administration of DMF did not result in changes in the levels of NAA and m-Ins during the 24-month treatment period. This may suggest that hippocampal neuronal integrity and the level of microglial gliosis was not significantly impacted on during this time frame consistent with no significant change in clinical parameters over this time period.

There were no metabolic changes in the HCs brain between baseline and 2 years follow up. This confirmed the reliability of the MRS technique, and that changes observed in the MS cohort are clinically meaningful.

We observed a trend for higher hippocampal GSH in the RRMS group at baseline compared to the HCs. However, the variability in these levels was high and hence it did not reach significance. This finding may suggest a variable level of oxidative status in the hippocampus within our RRMS cohort, at the pre-treatment onset time point, although none of the patients had received disease modifying therapies within the preceding month, or steroid treatment in the preceding three months.

A significant reduction in GSH levels in the fronto-parietal region has been reported by others in secondary progressive MS patients compared to RRMS<sup>200</sup>. The same study also reported a trend for reduced levels of GSH in this same region in RRMS compared to HCs. We know that our hippocampal voxel was comprised of approximately equal portions white and grey matter, with an increase of WM fraction during the duration of our study, however, the cellular source of the GSH cannot be determined with certainty. Others have shown at 7T, a differential reduction of GSH in the grey matter of MS patients, with no impact on white matter GSH<sup>196</sup>. In studies where reduced levels of GSH in progressive MS have been shown<sup>200</sup>, spectral editing techniques were applied to optimize GSH localisation, this differed in our study in which we have undertaken a series of *in-vitro* scans, using GSH phantoms, to validate our LCModel post-processing quantification techniques, to confirm an accurate measurement of GSH.

It has been hypothesized that a possible mode of action of DMF is by its anti-oxidative effects via modulation of GSH activity<sup>195, 220</sup>. This has been illustrated *in-vitro*<sup>220</sup> following DMF administration, however, the current study is the first *in-vivo* investigation of the impact of DMF treatment on hippocampal GSH metabolism in MS patients. We saw an initial decline

in GSH levels during the first month of treatment. It should be noted that the dosing regimen for DMF involves a weekly dose escalation over a 4 week period, until the recommended therapeutic level (480mg daily) is achieved. Between the first and 24 months of treatment, we observed an increasing trend for GSH levels within the hippocampus, approaching that seen in age and sex-matched healthy controls. Although not conclusive, our findings do support *in-vitro* studies which have demonstrated an increase in GSH levels in astrocytes following addition of DMF <sup>220</sup>. A corresponding decreasing trend in lesion volume within the voxel was observed during this period but did not reach significance. It may be warranted to investigate a longer DMF treatment period in a larger cohort to determine an association between hippocampal GSH levels and treatment efficacy, but our study suggests that GSH is a more sensitive marker than morphological changes.

We saw a correlation between attention and processing speed, with an increase in hippocampal m-Ins levels over 12 months. This may suggest an increase in hippocampal gliosis with altered cognitive function in our MS cohort. It also indicates that hippocampal m-Ins levels may be a surrogate marker for cognitive function, although larger longitudinal studies are warranted to verify this association. The cognitive domains evaluated by the ARCS displayed associations with hippocampal NAA of RRMS at T24 only. This result is consistent with previous study<sup>216</sup> that showed that decreasing NAA correlated with cognitive dysfunction as well as with disability in RRMS patients using H-MRS. We have recently shown that there is a complex interplay between mood disorders such as depression, anxiety and stress with cognitive performance evidenced by lower ARCS scores in RRMS <sup>221</sup>.

Using Positron emission tomography (PET) imaging, Colasanti et al.<sup>222</sup> have demonstrated hippocampal microglial activation to be associated with brain connectivity and depressive symptoms. Changes in connectivity with the hippocampus have also been demonstrated in depressed MS patients with alterations being more prominent in depressed compared to non-depressed patients <sup>223</sup>. As expected, the DASS self-report questionnaire confirmed higher levels of depression, anxiety and stress in the RRMS cohort compared to HCs. We also observed an association between m-Ins, tCho and Cr levels with mood symptoms at T12 and T24. This may represent an increase in gliosis in the hippocampus with increased depression, anxiety and stress symptoms in our cohort.

Despite not detecting any alterations in hippocampal Glx levels, we did observe a positive correlation between hippocampal Glx and anxiety at T12, and between Glx and MSSS levels at baseline. However, Glx was negatively correlated with disease duration at baseline and T24,

and with EDSS at baseline. Glx correlation with EDSS level at baseline has been reported by Chard et al. in normal appearing white matter and normal appearing cortical grey matter<sup>150</sup>. However, no correlation between Glx and disease duration was found by Chard et al. Others have demonstrated altered levels of glutamate (Glu) in multiple sclerosis, although regional variations have been noted<sup>40</sup>. Elevation in Glu has been observed in white matter lesions but not in normal appearing white matter<sup>97</sup> while in the hippocampus, a depletion in Glu and Glx was measured<sup>40</sup>, which was in turn shown to be associated with visual and verbal memory impairment. The underlying pathophysiological and metabolic changes associated with MS anxiety have not been evaluated as extensively as those for MS depression. Further studies are needed to fully appreciate the relevance of a link between hippocampal Glx and anxiety in MS.

This study is the first to illustrate a change in hippocampal metabolism associated with the onset of treatment with DMF in RRMS patients. However, there are a number of limitations to this study. The findings are preliminary and need to be confirmed in a larger patient cohort over an extended treatment period to enable longer term impacts of DMF on disease outcomes and metabolic changes to be more fully explored. In the current study we did not employ spectral editing schemes to optimize detection of GSH as utilized in other studies which have investigated the changes in GSH associated with MS<sup>196, 224</sup>. We have instead, undertaken a series of *in-vitro* investigations to support the validity of spectral post-processing and quantification using LCmodel for our MRS spectral analysis.

## **4.5 Conclusion**

This study demonstrated that MRS is a sensitive marker of disease activity with several metabolites correlated with clinical parameters, but also capable to detect a treatment effect prior to volumetric change. We have shown that treatment with DMF may impact on hippocampal metabolism, specifically glutathione levels, which supports its assumed antioxidant mode of action, resulting in an anti-inflammatory effect in the MS brain following DMF treatment.

## **Acknowledgements**

The authors thank the patients and controls who participated in this study and the Imaging Centre of the University of Newcastle and Hunter Medical Research Institute.

## **Funding**

Independent investigator- initiated grant provided by Biogen Pharmaceuticals Pty Ltd.

### **Availability of data and materials**

Availability of data and materials are subject to guidelines of local Hunter New England Local Health District Human Research Ethics Committee.

### **Authors' contributions**

OA has been involved in writing, compiling and revising the manuscript critically to suit publication standards. JLS, KR, RL and SR contributed significantly on study design, data collection, revising, literature and critical suggestions to reshape the manuscript. All authors read and approved the final version of manuscript.

### **Ethics approval and consent to participate**

This study was approved by Institutional Review Board from the Hunter New England Local Health District Human Research Ethics Committee (HNEHREC Reference No: 4/09/10/3.01), Newcastle, NSW, Australia.

### **Consent for publication**

Written informed consent was obtained from the patients/healthy subjects for publication of their individual details and accompanying images in this manuscript. The consent forms are held by the corresponding author in the patients' clinical notes and is available for review by the Editor-in-Chief upon request.

### **Competing interests**

OA, KR, RL and SR have no competing interests. JLS has accepted travel compensation from Novartis, Biogen and Merck. Her institution receives the honoraria for talks and advisory board commitment and as well as research grants from Biogen, Genzyme Sanofi, Merck, Novartis, Roche and TEVA.

## **Chapter 5 : Effect of dimethyl fumarate (Tecfidera) on microstructure and biochemistry in the brain of MS patients**

Oun Al-iedani, Karen Ribbons, Saadallah Ramadan, Jeannette Lechner-Scott

### **ABSTRACT**

The effect of dimethyl fumarate (DMF) in MS is thought to be partly due to its anti-oxidative properties. However, its impact on neurometabolite profiles and anti-inflammatory status of the brain has not been evaluated. In this study, non-invasive atrophy measures and one-dimensional proton magnetic resonance spectroscopy (1D H-MRS) were acquired from the pre-frontal cortex (PFC) and posterior cingulate gyrus (PCG) to quantify neurometabolite changes in RRMS patients compared to healthy controls (HCs) and evaluate the metabolic impact of DMF treatment longitudinally over 24 months. H-MRS was undertaken on 20 RRMS patients, who were predominantly female and early in their disease course with mild disability (EDSS  $2\pm 0.18$ ), prior to and up to 24 months post-inception of DMF treatment and 20 age and sex-matched HCs. Spectroscopic data were acquired from the PFC and PCG (3.375ml and 27ml, PRESS, TE 30ms) at 3 Tesla. Using 1D H-MRS, we identified a significant reductions in PFC N-acetylaspartate/tCr (NAA/tCr, -6%,  $p= 0.05$ ) and PCG glutamine+glutamate/total creatine (Glx/tCr, -9%,  $p=0.001$ ) and increased PFC total choline (tCho/tCr, +13%,  $p=0.02$ ) in RRMS patients, before starting DMF, compared to HCs. Following treatment, Post hoc tests revealed that PFC NAA levels significantly increased over 12 months in the RRMS group ( $F=2.6, p<0.05$ ), but stabilised and didn't significantly change between 12 and 24-month period ( $p=0.1$ ). Also, PCG NAA ( $F=3.95, p=0.02$ ) and tCho/tCr ( $F=3.47, p=0.03$ ) levels were altered significantly over the 24-month treatment period. This study demonstrated that several metabolites evaluated by 1D H-MRS represent sensitive markers of MS disease activity. Further studies with longer treatment durations are warranted to investigate the impact of DMF on metabolic changes in the MS brain and their association with disease activity.

## 5.1 Introduction

There has been a fundamental shift in treatment goal for multiple sclerosis. Newer treatments have not only shown the reduction of relapse rate and T2 lesion load but also brain atrophy, which seems to be more related to long term disability<sup>225</sup>. Conventional MRI techniques have been the main imaging tool for diagnosis as well as on-going monitoring for MS pathology<sup>4</sup> reflecting inflammatory activity via T2 lesions and brain damage via atrophy measurements.

MRI is an important tool for monitoring the efficacy of disease-modifying treatments and has been used as secondary outcome measure for most treatment trials predominantly focusing on lesion load and contrast enhancement. Conventional MRI has demonstrated the efficacy in the use of glatiramer acetate (GA), interferon (IFN)-b, and natalizumab in RRMS to reduce MRI disease activity<sup>226,227</sup>. However, there are several disadvantages to this technique. Firstly, MRI features of MS are not specific to its pathological substrates which contribute to the development of permanent disability. MRI is not able to quantify the damage in normal appearing white matter and to detect and quantify damage to grey matter. Also, the clinical manifestation of MS plaques in different anatomical locations such as spinal cord and optic nerves are variable.

Advanced MRI techniques such as magnetic resonance spectroscopy, capable of exploring the metabolic changes of the MS brain, are described as a non-invasive virtual biopsy with the potential to provide biomarkers for early detection and monitoring of disease progression. This technique may allow a better understanding of the pathophysiology of the symptoms and aid in the development of new treatments. Some treatment efficacy studies have used H-MRS to assess changes in the metabolic profile of the MS brain to investigate if drug therapies can reverse or prevent the progression of neuronal injury<sup>228, 229</sup>. Studies such as Sarchielli et al, Khan et al and Schubert et al have explored the treatment efficacy of IFN and GA therapy using H-MRS<sup>228, 230-232</sup>. Interferon studies have demonstrated conflicting results of improvement or stabilization to little effect on NAA. Khan et al found that NAA/Cr increased significantly with GA compared with control group, and suggested that this may be due to axonal metabolic recovery<sup>230, 233</sup>.

H-MRS, however, hasn't been used to assess cross-sectional and longitudinal effects of disease-modifying treatment such as dimethyl fumarate (DMF). DMF is a disease-modifying treatment for relapsing-remitting MS (RRMS). Due to its neuroprotective and

immunomodulatory effects, it seems to protect neural stem cells from oxidative stress through the activation of nuclear factor erythroid-2-related factor (Nrf2) transcriptional pathway<sup>234</sup>. Two major DMF studies demonstrated its effect on reducing relapse rate and delay disease progression as well as significant reduction of new lesion formation and brain atrophy<sup>235, 236</sup>.

H-MRS is a sensitive method to detect the pathological process within the MS brain and different tissue types (MS lesion, grey matter and NAWM). Brain metabolites differ within the MS lesions, NAWM and grey matter in various brain regions such as hippocampus, cortex and sub-cortical regions<sup>28, 41, 42, 76, 237</sup>. These studies confirmed decreased levels of NAA and choline and increased m-Ins in NAWM and cortex regions and indicated brain tissue loss and clinical progression of MS. Furthermore, NAA and NAA/Cr ratio showed decreased levels in WML compared to NAWM regions<sup>144</sup> suggesting axonal loss but dilution due to increased water content may cause smaller changes<sup>67, 238</sup>. Decrease in NAA correlates with EDSS and increased m-Ins in chronic lesion was found to be associated with gliosis<sup>68, 154, 216</sup>. Another H-MRS study showed increased Glu concentration in MS lesions and NAWM, which may be due to glutamate mediated excito-toxicity. This study found that increased Glu levels was positively correlated with visuospatial memory, hippocampal, thalamic and cingulate regions. The development of novel and non-invasive MR techniques such as H-MRS enables monitoring of a number of chemical entities in the MS brain, including glutathione (GSH)<sup>39, 159</sup>. Some found a positive association between the levels of GSH in this region with cognitive function, including memory and processing speed<sup>200</sup>.

The objective of this study is to evaluate the amount of axonal injury and brain metabolites in relapsing-remitting MS patients compared to healthy controls using H-MRS technique, to detect pathology early and treat appropriately to prevent long term disability. Firstly, an MS cohort was studied in a cross-sectional manner compared to age and sex matched healthy controls at baseline. The scan was repeated at two years follow up. An open-label longitudinal observational study was conducted to evaluate the impact of DMF treatment on the pre-frontal cortex (PFC) and posterior cingulate gyrus (PCG) metabolic profile at pre and post treatment onset at four time points. Lastly, the correlation between brain metabolites and severity of clinical and neuropsychological symptoms was analysed at three time points at baseline, 12 and 24 months following the initiation of DMF treatment in two regions; PFC and PCG.

## 5.2 Methods

### 5.2.1 Patients and Healthy Control Subjects

Twenty patients with confirmed RRMS, in accordance with the McDonald criteria<sup>17</sup>, aged between 20 to 55 years, who were considered eligible to commence DMF treatment by their treating neurologist, were included in this study. HCs (N=20) were age ( $\pm 2$  years) and sex-matched to the RRMS cohort. Out of the remaining 20 RRMS patients, 7 could not be evaluated at 2 years due to various reasons such as pregnancy, having stopped DMF due to side effects or patient's choice.

All patients were recruited from the John Hunter Hospital, Newcastle, Australia, MS outpatient clinic. Age and sex-matched HCs were derived from the Hunter Medical Research Institute (HMRI) research register and needed to comply to the study inclusion criteria, which included passing an MRI safety clearance, as well as being able to comply with all study procedures. Institutional Review Board approval was obtained from the Hunter New England Local Health District Human Research Ethics Committee, with written informed consent obtained from all subjects prior to undertaking any study-related procedures. All scans were conducted between December 2015 and March 2018.

### 5.2.2 Study design

In the RRMS cohort, an open-label longitudinal observational study was conducted to evaluate the impact of DMF treatment on the PFC and PCG metabolite profile. We also conducted cross-sectional evaluation prior to and at 24 months post DMF treatment inception, between RRMS patients and HCs. MRI/H-MRS data was acquired from the RRMS cohort at five different time points; baseline (T0, pre-DMF onset), 1 month (T1), 6 months (T6), 12 months (T12) and 24 months (T24) post inception of DMF treatment onset. HCs were scanned at baseline and 24 months. DMF dosing was escalated over the first month of treatment, to achieve a therapeutic dose of 480 mg/day according to the following regime: 120 mg/day week 1, 240 mg/day week 2, 360 mg/day week 3 and 480 mg/day from week 4 onwards.

### 5.2.3 Binary mask for the voxel segmentation

A binary mask of an MRS voxel  $1 \times 1 \times 1 \text{ cm}^3$  for PFC and  $3 \times 3 \times 3 \text{ cm}^3$  for PCG regions (Figure 1) was created using the “mask()” function within the SPM toolbox. To determine the fractional quantities of GM, WM and CSF within MRS voxels, partial volume masks for each tissue types were created using FSL FAST (Figure 5-1) as described by Quadrelli et al. for single voxel segmentation<sup>203</sup>. These masks were overlaid onto the high-quality T1-

MPRAGE structural images. For accuracy in the MRS voxel re-positioning, during longitudinal re-assessment, MPRAGE data was reconstructed into 1mm coronal and axial slices on the scanner.

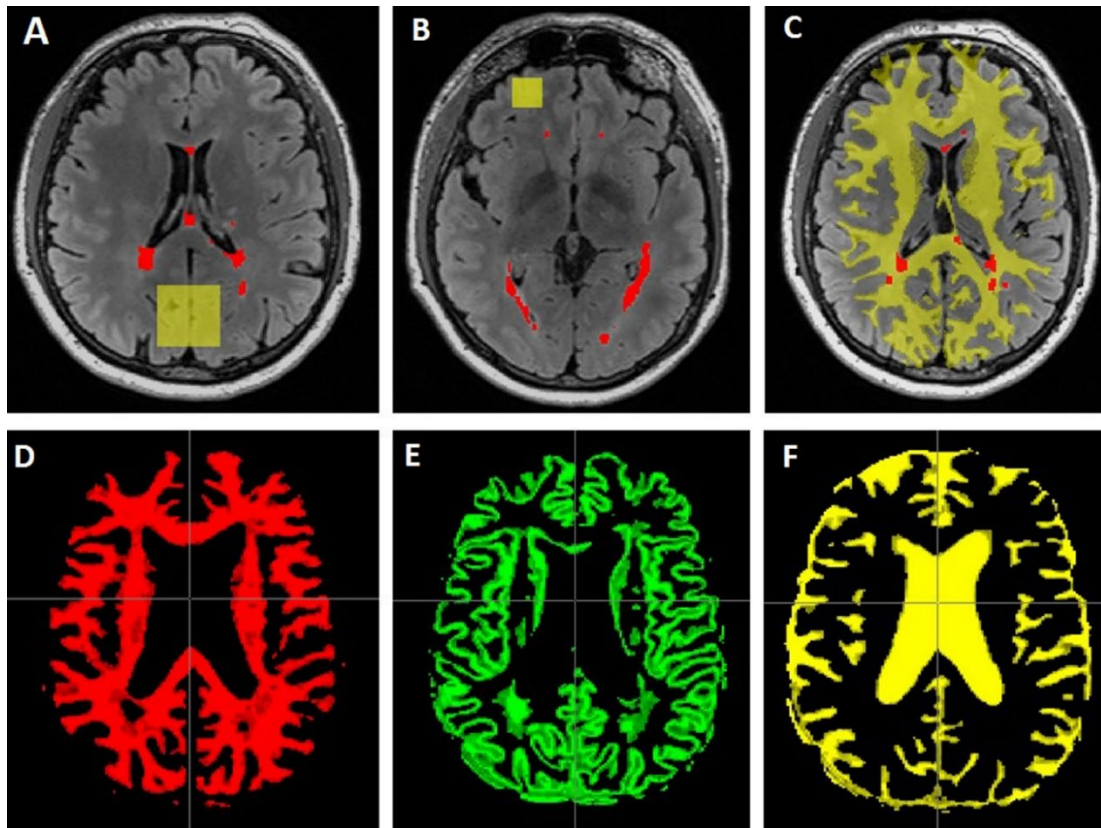


Figure 5-1. Reconstructed MRS voxels displayed as a mask overlying the T2-FLAIR images from a RRMS patient showing lesion map (red colour pixels), (A) PCG mask, (B) PFC mask and (C) lesion map on global white matter. The results of partial volume segmentation using FSL FAST produced (D) WM mask, (E) GM mask, and (F) CSF mask.

#### 5.2.4 MRI Acquisition and Structural assessments

All MRI/H-MRS scans were undertaken on a 3T Prisma (Siemens Healthineers, Erlangen, Germany) MRI scanner equipped with a 64-channel head and neck coil located at the HMRI, Newcastle, NSW, Australia. Experimental parameters of the three-dimensional isotropic T1-weighted Magnetization-Prepared Rapid Gradient Echo (MPRAGE) were as follows; sagittal orientation, TR/TE/TI=2000/3.5/1100 ms, 7° flip angle, field of view (FOV) =256x256 mm, pixel size =1x1x1 mm<sup>3</sup>, NEX=4 and acquisition time =5 minutes. Three-dimensional T2 FLuid-Attenuated Inversion Recovery (T2-FLAIR) sequence, TR/TE/TI =5000/386/1800ms, 12° flip

angle, FOV=256x256 mm, pixel size=1x1x1 mm<sup>3</sup>, echo train duration=858ms, NEX=1 and acquisition time=4 minutes.

Brain and skull images were extracted from the whole brain T1 3D MPRAGE data using SIENAX<sup>239</sup>. The brain image was co-registered to MNI152 space<sup>240, 241</sup> to determine the volumetric scaling factor to normalise for head size (Figure 5-2). Total brain volume, including grey matter (GM), white matter (WM), peripheral grey matter and ventricular CSF volumes were calculated with partial volume estimation in FSL FAST<sup>242</sup>.

Longitudinal annualised atrophy changes in percentage brain volume change (PBVC) for 13 RRMS patients in baseline, T12 and T24 were assessed using SIENA<sup>201</sup>.

LST toolbox<sup>243</sup> was used to generate an initial binary lesion map along voxels that are hyperintense in the T2-FLAIR image, resulting in a lesion probability map with a threshold of 0.1. This was followed by lesion filling within the T1 MPRAGE, using the binary lesion mask for each participant and a threshold of 0.5. This minimises errors in partial volume segmentation and improves the final volume measurements<sup>244</sup>. Partial volume segmentation of the lesion filled T1 structural image was segmented using FSL FAST (Battaglini *et al.*, 2012). Lesions within the MRS voxel were segmented using the lesion growth algorithm described by Quadrelli *et al*<sup>203</sup>.

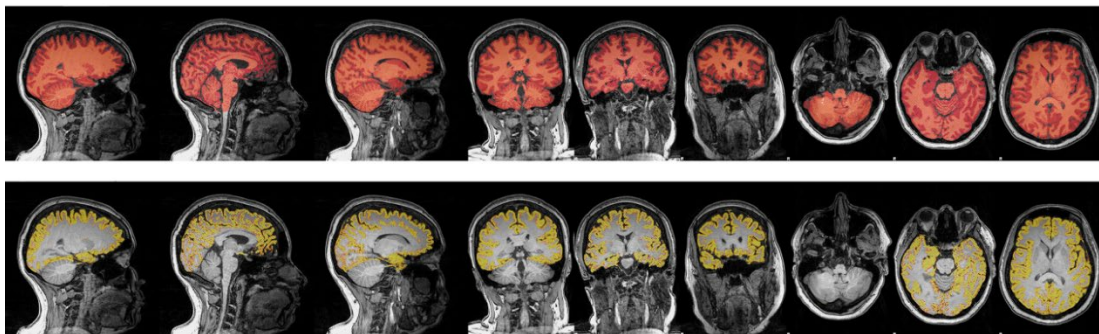


Figure 5-2. Brain tissue volume, normalised for subject head size, was estimated with SIENAX. Final SIENAX segmentation results of whole brain (top row) and peripheral cortex masked segmentation (bottom row).

### 5.2.5 H-MRS Acquisition, Post-Processing and Analyses

One-dimensional (1D) H PCG and PFC H-MRS was applied using a Point RESolved Spectroscopy (PRESS) sequence at short echo time, acquired from the regions of interest (ROI), as shown in Figure 5-3.

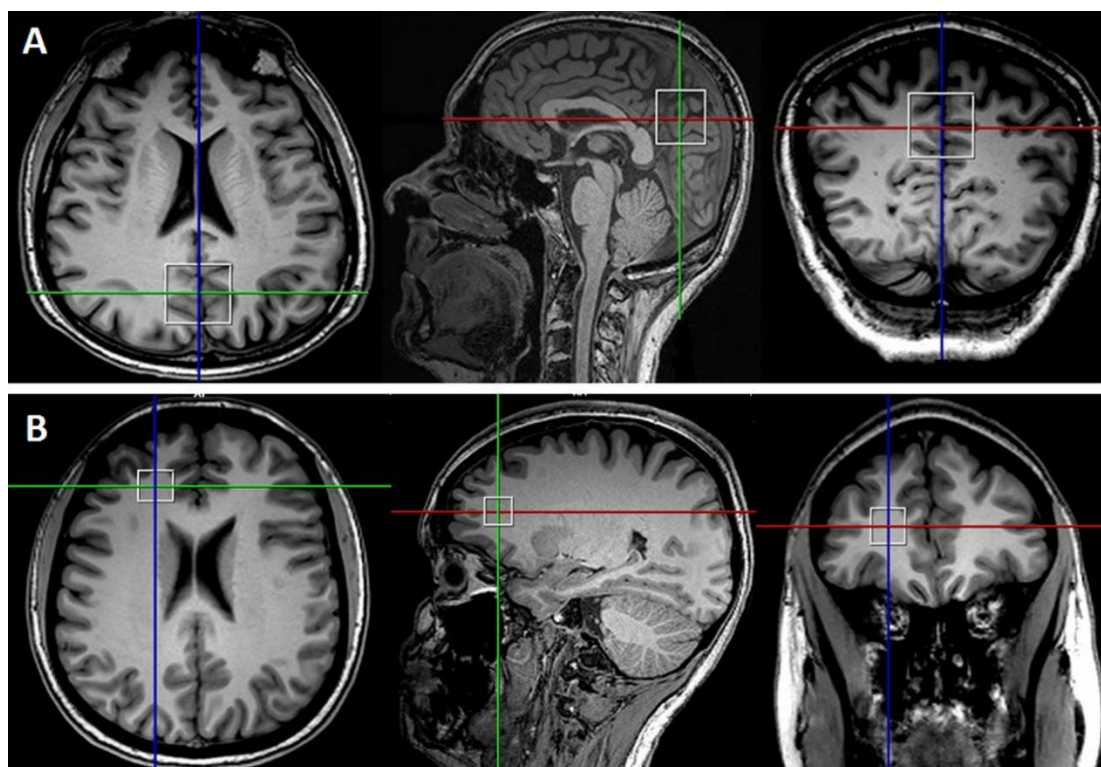


Figure 5-3. T1-weighted MR images in coronal, sagittal and axial planes demonstrating the (A) PCG and (B) PFC voxels size and position (white box).

The following parameters were used: TR/TE=2000/30ms, PFC voxel size = $15 \times 15 \times 15 \text{ mm}^3$ , PCG voxel size = $30 \times 30 \times 30 \text{ mm}^3$ , averages = 96, vector size = 1024 points, preparation scans = 4, RF offset frequency = 3.2 ppm and water suppression was enabled. Water reference was also acquired (4 averages) from the same voxel position and size after disabling RF part of water suppression module.

Single voxel 1D H-MRS was transferred offline and analysed with LCModel using a basis set specifically designed for 3T and TE=30ms with water normalization. This technique allowed the estimation of overlapping resonant metabolites such as glutamine+glutamate (Glx) at short TE. A water reference scan was used for eddy-current correction as well as partial volume correction in LCModel by adjusting ‘WCONC’ parameter based on percentages of

WM, GM and CSF as described in the LCModel manual. Concentrations of the brain metabolites were expressed as a ratio with respect to total creatine (creatine (Cr)+phosphocreatine (PCr) = tCr) with Cramer-Rao lower bound (CRLB (SD %)) less than or equal to 20% accepted. Samples of *in-vivo* MR spectra from PFC and PCG analysed by LCModel are shown in Figure 5-4.

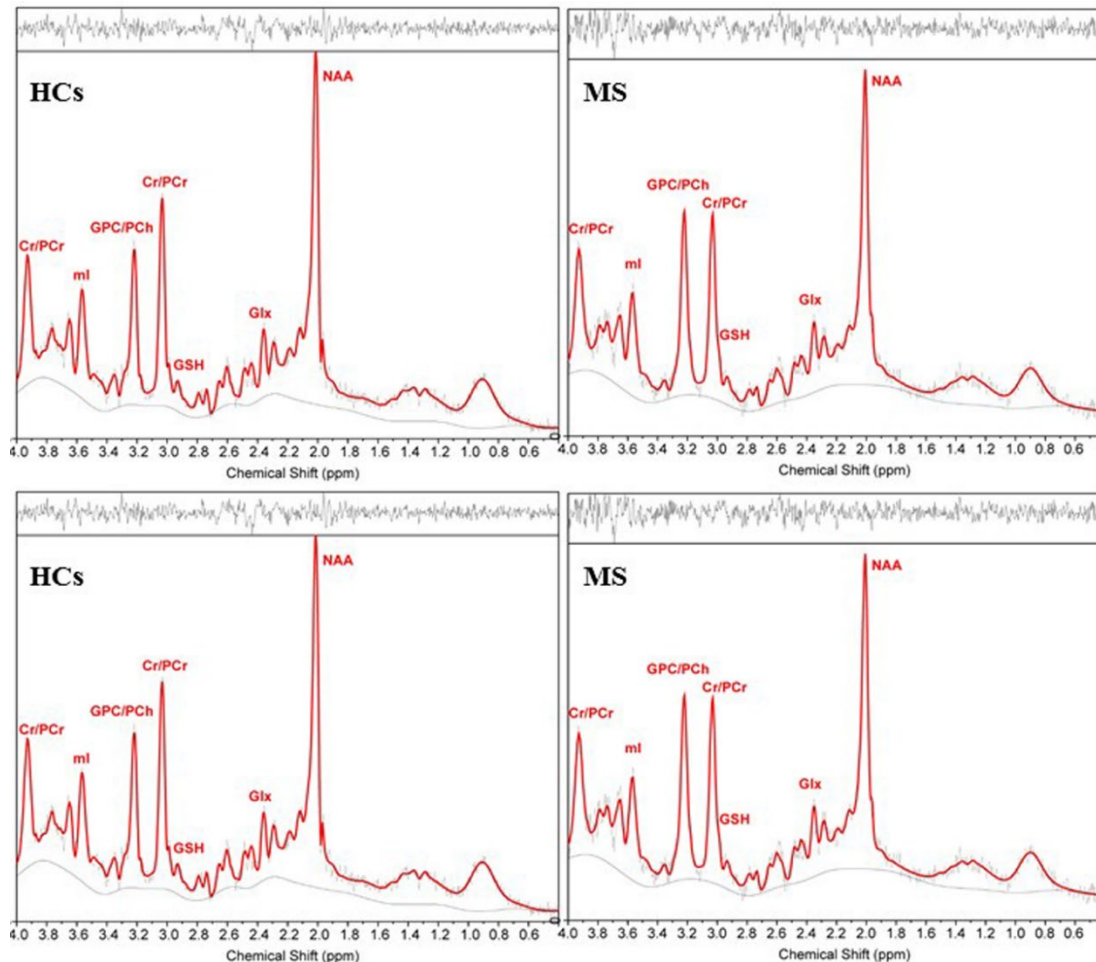


Figure 5-4. Samples of *in-vivo* MR spectra from PFC (top) and PCG (bottom) regions analysed by LCModel indicating the major brain metabolites at 3T and short TE (30ms).

### Quality Control

Maintenance of quality control for MRI and H-MRS data was carried out by weekly scanning of the American College of Radiologists (ACR) phantom and spherical GE spectroscopic phantom<sup>165</sup> containing stable brain metabolites at physiological pH and concentrations.

### 5.2.6 Clinical Assessments

All patients underwent a comprehensive neurological examination for disability status. Disability status was evaluated in the RRMS group, prior to and at 12 and 24 months following the inception of DMF treatment, by applying the Expanded Disability Severity Scale (EDSS). EDSS is the most common tool used to evaluate the classification of disability in MS patients. It allows neurologists to assign a Functional System Score (FSS) to 7 values including Pyramidal, Cerebellar, Brainstem, Sensory, Bowel and Bladder, Visual, Cerebral. All EDSS evaluations were performed by a neurologist who had undertaken appropriate neuro status certification training. The Multiple Sclerosis Severity Score (MSSS) was calculated using the EDSS and duration of disease for each patient according to the algorithms provided by Roxburgh et al.<sup>207</sup>.

Similarly, all study participants (RRMS and HCs) were assessed for cognitive performance at baseline, 12 and 24 months using the Audio Recorded Cognitive Screen (ARCS), which is a valid and reliable instrument for administering neuropsychological tests of cognitive function to unsupervised individuals<sup>13</sup>. The ARCS assesses the performance in the domains of memory, verbal fluency, language (object naming), visuospatial function and attention with elements from each domain given a score which is used to derive an overall ‘global’ cognitive performance score. Studies to date indicate that elements of the ARCS have good to excellent test-retest characteristics and generate results that correspond closely to those obtained with conventional administration of the same tests in an alternate form. The verbal new learning/memory test component of the ARCS demonstrates excellent concurrent validity against the well-characterised Rey Auditory Verbal Learning Test and the HAT-B component of the ARCS provides a valid measure of executive functioning.

The Symbol Digit Modalities Test (SDMT) was undertaken concurrently as a measure of attention and information processing speed presented in the visual modality. As described by Drake et al.<sup>245</sup>: “Patients view a key presenting nine numbers paired with unique symbols. Below the key is an array of symbols paired with empty spaces, the patient’s task being to voice the matching number for each symbol as rapidly as possible.”, the SDMT has been shown to be an appropriate screening tool for evaluating cognitive impairment in MS patients<sup>245, 246</sup> that is comparable to other psychometric and questionnaire methods.

The mental health status of participants was assessed using the short version of the Depression Anxiety Stress Scale (DASS-21)<sup>208</sup>. Higher scores were indicative of higher levels

of depression, stress and anxiety. All scores, derived from the 21-point scale, were multiplied by 2 to enable comparison to the full 42-point scale DASS and determine clinical cut offs for symptom severity.

Fatigue status was determined using the Modified Fatigue Impact Scale (MFIS), a modified form of the Fatigue Impact Scale<sup>209</sup>. The questionnaire was based on items derived from interviews with MS patients concerning how fatigue impacts their lives. This instrument provided an assessment of the effects of fatigue in terms of physical and cognitive functioning.

### **5.2.7 Statistical Analysis**

To investigate the significant difference between MS and HCs groups, T-tests were applied using SPSS, for independent and paired sample analyses. Major brain metabolites (NAA, Cr, total choline (tCho), m-Ins, GSH and Glx) were analysed from MS patients and HCs at different time points. The level of significant change in metabolite levels associated with onset of DMF treatment was assessed using repeated measures ANOVA, adjusted for appropriate covariates, followed by post hoc testing using Least Significant Difference (LSD). Additionally, the correlation between clinical symptoms and metabolite levels was performed using the correlation coefficient for non-parametric correlations (Spearman's rho).

## **5.3 Results**

### **5.3.1 Participant demographics and characteristics**

All of the 20 recruited RRMS patients met the enrollment criteria. Patients were predominantly female, early in their disease course with mild disability (EDSS 2±0.18) (Table 5-1). Cross-sectional evaluation showed significant differences in severity of mood symptoms, fatigue status and cognition impairment in the RRMS patients compared to age and sex-matched HCs at baseline and at two years (Table 5-1). There were no significant changes in levels of clinical symptoms for HCs during the 24-months period (baseline and 24 months) (Table 5-1). Reliable data were obtained from HCs and MS participants at each time point. Additionally, using repeated measures of ANOVA, longitudinal analysis (DMF treatment effect) showed that no statistical change was observed in the level of any clinical symptoms, EDSS, MSSS and disease duration for DMF treatment for 13 RRMS patients at three time points (T0, T12 and T24) over the two years ( $p>0.4$ ,  $F<0.7$ ). We observed no statistical changes in the level of severity of disability at DMF treatment onset and at the 24 months post-DMF treatment.

Table 5-1. Cross-sectional analysis of mean demographic scores and disease-related variables for MS and HCs groups at baseline and 2 years.

Characteristics	Baseline			2 yrs follow up		
	HCs(N=20)	MS(N=20)	<i>p</i> -value	HCs(N=13)	MS(N=13)	<i>p</i> -value
Sex (% female)	80%	80%	0.884	85%	85%	0.684
Age	35±1.62	35±1.64	0.921	37±1.62	37±1.64	0.721
Disease Duration (yrs)	-	5±1.3	-	-	6±1.50	-
EDSS	-	2±0.18	-	-	2±0.41	-
MSSS	-	3.75±0.4	-	-	3±0.71	-
Total ARCS	93±2.84	82±3.44	0.015	95±4.05	83±5.33	0.096
Memory	92±2.78	87±4.74	0.346	96±2.34	83±7.94	0.173
Fluency	92±4.02	81±3.44	0.053	92±5.72	84±5.84	0.333
Visuospatial	100±0.6	102±0.92	0.040	100±1.54	101±1.01	0.211
Language	92±4.16	81±4.43	0.066	94±6.12	80±3.83	0.066
Attention	101±2.43	91±3.42	0.015	101±2.37	97±4.62	0.437
SDMT	63±3.27	52±2.51	0.010	64±2.49	53±3.47	0.020
DASS-21	10±1.76	36±5.95	0.000	8±1.67	23±4.57	0.006
Stress	6±1.29	17±2.54	0.001	5±0.82	15±2.71	0.003
Anxiety	2±0.53	10±2.07	0.000	1±0.41	5±1.27	0.004
Depression	2±0.34	10±1.94	0.000	2±0.97	6±1.81	0.044
MFIS	12.95±2.48	37.4±3.87	0.000	12±4.44	29±4.47	0.010
Physical fatigue	5±1.06	18.1±2.03	0.000	5±2.27	13.1±2.36	0.021
Cognitive fatigue	7.9±1.64	19.32±2.06	0.000	7±2.27	16±2.34	0.008

Data are expressed as mean values ± SEM. MFIS: Modified Fatigue Impact Scale; SDMT: symbol digit modalities test; DASS-21: depression anxiety stress scales; EDSS: expanded disability status scale; MSSS: multiple sclerosis severity score; ARCS: audio recorded cognitive screen.

### 5.3.2 Morphology (whole brain and voxel characteristics)

There was a significant variation in the MRS voxel composition (GM, WM and CSF fractions) between HCs and MS patients using cross-sectional analysis, with a significant reduction in the GM fraction and a reciprocal 8% increase in CSF within the PFC voxel in the RRMS cohort at baseline (pre-DMF onset) compared to the HC group. We observed no significant difference at 24 months follow up post-DMF treatment start in PFC voxel composition between HCs and MS patients (Table 5-2). In contrast, there was no significant variation in the MRS voxel composition between HCs and MS patients using cross-sectional analysis, with a reduction in the GM fraction (-9%) within the PCG voxel in the RRMS cohort at baseline (pre-DMF onset) compared to the HC group. We observed no significant difference at 24 months follow up post-DMF treatment start in PCG voxel composition between HCs and MS patients (Table 5-3).

In addition, we observed no significant change in the total brain volume between the RRMS cohort and HCs at baseline and also at 2yrs (Table 5-2). Interestingly, within the RRMS cohort, longitudinal analysis of both PFC and PCG regions showed the onset of DMF treatment had no significant impact on the MRS voxel composition (GM, WM and CSF fractions) ( $F < 3.2$ ,  $p > 0.06$ ) up to 24 months post-treatment (Table 5-2 and Table 5-3). We saw no significant change in the whole brain T2-FLAIR lesion load, during the 24-month DMF treatment period ( $F = 1.24$ ,  $p = 0.12$ ) (Table 5-2). There was no detectable morphological changes during the 24-months DMF treatment period.

Annualised atrophy changes of PBVC were analysed for 13 RRMS patients at three time periods (T0 vs T12, T12 vs T24 and T0 vs T24), yielding  $-0.35 \pm 0.14$ ,  $-0.40 \pm 0.12$  and  $-0.55 \pm 0.19$ , respectively. No substantial change was observed in the average annualised rate of brain volume loss between 1<sup>st</sup> and 2<sup>nd</sup> year of treatment with DMF. PBVC which was analysed for the matched 13 HCs for only one time period (T0 vs T24), yielding  $(-0.19 \pm 0.11)$ , is significantly lower atrophy rate than that observed in the patient cohort.

Table 5-2. Mean values of spectroscopic voxel segmentation of PFC region and volume of brain fractions for RRMS patients compared to HCs showing treatment effect across time points.

	Regions	HCs	MS baseline	T1	T6	T12	T24	HCs(2yrs)	F	<i>p</i>	
<b>Sample size</b>		<b>N=20</b>						<b>N=13</b>			
<b>MRS voxel</b>	<b>CSF%</b>	1.12±0.004	1.21±0.003 <sup>a</sup>	1.15±0.002	1.14±0.002	1.16±0.004	1.14±0.002	1.11±0.001	2	0.09	
	<b>GM%</b>	15±0.02	10±0.01 <sup>a</sup>	12±0.011	12±0.016	15±0.02	12±0.01	14±0.02	1.8	0.101	
	<b>WM%</b>	85±0.011	88±0.03	86±0.02	86±0.03	84±0.02	86±0.01	86±0.02	1.9	0.112	
	<b>LV(mm<sup>3</sup>)</b>	-	0.004±0.003	0.007±0.003	0.007±0.004	0.005±0.004	0.007±0.006	-	1.61	0.144	
<b>Whole brain (mm<sup>3</sup>)</b>	<b>WBV</b>	1630±24	1605±26	-	-	-	1601±17	1625±22	-	-	
	<b>CSF</b>	32±4	36±4	-	-	-	35±2.5	31±3.9	-	-	
	<b>GM</b>	847±17	831±16				828±15	842±16			
	<b>WM</b>	784±11	774±14				772±6	783±11			
	<b>T2 lesion volume</b>	-	4.9±0.9	4.83±0.88	4.82±0.98	4.7±0.98	4.7±0.98	-	1.24	0.120	

**a:**  $p \leq 0.001$  MS vs HCs at baseline. CSF: cerebrospinal fluid; LV (mm<sup>3</sup>): lesion volume within MRS voxel; GM: grey matter; H-MRS: magnetic resonance spectroscopy; T1:1 month of treatment; T6: 6 months of treatment; T12: 12 months of treatment; T24: 24 months of treatment; WM: white matter; WBV: whole brain volume.

Table 5-3 Mean values of spectroscopic voxel segmentation of PCG region and volume of brain fractions for RRMS patients compared to HCs showing treatment effect across time points.

	Regions	HCs	MS baseline	T1	T6	T12	T24	HCs(2yrs)	F	<i>p</i>	
<b>Sample size</b>		<b>N=20</b>					<b>N=13</b>				
<b>MRS voxel</b>	<b>CSF%</b>	11±0.012	12±0.01	11±0.02	11.7±0.01	12±0.01	11.1±0.01	11±0.01	3.2	0.06	
	<b>GM%</b>	51.7±0.03 <sup>a</sup>	47.6±0.03	51±0.03	48.5±0.02	51±0.01	51±0.03	50.7±0.02	0.8	0.40	
	<b>WM%</b>	37.2±0.01	37.8±0.03	37.9±0.02	39.7±0.02	37±0.01	37.1±0.01	37.8±0.03	0.4	0.70	
	<b>LV(mm<sup>3</sup>)</b>	-	0.004±0.003	0.007±0.003	0.007±0.004	0.005±0.004	0.007±0.006	-	1.61	0.144	
<b>Whole brain (mm<sup>3</sup>)</b>	<b>WBV</b>	1630±24	1605±26	-	-	-	1601±17	1625±22	-	-	
	<b>CSF</b>	32±4	36±4	-	-	-	35±2.5	31±3.9	-	-	
	<b>GM</b>	847±17	831±16				828±15	842±16			
	<b>WM</b>	784±11	774±14				772±6	783±11			
	<b>T2 lesion volume</b>	-	4.9±0.9	4.83±0.88	4.82±0.98	4.7±0.98	4.7±0.98	-	1.24	0.120	

**a:**  $p \leq 0.001$  MS vs HCs at baseline. CSF: cerebrospinal fluid; LV (mm<sup>3</sup>): lesion volume within MRS voxel; GM: grey matter; H-MRS: magnetic resonance spectroscopy; T1:1 month of treatment; T6: 6 months of treatment; T12: 12 months of treatment; T24: 24 months of treatment; WM: white matter; WBV: whole brain volume.

### 5.3.3 MR Spectroscopy

#### 5.3.3.1 H-MRS of PFC region

Using single voxel 1D H-MRS, cross-sectional analysis identified a statistically significant reduction in PFC NAA/tCr (-6%,  $p=0.05$ ) and increase in tCho/tCr (+13%,  $p=0.02$ ) in the total RRMS cohort at baseline, compared to HCs (Figure 5-5). We also observed significant increase in m-Ins/tCr (+8%,  $p=0.05$ ) and reduction in PFC Glx/tCr (-13%,  $p=0.03$ ) at baseline in the total RRMS cohort compared to HCs (Figure 5-5). In contrast, we did not observe any significant differences in the levels of PFC Cr, Glu or GSH between the RRMS group at baseline compared to HCs (Table 5-4). When assessing only the cohort that was followed up (N=13), cross-sectional analysis showed no statistical significance ( $p>0.05$ ) in PFC metabolites (NAA, Glx, Cr, tCho, m-Ins and GSH) between the RRMS cohort (N=13) and matched HCs (N=13) at the 24 month time point.

Longitudinal analysis showed the onset of treatment with DMF did not significantly impact on the levels of PFC m-Ins, Glx, GSH or Cr in the RRMS group. However, as the DMF treatment progressed, the mean PFC NAA levels were altered significantly over the 24-month treatment period ( $F=2.6$ ,  $p<0.05$ ) (Figure 5-5 and Table 5-4), but stabilised and didn't significantly change between T12 ( $1.376\pm 0.029$ ) and T24 ( $1.38\pm 0.03$ ) to approach levels seen in the HC group.

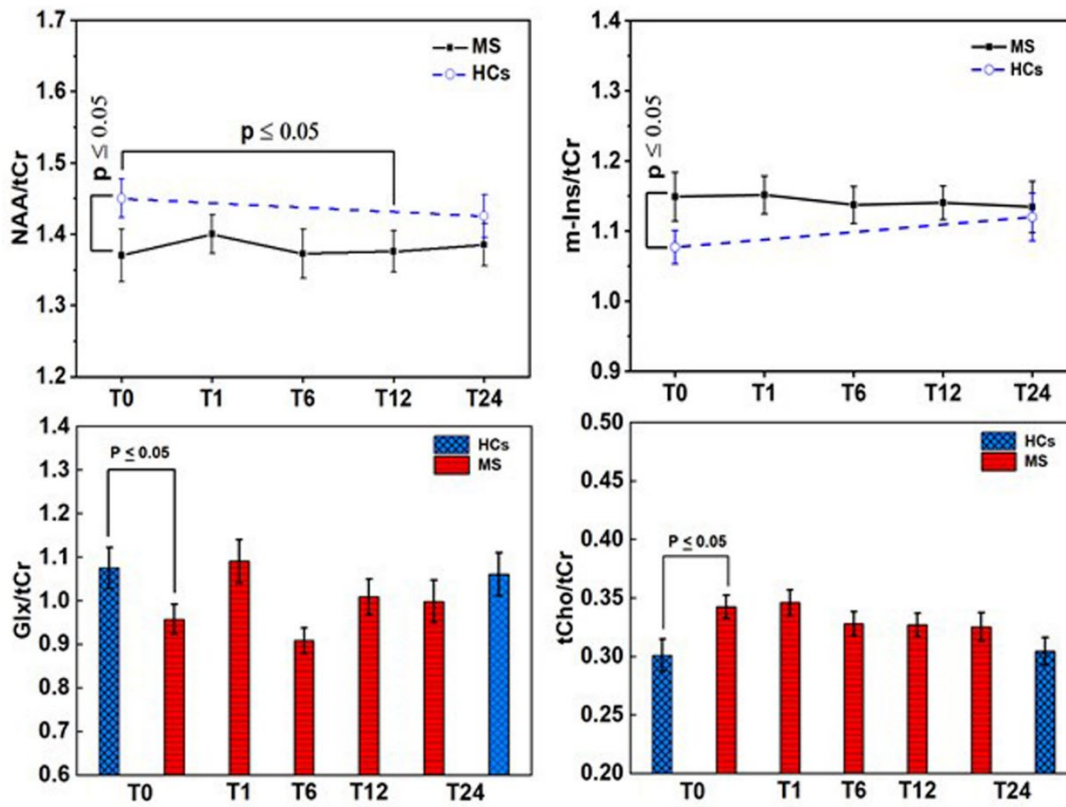


Figure 5-5. PFC neurometabolite/tCr ratio in HCs and RRMS pre and post inception of DMF treatment.

Table 5-4. Mean values of neurometabolite/tCr of PFC region in HCs and RRMS pre and post inception of DMF treatment, showing treatment effect across time points.

PFC voxel	HCs	MS baseline	T1	T6	T12	T24	HCs(2yrs)	F	<i>p</i>	
Sample size	N=20						N=13			
GSH	0.396±0.025	0.378±0.021	0.409±0.033	0.351±0.016	0.390±0.034	0.408±0.03	0.412±0.03	1.81	0.17	
Glx	1.075±0.047	0.957±0.034*	1.090±0.144	0.908±0.029	1.021±0.064	1.002±0.04	1.065±0.05	1.12	0.38	
tNAA	1.458±0.027	1.37±0.036*	1.409±0.037	1.372±0.034	1.376±0.029	1.38±0.03	1.428±0.04	2.6	0.05	
Cr	0.615±0.034	0.634±0.031	0.609±0.031	0.600±0.027	0.64±0.042	0.610±0.06	0.593±0.05	0.26	0.89	
Glu	1.04±0.04	0.931±0.035	1.006±0.08	0.891±0.026	0.935±0.043	0.944±0.04	1.05±0.05	0.84	0.51	
m-Ins	1.076±0.023	1.149±0.034	1.151±0.037	1.137±0.026	1.142±0.037	1.134±0.03	1.12±0.03	0.22	0.9	
tCho	0.301±0.0137	0.342±0.01*	0.345±0.011	0.327±0.010	0.324±0.011	0.325±0.012	0.304±0.012	2.44	0.06	
GPC	0.287±0.013	0.33±0.009**	0.332±0.008	0.323±0.012	0.320±0.011	0.318±0.02	0.292±0.015	2.7	0.05	

\*  $p \leq 0.05$ ; \*\*  $p \leq 0.01$ .

### 5.3.3.2 H-MRS of PCG region

Using single voxel 1D H-MRS, cross-sectional analysis identified a statistically significant reduction in PCG Glx/tCr (-9%,  $p=0.001$ ) and Glu/tCr (-8%,  $p=0.02$ ) in the total RRMS cohort at baseline, compared to HCs (Figure 5-6). In contrast, we did not observe any significant difference in the level of PCG NAA, m-Ins or GSH between the RRMS group at baseline compared to HCs (Table 5-5). When assessing only the cohort that was followed up ( $N=13$ ), cross-sectional analysis showed no statistical significance ( $p>0.05$ ) in PCG metabolites (NAA, Glx, Cr, tCho, m-Ins and GSH) between the RRMS cohort ( $N=13$ ) and matched HCs ( $N=13$ ) at the 24 month time point.

Longitudinal analysis showed the onset of treatment with DMF did not significantly impact on the levels of PCG Glx, GSH or Cr in the RRMS group. However, as the DMF treatment progressed, the mean of neurometabolite of PCG NAA, GSH, Glu and m-Ins levels were altered significantly over the 24-month treatment period ( $F=3.9, p<0.05$ ) ( $F=2.75, p<0.05$ ) ( $F=2.65, p<0.05$ ) ( $F=3.67, p<0.05$ ) respectively (Figure 5-6 and Table 5-5).

Post hoc tests revealed that there was a statistically significant differences in NAA levels from the baseline pre-treatment time point to T24 ( $1.4\pm 0.03$  vs  $1.37\pm 0.02$ ,  $p=0.03$ ). tCho levels revealed statistically significant differences between the baseline pre-treatment time point and T24 ( $1.4\pm 0.03$  vs  $1.37\pm 0.02$ ,  $p=0.03$ ) and tCho levels remained statistically significant between the first month of treatment onset and 12 months ( $0.45\pm 0.03$ ,  $p=0.035$ ). GPC demonstrated a significant difference in pre-treatment and two years of treatment inception and also, between 1 and 24 months (Table 5-5).

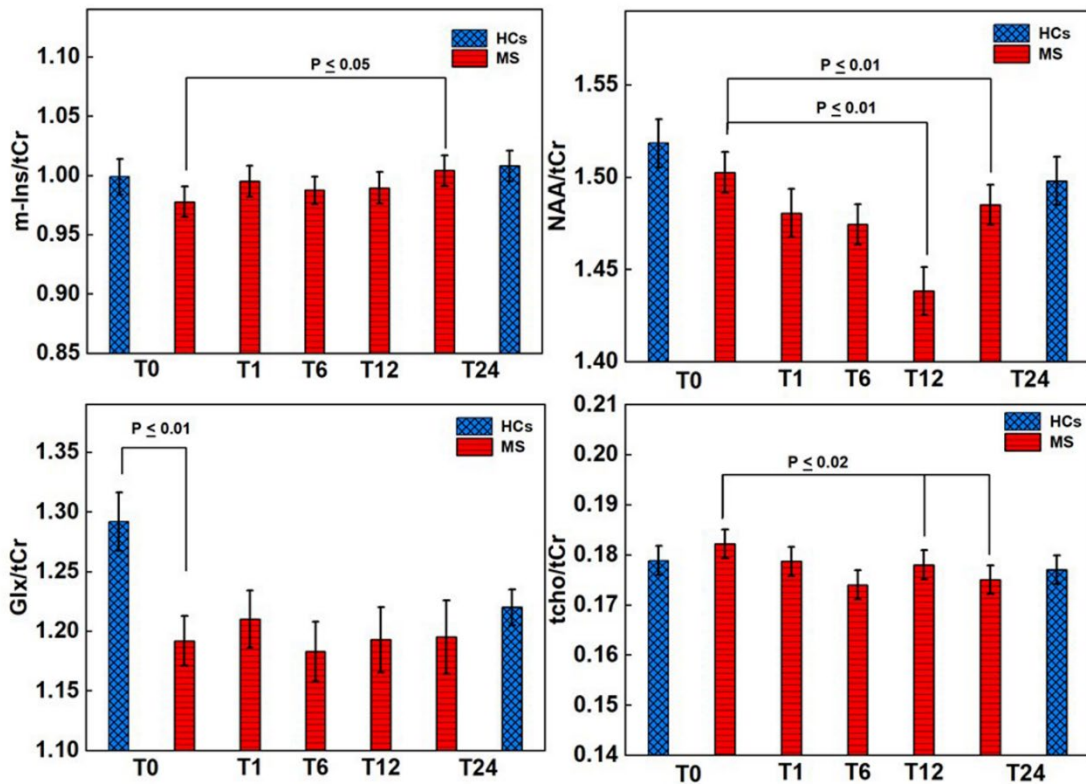


Figure 5-6. PCG neurometabolite / tCr ratio in HCs and RRMS pre and post inception of DMF treatment.

Table 5-5 Mean values of neurometabolite/tCr of PCG region in HCs and RRMS pre and post inception of DMF treatment, showing treatment effect across time points.

Region	HCs	MS baseline	T1	T6	T12	T24	HCs(2yrs)	F	p	
Sample size	N=20						N=13			
GSH	0.233±0.004	0.225±0.004	0.232±0.006	0.217±0.003	0.219±0.006	0.221±0.005	0.237±0.005	2.75	0.05	
Glx	1.292±0.022	1.187±0.026**	1.21±0.027	1.183±0.028	1.193±0.027	1.195±0.04	1.220±0.02	0.43	0.78	
NAA	1.405±0.025	1.376±0.024	1.371±0.019	1.363±0.026	1.341±0.022	1.361±0.03	1.380±0.02	3.95	0.02	
Cr	0.581±0.007	0.551±0.009	0.563±0.005	0.567±0.007	0.574±0.007	0.577±0.01	0.583±0.007	1.84	0.16	
Glu	1.185±0.024	1.105±0.021*	1.117±0.024	1.074±0.025	1.084±0.027	1.09±0.031	1.163±0.02	2.65	0.05	
tCho	0.179±0.004	0.183±0.004	0.177±0.003	0.174±0.004	0.178±0.004	0.175±0.004	0.177±0.005	3.47	0.03	
m-Ins	0.999±0.016	0.978±0.017	0.995±0.015	0.988±0.012	0.989±0.013	1.013±0.017	1.008 ±0.02	3.67	0.02	

\*  $p \leq 0.05$ ; \*\*  $p \leq 0.01$ .

#### **5.3.4 Correlation of PFC metabolites with clinical and volumetric measures**

We investigated associations between clinical symptoms and PFC metabolite levels at the baseline, 12-month and 24-month post-DMF treatment onset. The clinical symptoms that showed the strongest associations with PFC metabolite levels were related to mood status at baseline and T12 (Table 5-6). There was a negative correlation between the levels of PFC NAA, GSH, Glx and Glu with the overall severity of mood symptoms (total DASS-21 scores), as well as the levels for each domain, depression, anxiety and stress (Table 5-6), while m-Ins levels showed an association with the mood status were positively. The cognitive domains evaluated by the ARCS ( $r=0.527$ ) and memory ( $r=0.595$ ) displayed associations with PFC NAA only at baseline, while processing speed and attention, determined by the SDMT, showed no correlation with PFC neurometabolites over 2yrs follow up treatment. Other clinical symptoms that showed associations with PFC metabolite levels were related to disability status, MSSS score, at baseline and T12 (Table 5-6). There was a negative correlation between the levels of PFC Glx and Glu with the EDSS score at baseline, while NAA levels showed an association with MSSS ( $r=0.542$ ) at T12 only. There was evidence for PFC axonal integrity (NAA/tCr) to be negatively correlated with whole brain lesion volume score ( $r=-0.704$ ) at T12 while positively correlated with total brain volume ( $r=0.632$  and  $0.566$ ) at T12 and T24 for tCho/tCr.

Table 5-6. Spearman's correlation between PFC neurometabolites ratios and cognitive functions in RRMS across 24 month study period. Only statistically significant changes are listed.

Time points	Metabolite/tCr	Clinical parameters					
		DASS-21	Stress	Depression	EDSS	TL-volume	
T0	Glu	DASS-21	Stress	Depression	EDSS	TL-volume	
		-0.606**	-0.547*	-0.472*	-0.501*	-0.700**	
	NAA	DASS-21	Stress	Depression	Anxiety	TARCS	Memory
		-0.673**	-0.616**	-0.470*	-0.589**	0.527*	0.595**
	m-Ins	DASS-21	Stress	Depression			
		0.610**	0.509*	0.695**			
	GSH	DASS-21	Stress				
		-0.458*	-0.515*				
	Glx	DASS-21	Stress		EDSS	TL-volume	
		-0.560*	-0.509*		-0.556*	-0.624**	
T12	m-Ins			Depression			
				0.493*			
	NAA	DASS-21	Stress	Depression		TL-volume	MSSS
		-0.611*	-0.540*	-0.579*		-0.704**	0.542*
	tCho						WBV
							0.632**
Glx				Anxiety		WBV	
				-0.464*		0.530*	
T24	tCho				GMV	WBV	
					0.599*	0.566*	
	Glu	D-D					
		-0.622*					
	NAA	D-D					
-0.592*							

\*  $p \leq 0.05$ ; \*\* $p \leq 0.01$ . Cr: creatine; DASS-21: depression anxiety stress scales; D D: disease duration; EDSS: expanded disability status scale; Glx: glutamate+glutamine; Glu:glutamate; GMV: grey matter volume; GSH: glutathione; NAA: N-acetylaspartate; m-Ins: myo-inositol; TARCS: total audio recorded cognitive screen;

tCho: total choline; TL volume: total lesion volume; T0: baseline; T12: 12 months of treatment; T24: 24 months of treatment; WBV: whole brain volume; WM: white matter.

### **5.3.5 Correlation of PCG metabolites with clinical and volumetric measures**

We investigated associations between clinical symptoms and PCG metabolite levels at the baseline, 12-month and 24-month post-DMF treatment onset. The clinical symptoms that showed the strongest associations with PCG metabolite levels were related to mood status at baseline (Table 5-7). There was a negative correlation between the levels of PCG NAA and Glx with the levels for each domain, depression and anxiety (Table 5-7), while m-Ins levels showed association with the overall severity of mood symptoms (total DASS-21 scores), as well as the levels for each domain, depression ( $r=0.540$ ) and stress ( $r=0.703$ ). The cognitive domains evaluated by the ARCS displayed associations with PCG NAA only at T12, while processing speed, determined by the SDMT, showed correlation with PCG neurometabolite (GSH( $r=-0.477$ ), GPC( $r=0.488$ )) at baseline. Other clinical symptoms that showed associations with PCG metabolite levels were related to disability status, MSSS score, at baseline and T12 (Table 5-7). There was a negative correlation between the levels of PCG Glu with the EDSS score at T12, while NAA and m-Ins levels showed an association with MSSS ( $r=-0.513$ ,  $r=0.615$ ) at baseline only. There was evidence for PCG axonal integrity (NAA/tCr) to be negatively correlated with whole brain lesion volume score ( $r=-0.488$ ,  $r=-0.754$ ) at baseline and T12.

Table 5-7 Spearman's correlation between PCG neurometabolites ratios and cognitive functions in RRMS across 24 month study period. Only statistically significant changes are listed.

Time points	Metabolite/tCr	Clinical parameters_PCG					
T0	m-Ins	DASS-21	Stress	Depression		MSSS	
		0.688**	0.703**	0.540*		0.615**	
	GSH	DASS-21		Depression		SDMT	
		0.522*		0.583*		-0.477*	
	GPC					SDMT	
						0.488*	
NAA			Depression	Anxiety	TL-volume	MSSS	
			-0.475*	-0.609**	-0.488*	-0.513*	
Glx				Anxiety	TL-volume		
				-0.575*	-0.495*		
T12	m-Ins					MSSS	
						-0.470*	
	NAA	TARCS				TL-volume	
		0.522*				-0.754**	
	tCho	TARCS			Anxiety		EDSS
		-0.543*			0.503*		0.459*
Glx	TARCS				TL-volume		
	0.624*				-0.773**		
GPC	TARCS						
	-0.462*						
Glu					TL-volume	EDSS	
					-0.763**	-0.532*	
T24	GSH	DASS-21					
		-0.594*					

\*  $p \leq 0.05$ ; \*\* $p \leq 0.01$ . DASS-21: depression anxiety stress scales; EDSS: expanded disability status scale; Glx: glutamate+glutamine; Glu:glutamate; GSH: NAA: N-acetylaspartate; m-Ins: myo-inositol; MSSS: multiple sclerosis severity score; SDMT: symbol digit modalities test; TARCS: total audio recorded cognitive screen; tCho: total choline; TL volume: total lesion volume; T0: baseline; T12: 12 months of treatment; T24: 24 months of treatment.

## 5.4 Discussion

Our cohort of 20 RRMS patients was clinically stable while undergoing treatment with DMF. PFC and PCG are involved in cognition and decision making, and learning and memory functions, respectively. In MS, changes in pre-frontal cortex and posterior cingulate gyrus proliferation, lesion load, GM volume loss, NAWM volume have been associated with alterations in cognitive and mood function in MS patients<sup>211</sup>. There is ample evidence of impaired cognitive function and higher levels of mood and fatigue symptoms in RRMS compared to matched healthy subjects<sup>247</sup>. Furthermore, studies have proposed that the PCG and PFC might be sensitive to the progression of clinical and cognitive disabilities in MS patients and might play an important role in improvement of cognitive performance<sup>248-250</sup>. Despite their relatively short disease duration and low disability score, our RRMS cohort displayed cognitive impairment, evidenced by poorer visuospatial, fluency and attention scores, as well as lower overall performance scores on the ARCS than the HCs. Similarly, the RRMS cohort had worse attention and processing speed in comparison to HCs, resulting in lower SDMT scores. Our study demonstrated no statistical change in the level of clinical symptoms, EDSS, MSSS for the study periods (T0-T12 and T12-T24) while being treated with DMF over the two years. These results cannot be interpreted as supportive of predicting progression of disability, however, DMF can be considered as an agent that provides possible stabilization of symptoms during the two-year period, and investigation of DMF efficacy over a longer period of time is warranted.

In spite of the fact that the whole brain lesion load was low in our patient group, our findings indicated a reduction in total brain volume and partial GM volume within the PFC and PCG voxels with a reciprocal increase in CSF, compared to healthy controls in cross-sectional and longitudinal studies. Reduction in brain volumes have been correlated with increased risk of disease progression rates and decrease of treatment effect in MS <sup>212</sup>.

Previous literature <sup>213</sup> reported a faster rate of atrophy in MS patients (0.5–1.35% per year) compared to age-matched HCs (0.1–0.3% per year), which is consistent with our annual PBVC value of -0.4 and -0.55 for RRMS cohort and -0.19 for HCs group over 2 years. Therefore, the average annualised rate of brain volume loss over 2 years while receiving treatment with DMF, might suggest an effect of DMF on brain volume, which was described in pivotal trials of DMF vs placebo <sup>214</sup>. A lower rate of brain volume loss has been associated with benefit on disease progression in MS <sup>215</sup>.

Using single voxel H-MRS technique, we confirmed the importance of NAA and m-Ins as indicators of axonal loss and gliosis <sup>31, 216</sup>. In this project, we observed a significant reduction of NAA and Glx, an increase in m-Ins and tCho levels in PFC region of RRMS in comparison to age and sex-matched healthy individuals in the cross-sectional analyses. Increased tCho levels in NAWM compared to healthy controls might indicate cell membrane turnover, as seen in pathological process like inflammation <sup>31</sup> and myelin breakdown or maybe the result of remyelination in chronic lesions <sup>251</sup>. Furthermore, these metabolic changes were associated with morphological changes within the brain including increased CSF volume, total brain volume loss and T2 white matter lesion load. In contrast, we found a significant reduction in Glx and Glu in the PCG region when compared to age and sex-matched healthy individuals in the cross-sectional analyses. Our finding of PCG Glu is consistent with other H-MRS studies in RRMS <sup>40</sup> that have shown reduction in Glu (neurotransmitter) levels in cingulate and parietal regions reflected the same pathological process of early loss of neuronal integrity in reduced NAA <sup>252</sup>.

However, longitudinal metabolic changes in this cohort of patients are worth mentioning in particular after the commencement of various disease-modifying therapeutic (DMT) agents. Several studies demonstrated changes in metabolic profiles especially NAA and m-Ins in patients with DMTs. The role of NAA as a marker of neuronal integrity was supported by the reduction in NAA levels associated with lower grey matter content in the PFC voxel compared to that seen in the same region in healthy controls. Other studies have shown an increase in white matter NAA content following treatment with MS disease-modifying therapy<sup>217</sup>. Reduced level of NAA in the grey matter of MS patients has also been recently established<sup>155</sup> further supporting the importance of NAA as a disease marker. Increased m-Ins in NAWM and cortex regions indicates brain tissue loss and clinical progression of MS<sup>28,237</sup>. Increased levels of m-Ins have been detected by others in the CSF from MS patients<sup>218</sup> and also in the T1-weighted hypo-intense chronic MS lesions<sup>219</sup>, the latter thought to be associated with astrogliosis around the lesion<sup>68</sup>.

Efficacy of Interferon therapy in RRMS cohorts using H-MRS studies have yielded conflicting results that range from stabilization to weak effect on NAA<sup>231,253</sup>. Khan et al. found that averaged NAA/Cr ratio in corpus callosum/adjacent white matter increased significantly with GA compared with control group, and suggested that this may be due to axonal metabolic recovery<sup>230,233</sup>. However, in the current study, the change in the level of PFC NAA/tCr in MS after the administration of DMF stabilised in the first 12 months but did not significantly change thereafter over the period of 2 years. This may suggest that the PFC neuronal integrity and the level of microglial gliosis were not significantly impacted during this time period consistent with insignificant changes in clinical parameters over this time period. These results agree with our selected RRMS cohort that were active to start off with and then stabilized upon treatment. There were no metabolic changes in the HCs brain between baseline and 2 years follow up which confirms the reliability of the H-MRS technique, and that changes observed in the MS cohort can be conceived as clinically relevant.

MRS study of MS patients undergoing GA and INF-b treatment yielded GSH reduction in the fronto-parietal region in secondary progressive MS patients compared to RRMS<sup>200</sup>. The same study also reported a trend towards reduced levels of GSH with no significant difference in this same region in RRMS compared to HCs. We understand that our PFC voxel was comprised of higher white matter than grey matter compositions, with an increase of WM fraction during the duration of our study. Our finding found that the effects of DMF on GSH concentrations in PFC and PCG did not differ between RRMS and controls over 2yrs despite a trend for reduced levels of GSH in RRMS. Similarly, the whole brain and GM volumes were lower in RRMS than in controls in PFC and PCG regions. These results indicate that neurodegeneration is evident even in early forms of RRMS possibly due to oxidative stress due to GSH depletion. This is in concordance with other study albeit under different treatment regimes. This study was not powered to distinguish GSH concentration differences among different disease-modifying therapies<sup>200</sup>.

A corresponding decreasing trend in lesion volume within the PFC and PCG voxel was observed during this period but did not reach significance. It may be warranted to investigate a longer DMF treatment period in a larger cohort to determine an association between PFC and PCG metabolic levels and treatment efficacy. However, our finding suggests that H-MRS of brain metabolites in both regions are a more sensitive marker than morphological changes.

The clinical symptoms that showed the strongest associations with PFC metabolite levels were related to mood at baseline and T12. We observed correlations between the overall severity of mood symptoms (total DASS-21 scores), as well as the levels for each domain, depression and stress, with a decrease in PFC NAA levels and increase PFC m-Ins over 12 months. This may suggest a decrease in PFC neuronal integrity and mitochondrial dysfunction with altered mood function in our MS cohort. It also suggests a possible increase in PFC gliosis with altered cognitive function in our MS cohort. The cognitive domains evaluated by the ARCS and memory displayed

associations with PFC NAA of RRMS at baseline only. This result is consistent with a previous study <sup>216</sup> that showed that decreasing NAA correlated with cognitive dysfunction as well as with disability in RRMS patients using H-MRS. Furthermore, other findings have indicated a reduction in NAA and Cho and increased in m-Ins in NAWM have correlated with decreasing memory scores and suggesting that these brain metabolites may be described as indicators of cognitive performance in RRMS <sup>247</sup>. We have recently shown that there is a complex interplay between mood disorders such as depression, anxiety and stress with cognitive performance evidenced by lower ARCS scores in RRMS <sup>221</sup>. However, decrease of NAA/tCr and increase of m-Ins ratios within the PFC region (predominately in white matter) do not show a significant correlation with fatigue scores nor cognition in our MS cohort. This result is consistent with a previous H-MRS study that showed that there was no significant correlation between the NAA/Cr and m-Ins/Cr levels and fatigue or cognitive performance in RRMS <sup>248</sup>.

As expected, the DASS self-report questionnaire confirmed higher levels of depression, anxiety and stress in the RRMS cohort compared to HCs. We also observed an association between GSH and Glu levels with mood symptoms at baseline and T12. This may represent an increase in oxidative stress and glial changes in the PFC with increased depression, anxiety and stress symptoms in our cohort.

In cross-sectional analysis, we detected a significant alteration in PFC Glx level. Thus, we did observe a negative correlation between PFC Glx and stress at baseline, and between Glx and anxiety levels at T12. However, Glx was negatively correlated with EDSS at baseline. Glx correlation with EDSS level at baseline has been reported by Chard et al. in normal appearing white matter and normal appearing cortical grey matter <sup>150</sup>. However, no correlation between Glx and disease duration was found in our study. De Stefano et al. reported that NAA and NAA/Cr were significantly correlated with EDSS in different H-MRS studies in NAWM <sup>254</sup> suggesting that neuronal damage within NAWM is a mechanism of disability <sup>43, 255</sup>, but Gustafsson et al. found a weak correlation between NAA and EDSS <sup>256</sup>. However, no correlation between PFC

NAA/tCr and EDSS score was found in our study. Others have demonstrated altered levels of glutamate (Glu) in multiple sclerosis, although regional variations have been noted<sup>40</sup>. Elevation in Glu has been observed in white matter lesions but not in normal appearing white matter<sup>97</sup> while in the cingulate regions, a depletion in Glu and Glx was measured<sup>40</sup>, which was in turn shown to be associated with visual and verbal memory impairment.

In addition to the above, we observed a negative correlation between the levels for each domain, depression and anxiety and PCG NAA levels and also a positive correlation between the overall severity of mood symptoms (total DASS-21 scores), as well as depression and stress and PCG m-Ins at baseline only. This may suggest an increase in PCG neuronal integrity and mitochondrial dysfunction with altered mood function in our MS cohort. We reported a correlation between processing speed, with an increase in PCG GPC levels at baseline. This may suggest an increase in PCG demyelination or inflammation with altered cognitive function in our MS cohort. The cognitive domains evaluated by the ARCS displayed associations with PCG NAA and tCho of RRMS at T12 only. This result is consistent with a previous study<sup>216</sup> that showed that decreasing NAA correlated with cognitive dysfunction as well as with disability in RRMS patients using H-MRS. Furthermore, other findings have indicated a reduction in NAA and Cho and increased in m-Ins in NAWM that have correlated with decreasing memory scores and suggesting that these brain metabolites may be indicators of cognitive performance in RRMS<sup>247</sup>. However, decrease of NAA/tCr and increase of m-Ins ratios within PCG region do not show a significant correlation with fatigue scores of MS cohort. This result is consistent with previous H-MRS study that showed that there was no significant correlation between the NAA/Cr and m-Ins/Cr levels and fatigue or cognitive performance in PCG region of RRMS<sup>248</sup>.

As expected, the DASS self-report questionnaire confirmed higher levels of depression and anxiety in the RRMS cohort compared to HCs. We observed an association between GSH and Glx levels with mood symptoms at baseline. This may

represent an increase in oxidative stress and glial changes in the PCG with increased depression, anxiety symptoms in our cohort.

In cross-sectional analysis, we detected a significant alteration in PCG Glx level. Thus, we did observe a negative correlation between PCG Glx and anxiety at baseline. However, only Glu was negatively correlated with EDSS at T12. Glx correlation with EDSS level at baseline has been reported by Chard et al. in normal appearing white matter and normal appearing cortical grey matter<sup>150</sup>. NAA and NNA/Cr was significantly correlated with EDSS in different H-MRS studies in NAWM<sup>254</sup> suggesting that neuronal damage within NAWM is a mechanism of disability<sup>43,255</sup>, but another study found a weak correlation between NAA and EDSS<sup>256</sup>. However, no correlation between PCG NAA/tCr and EDSS score was found in our study, but PCG NAA/tCr and m-Ins/tCr were correlated with MSSS score of RRMS cohort. This may suggest an increase in PCG neuronal integrity and PCG gliosis with altered MSSS function in our MS cohort. Others have demonstrated altered levels of Glu in multiple sclerosis, although regional variations have been noted<sup>40</sup>. Elevation in Glu has been observed in white matter lesions but not in normal appearing white matter<sup>97</sup> while in the cingulate regions, a depletion in Glu and Glx was reported<sup>40</sup>, which was in turn shown to be associated with visual and verbal memory impairment.

To the best of our knowledge, the current study is the first *in-vivo* investigation of the impact of DMF treatment on the PFC and PCG metabolism in MS patients. It should be noted that the dosing regimen for DMF involves a weekly dose escalation over a 4 week period, until the recommended therapeutic level (480mg daily) is achieved. Between the first and 24 months of treatment, we observed a slightly increasing trend for Glx and levels within the PFC and PCG, not approaching that seen in age and sex-matched healthy controls. Furthermore, we observed a slightly decreasing trend for m-Ins and tCho levels within the PFC and PCG, but not close in age and sex-matched healthy controls at T24 month. These longitudinal metabolic changes in MS patients results indicate that disease progression rates is evident in RRMS from lower brain

volumes than from effect of therapy in MS due to metabolic changes over 2years of DMF treatment <sup>212</sup>.

There are, however, a number of limitations to this study. The findings are preliminary and need to be confirmed in a larger patient cohort over an extended treatment period to enable longer term impacts of DMF on disease outcomes and metabolic changes to be more fully explored. In the current study, we did not employ spectral editing schemes to optimize detection of GSH as utilized in other studies which have investigated the changes in GSH associated with MS <sup>196, 224</sup>. We have instead, undertaken a series of *in-vitro* investigations to support the validity of spectral post-processing and quantification using LCmodel for our H-MRS spectral analysis.

## **5.5 Conclusion**

This study demonstrated that H-MRS is a sensitive marker of disease activity with several metabolites correlated with clinical parameters, but also capable to detect a treatment effect prior to volumetric change. We have shown that treatment with DMF may impact on PFC metabolism, specifically NAA/tCr levels. It may be warranted to investigate a longer DMF treatment period in a larger cohort to determine an association between PFC and PCG metabolic levels and treatment efficacy. However, our finding suggests that H-MRS of brain metabolites in both regions are a more sensitive marker than morphological changes. The clinical symptoms that showed the strongest associations with PFC metabolite levels were related to mood status at baseline and T12.

**Funding**

Independent investigator- initiated grant provided by Biogen Pharmaceuticals Pty Ltd.

**Availability of data and materials**

Availability of data and materials are subject to guidelines of local Hunter New England Local Health District Human Research Ethics Committee. All authors contributed to revising, literature and critical suggestions to reshape the manuscript.

**Ethics approval and consent to participate**

This study was approved by Institutional Review Board from the Hunter New England Local Health District Human Research Ethics Committee (HNEHREC Reference No: 4/09/10/3.01), Newcastle, NSW, Australia.

## **Chapter 6 : Cross sectional evaluation of neurometabolic alterations in RRMS with fingolimod and injectable treatment using advanced MRS**

Oun Al-iedani, Karen Ribbons, Saadallah Ramadan, Rod Lea, Jeannette Lechner-Scott

### **ABSTRACT**

Disease modifying therapies (DMT) for MS treatment is essential to understand the underlying pathology resulting in disease progression. Treatment response studies using one-dimensional proton magnetic resonance imaging (1D H-MRS) have demonstrated a significant increase in N-acetylaspartate/creatine (NAA/Cr) in RRMS patients and improvement in fatigue symptoms. It is important to develop new and meaningful imaging biomarkers to evaluate the clinical efficacy of treatment radiologically. In this study, non-invasive H-MRS technique was applied to evaluate the amount of axonal injury and brain metabolites in RRMS patients on two DMTs; fingolimod and injectables. These were compared to healthy controls in a cross-sectional evaluation in three brain regions of hippocampus, pre-frontal cortex (PFC) and posterior cingulate gyrus (PCG). Metabolites were correlated with clinical severity and neuropsychological symptoms.

RRMS patients who have been on fingolimod (N=52) and interferon (INF) or glatiramer acetate (GA) (N=46) for a minimum of six months were included in this study. Patients were predominantly female (77%) with mild expanded disability status scale (EDSS:  $2\pm 0.12$ ). Using H-MRS, we identified a significant reduction in

NAA/total Cr (tCr) in hippocampus (-17%,  $p=0.001$ ), PCG (-7%,  $p=0.001$ ) and PFC (-9%,  $p=0.001$ ). In PFC a significant increase in myo-inositol (m-Ins)/tCr (+5%,  $p=0.03$ ) was identified. NAA was positively correlated with cognitive domain (memory and total audio recorded cognitive screen (TARCS)) and m-Ins was positively correlated with mood symptoms in hippocampus. H-MRS proved to be a sensitive marker of disease activity with several metabolites correlated with clinical parameters. A longitudinal study is required to investigate association between hippocampus, PFC and PCG metabolic levels and treatment efficacy.

## 6.1 Introduction

Conventional MRI and clinical assessments are fundamental methods for monitoring disease severity of multiple sclerosis (MS) patients. MRI is sensitive at detecting MS plaques in the brain and spinal cord, reflecting inflammatory activity. New T2 lesions, total lesion load and atrophy are all markers linked to disease progression<sup>216,257</sup>. MRI has a prominent role in the diagnosis and clinical management of MS pathology<sup>69,258</sup>. However, disease in the normal appearing brain tissue (both white and grey matter) is undetectable with routine imaging and progression of disability during the course of the disease cannot be reliably measured where the association between clinical findings and radiological disease severity is limited<sup>259,260</sup>. Furthermore, the clinical manifestation of MS plaques in different anatomical locations such as spinal cord and optic nerves are variable and contributes differently to overall disability scores like EDSS. Damage to the normal appearing brain tissue<sup>28</sup> during the progression of the disease leads to atrophy and eventual disability<sup>261,262</sup>. In particular, the degree of spinal cord atrophy correlates with disability status<sup>263</sup>, while grey matter volume<sup>262,264</sup> correlates with cognitive impairment and physical disability of MS patients. On the other hand, the primary outcome of MRI measures as a potential biomarker for monitoring the efficacy of disease modifying treatments (DMT) is increased. Therapeutic trials using MRI have demonstrated the efficacy of all DMTs

including injectable glatiramer acetate (GA), interferon (IFN-b) and natalizumab in relapse-remitting MS (RRMS) in reducing MRI-detected disease activity<sup>226, 227</sup>.

In the last decade, disease modifying therapies for MS treatment were deemed vital to understand the underlying pathology resulting in disease progression and therefore have assisted in developing new meaningful imaging biomarkers to evaluate the clinical efficacy of treatment radiologically. Current immunomodulatory drugs such as GA and IFN-b and newer oral drugs like fingolimod have not only shown the reduction of relapse rate and T2 lesion load but also brain atrophy, which seems to be related to long term disease and disability<sup>265</sup>.

A non-invasive, advanced MRI technique of proton magnetic resonance spectroscopy (H-MRS) enables monitoring of metabolic alterations in relatively small volumes of interest. This has the potential to provide biomarkers for early detection and to monitor disease progression of the MS brain. H-MRS may allow better understanding of the pathophysiology of the symptoms and aid in the development of new treatments. Few studies have used H-MRS to monitor the response to the disease modifying therapies in RRMS and to assess if immunomodulatory therapies can reverse or prevent the progression of neuronal injury<sup>228, 229, 253</sup>. Additionally, the majority of these studies evaluated the impact of IFN-b on RRMS in longitudinal studies with different intervals and cohorts<sup>229, 231, 232, 253</sup>.

Interferon studies have demonstrated conflicting results of improvement or stabilization related to the level of N-acetylaspartate (NAA) and creatine (Cr) in white matter lesions and normal appearing white matter during the treatment. If confirmed, this could potentially reflect a positive effect of the treatment on the disease progression<sup>228, 231, 253</sup>. Khan et al has explored the treatment efficacy of GA therapy using H-MRS. They found that NAA/Cr increased significantly after treatment with GA compared to the control group and suggested that this may be due to axonal metabolic recovery. They also found that NAA/Cr was associated with disability level<sup>230, 233</sup>. Furthermore,

they found that GA treatment has demonstrated a significant improvement in axonal integrity and fatigue symptoms <sup>266</sup>.

H-MRS, however, hasn't been used to assess cross-sectional and longitudinal effects of disease modifying treatment such as fingolimod. The clinical trial FREEDOMS evaluated quantitative MRI techniques such as lesion load and brain volume changes in relapsing-remitting MS patients from baseline at 6, 12 and 24 months post treatment inception. The study showed reduced brain volume loss within 6 months of inception of treatment <sup>267</sup>. However, this may be due to the endothelial effect of fingolimod or early oedema rather than inhibiting atrophy <sup>268</sup>. Fingolimod has shown a clear benefit in preventing brain atrophy early <sup>267</sup>, which has always been associated with lower cognitive decline. This highlights the importance of the interrogation of microstructural and biochemical changes that occur after treatment. The development of novel and non-invasive MR techniques such as H-MRS can enable monitoring of many chemical entities in the MS brain, including NAA, myo-inositol (m-Ins) and glutathione (GSH) <sup>39, 159</sup>.

H-MRS can diagnose MS pathological processes in different tissue types; MS lesions and normal-appearing white matter (NAWM). Clinically, metabolite levels within the MS lesions, NAWM and grey matter in various brain regions such as hippocampus, cortex and sub-cortical regions <sup>28, 41, 42, 76, 237</sup> can be evaluated. These studies have demonstrated decreased levels of NAA and choline and increased m-Ins in NAWM and cortex regions and atrophy in clinical progression of MS. To date, studies have demonstrated metabolic changes in multiple regions in the MS brain and these are not limited to active white matter lesions but also NAWM<sup>269</sup>. NAA is the most commonly evaluated metabolite in the MS brain with reduction in NAA associated with axonal loss, neuronal damage and mitochondrial dysfunction <sup>270</sup>. Also, NAA and NAA/Cr ratio showed decreased levels in WML compared to NAWM regions<sup>144</sup>, indicating axonal loss and dilution due to increased water content that may cause smaller changes <sup>67, 238</sup>.

Furthermore, decrease in NAA has been correlated with Expanded Disability Status Scale (EDSS)<sup>217</sup> and disease course<sup>37,43</sup> with the levels differing between brain regions<sup>28</sup> and between lesions and NAWM<sup>269</sup> and increased m-Ins in chronic lesions was found to be associated with gliosis<sup>68, 154, 216</sup>. Increased neurotransmitter glutamate (Glu) concentration in MS lesions and NAWM was shown in another study which may be due to glutamate mediated excito-toxicity.

Responsible for executive functioning, pre-frontal cortex (PFC) forms an integral part in cognitive function. Posterior cingulate gyrus (PCG), on the other hand, part of the limbic system with mutual connections with medial temporal lobe and hippocampal formation, acts as a hub for important structural and functional connections involved largely in memory processing. Both PFC and PCG regions are key areas in the default mode network in normal cognition<sup>249</sup> and in cognitive processing of MS<sup>271, 272</sup>.

The pathology of PCG has a major impact on cognition of patients with several pathological processes including neuronal loss, and white matter integrity. This can contribute to cognitive decline, effecting neuropsychological performance in patients with RRMS, and improvement is associated with changes of activity with increased connections associated with PCG, PFC and anterior cingulate cortex (ACC). The pathological processes underlying cognitive impairments in RRMS are complex which stems from disarrayed neurometabolite levels<sup>37</sup>, disruption of the integrity of brain connectivity<sup>273</sup> as well as abnormalities in structural pathways and functional cognitive networks.

In MS, changes in PFC and PCG proliferation, lesion load, GM volume loss, NAWM volume have been associated with alterations in cognitive and mood function in MS patients. PCG and PFC might be sensitive to the progression of clinical and cognitive disabilities of MS patients and might play an important role in monitoring cognitive performance. Increased Glu levels in these regions correlate positively with cognitive performance in H-MRS studies, in particular visuospatial memory with levels in hippocampal, thalamic and cingulate regions. Additionally, positive association was

seen in the levels of GSH in the hippocampus region effecting memory and processing speed <sup>200</sup>.

Hippocampal pathology in MS includes the presence of demyelinating lesions leading to functional connectivity changes in addition to regional atrophy. In MS, this hippocampal dysfunction has been associated with memory impairment <sup>274</sup>, overall cognitive deficit and depression <sup>275</sup>. Global GM and WM atrophy, and specifically hippocampal atrophy, have been correlated with visual-spatial and verbal memory deficits <sup>276</sup>. Additionally, hippocampal atrophy has been correlated with decreased functional connectivity <sup>277</sup>. MS treatments have been shown to potentially improve hippocampal function. In mice, the immunomodulatory agent fingolimod has been shown to enhance hippocampal neurogenesis <sup>278</sup> and in vitro enhance growth of neural stem cells <sup>279</sup>. However, to date, the *in-vivo* human impact of MS treatments on hippocampal, PFC and PCG metabolism has not been shown.

The objective of this study is to evaluate the amount of axonal injury and brain metabolites in RRMS patients compared to healthy controls using H-MRS technique. This will aid in detecting pathology early and treat appropriately to prevent long term disability. Firstly, a MS cohort has been studied in a cross-sectional manner compared to age and sex-matched healthy controls at baseline. Then, healthy controls (HCs) were correlated with each treatment group of fingolimod and injectables (interferon and GA). The changes in metabolic concentrations were studied in three brain regions of hippocampus, PFC and PCG. Lastly, the correlation between brain metabolites and severity of clinical and neuropsychological symptoms will be analysed in a cross-sectional manner between neurometabolites, volumetric MRI data and clinical symptoms of MS with different treatments. In this study, we want to demonstrate, that the effect of fingolimod is associated with preventing cognitive decline as measured by the Symbol Digit Modalities Test (SDMT) and the Audio Recorded Cognitive Screen (ARCS).

## **6.2 Methods**

### **6.2.1 Patients and Healthy Control Subjects**

Ninety eight patients with confirmed RRMS, in accordance with the McDonald criteria <sup>17</sup>, aged between 20 to 55 years, who were undergoing immunomodulatory therapy for a minimum of 6 months with no new clinical symptoms or change in their disability status in the last 6 months, were included in the study. Patients were eligible if they had an EDSS score from 1–4 and are able to walk a minimum of 500m. Patients were excluded if they had a comorbid diagnosis of other neurological or psychiatric conditions; impaired capacity to consent; any contraindication to MRI scanning, or treatment with glucocorticoids within the last three months. HCs were age ( $\pm 2$  years) and sex-matched to the RRMS cohort receiving oral (fingolimod), injectable (interferon or GA) disease modifying therapy.

All patients were recruited from the John Hunter Hospital, Newcastle, Australia, MS outpatient clinic. Age and sex-matched HCs were derived from the Hunter Medical Research Institute (HMRI) research register and needed to comply to the study inclusion criteria, which included passing an MRI safety clearance, as well as being able to comply with all study procedures. Institutional Review Board approval was obtained from the Hunter New England Local Health District Human Research Ethics Committee, with written informed consent obtained from all subjects prior to undertaking any study-related procedures. All scans were conducted between December 2014 and June 2017.

### **6.2.2 Study design**

In the RRMS cohort, a cross-sectional observational study was conducted to evaluate the impact of disease modifying therapy (fingolimod and injectable) on the hippocampal, PFC and PCG metabolite profile. We also conducted MRI/MRS cross-sectional evaluation of RRMS/HCs neurometabolite profile changes from these three regions of interest at baseline. Additionally, all participants underwent a neurological examination for clinical assessments. RRMS participants have received fingolimod or

injectable disease therapies in accordance with the manufacturers guidelines and as specified by their treating neurologist. Dosing summaries for each of these compounds are shown in the Table 6-1.

Table 6-1. Dosing summaries for fingolimod or injectable disease therapies compounds of RRMS patients.

# of Participants Entered Treatment	Type of Study Drug	Compound	Min Dose	Frequency
52 RRMS	Investigational	Fingolimod	0.5mg	Daily
46 RRMS	Comparator	Interferon beta- 1a (Avonex)	30mcg	Weekly
	Comparator	Interferon beta- 1a (Rebif)	44mcg /0.5ml	Daily
	Comparator	Betaferon	250mcg/ml	Every other
	Comparator	Copaxone	20mg/ml	Daily

Fingolimod or injectable disease therapies compounds dosing was evaluated according the following regime: fingolimod (0.5mg/day), interferon beta- 1a (Rebif) (44mcg /0.5ml day), Copaxone (20mg/ml day).

### 6.2.3 Binary mask for the voxel segmentation

A binary mask of an MRS voxel for hippocampal, PFC and PCG regions (Figure 6-1) was created using the “mask()” function within the SPM toolbox. To determine the fractional quantities of GM, WM and CSF within MRS voxels, partial volume masks for each tissue type were created using FSL FAST (Figure 6-1) as described by Quadrelli et al. for single voxel segmentation<sup>203</sup>. These masks were overlaid onto the high-quality T1-MPRAGE structural images. For accuracy in the MRS voxel re-positioning, during longitudinal re-assessment, MPRAGE data was reconstructed into 1mm coronal and axial slices on the scanner.

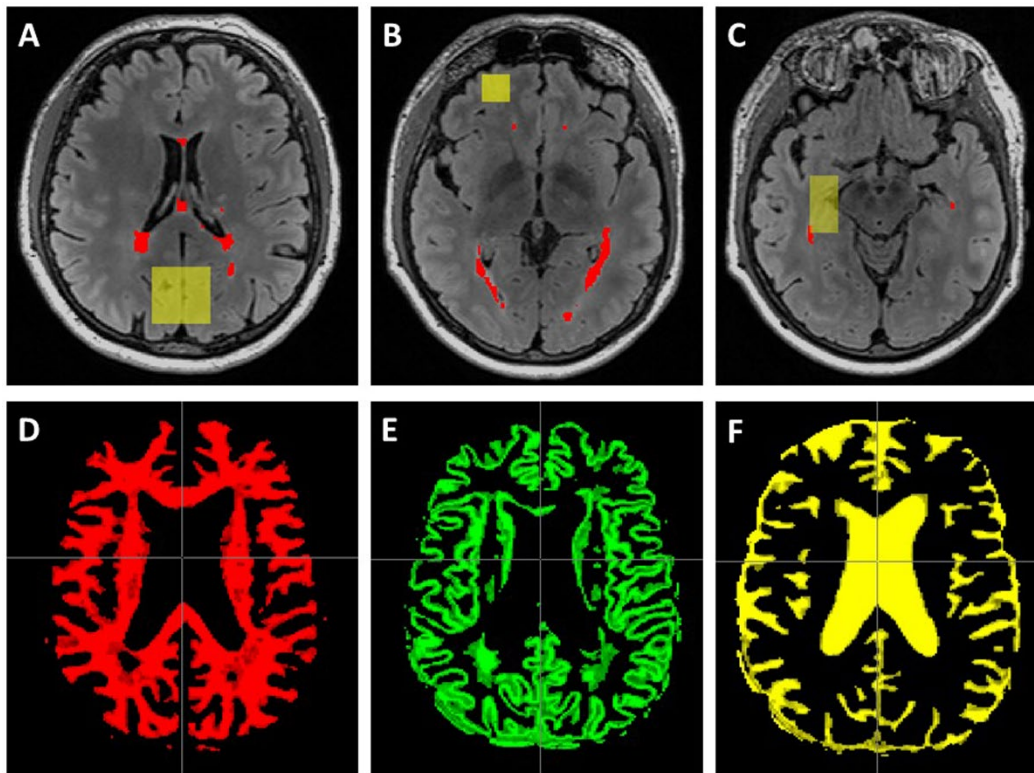


Figure 6-1. Reconstructed MRS voxels displayed as a mask overlying the T2 FLAIR images and lesion map (red colour), (A) PCG mask, (B) PFC mask and (C) hippocampal mask. The results of partial volume segmentation using FSL FAST, (D) WM mask, (E) GM mask, and (F) CSF mask.

#### 6.2.4 MRI acquisition and structural assessments

All MRI/MRS scans were undertaken on a 3T Prisma (Siemens Healthineers, Erlangen, Germany) MRI scanner equipped with a 64-channel head and neck coil located at the HMRI, Newcastle, NSW, Australia. Experimental parameters of the three-dimensional isotropic T1-weighted Magnetization-Prepared Rapid Gradient Echo (MPRAGE) were as follows; sagittal orientation, TR/TE/TI=2000/3.5/1100 ms, 7° flip angle, field of view (FOV)=256x256 mm, pixel size =1x1x1 mm<sup>3</sup>, NEX=4 and acquisition time =5 minutes. Three-dimensional T2 FLuid-Attenuated Inversion Recovery (T2-FLAIR) sequence, TR/TE/TI =5000/386/1800ms, 12° flip angle,

FOV=256x256 mm, pixel size=1x1x1 mm<sup>3</sup>, echo train duration=858ms, NEX=1 and acquisition time=4 minutes.

Brain and skull images were extracted from the whole brain T1 3D MPRAGE data using SIENAX<sup>239</sup>. The brain image was co-registered to MNI152 space<sup>240, 241</sup> to determine the volumetric scaling factor to normalise for head size (Figure 6-2). Total brain volume, including grey matter (GM), white matter (WM), peripheral grey matter and ventricular CSF volumes were calculated with partial volume estimation in FSL FAST<sup>242</sup>.

LST toolbox<sup>243</sup> was used to generate an initial binary lesion map along voxels that are hyperintense in the T2 FLAIR image, resulting in a lesion probability map with a threshold of 0.1. This was followed by lesion filling within the T1 MPRAGE, using the binary lesion mask for each participant and a threshold of 0.5. This minimises errors in partial volume segmentation and improves the final volume measurements<sup>244</sup>. Partial volume segmentation of the lesion filled T1 structural image was segmented using FSL FAST (Battaglini *et al.*, 2012). Lesions within the MRS voxel were segmented using the lesion growth algorithm described by Quadrelli *et al*<sup>203</sup>.

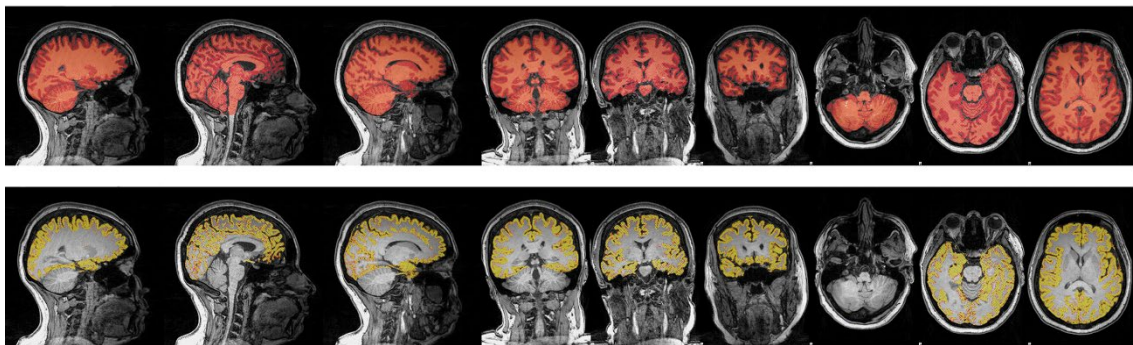


Figure 6-2. Brain tissue volume, normalised for subject head size, was estimated with SIENAX. Final SIENAX segmentation results of whole brain (top row) and peripheral cortex masked segmentation (bottom row).

### 6.2.5 H-MRS Acquisition, Post-Processing and Analyses

One-dimensional (1D) H-MRS of the hippocampus, PCG and PFC were acquired using a Point RESolved Spectroscopy (PRESS) sequence at short echo time, acquired from the regions of interest (ROI), as shown in Figure 6-3.

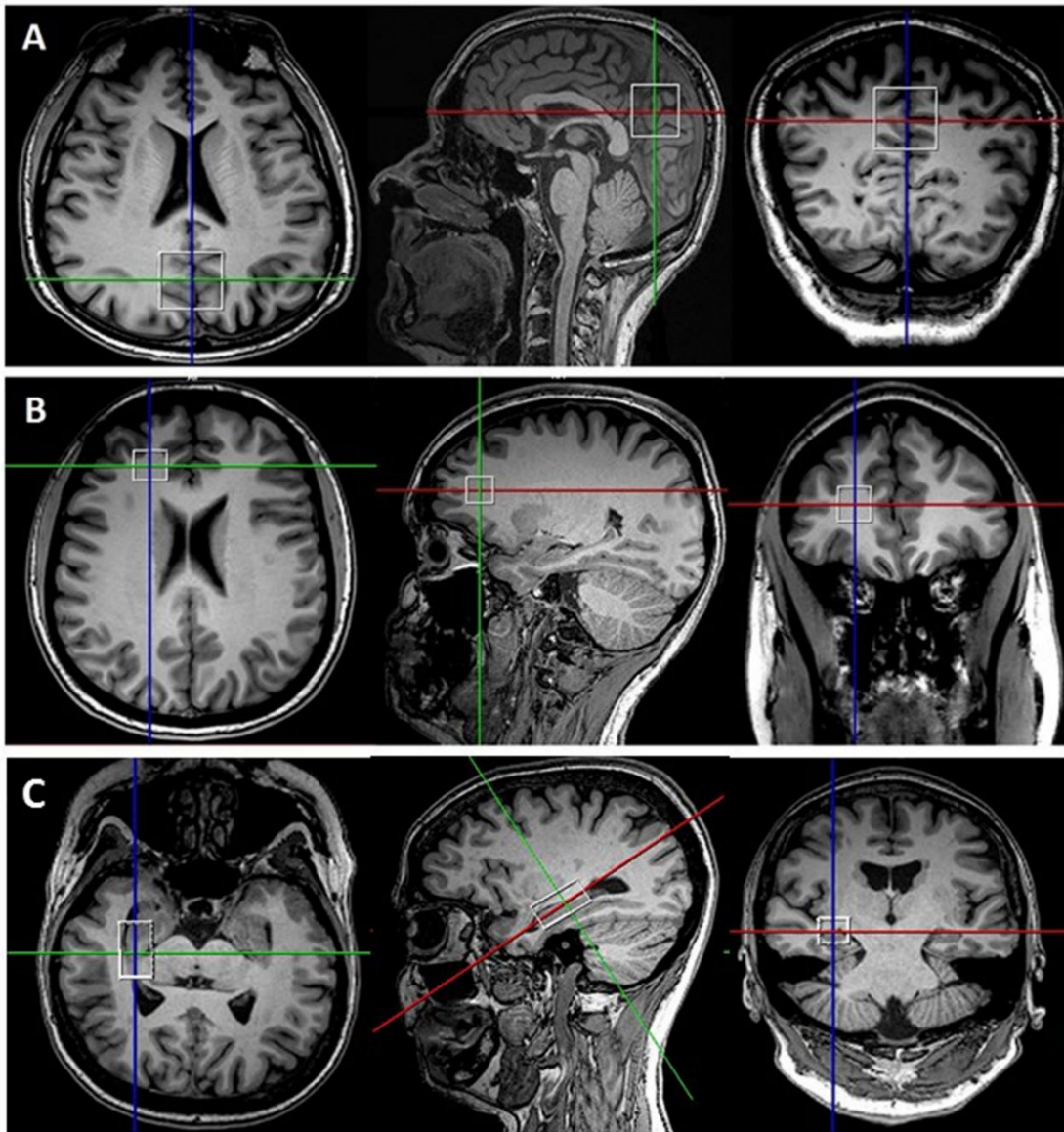


Figure 6-3. T1-weighted MR images in coronal, sagittal and axial planes demonstrating the PCG (A), PFC (B) and hippocampal (C) voxels sizes and positions (white box).

The following parameters were used: TR/TE=2000/30ms, hippocampal voxel size =30x15x15 mm<sup>3</sup>, PFC voxel size =15x15x15 mm<sup>3</sup>, PCG voxel size =30x30x30 mm<sup>3</sup>, averages = 96, vector size =1024 points, preparation scans =4, RF offset frequency =3.2 ppm and water suppression was enabled. Water reference was also acquired (4 averages) from the same voxel position and size after disabling RF part of water suppression module.

Single voxel 1D MRS was transferred offline and analysed with LCModel using a basis set specifically designed for 3T and TE=30ms with water normalization. This technique allowed the estimation of overlapping resonant metabolites such as glutamine+glutamate (Glx) at short TE. A water reference scan was used for eddy-current correction as well as partial volume correction in LCModel by adjusting 'WCONC' parameter based on percentages of WM, GM and CSF as described in the LCModel manual. Concentrations of the brain metabolites were expressed as a ratio with respect to total creatine (Cr+phosphocreatine (PCr) = tCr) with Cramer-Rao lower bound (CRLB (SD %)) less than or equal 20% accepted. Samples of *in-vivo* MR spectra from PFC and PCG analysed by LCModel are shown in Figure 6-4.

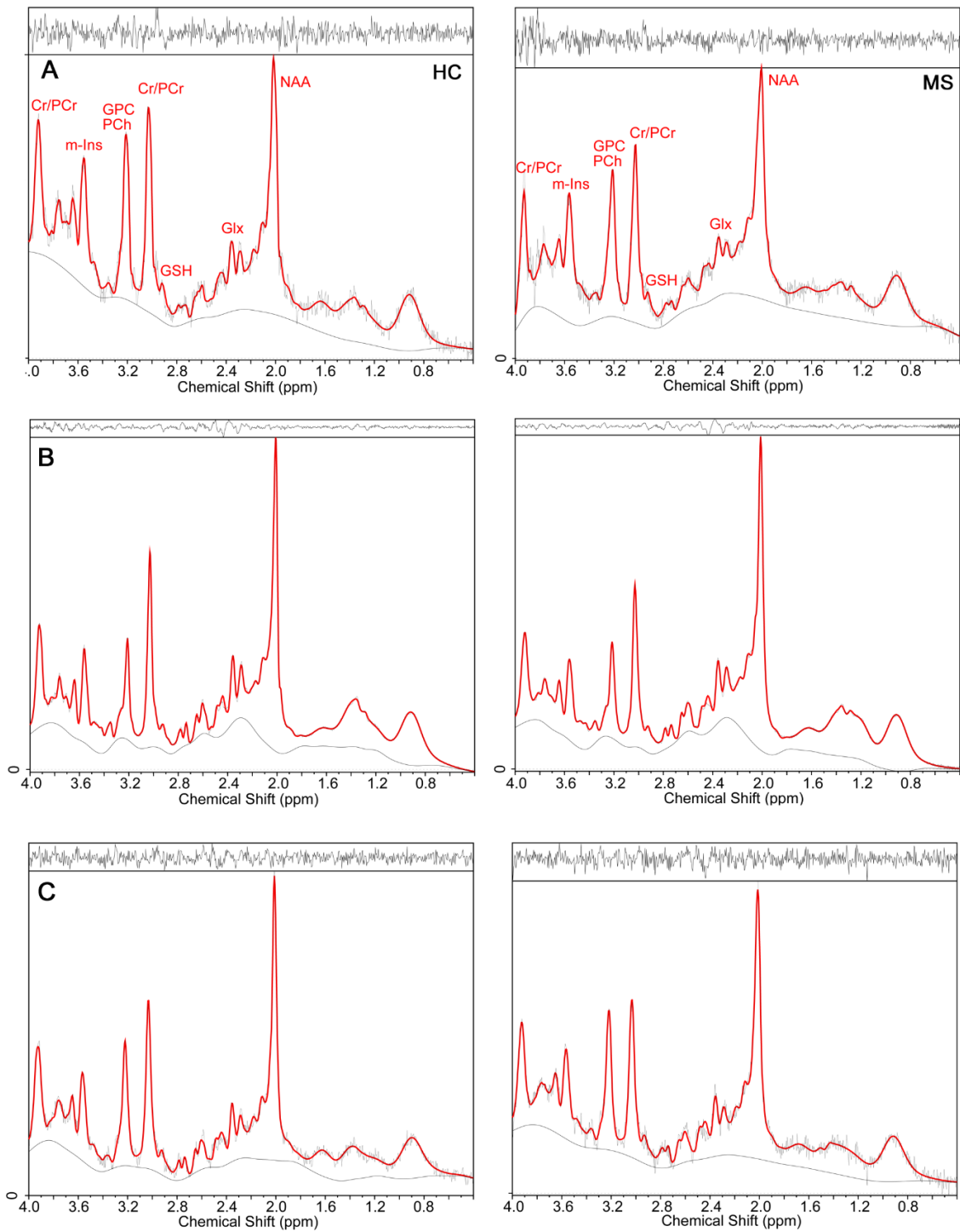


Figure 6-4. Samples of in-vivo MR spectra levels from HCs (left) and MS patients (right) for (A) hippocampal, (B) PCG and (C) PFC regions analysed by LCModel indicating the major set of brain metabolites at 3T and short TE.

### *Quality Control*

Maintenance of quality control for MRI and MRS data was carried out by weekly scanning of the American College of Radiologists (ACR) phantom and spherical GE spectroscopic phantom<sup>165</sup> containing stable brain metabolites at physiological pH and concentrations.

### **6.2.6 Clinical Assessments**

All RRMS patients underwent a comprehensive neurological examination for disability status by applying the EDSS. The EDSS is the most common tool used to evaluate the classification of disability in MS patients. It allows neurologists to assign a Functional System Score (FSS) to 7 functional systems including: Pyramidal, Cerebellar, Brainstem, Sensory, Bowel and Bladder, Visual and Cerebral. All EDSS evaluations were performed by a neurologist who had undertaken appropriate neuro status certification training. The MS Severity Score (MSSS) was calculated using the EDSS and duration of disease for each patient according to the algorithms provided by Roxburgh et al.<sup>207</sup>.

Similarly, all study participants (RRMS and HCs) were assessed for cognitive performance at baseline using ARCS, which is a valid and reliable instrument for administering neuropsychological tests of cognitive function to unsupervised individuals<sup>13</sup>. The ARCS assesses the performance in the domains of memory, verbal fluency, language, visuospatial function and attention with elements from each domain given a score which is used to derive an overall ‘global’ cognitive performance score. Studies to date indicate that elements of the ARCS have good to excellent test-retest characteristics and generate results that correspond closely to those obtained with conventional administration of the same tests in alternate form.

The SDMT was undertaken concurrently as a measure of attention and information processing speed presented in the visual modality. As described by Drake et al.<sup>245</sup>: *“Patients view a key presenting nine numbers paired with unique symbols. Below the*

*key is an array of symbols paired with empty spaces, the patient's task being to voice the matching number for each symbol as rapidly as possible.*" The SDMT has been shown to be an appropriate screening tool for evaluating cognitive impairment in MS patients<sup>245, 246</sup> that is comparable to other psychometric and questionnaire methods.

The mental health status of participants was assessed using the short version of the Depression Anxiety Stress Scale (DASS-21)<sup>208</sup>. Higher scores were indicative of higher levels of depression, stress and anxiety. All scores, derived from the 21-point scale, were multiplied by 2 to enable comparison to the full 42-point scale DASS and determine clinical cut offs for symptom severity.

Fatigue status was determined using the Modified Fatigue Impact Scale (MFIS), a modified form of the Fatigue Impact Scale<sup>209</sup>. The questionnaire was based on items derived from interviews with MS patients concerning how fatigue impacts their lives. This instrument provided an assessment of the effects of fatigue in terms of physical and cognitive functioning.

### **6.2.7 Statistical Analysis**

To investigate the significant difference between MS and HCs groups, T-tests were applied using SPSS, for independent sample analyses. Major brain metabolites (NAA, Cr, total choline (tCho; glycerophosphocholine (GPC)+phosphocholine(PCh)+free choline (Cho)), m-Ins, GSH and Glx) were analysed from RRMS groups and HCs in cross-sectional study. The level of significant change in metabolite levels associated with the three treatment groups was assessed using General Linear Model - Univariate, each metabolite is the dependent variable and treatment is a fixed factor adjusted for appropriate covariates, followed by post hoc testing using Least Significant Difference (LSD). Additionally, correlation between clinical symptoms and metabolite levels was performed using the correlation coefficient for non-parametric correlations (Spearman's rho). Since this study was largely exploratory in nature and consisted of

multiple test variables, we chose to use a relaxed significance threshold of 0.05 and interpret results accordingly.

## 6.3 Results

### 6.3.1 Participant demographics and characteristics

RRMS patients had an average disease duration of  $8.2 \pm 0.6$  years, with mild disability (EDSS  $2 \pm 0.12$ ) and mean MSSS of  $2.9 \pm 0.2$  and were predominantly female (77%) with a mean age of  $44 \pm 1.04$  years, and undergoing treatment for the last  $3.2 \pm 0.3$  years with fingolimod (N=52), interferon or GA (N=46) (Table 6-2). Cross-sectional evaluation showed significant differences in severity of mood symptoms, fatigue status and cognition impairment in the RRMS patients compared to age and sex-matched HCs at baseline (Table 6-2). Additionally, cognitive function, fatigue and mood status evaluation of RRMS treatments group (fingolimod and injectable) were statically significant compared to age and sex-matched HCs at baseline. Therefore, we observed no statistical changes in the level of severity of disability at oral and injectable treatment of cross-sectional evaluation.

Table 6-2. Cross-sectional analysis of mean demographic scores and disease-related variables for RRMS (fingolimod and injectables) and HCs groups at baseline.

Characteristics	Baseline			
	HCs (N=51)	Total MS (N=98)	RRMS (fingolimod ) N=52	RRMS (injectable) N=46
Sex (% female)	74%	77%	70%	84%
Age	$41 \pm 1.4$	$44 \pm 1.04$	$44 \pm 1.3$	$44 \pm 1.71$
Disease Duration (yrs)	-	$8.2 \pm 0.64$	$9 \pm 6.5$	$7.6 \pm 0.9$
EDSS	-	$2 \pm 0.12$	$2 \pm 1.3$	$1.86 \pm 0.16$
MSSS	-	$2.9 \pm 0.2$	$3 \pm 0.3$	$2.8 \pm 0.25$

AAR	-	1±0.22	1±0.22	1±0.22
Total ARCS	93±2.36	86±1.69*	87±2.4*	88±2.3
Memory	93±1.92	88±2.17	87±3.3	90±2.6
Fluency	94±2.56	85±1.54**	84±2.3**	85±1.8**
Visuospatial	100±0.56	102±0.80*	102±0.6*	99±1.5
Language	90±3.57	89±2.23	89±2.8	90±3.4
Attention	99±1.86	94±1.46*	94±1.9*	95±2.3
SDMT	60±1.55	50±0.97**	50±1.4**	50±1.3**
DASS-21	12±1.90	24±2.38**	25±3**	22±3.7*
Stress	6±0.99	12±1.01**	12±1.4**	10±1.4*
Anxiety	3±0.60	7±0.78**	7±1**	6±1.2*
Depression	3±0.57	7±0.88**	7±1.2**	6±1.3*
MFIS	13±1.50	30±1.74**	34±2.5**	25±2.3**
Physical fatigue	6±0.76	15±0.93**	17±1.3**	12±1.2**
Cognitive fatigue	8±0.92	15±0.91**	16±1.3**	13±1.2**

Data are expressed as mean values ± SEM. AAR: annual relapse rate; DASS-21: depression anxiety stress scales; EDSS: expanded disability status scale; MFIS: Modified Fatigue Impact Scale; MSSS: MS severity score; SDMT: symbol digit modalities test; Total ARCS: Total audio recorded cognitive screen.

### 6.3.2 Morphology (whole brain and MRS voxel characteristics)

There was a significant variation in the MRS voxel composition (GM, WM and CSF fractions) between HCs and MS patients using cross-sectional analysis, with a significant reduction in the WM fraction(-14%) and a reciprocal 15% increase in CSF within the hippocampal voxel in the 52 RRMS (fingolimod cohort) at baseline compared to 51 age and sex-matched HCs group. We observed no significant difference at baseline in PFC and PCG voxels composition between HCs and RRMS patients (fingolimod cohort) (Table 6-3). Moreover, there was an identical statistical significance in the hippocampal voxel composition with a significant reduction in the

WM fraction (-15%) between HCs and RRMS (injectable cohort) as well as HCs and RRMS patients (both cohorts).

In addition, we observed a significant reduction in the total brain volume between the RRMS (fingolimod cohort) and age and sex-matched HCs at baseline (Table 6-3). Interestingly, within the RRMS (fingolimod cohort) and (injectable cohort) as the RRMS (both groups), brain tissue volume fraction (CSF, GM, WM and pGM) were statistically significant compared with HCs group. The findings showed a significant reduction in GM (-3%), WM (-5%) and pGM (-3%) with a reciprocal 40% increase in CSF (Table 6-3).

Table 6-3. Mean values of spectroscopic voxel segmentation of hippocampal, PCG and PFC regions and volume of brain fractions for RRMS patients compared to age and sex-matched HCs at baseline.

	Regions	HCs	RRMS (fingolimod)	RRMS (injectable)
<b>Sample size</b>		<b>N=51</b>	<b>N=52</b>	<b>N=46</b>
<b>MRS voxel Hippocampus</b>	<b>CSF%</b>	4.1±0.011	4.7±0.004	5.2±0.008
	<b>GM%</b>	39.8±0.006	46.3±0.004*	46.1±0.007*
	<b>WM%</b>	55.5±0.013	48.7±0.007*	48.4±0.018*
	<b>LV(mm<sup>3</sup>)</b>	-	0.82±0.03	0.431±0.012
<b>MRS voxel PCG</b>	<b>CSF%</b>	11.8±0.007	13.2±0.005	13.9±0.008*
	<b>GM%</b>	51±0.004	50±0.003	50±0.005
	<b>WM%</b>	36.6±0.007	36.2±0.004	35.9±0.006
	<b>LV(mm<sup>3</sup>)</b>	-	0.04±0.01	0.06±0.01
<b>MRS voxel PFC</b>	<b>CSF%</b>	1.8±0.003	1.85±0.003	1.9±0.006
	<b>GM%</b>	13.9±0.011	13.6±0.008	12.4±0.014
	<b>WM%</b>	83.7±0.03	84.6±0.01	85.5±0.01
	<b>LV(mm<sup>3</sup>)</b>	-	0.85±0.7	1.68±1.67
<b>Whole brain (mm<sup>3</sup>)</b>	<b>WBV</b>	1621±11	1562±13**	1560±10**
	<b>PGM</b>	671±6	652±7*	648±5*
	<b>CSF</b>	30±1	42±3**	41±3**
	<b>GM</b>	833±7	809±8*	808±6*

	<b>WM</b>	787±6	752±6**	752±6**
	<b>T2 lesion volume</b>	-	6.2±0.7	5±0.9

\*  $p \leq 0.05$ ; \*\*  $p \leq 0.01$  RRMS vs HCs at baseline. CSF: normalised ventricular volume; LV (mm<sup>3</sup>): lesion volume within MRS voxel; GM: normalised grey matter; MRS: magnetic resonance spectroscopy; pGM: normalised cortical grey matter; WM: normalised white matter; WBV: normalised whole brain volume.

### 6.3.3 MR Spectroscopy

Using single voxel H-MRS, cross-sectional analysis identified a statistically significant reduction in hippocampal NAA/tCr (-17%,  $p=0.001$ ) (-15%,  $p=0.01$ ) and increase in Glx/tCr (+16%,  $p=0.001$ ) (+15%,  $p=0.02$ ) in RRMS (fingolimod cohort) and (injectable cohort) at baseline, compared to HCs (Table 6-4) and (Figure 6-5). We also observed significant reduction in PCG NAA/tCr (-7%,  $p=0.001$ ) (-6%,  $p=0.001$ ) and reduction in PCG Cr/tCr (-7%,  $p=0.02$ ) (-5%,  $p=0.02$ ) in RRMS (fingolimod cohort) and (injectable cohort) at baseline, compared to HCs (Table 6-4) (Figure 6-6). However, PCG Glx/tCr level (1.166±0.015) in RRMS (injectable cohort) was significantly lower than HCs (1.25±0.017) with significant reduction by (-7%,  $p=0.01$ ). In contrast, we did not observe any significant difference in the level Glu or GSH and tCho of hippocampal and PCG regions between the RRMS (fingolimod cohort) at baseline compared to HCs (Table 6-4).

On another region of RRMS patients who had fingolimod treatment, cross-sectional analysis identified a statistically significant reduction in PFC NAA/tCr (-9%,  $p=0.001$ ) and increase in m-Ins/tCr (+5%,  $p=0.03$ ) in RRMS group at baseline, compared to matched HCs (Table 6-4) (Figure 6-7). When assessing only the RRMS, injectable cohort (N=46), cross-sectional analysis showed statistical significance reduction in PFC (NAA, -14%,  $p=0.03$ ) and (GSH, -10%,  $p=0.03$ ) between the RRMS cohort and HCs. We also observed significant increase in PFC metabolites/tCr ratio (m-Ins, +7%,  $p=0.01$ ) in RRMS at baseline, compared to HCs (Figure 6-7). However, no statistically significant difference was observed in PFC metabolites/tCr ratio of (Glx,

tCho and Cr or PCr) data between RRMS group compared to HCs at baseline. When assessing only the RRMS, (fingolimod cohort) (N=52), we observed a significant reduction in the levels of tNAA/tCr ratio in hippocampal, PCG and PFC regions in the RRMS cohort compared to HCs at baseline (Figure 6-8).

On the other side of this study, MRS finding showed that there was statistically significant reduction in the levels of hippocampal metabolites/tCr ratio (NAA, -16%,  $p=0.01$ ) and (Glu, -8%,  $p=0.02$ ) in the total RRMS cohort compared to HCs (Figure 6-8). Moreover, compared with the HCs, the hippocampal Glx/tCr was higher (+17%,  $p=0.002$ ) in the total RRMS patients (Figure 6-9). In contrast, we did not observe any significant difference in the level of the other hippocampal metabolites/tCr ratio between the RRMS group at baseline compared to HCs.

When assessing PCG metabolites profiles for total RRMS patients, a statistically significant reduction in metabolite to tCr ratios was identified for (NAA, -6%,  $p=0.001$ ), (Glx, -6%,  $p=0.01$ ) and (Glu, -5%,  $p=0.002$ ) in the total RRMS cohort compared to HCs (Figure 6-9). However, no statistical significance ( $p<0.05$ ) in PCG metabolites levels was identified for tCho, m-Ins and GSH between the RRMS cohort and HCs at the baseline.

Cross-sectional analysis for PFC metabolites/tCr ratio showed a significant reduction in (NAA, -9%,  $p=0.001$ ) and (Glu, -6%,  $p=0.04$ ) and increase in (m-Ins, +6%,  $p=0.01$ ) in the total RRMS cohort compared to HCs (Figure 6-9). No statistically significant difference ( $p<0.05$ ) was observed in PFC metabolites levels (tCho, Glx, GSH and Cr or PCr) between RRMS cohort at baseline compared to HCs.

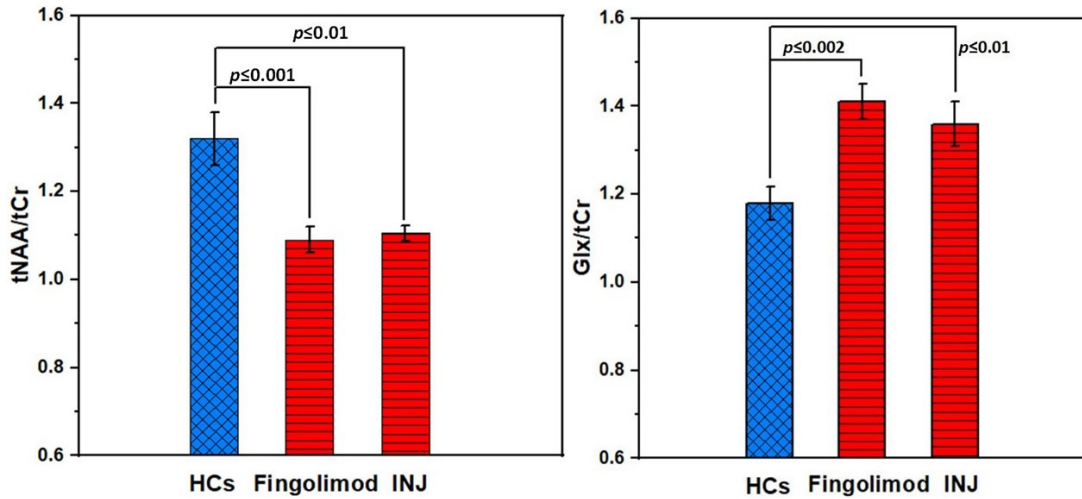


Figure 6-5. Hippocampal neurometabolite/tCr ratio (tNAA and Glx) in HCs and RRMS fingolimod and injectables (INJ: GA+interferon) disease modifying therapies.

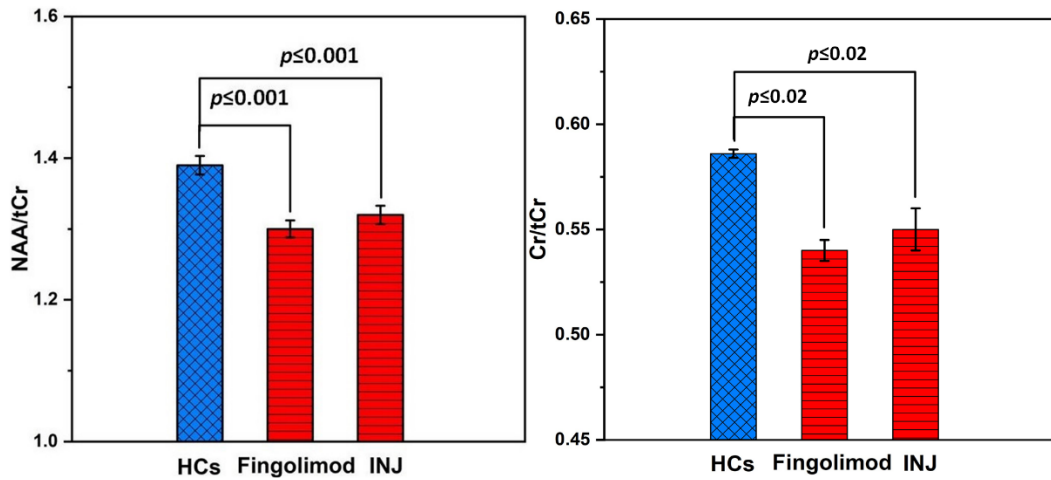


Figure 6-6. PCG neurometabolite/tCr ratio (tNAA and Cr) in HCs and RRMS fingolimod and injectable treatments (INJ: GA+interferon).

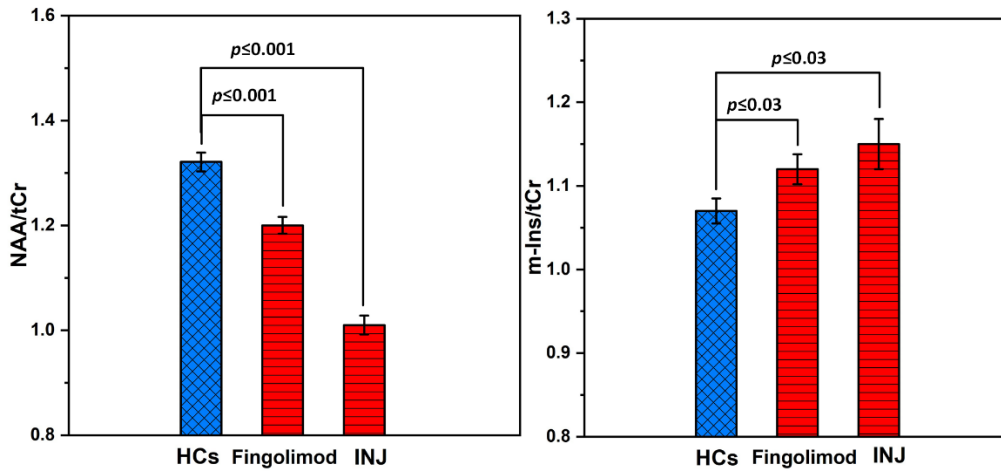


Figure 6-7. PFC neurometabolite / tCr ratio (NAA and m-Ins) in HCs and RRMS fingolimod and injectable (INJ: GA+interferon) disease modifying therapies.

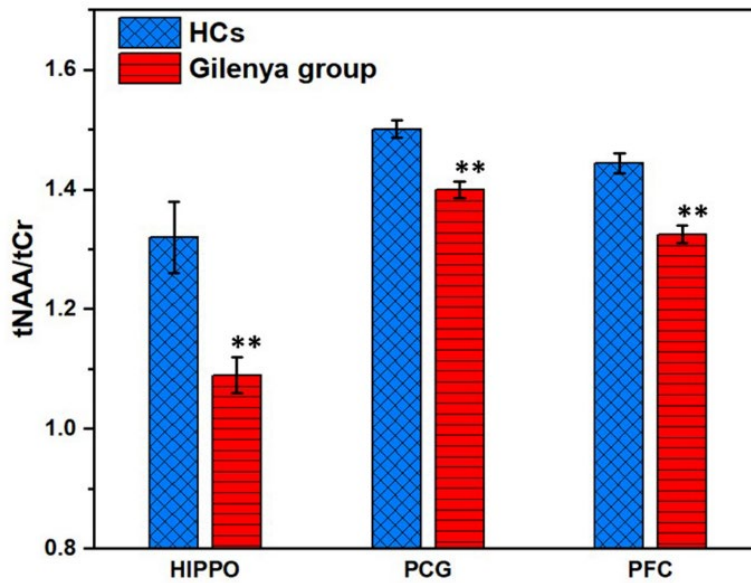


Figure 6-8. Comparison the levels neurometabolite/tCr ratio (tNAA) in HCs and RRMS fingolimod (Gilenya) in three regions hippocampal (HIPPO), PCG and PFC. \*\* $p \leq 0.001$  RRMS (fingolimod group) vs HCs at baseline.

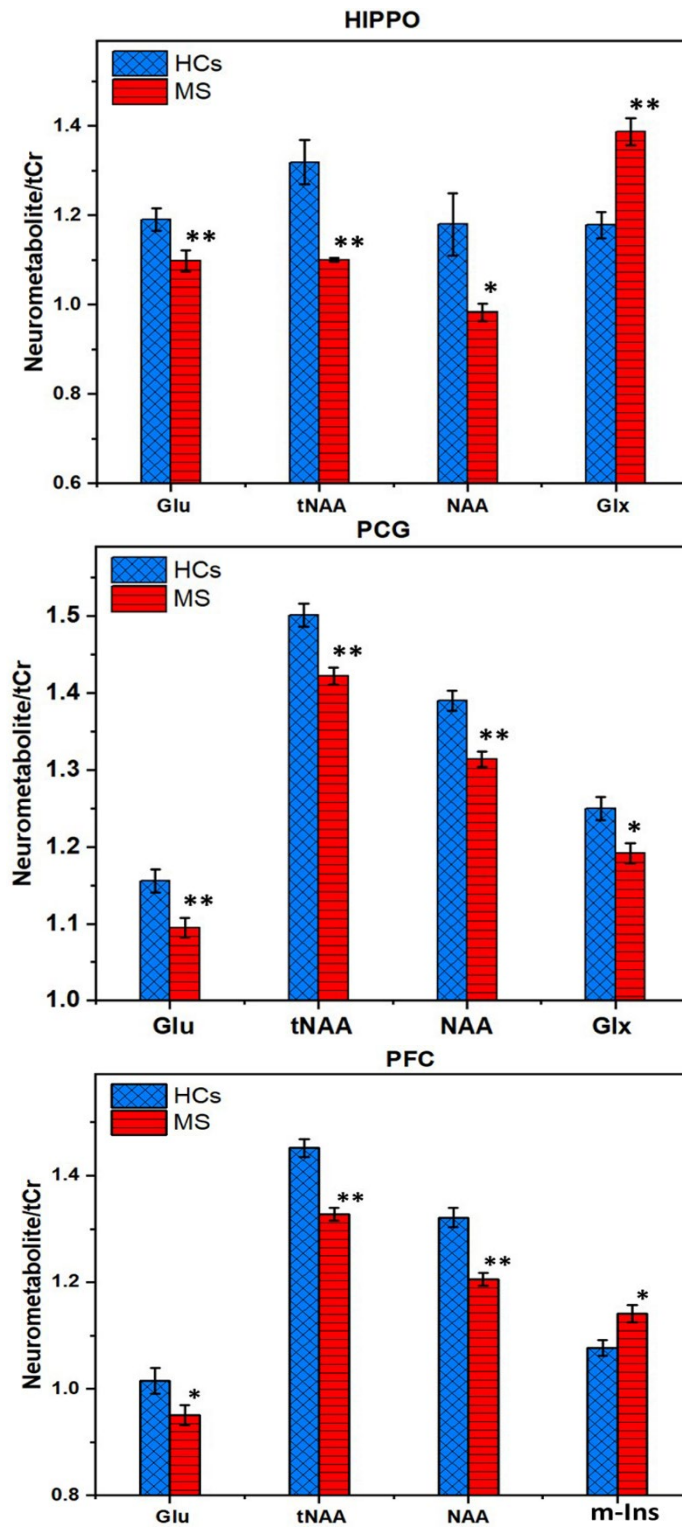


Figure 6-9. Comparison of the neurometabolite/tCr ratio (tNAA, NAA, Glx, Glu and m-Ins) in HCs and total RRMS in three regions of hippocampal (HIPPO), PCG and PFC. \*  $p \leq 0.01$ , \*\*  $p \leq 0.001$  RRMS vs HCs at baseline.

Table 6-4. Mean values of brain-metabolite/tCr of hippocampal, PCG and PFC regions in HCs and RRMS (fingolimod and injectable cohorts). \*  $p \leq 0.05$ ; \*\* $p \leq 0.01$  RRMS vs HCs at baseline.

Regions	Metabolite	HCs	RRMS fingolimod cohort	RRMS injectable cohort
MRS voxel Hippocampus	Sample size	N=51	N=52	N=46
	GSH	0.362±0.13	0.477±0.032	0.484±0.021
	Glx	1.179±0.038	1.411±0.040**	1.36±0.05**
	tNAA	1.320±0.060	1.09±0.03**	1.05±0.018**
	NAA	1.180±0.08	0.969±0.024*	1±0.019*
	tCho	0.319±0.008	0.311±0.006	0.325±0.006
	Glu	1.174±0.04	1.117±0.031	1.078±0.037*
	m-Ins	1.541±0.028	1.546±0.034	1.414±0.04
MRS voxel PCG	GSH	0.23±0.003	0.24±0.004	0.233±0.006
	Glx	1.25±0.015	1.21±0.02	1.167±0.018*
	tNAA	1.501±0.015	1.400±0.014**	1.434±0.017**
	NAA	1.4±0.013	1.3±0.012*	1.326±0.014*
	Cr	0.580±0.003	0.540±0.005*	0.553±0.01*
	Glu	1.15±0.015	1.11±0.02	1.073±0.016
	m-Ins	0.98±0.011	0.96±0.012	0.96±0.014
	tCho	0.18±0.002	0.17±0.002	0.176±0.003
MRS voxel PFC	GSH	0.4±0.016	0.41±0.032	0.36±0.01*
	Glx	1.05±0.002	1±0.02	0.96±0.03*
	tNAA	1.444±0.017	1.325±0.015**	1.329±0.02**
	NAA	1.32±0.02	1.2±0.016*	1.2±0.02*
	Glu	1.02±0.02	0.97±0.02	0.925±0.03*
	m-Ins	1.077±0.016	1.126±0.018*	1.158±0.03*
	tCho	0.314±0.008	0.316±0.006	0.325±0.008

#### 6.3.4 Correlation of hippocampal metabolites with clinical and volumetric measures

We investigated associations between clinical symptoms and hippocampal metabolite levels for RRMS (fingolimod cohort) at the baseline. The clinical symptoms that showed the associations with hippocampal metabolite levels were related to mood status and cognitive domains (Table 6-5). There was a positive correlation between the levels of hippocampal m-Ins, with the overall severity of mood symptoms (DASS-21,

$r=0.364$ ) and depression ( $r=0.368$ ) (Table 6-5). The cognitive domains evaluated by ARCS ( $r=0.402$ ) and memory ( $r=0.428$ ) displayed associations with hippocampal NAA only, while processing speed and attention, determined by the SDMT, showed no correlation with hippocampal neurometabolites for RRMS (fingolimod cohort) at baseline. Other hippocampal neurometabolite levels (tCho and GPC) were positively correlated with total brain and grey matter volumes.

The clinical symptoms that showed the associations with volumetric MRI measures were related to disability status and cognitive domains (Table 6-5). There was a negative correlation between ventricular volume, with the cognitive domains, processing speed ( $r=-0.29$ ) and attention ( $r=-0.308$ ) (Table 6-5), while disability status (EDSS,  $r=0.355$ ) was positively correlated with ventricular volume.

The cognitive domains evaluated by processing speed and attention, determined by the SDMT displayed positive correlation with GM, WM and total brain volumes, while disability status of RRMS (fingolimod cohort) (EDSS,  $r=-0.403$ ,  $r=-0.379$ ), showed negatively correlation with GM and total brain volumes respectively at baseline. However, mood status and cognitive domains (ARCS and memory), showed no correlation with MRI measurements for RRMS (fingolimod cohort) at baseline.

For total RRMS (fingolimod and injectable cohort) at baseline, the mood symptoms (depression,  $r=-0.3$ ) were negatively correlated with hippocampal NAA. Moreover, hippocampal axonal integrity (NAA/tCr) was negatively correlated with ventricular volume ( $r=-0.306$ ) at baseline. Volumetric MRI measures correlated with clinical symptoms related to disability status (EDSS) and cognitive domains in total RRMS showing similar trend to the fingolimod cohort at baseline. However, mood symptoms (DASS-21,  $r=-0.335$ ) were negatively correlated with WM volume.

Table 6-5. Spearman's correlation between hippocampal neurometabolite ratios and cognitive functions and volumetric measures in RRMS (fingolimod cohort) at baseline. Only statistically significant changes are listed.

Measurements	Parameters	Clinical parameters		
MRS measure	NAA	TARCS	Memory	
		0.402*	0.428*	
	m-Ins		DASS-21	Depression
			0.364**	0.368**
	tCho	GMV	WBV	
		0.292*	0.283*	
MRI measure	CSFV	Attention	SDMT	EDSS
		-0.308*	-0.293*	0.355**
	GMV	Attention	SDMT	EDSS
		0.278*	0.352*	-0.403**
	WMV		SDMT	
			0.316*	
	WBV	Attention	SDMT	EDSS
		0.374*	0.375*	-0.379**

\*  $p \leq 0.05$ ; \*\* $p \leq 0.01$ . DASS-21: depression anxiety stress scales; CSFV: ventricular volume; EDSS: expanded disability status scale; GMV: grey matter volume; NAA: N-acetylaspartate; m-Ins: myo-inositol; TARCS: total audio recorded cognitive screen; tCho: total choline; WBV: whole brain volume; WMV: white matter volume.

### 6.3.5 Correlation of PCG metabolites with clinical measures

The correlation between clinical symptoms and PCG metabolite levels and volumetric MRI measures for RRMS (fingolimod cohort) were investigated in this study. The clinical symptoms that showed associations with PCG metabolite levels were related to cognitive domains (Table 6-6). The cognitive domains evaluated by the ARCS displayed associations with PCG GSH, m-Ins and tCho with negatively correlation at baseline. While processing speed, determined by the SDMT, and attention domains showed correlation with PCG neurometabolites (GSH( $r=-0.395$ ) and tCho ( $r=-0.343$ )) at baseline. Moreover, there was a negative correlation between the levels of PCG GSH and tCho with memory ( $r=-0.431$  and  $-0.436$ ) (Table 6-6).

Other clinical symptoms that showed associations with PCG metabolite levels were related to disability status, MSSS score at baseline (Table 6-6). Interestingly, there was

a negative correlation between the levels of PCG NAA with the MFIS score ( $r=-0.315$ ) and ventricular volume ( $r=-0.425$ ). This correlation supports the notion that PCG axonal integrity (NAA/tCr) is leading to increased ventricular volume (atrophy).

For total RRMS (fingolimod and injectable cohort) at baseline, the cognitive domains (TARCS,  $r=-0.285$  and  $r=-0.329$ ) showed negative correlation with PCG m-Ins and tCho respectively. Moreover, the memory and attention domains ( $r=-0.285$  and  $r=-0.329$ ) showed negative correlations with PCG m-Ins ( $r=-0.228$  and  $r=-0.341$ ) and tCho ( $r=-0.302$  and  $r=-0.289$ ) respectively. Disability status and MSSS score showed positive associations with PCG tCho levels at baseline. Additionally, there was a negative correlation between the levels of PCG NAA with ventricular volume ( $r=-0.315$ ), while ventricular volume was positively correlated with PCG m-Ins ( $r=0.267$ ).

Table 6-6. Spearman’s correlation between PCG neurometabolites ratios and cognitive functions in RRMS (fingolimod cohort) at baseline. Only statistically significant changes are listed.

Measurements	Parameters	Clinical parameters				
MRS measure	GSH	TARCS	Memory	Attention	SDMT	EDSS
		-0.365*	-0.431**	-0.318*	-0.395*	0.331*
	m-Ins	TARCS		Attention		
		-0.343*		-0.326*		
	tCho	TARCS	Memory		SDMT	MSSS
		-0.446**	-0.436**		-0.343*	0.336*
	NAA	MFIS	CSFV			
		-0.315*	-0.425**			

\* $p \leq 0.05$ ; \*\* $p \leq 0.01$ . EDSS: expanded disability status scale; GSH: glutathione; MFIS: modified fatigue impact scale; NAA: N-acetylaspartate; m-Ins: myo-inositol; MSSS: MS severity score; SDMT: symbol digit modalities test; TARCS: total audio recorded cognitive screen; tCho: total choline; CSFV: ventricular volume.

### 6.3.6 Correlation of PFC metabolites with clinical measures

The Correlation between the clinical symptoms and PFC metabolite levels indicated that there was a negative correlation between the levels of PFC GSH and Glx with the mood symptoms for each domain, anxiety (GSH,  $r=-0.351$ ) and depression

(Glx,  $r=-0.312$ ) (Table 6-7). While PFC Glx levels showed an association with the cognitive domain (attention,  $r=-0.362$ ). However, the cognitive domain evaluated by the ARCS and disability status score, showed no correlation with PFC neurometabolite for RRMS (fingolimod cohort) at baseline.

The cognitive domains evaluated by processing speed and attention, determined by the SDMT displayed positive correlations with GM, WM and total brain volumes, while disability status of RRMS (fingolimod cohort) (EDSS,  $r=-0.403$ ,  $r=-0.379$ ), showed negative correlations with GM and total brain volumes respectively at baseline. However, mood status and cognitive domains (TARCS and memory), showed no correlated with MRI measurements for RRMS (fingolimod cohort) at baseline.

For total RRMS (fingolimod and injectable cohort) at baseline, the mood status (anxiety,  $r=-0.201$ ) showed negative correlation with PFC GSH. Additionally, there was a negative correlation between the levels of PFC NAA with ventricular volume ( $r=-0.274$ ), while grey matter volume was negatively correlated with PFC m-Ins ( $r=-0.267$ ). Volumetric MRI measures (ventricular, grey matter and total brain volumes) correlated with clinical symptoms related to disability status (EDSS) and cognitive domains (SDMT) in total RRMS showing similar trend to the fingolimod cohort at baseline. However, mood symptoms (DASS-21,  $r=-0.211$ ) were negatively correlated with WM volume.

Table 6-7. Spearman’s correlations between PFC neurometabolite ratios and cognitive functions in RRMS (fingolimod cohort) at baseline. Only statistically significant changes are listed.

Measurements	Parameters	Clinical parameters		
MRS measure	GSH	Anxiety		
		-0.351*		
	Glx	Depression	Attention	
		-0.312*	-0.362**	

\*  $p \leq 0.05$ ; \*\* $p \leq 0.01$ . EDSS: expanded disability status scale; Glx: glutamate+glutamine; GSH: glutathione; SDMT: symbol digit modalities test; TARCS: total audio recorded cognitive screen.

## 6.4 Discussion

A cohort of 98 RRMS patients, on immunomodulatory therapy of fingolimod, interferon or GA for a minimum of 6 months with no new clinical symptoms or change in their disability status in the last 6 months, were included in the study.

The hippocampus controls learning and memory in the brain with highest degree of neuroplasticity, with regional neurogenesis throughout life. Changes in hippocampal proliferation, lesion load, volume and connectivity correlates with alterations in cognitive and mood functions in MS experimental autoimmune encephalomyelitis (EAE) mouse models<sup>210</sup> and MS patient studies<sup>211</sup>. Recently, we demonstrated a trend of rebound effect of GSH in the hippocampus following 24 months of DMF treatment, suggesting recovery from inflammation due to anti-oxidative effect of DMF treatment<sup>280</sup>.

The PFC and PCG, are responsible for the functions of cognition, decision making and learning. In MS, changes in PFC and PCG metabolism, lesion load, GM volume loss and NAWM volume are associated with alterations in cognitive and mood function<sup>211</sup>. Studies have shown that changes to PCG and PFC may be sensitive to the progression of clinical and cognitive disabilities of MS patients and may play an important role in improvement of cognitive performance<sup>248-250</sup>. Although our study cohort had a relatively short disease duration and low disability score, they showed cognitive deficits in all domains compared to matched HC, independent of their treatment. The entire cohort had lower SDMT scores due to poor attention and processing speeds in comparison to HCs. There was no statistical difference in the level of clinical symptoms, EDSS, MSSS at baseline between treatment groups.

Using H-MRS techniques, a reduction in NAA or NAA/Cr and increased m-Ins have been confirmed as the most consistent neurometabolic abnormality in NABM in the RRMS by other studies <sup>28, 68, 281</sup>. In this project, we confirmed the importance of NAA and m-Ins as indicators of axonal loss and gliosis <sup>31, 150, 216</sup>. We observed a significant reduction of NAA and increase in Glx levels in hippocampus, predominantly containing normal appearing white and grey matter in both fingolimod and injectable treatment groups, in comparison to age and sex-matched healthy controls in the cross-sectional analyses. Reduced level of NAA in the grey matter of MS patients has also been recently established, <sup>155</sup> further supporting the importance of NAA as a disease marker. Decreased Glx (Glutamate +Glutamine) levels in NAWM than in controls have been reported by others <sup>150, 237</sup>. However, this contradicts with the finding of Kantorova et al. <sup>282</sup> of higher concentration of Glx and increased Glu concentration by Srinivasan et al. <sup>76</sup> and Geurts et al. <sup>28</sup>. Glutamate (with excitotoxicity properties) may represent Glx due to the general problem of separating and correctly quantifying the components of the Glx resonances due to their strong overlap at 3T <sup>237</sup>. Similarly, our findings showed increase in Glx/Glu and decreased NAA in hippocampal NAWM. This justifies the clinical progression of MS patients, as a result of primary neuroaxonal loss due to inflammatory processes <sup>281</sup>. Furthermore, these metabolic changes were associated with morphological changes within the brain including increased CSF volume, total brain volume loss and T2 white matter lesion load. Our MR spectroscopy findings showed that there was no significant change in hippocampal metabolites between fingolimod and injectable treatment groups and the total RRMS compared to healthy control group. RRMS patients on immunomodulatory therapy of interferon or GA, has shown a lack of significant impact of treatment on brain metabolites during the first 6 months in other MR spectroscopy studies <sup>228, 232</sup>.

In contrast, we found a significant reduction in PCG Glx and Glu of total RRMS group in cross-sectional analyses. This PCG finding is similar to other RRMS MRS studies with reduced Glu (neurotransmitter) concentrations in cingulate and parietal

regions indicating early loss of neuronal integrity. Our finding of PCG Glu is consistent with another MRS study in RRMS<sup>40</sup> that have shown reduction in Glu levels in cingulate and parietal regions reflected the same pathological process of early loss of neuronal integrity in reduced NAA<sup>252</sup>.

Both PFC and PCG demonstrated changes in metabolic profiles especially NAA and m-Ins in RRMS patients with fingolimod and injectable treatments. Out of the three regions, only PCG NAA levels correlated negatively with higher ventricular volume, suggesting that NAA is a marker for neuronal integrity. Therefore, NAA may be a more sensitive marker of brain atrophy. Increase in NAA in white matter has been demonstrated in other MS studies following DMT<sup>217</sup>. Decreased levels of Cr in PCG were seen in our study which is consistent with other studies<sup>70</sup>, and indicative of neuroaxonal alterations which is likely associated with decreases in NAA and Cr levels.

In our study, we observed a significant increase in PFC m-Ins in both treated MS cohorts in agreement with previous studies in NAWM and cortical grey matter indicating brain tissue loss and clinical progression of MS<sup>28, 150, 237</sup>. Increased m-Ins levels in MS whole-brain have been shown in other studies<sup>219</sup> as well as in T1 hypointense chronic lesions<sup>218</sup> suggests astrogliosis around the lesion<sup>68</sup>.

Several studies demonstrated changes in metabolic profiles especially NAA and m-Ins in patients with DMTs. MRS studies have been used to investigate the efficacy of interferon treatment showing conflicting results of improvement or stabilization of the disease with minimal effect on NAA in white matter lesion and NAWM<sup>228, 253</sup>. Kahn et al. reported significant increase in averaged NAA/Cr ratio in the corpus callosum adjacent white matter with GA when compared to healthy controls suggesting axonal metabolic recovery<sup>230, 233</sup>.

Another H-MRS study showed that GSH concentrations in the fronto-parietal region had significant reduction in secondary progressive MS patients compared to RRMS who were on GA and beta interferon treatment<sup>200</sup>. The same study also reported

a trend towards reduced levels of GSH with no significant difference in this same region in RRMS compared to HCs. However, our findings show reduced levels of GSH with significant difference in PCG in RRMS (interferon or GA group). This difference in GSH levels may have resulted from differences in sample size of RRMS and H-MRS protocol (acquisition parameters). Similarly, our previous study demonstrated the trend of GSH recovery in the hippocampus following 2 years of DMF treatment, suggesting recovery from inflammation as a result of anti-oxidative effect of DMF <sup>280</sup>.

Although our patient cohort was young and had relatively short disease duration, the whole brain volumetric measures were lower and ventricular volumes were higher in RRMS than in controls. This suggests neurodegeneration in RRMS starts early and might be related to oxidative stress from GSH reduction. This correlates with other studies even investigating other treatment regimens <sup>200</sup>.

To the best of our knowledge, the current study is the first cross-sectional *in-vivo* investigation comparing the impact of fingolimod, interferon or GA treatment on the hippocampus, PFC and PCG metabolism in RRMS patients. Therefore, longitudinal studies are required to further clarify the above findings. Furthermore, it may be warranted to investigate a longer fingolimod, interferon or GA treatment period in a larger cohort to determine an association between hippocampus, PFC and PCG metabolic levels and treatment efficacy. However, our findings suggest that MRS of brain metabolites in these three regions are a more sensitive marker than morphological changes.

The clinical symptoms that showed the best associations with hippocampal metabolite levels of RRMS (fingolimod group) were related to mood status and cognitive domains. We saw a positive correlation between the levels of hippocampal m-Ins, with the total DASS-21 scores and depression. This may indicate that an increase in gliosis leads to altered mood function in our RRMS cohort. Moreover, the cognitive domains evaluated by the ARCS displayed associations with hippocampal NAA, in particular memory. This may suggest that a decrease in hippocampal neuronal

integrity and mitochondrial dysfunction results in altered cognitive function in RRMS. Also, our results are consistent with a previous study<sup>216</sup> that showed that decreasing NAA correlated with cognitive dysfunction as well as with disability in RRMS patients<sup>254</sup>. Other studies have shown a reduction in NAA and Cho and increase in m-Ins in NAWM correlating with decreased memory scores. Therefore, brain metabolic levels may be an indicator of cognitive performance in RRMS<sup>247</sup>. There is complex association between mood disorders such as depression, anxiety and stress with cognitive performance shown by the lower ARCS scores<sup>221</sup>. However, decrease of NAA/tCr and increase of m-Ins ratios within hippocampal regions do not show a significant relationship with fatigue scores of the RRMS cohort. This result is consistent with a previous MRS study showing that there was no significant correlation between the NAA/Cr and m-Ins/Cr levels and fatigue in RRMS<sup>248</sup>. Although we cannot evaluate the level of atrophy in a cross-sectional design, we noted there was a positive correlation with grey matter and total brain volumes with cognitive function as, determined by the SDMT. In addition to cognition, disability status as measure by EDSS showed negative correlation with grey matter and total brain volumes at baseline. This may represent the relationship between axonal loss and level of atrophy as a key element in the development of clinical disability and brain volume loss in MS.

As expected, the DASS self-report questionnaire confirmed higher levels of depression, anxiety and stress in the RRMS cohort compared to HCs. We also observed an association between PFC GSH and Glx levels with mood symptoms at baseline. This may represent an increase in oxidative stress and glial changes in the PFC with increased depression and anxiety symptoms in our RRMS cohort.

In our cross-sectional analysis, we detected significant alterations in PFC Glx level. We observed a negative correlation between PFC Glx and depression at baseline. Glx correlation with EDSS level at baseline has been reported by Chard et al. in normal appearing white matter and normal appearing cortical grey matter<sup>150</sup>. However, our findings showed there was no correlation between PFC Glx and EDSS at baseline, most

likely as our cohort was relatively young with a short disease duration. NAA/Cr was significantly correlated with EDSS ( $r=-0.7$ ,  $p=0.001$ ) in different MRS studies in NAWM<sup>254</sup> suggesting that neuronal damage within NAWM is a mechanism of disability<sup>43, 255</sup>, but another study found a weak correlation between NAA and EDSS ( $r=-0.4$ )<sup>256</sup>. Others have demonstrated altered levels of Glu in MS, although regional variations have been noted<sup>40</sup>. Elevation in Glu has been observed in white matter lesions but not in NAWM<sup>97</sup> while in the cingulate regions, a depletion in Glu and Glx was measured<sup>40</sup>, which was in turn shown to be associated with visual and verbal memory impairment.

On the other side, we observed a negative correlation between the PCG NAA levels and total fatigue (MFIS) and ventricular volume in RRMS (fingolimod group). This result is consistent with previous MRS studies that showed that there was no significant correlation between NAA/Cr level and cognitive performance in PCG region of RRMS<sup>248</sup>, while our result is not consistent with this MRS study that showed that there was no significant correlation between NAA/Cr level and fatigue in PCG region of RRMS. This may be because we did not select particularly fatigued patients. We detected a correlation between the total ARCS, with an increase in PCG m-Ins levels at baseline. This may suggest an increase in PCG gliosis with altered cognitive function in RRMS cohort. The cognitive domains evaluated by the ARCS displayed associations with PCG tCho of RRMS. This may represent an increase in tCho levels in NAWM compared to controls, indicating increased cell membrane turnover as seen in pathological processing, mainly with inflammation<sup>31</sup> and myelin breakdown which may result from remyelination in chronic lesions<sup>251</sup>. Furthermore, other findings have indicated a reduction in NAA and Cho and increase in m-Ins in NAWM are correlated with decreasing memory scores and suggesting that these brain metabolites may be indicators of cognitive performance in RRMS<sup>247</sup>.

We also observed an association between PCG GSH levels with the cognitive domains evaluated by the total ARCS like memory, while processing speed was

determined by the SDMT, and attention domains showed negative correlation with PCG GSH. This may represent an increase in oxidative stress and glial changes in the PCG with decreased cognitive function as well as with disability in RRMS cohort.

Due to their short disease duration, the whole brain lesion load was low in our patient group, however a reduction in total brain volume, WM, GM and cortical grey matter with reciprocal increase in ventricular volume was already seen. In voxel characterization findings, hippocampal white matter fraction was significantly decreased, and partial GM volume was significantly increased compared to healthy controls in cross-sectional evaluation in the fingolimod cohort. In contrast, there was no significant difference in PFC and PCG morphology. Increased risk of disease progression rates and decrease of treatment effect in MS <sup>212</sup> has been correlated with lower brain volumes and suggests that disease processes other than white matter demyelination are occurring in the MS brain. Faster rates of atrophy in MS patients (0.5-1.35% per year) compared to age-matched HCs (0.1-0.3% per year) has been previously published <sup>213</sup>. The rate of brain atrophy has shown to be a potential biomarker of disease progression in MS <sup>215</sup> and in particular regional grey matter atrophy has shown to have a high correlation with cognitive performance <sup>283</sup>. Also, lower rate of brain volume loss is associated with decrease in disease progression in MS <sup>215</sup>.

This study is the first to illustrate a change in hippocampus, PFC and PCG metabolism associated with treatment with fingolimod, interferon or GA in RRMS patients. However, there are a number of limitations to this study. The findings are cross-sectional and need to be confirmed over an extended treatment period to enable longer term impacts of fingolimod, interferon or GA on disease outcomes and metabolic changes to be more fully explored. In the current study we did not employ spectral editing schemes to optimize detection of GSH as utilized in other studies which have investigated the changes in GSH associated with MS <sup>196, 224</sup>.

## **6.5 Conclusion**

This study demonstrated that MRS is a sensitive marker of disease activity with several metabolites correlated with clinical parameters. The current study is the first cross-sectional *in-vivo* investigation comparing the impact of fingolimod, interferon or GA treatment on the hippocampus, PFC and PCG metabolism in RRMS patients. Longitudinal studies are required to further clarify metabolic difference over time, and to determine an association between hippocampus, PFC and PCG metabolic levels and treatment efficacy. However, our findings suggest that MRS of brain metabolites in these three regions are more sensitive markers than morphological changes.

### **Funding**

Independent investigator-initiated grant provided by Novartis Pharmaceuticals Australia Pty Ltd

### **Availability of data and materials**

Availability of data and materials are subject to guidelines of local Hunter New England Local Health District Human Research Ethics Committee. All authors contributed to revising, literature and critical suggestions to reshape the manuscript.

### **Ethics approval and consent to participate**

This study was approved by Institutional Review Board from the Hunter New England Local Health District Human Research Ethics Committee (HNEHREC Reference No: 4/09/10/3.01), Newcastle, NSW, Australia.

## **Chapter 7 : Spiral-MRSI and tissue segmentation of normal-appearing white matter and white matter lesions in relapsing remitting Multiple Sclerosis patients**

Oun Al-iedani, Karen Ribbons, Neda Gholizadeh, Jeannette Lechner-Scott, Scott Quadrelli, Rodney Lea, Ovidiu Andronesi, Saadallah Ramadan

### **ABSTRACT**

**BACKGROUND:** Conventional MRI is inadequate to understand the pathological changes of Multiple sclerosis (MS). Novel H-MRS methods might add clinical value and potentially identify new biomarkers. Additionally, it may quantify neuronal damage within white matter lesions (WML) and normal-appearing white matter (NAWM).

**PURPOSE:** To evaluate the performance of novel spiral MRSI and tissue segmentation pipeline of the brain, and neurometabolic changes in NAWM and WML of stable relapsing-remitting MS (RRMS) compared to age and sex-matched HCs.

**STUDY TYPE:** Observational

**POPULATION:** Sixteen RRMS patients and nine HCs.

**FIELD STRENGTH/SEQUENCE:** 3T/ Spiral 3D MRSI (LASER-GOIA-W[16,4])

**ASSESSMENT:** MRSI data from a large volume of interest (VOI) 320cm<sup>3</sup> and analyzed using LCModel. Brain volume and WML quantifications were performed using SIENAX and SPM. Support vector machine (SVM) was used to classify tissue types and assessed by accuracy, sensitivity and specificity.

**STATISTICAL TEST:** A receiver operating characteristic curve was used to evaluate and compare the diagnostic performance of metabolites between the two groups. MRSI data and voxel tissue segmentation were also compared between the two cohorts using T-tests.

**RESULTS:** Compared to HCs, RRMS demonstrated a statistically significant reduction in all mean brain tissues and increase in CSF volume. Within VOI, WM decreased (-10%) and CSF increased (41%) in RRMS compared to HCs ( $p < 0.001$ ). MRSI revealed that total creatine (tCr) ratios of N-acetylaspartate and glutamate+glutamine in WML were significantly lower than NAWM-MS (-9%, -8%) and HCs (-14%, -10%), respectively. Myo-inositol/tCr in WML was significantly higher than NAWM-MS (14%) and HCs (10%). SVM of MRSI yielded accuracy, sensitivity and specificity of 86%, 95%, and 70%, respectively for HCs vs WML, which were higher than HC vs NAWM and WML vs NAWM models.

**DATA CONCLUSION:** This study demonstrates the benefit of MRSI in evaluating neurometabolic changes in NAWM. SVM of MRSI data may be suited for clinical monitoring and progression of MS patients. Longitudinal MRSI studies are warranted.

## 7.1 Introduction

Multiple Sclerosis (MS) is an immune-mediated demyelinating condition in which inflammatory cells attack the central nervous system, leading to varying extents of neuroaxonal injury, demyelination and gliosis, affecting both the brain and spinal cord.<sup>67, 68</sup>

The diagnosis and management of MS have become increasingly reliant on MRI. Conventional MRI is essential to monitor inflammatory activity in the form of white matter lesion (WML) as well as MS brain tissue atrophy (parenchymal brain volume loss) in order to assess active or chronic stages, which will determine treatment choices.

However, conventional MRI is not adequate to understand all pathological changes relevant to MS, especially in the progressive phase, such as axonal loss and neuronal damage, oxidative stress, inflammatory and demyelination processes. Novel MR methods such as single voxel (SV) or H-MRS<sup>37</sup> and multi-voxel MRS imaging (MRSI)<sup>38</sup> can differentiate these pathological processes within MS lesions, as well as in normal-appearing white matter (NAWM), which improves the specificity of the diagnosis and aids clinical management of MS.<sup>39</sup>

In the research arena to date, single voxel and MRSI techniques have been used to evaluate the neurometabolic changes in the MS brain. For instance, a reduction of NAA level reflects axonal degeneration and mitochondrial dysfunction<sup>39</sup>, whereas brain inflammation leads to an increase in myo-inositol (m-Ins) and Cr levels due to increased glial (astrocytic) proliferation and energy metabolism.<sup>216</sup> Additionally, an increase in Cho levels is thought to be associated with abnormal membrane turnover from myelin breakdown indicating inflammation and demyelination.<sup>190</sup>

Clinically, MRSI is more suitable than SV methods due to its ability to obtain important metabolic information with extended spatial coverage. Several reports have shown that using SV and MRSI methods coupled with tissue segmentation can evaluate spectroscopic changes of brain metabolites within WML, NAWM and grey matter (GM) in the hippocampus as well as other brain regions in MS patients.<sup>42, 43, 45, 46</sup> Several studies have shown a decrease in NAA and NAA/Cr ratio in WML compared to NAWM regions.<sup>38, 144, 269, 284</sup> Lower NAA ( $p < 0.05$ ) levels were found in NAWM region of MS patients compared to healthy controls (HCs).<sup>43, 284, 285</sup> Increased m-Ins in WML relative to corresponding NAWM was shown in MS patients<sup>37, 38, 269, 284</sup>, and again m-Ins in NAWM in MS patients was increased compared with HCs.<sup>46, 269</sup> Another MRSI study at 3T, showed that NAA/Cr of MS patients was significantly decreased ( $p < 0.0001$ ) in NAWM compared to HCs.<sup>286</sup> Recently, Marshall et al.<sup>27</sup> have shown significant increase in m-Ins and decrease in NAA/Cr ratios in WML compared to NAWM in MS patients by applying semi-LASER MRSI at 3T. Most conventional 2D

and 3D MRSI in the above studies used PRESS which suffer from suboptimal data quality, limited spatial coverage and resolution, long acquisition times and localization artifacts. However, in spite of the above encouraging results of MRSI applications, the challenge is to perform metabolic mapping of the majority of the brain, with high spatial resolution, improved localization and short acquisition times.

Methodological improvements have been achieved to enable fast MRSI acquisition. Interestingly, a few studies have applied fast 3D MRSI methods to cover large regions of the MS brain and to evaluate brain-metabolites in MS lesions, WML, NAWM and cortical grey matter. These fast MRSI studies mostly used echo planar spectroscopic imaging (EPSI)<sup>47-50</sup>, a technically demanding sequence with specialized acquisition and processing requirements, with suboptimal point spread function behavior.

Thus, 3D MRSI with accelerated spiral phase-encoding, localization by *adiabatic selective refocusing* (LASER) sequence and GOIA-W[16,4] RF pulses<sup>287, 288</sup> is proposed in the current study, to investigate metabolic changes in NAWM and WML of RRMS compared to age and sex-matched HCs. We aimed to evaluate the performance of fast spiral MRSI techniques, coupled with tissue segmentation of the majority of the brain, to identify neurometabolic differences in NAWM and WML of stable RRMS patients, compared to age and sex-matched HCs. To evaluate the differences in large spectroscopic data sets in the entire volume of interest (VOI), Support Vector Machine (SVM) method with multi-models of normal appearing white matter and regions of white matter lesions compared to HCs have been applied.

## **7.2 Methods**

### **7.2.1 Patients and Healthy Control Subjects**

Sixteen RRMS patients aged between 20 to 55 years, diagnosed with RRMS according to the McDonald criteria were recruited from a single center.<sup>17</sup> All RRMS patients were undergoing treatment with natalizumab for a minimum of 6 months prior to inception of the study. Nine sex-matched healthy control participants were matched within  $\pm 2$  years of age to the RRMS cohort.

All patients were recruited from the outpatient clinic at the John Hunter Hospital in Newcastle, Australia. Age and sex-matched HCs were recruited from the Hunter Medical Research Institute (HMRI) research register and all participants needed to comply with the study inclusion criteria, which included passing an MRI safety clearance, as well as being able to comply with all study procedures. Institutional Review Board approval was obtained from the Hunter New England Local Health District Human Research Ethics Committee, with written informed consent obtained from all subjects prior to undertaking any study-related procedures. All scans were conducted between May 2016 and June 2018.

### **7.2.2 MRI protocol and Structural assessments**

All study scans were undertaken on a 3T Prisma (Siemens Healthineers, Erlangen, Germany) MRI scanner with a 64 channel head and neck coil. Structural imaging using 3D T1-MPRAGE was performed as follows: volumetric sequence, TR/TE/TI=2000/3.5/1100 ms, 7-degree flip angle, FOV=256x256 mm, image voxel size=1x1x1 mm<sup>3</sup>, NEX=4 and acquisition time=5 minutes. 3D T2-FLuid Attenuated Inversion Recovery (T2-FLAIR) sequence was acquired with TR/TE/TI=5000/386/1800 ms, 12° flip angle, FOV=256x256 mm, image voxel size=1x1x1 mm<sup>3</sup>, echo train duration=858 ms, NEX=1 and acquisition time=4 minutes 12 sec.

### 7.2.3 Validation of MRSI voxel coordinates in vitro and in vivo

For the purpose of segmenting individual MRSI voxels, two experiments were performed to validate the determination of multi-voxel centroid coordinates from the VOI centroid coordinates reported in the Siemens exported '.rda' file (*VOIPositionSag*, *VOIPositionCor*, *VOIPositionTra* and *VOIPhaseFOV*, *VOIReadoutFOV*, *VOIThickness*). A 2x2 cm<sup>2</sup> VOI matrix was defined on the American College of Radiology (ACR) phantom as shown in Figure 7-1A, fitting exactly to the ACR phantom built-in grid. The centroid coordinates of each of the four voxels VOI were calculated using an in-house MATLAB code (2015b, The MathWorks, Inc., Natick, MA, USA) and were compared to the expected coordinates based on the precisely built-in grid inside the phantom. MRSI experiment with a 2x2 cm<sup>2</sup> VOI was also performed in vivo for validation (Figure 7-1B). For this experiment, fractional quantities of GM, WM and CSF within the VOI were determined using multi-voxel segmentation (2x2 voxel) approach which includes duplicating '.rda' file into multiple '.rda' files based on computed centroid for each voxel, as for phantom. This multi-voxel segmentation approach was validated by summation of the total fractional quantities from the multi-voxels (2x2) and comparing them to the total fractional quantities of the VOI as a single voxel.

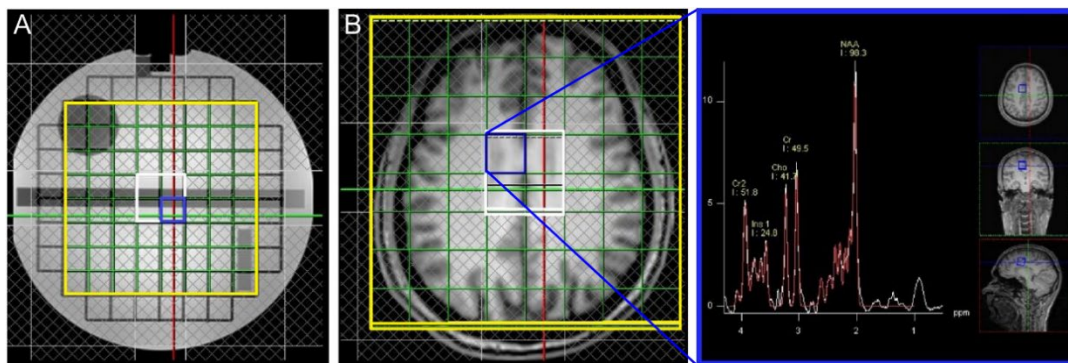


Figure 7-1 A. MRSI VOI (inner white box) and voxel location of interest (blue box) in an ACR phantom, B. In vivo MRSI multi-voxel VOI, voxel of interest location and corresponding spectrum.

#### 7.2.4 Binary mask for the segmentation of MRSI VOI

A binary mask of an MRSI slice ( $8 \times 10 \text{ cm}^2$ ) (Figure 7-2A) was created using the “mask()” function within the SPM toolbox. Masks were then created for each  $1 \times 1 \times 1 \text{ cm}^3$  voxel within the MRSI voxel within the VOI. To achieve this, synthetic data headers (‘.rda’ header) for each MRSI voxel within the VOI were created, using the above in-house MATLAB code. To determine the fractional quantities of GM, WM and CSF within individual VOI voxels, partial volume masks for each tissue type were created using FSL FAST (Figure 7-2. Pipeline of volumetric brain tissue segmentation from MRI and MRSI data. A. A binary mask of a MRSI single slice VOI ( $8 \times 10 \text{ cm}^2$ ) was created using the SPM toolbox. B. partial volume masks for each tissue type were created using FSL FAST. C. Partial volume segmentation of the lesion filled T1-MPRAGE structural images. D. Tissue segmentation of MRSI VOI (CSF, GM and WM) and lesion segmentation overlaid on the T2-FLAIR image. (remove full stop) as described by Quadrelli et al. for single voxel segmentation.<sup>289</sup> These masks were overlaid onto the high-quality T1-MPRAGE structural images. The existing in-house MATLAB code was modified for multi-voxel ‘.rda’ file input, which allowed the MRSI VOI to be co-registered with the T1-MPRAGE, to obtain the fractional quantities of each tissue type per voxel.

This method accounts for the partial volume effects of GM, WM, and CSF by using the respective partial volume estimation values of the MRSI voxels. Finally, MRSI voxels were re-classified into four types of tissues CSF, GM, NAWM and WML (see below) and the fractional volumes for each were calculated.

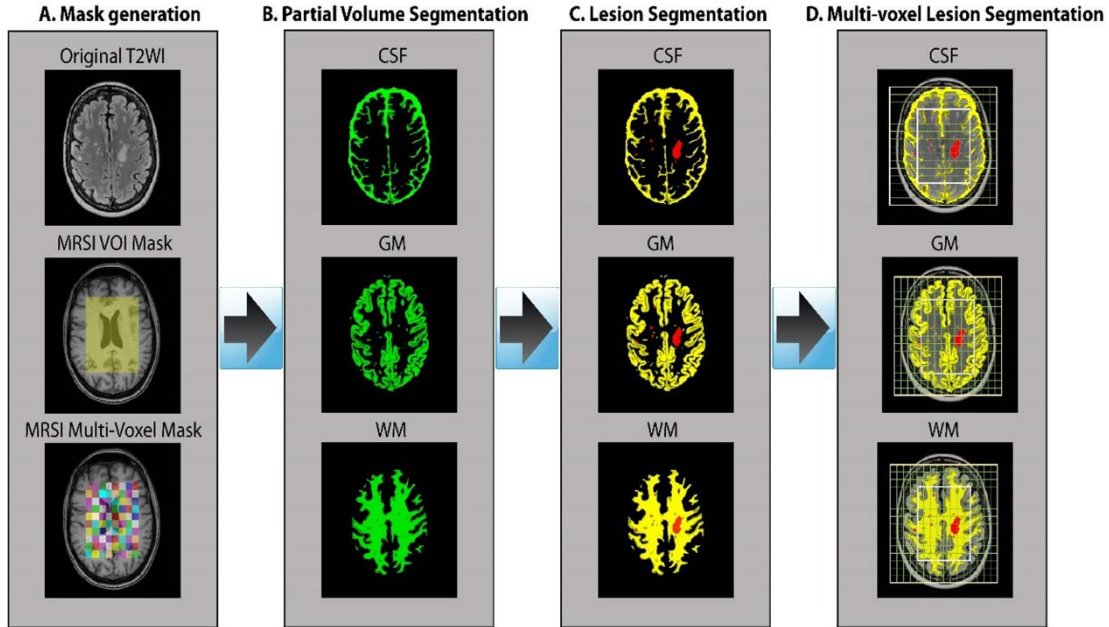


Figure 7-2. Pipeline of volumetric brain tissue segmentation from MRI and MRSI data. A. A binary mask of a MRSI single slice VOI (8x10 cm<sup>2</sup>) was created using the SPM toolbox. B. partial volume masks for each tissue type were created using FSL FAST. C. Partial volume segmentation of the lesion filled T1-MPRAGE structural images. D. Tissue segmentation of MRSI VOI (CSF, GM and WM) and lesion segmentation overlaid on the T2-FLAIR image.

### 7.2.6 White matter lesion quantification

SPM Lesion Segmentation Tool<sup>243</sup> was used to generate an initial binary lesion map from hyperintense T2-FLAIR image voxels, resulting in a lesion probability map with a threshold of 0.1. This was followed by T1-MPRAGE lesion filling, using the binary lesion mask for each participant and a threshold of 0.5. This minimizes errors in partial volume segmentation and improves the final volume measurements. Lesion segmented T1-MPRAGE structural image was performed using FSL FAST<sup>242</sup> (Figure 7-2C and D) as described below.

### 7.2.7 Brain volume quantification

Brain and skull images were extracted from the whole brain 3D T1-MPRAGE data using SIENAX.<sup>239</sup> The brain image was co-registered to MNI152 space<sup>241</sup> to determine the volumetric scaling factors to normalize for head size. Total brain volume and partial volumes, including white matter (WM), GM, peripheral grey matter (pGM) and ventricular CSF volumes were calculated using FSL FAST.<sup>242</sup>

### 7.2.8 Magnetic resonance spectroscopic imaging

3D 1H MRSI was applied using LASER sequence with adiabatic gradient-offset independent *adiabaticity* wideband (GOIA-W)[16,4] RF pulses. LASER-GOIA-W[16,4] RF pulses provide uniform excitation with sharp edges and large bandwidth, without outer-volume suppression bands. MRSI data were acquired with the following acquisition parameters: TR/TE: 2800/30 ms, six averages, spiral k-space sampling with simultaneously encoding one spectral and two spatial dimensions, vector size: 512 points, voxel size: 1x1x1cm<sup>3</sup>, delta frequency (offset): -2.7 ppm, water suppression enabled, VOI in (AP-RL-HF):10x8x4 cm, and FOV/matrix: 16×16×8 cm<sup>3</sup>, yielding a total acquisition time of 13.38 minutes. VOI was placed in the supratentorial brain parenchyma and included the frontal, parietal, occipital lobes as well as the superior aspect of temporal lobe, avoiding placement on the dura. The coronal (AP) slab extends from frontal to occipital lobes (10 cm), the sagittal (RL) slab extends from right to left cortical surfaces (8 cm), while transverse (HF) slab extends from parietal lobe to the superior aspect of the temporal lobe (4 cm). A single 1 cm slice with voxel size of 10x10x10 mm<sup>3</sup> within the VOI is shown in axial, sagittal and coronal MPRAGE planes in Figure 7-3 and included the corpus callosum, thalamus and the deep cortical white matter of frontal, parietal and occipital lobes.

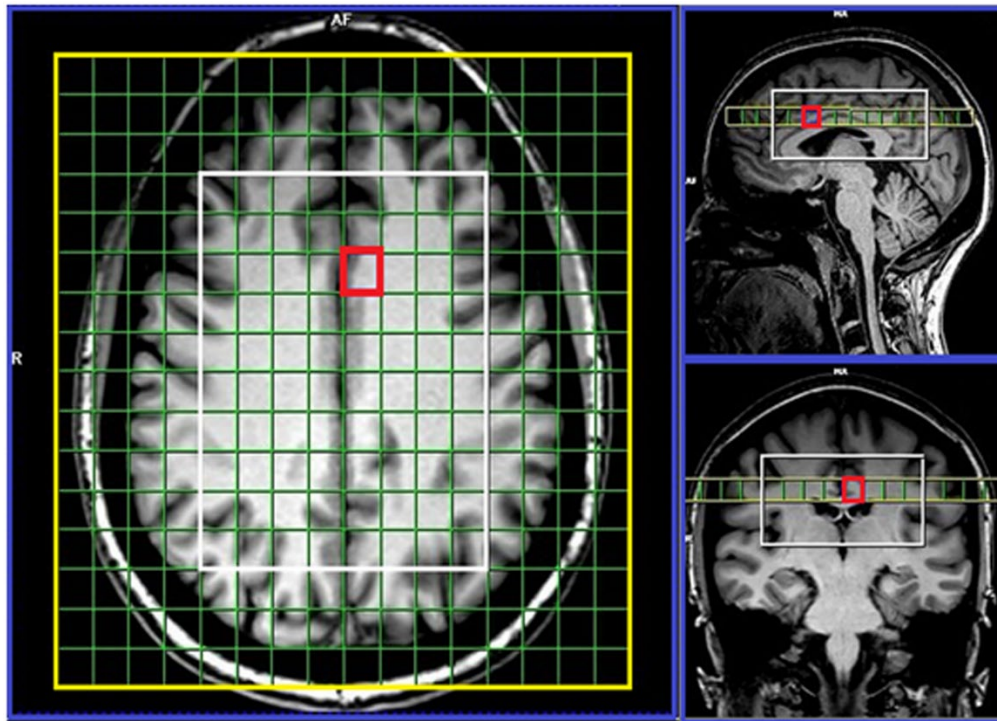


Figure 7-3. FOV (yellow box) and VOI (white box) positions in axial, sagittal and coronal MPRAGE planes with voxel size (red box,  $10 \times 10 \times 10$  mm<sup>3</sup>).

### 7.2.9 Post-processing and statistical analysis

The 3D 1H MRSI voxel was transferred offline and analyzed using an automated linear combination of model spectra LCMModel using a custom-made basis set for the GOIA-W[16,4] based LASER sequence<sup>287</sup> at TE of 30ms and 3T. Fast MRSI technique allowed 15 neurometabolites to be estimated such as NAA, Cr, PCr, m-Ins, Cho, glutamine+glutamate (Glx), glutathione (GSH) and glycerophosphorylcholine (GPC) as ratios to tCr (Cr+PCr). These MRSI detectable neurometabolites were evaluated in WMLs and NAWM in MS as well as in the WM and GM of HCs. Comparisons of neurometabolite ratios between groups were undertaken using T-tests.

Three binary SVM classifications with a radial basis function (RBF) kernel (RBF SVM), HCs vs NAWM, NAWM vs WML and HCs vs WML were built using a leave-one-out cross-validation method. A receiver operating characteristic (ROC) curve was

used to evaluate and compare the diagnostic performance of metabolites with a statistically significant difference between the two groups ( $p < 0.05$ ). The RBF SVM was defined by two parameters: misclassification cost ( $C$ ) and inverse of support vector's radius of influence ( $\gamma$ ). Optimal values of the parameters  $C$  and  $\gamma$  were calculated by performing a grid search of  $2^{-5}, \dots, 2^5$  for  $C$  and  $2^{-10}, \dots, 2^{10}$  for  $\gamma$  and the best combination was selected for each classifier. Due to the small sample size, a leave-one-out cross-validation was used to evaluate the performance of SVM classification models.

Spectroscopic data were reconstructed into  $10 \times 8 \times 4$  voxels with an individual voxel volume of  $1 \text{ cm}^3$ .  $^1\text{H}$  MRSI quality control of 320 spectral voxels per participant was ensured by excluding individual voxel spectra satisfying or more of the following conditions: water peak FWHM during shimming  $> 25$  Hz, Cramer-Rao lower bounds (CRLB(SD%))  $> 40\%$ , partial CSF voxel content  $> 40\%$  or partial lesion voxel content  $> 40\%$ . MRSI patient data with less than 30% of acceptable voxel spectral quality were also excluded.

## **7.3 Results**

### **7.3.1 Participant demographics and characteristics**

All of the 16 recruited RRMS patients were treated with natalizumab. Demographic and clinical parameters of the study cohorts are shown in Table 7-1. All patients were female with a mean age of 39 ( $\pm 9$ ), early in their disease course (disease duration of  $8 \pm 1.3$  years) and with mild disability (EDSS 2  $\pm$  0.4). The cross-sectional evaluation showed that the RRMS patients displayed a greater severity of mood symptoms, fatigue status and cognitive impairment compared to age and sex-matched HCs at baseline (Table 7-1).

Table 7-1. Cross-sectional analysis of mean demographic scores and disease-related variables for MS and HCs groups at baseline.

Characteristics	Baseline		
	HC (N = 9)	MS (N =16)	<i>p</i> -value
Sex (% female)	100%	100%	NA
Age	38±10	39±9	0.621
Disease Duration (yrs)	NA	8±1.3	NA
EDSS	NA	2±0.4	NA
MSSS	NA	3.66±0.5	NA
Total ARCS	96±3.66	84±4.59	0.05
Memory	93±3.11	87±3.23	0.181
Fluency	99±4.34	82±4.62	0.009
Visuospatial	101±0.5	96±4.43	0.3
Language	91±4.93	90±3.47	0.941
Attention	102±2.70	92±3.98	0.05
SDMT	65±2.91	50±2.81	0.001
DASS-21	14±2.26	22±3.56	0.05
Stress	8±1.22	11±2.06	0.251
Anxiety	2±0.48	5±1.11	0.016
Depression	4±1.32	6±1.24	0.312
MFIS	16±2.80	29±3.96	0.016
Physical fatigue	6±1.31	15±2.46	0.005
Cognitive fatigue	10±1.70	14±1.76	0.06

Data are expressed as mean values ± SEM. DASS-21: Depression Anxiety Stress Scales as a measure of the mental health status of participants; EDSS: Expanded Disability Status Scale to evaluate disability status of MS patients; MFIS: Modified Fatigue Impact Scale to assesses performance of fatigue status; MSSS: Multiple Sclerosis Severity Score calculated using the EDSS and duration of the disease; SDMT: Symbol Digit Modalities Test as a measure of attention and information processing speed presented in a visual modality; Total ARCS: Audio Recorded Cognitive Screen to assess the performance in the domains of memory, verbal fluency, visuospatial function and attention with elements from each domain score

### 7.3.2 Morphology (whole brain and voxel characteristics)

Volumetric segmentation data demonstrated a significant reduction in the mean whole brain normalised volume (WBV, -6%,  $p=0.008$ ), WM (-6%,  $p=0.007$ ) and GM (-5%,  $p=0.031$ ) volumes and a reciprocal 39% increase in CSF in RRMS compared to HCs (Table 7-2). On average, the RRMS group had a total lesion volume of 12 ml per patient.

Significant variations in the average VOI (MRSI voxels) composition (WM and CSF fractions) were found between HCs and MS patients. Compared with the HCs, the WM was lower (-10%,  $p=0.001$ ) and CSF was higher (41%,  $p=0.001$ ) in the VOI of MS patients (Table 7-2). Additionally, in the RRMS cohort, the average VOI lesion volume was 5.7 ml, while the average WM fraction in MRSI voxels was higher than GM and CSF fractions. Multi-voxel segmentation results showed that the CSF fraction percentage was significantly higher in WMLs (22%) compared with NAWM and HCs. WM voxels percentages were significantly higher in HCs (8%) compared with NAWM and WML, whereas there was no significant change of the GM fraction in these tissues ( $p>0.05$ , Table 7-2). Figure 7-4 shows tissue segmentation of MRSI data within individual VOI voxels with partial volume mask for WMLs, NAWM and GM overlaid on the T2-FLAIR in MS brain slice.

Table 7-2. Top: Mean values of tissue segmentation within MRSI VOI and whole brain for RRMS patients and HCs. \* Statistical significance ( $p < 0.05$ ). Bottom: Mean values of MRSI voxels volume fractions within WML and NAWM voxels of RRMS patients compared to HCs.\* Statistical significance ( $p < 0.05$ ).

<b>Volumetric Measure</b>	<b>Regions</b>	<b>HCs(N=9)</b>	<b>MS (N=16)</b>	<b>Mean Difference (MS vs HCs)</b>	<b><i>p-value</i></b>	
<b>MRSI VOI</b>	<b>%CSF</b>	0.69±0.006	1.2±0.009	41%	0.001*	
	<b>%GM</b>	29.4±0.005	29.7±0.007	1%	0.7	
	<b>%WM</b>	63.4±0.003	57.8±0.009	-10%	0.001*	
	<b>Lesion volume (mm3)</b>	NA	5.7±1.6	NA	NA	
<b>Whole brain (mm3)</b>	<b>Whole brain volume</b>	1659.98±22	1572.65±19	-6%	0.008*	
	<b>pGM volume</b>	694.76±11.4	660.23±10.8	-5%	0.039*	
	<b>CSF volume</b>	25.83±1.82	42.49±3.9	39%	0.001*	
	<b>GM volume</b>	858.13±13.8	816.46±12.03	-5%	0.031*	
	<b>WM volume</b>	801.84±11.2	756.18±11.01	-6%	0.007*	
	<b>Total lesion volume</b>	NA	12±5.6	NA	NA	
pGM: peripheral grey matter, NA: not applicable.						
<b>Voxel measure</b>	<b>HCs</b>	<b>NAWM</b>	<b>WML</b>	<b><i>p-value</i> HCs vs NAWM</b>	<b><i>p-value</i> HCS vs WML</b>	<b><i>p-value</i> NAWM vs WML</b>
<b>Voxel CSF</b>	0.043±0.006	0.093±0.012	0.120±0.013	0.000*	0.000*	0.013*
<b>Voxel GM</b>	0.253±0.015	0.256±0.014	0.227±0.014	0.191	0.1	0.061
<b>Voxel WM</b>	0.704±0.015	0.651±0.013	0.654±0.013	0.024*	0.032*	0.159
HCs: healthy controls, NAWM: MS normal-appearing white matter, GM: grey matter; WML: MS white matter lesion.						

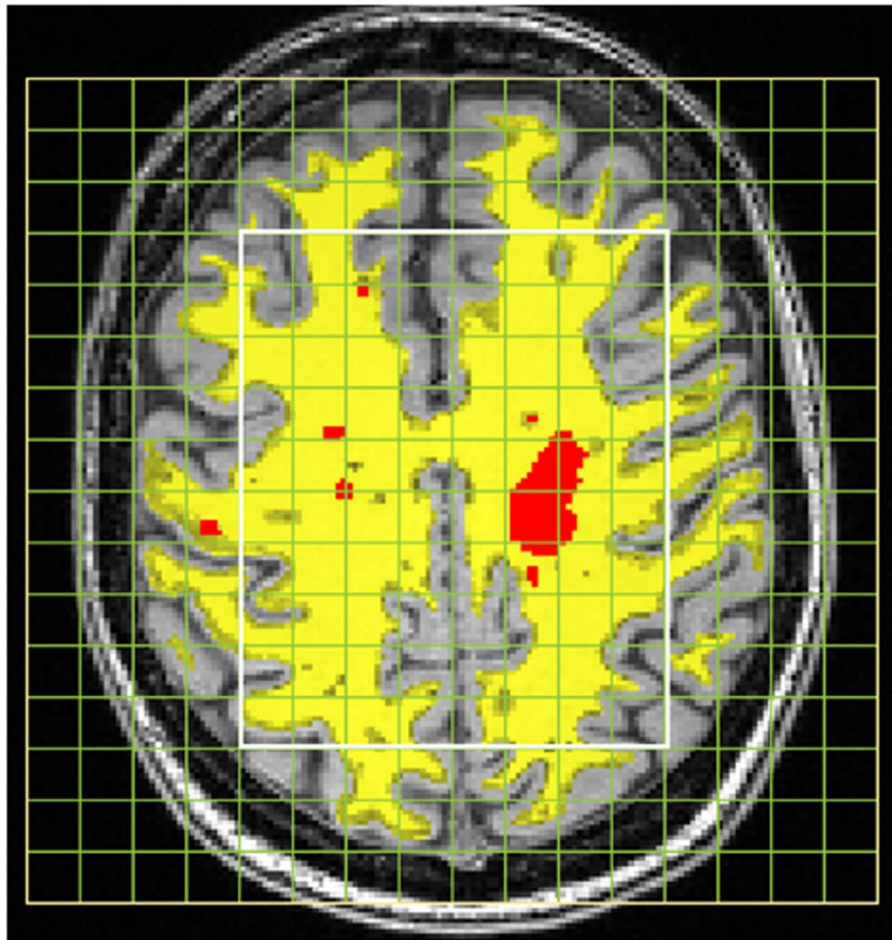


Figure 7-4. MRSI grid and tissue segmentation overlaid on the T2-FLAIR in MS brain slice. MRI color code: yellow indicates NAWM, red indicates WM lesions, grey indicates GM.

### 7.3.3 Magnetic resonance spectroscopic imaging

A high percentage of voxels (82%) of a total of 5120 (16 patients x320 voxels per patient) MRSI VOI voxels passed the spectral inclusion criteria. Spectral qualities of the VOI were validated in comparison with previously published MRSI reproducibility study<sup>290</sup> with a mean SNR of  $(8.43 \pm 1.29)$ . None of the patient or HC full data were excluded.

The performance of the fast MRSI technique and spectral quantification was assessed by measuring 15 analyzed neurometabolites with spectra obtained from RRMS and HCs voxels within 320 cm<sup>3</sup> VOI (Figure 7-5). Based on these quantitative investigations, coupled with spectroscopic voxel tissue segmentation, NAA/tCr, total NAA/tCr (tNAA/tCr) and Glx/tCr in WML were significantly lower than NAWM-MS (-9%, -5%, -8%) and HCs (-14%, -8%, -10%) within deep cortical white matter in both posterior parietal lobes. m-Ins/tCr and GPC/tCr in WML were significantly higher than NAWM-MS (12%, 15%) and HCs (10%, 17%). On the other hand, we observed lower tNAA, Glx and higher m-Ins, GPC ratios to tCr in NAWM-MS compared with HCs in the deep cortical white matter. Summary of significant differences in the metabolite ratios in these three different tissues are compiled in Table 7-3 and metabolites with statistically significant differences are shown in Figure 7-6. This figure clearly shows the important finding of the differences not only between the metabolic levels in WML and NAWM in MS patients but also the significant difference in NAWM in MS and HC cohorts.

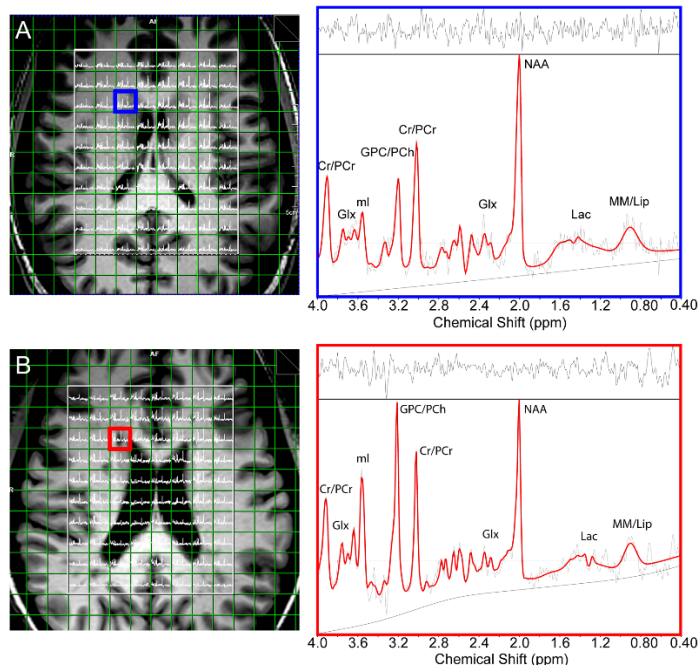


Figure 7-5. The LCModel fitting output of neurometabolites acquired from one MRSI voxel at similar voxel and slice position. Panel A: Healthy control, Panel B: MS brain.

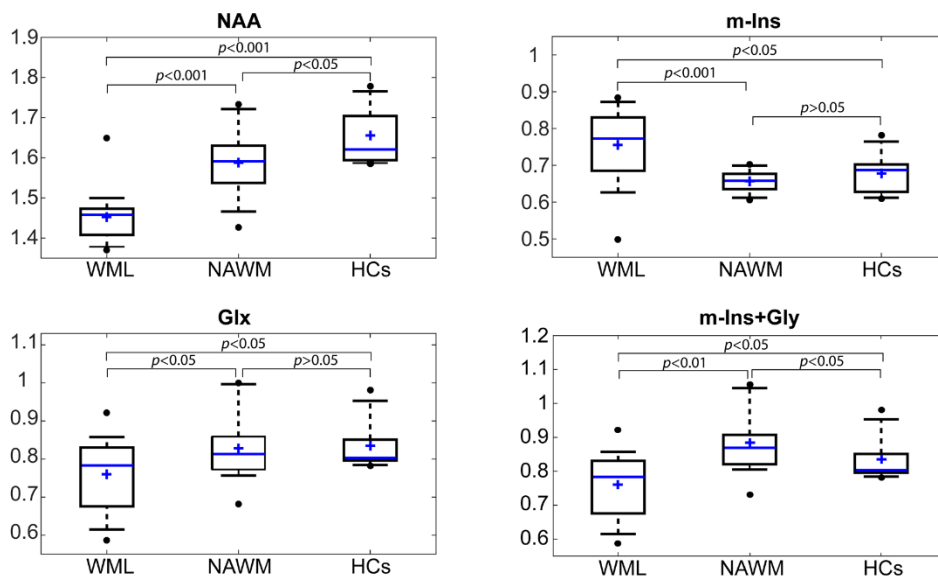


Figure 7-6. Box plot of statistically significant differences in the neurometabolic ratios (NAA/tCr, m-Ins/tCr, Glx/tCr and (m-Ins+Gly)/tCr) in three different tissues for WML, NAWM-MS and HC voxels.

Table 7-3. Summary of statistically significant differences in the metabolic ratios of three different tissues types from MRSI data; NAWM and WML for RRMS group compared to WM for HCs. Gly: glycine. \* Statistical significance ( $p < 0.05$ ).

Metabolite/tCr	HCs	NAWM	WML	<i>p-value</i> HCs vs NAWM	<i>p-value</i> HCs vs WML	<i>p-value</i> NAWM vs WML
<b>NAA</b>	1.655±0.024	1.588±0.022	1.453±0.016	0.05	0.001*	0.001*
<b>m-Ins</b>	0.678±0.018	0.657±0.008	0.755±0.026	0.219	0.051	0.001*
<b>GSH</b>	0.171±0.014	0.197±0.009	0.221±0.014	0.103	0.024*	0.159
<b>GPC</b>	0.218±0.010	0.222±0.011	0.263±0.012	0.446	0.021*	0.019*
<b>tNAA</b>	1.672±0.025	1.615±0.022	1.545±0.021	0.062	0.001*	0.029*
<b>m-Ins+Gly</b>	0.821±0.025	0.759±0.016	0.891±0.021	0.039*	0.044*	0.001*
<b>Glu</b>	0.71±0.020	0.745±0.024	0.654±0.019	0.392	0.048*	0.005*
<b>Glx</b>	0.835±0.021	0.824±0.021	0.760±0.024	0.851	0.047*	0.039*

To analyse the significant differences in spectroscopic data in its entirety within the VOI of the four slices (four 10mm slices), we measured the accuracy, sensitivity and specificity for three different classification models of HCs vs NAWM, NAWM vs WML, HCs vs WML, by using RBF SVM method. The HCs vs WML classification model achieved higher area under the curve (AUC), accuracy, sensitivity and specificity (94%, 86%, 95%, and 70% respectively) compared to NAWM vs WML (84%, 76%, 73%, and 77% respectively) and HCs vs NAWM (63%, 62%, 79%, and 40% respectively) models, as summarized in Figure 7-7. The results of NAA and m-Ins in Figure 7-7A shows significant differences in WML and NAWM in MS patients and also in NAWM in MS and HC cohorts in the entire VOI (4 slices) which clarifies that the metabolic changes are global with the same trend of changes seen in Figure 7-6 of the single slice of VOI.

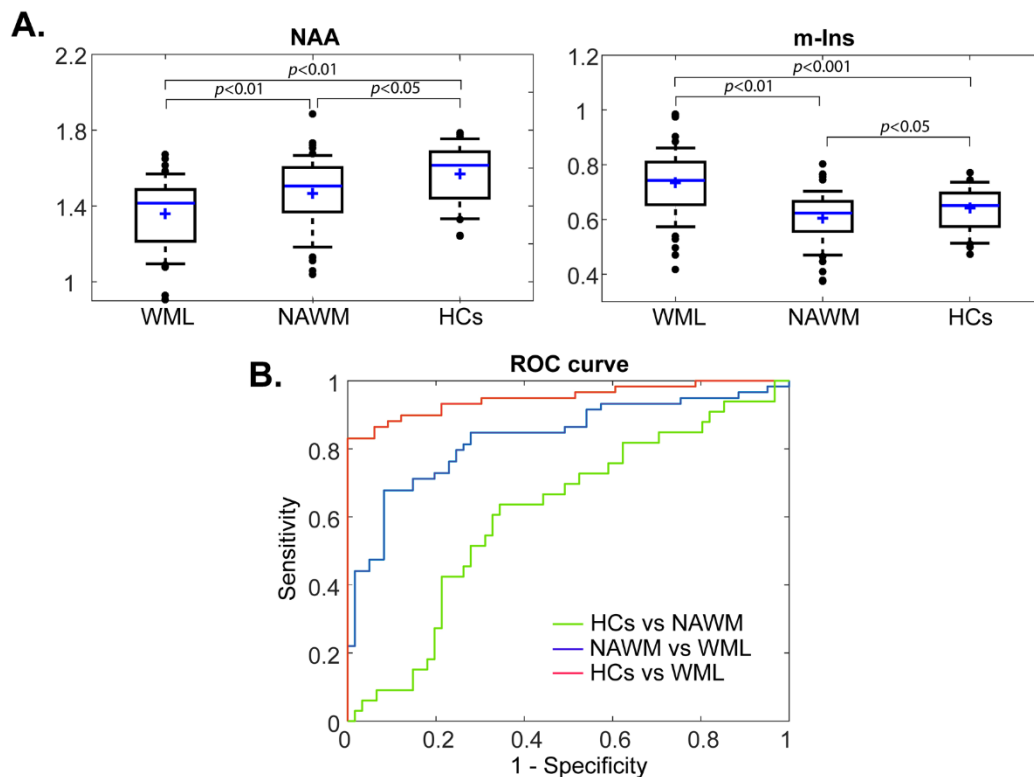


Figure 7-7. A. Box plot of significant differences in the neurometabolic ratios (NAA/tCr and m-Ins/tCr) for MS lesion voxels, NAWM-MS and HC voxels in four slices within large VOI (320 cm<sup>3</sup>). The statistically significant difference considered as  $p < 0.05$  between the two groups. B. The receiver operating characteristic (ROC) curves of three SVM classification (HCs vs NAWM, NAWM vs WML, HCs vs WML) using a leave-one-out cross-validation technique for major neurometabolites/tCr ratios yielding statistically significant differences between models.

## 7.4 Discussion

This study aimed to evaluate the role of fast spiral MRSI technique coupled with tissue segmentation of majority of the brain tissue to identify neurometabolic differences in NAWM and WML in MS patients compared to corresponding regions in HCs. To our knowledge, this is the first attempt to investigate neurometabolic changes in the majority of the brain using fast spiral MRSI (GOIA) with short echo time on RRMS coupled with multi-voxel segmentation. The major finding of this study is that fast spiral MRSI technique is reliable and robust in identifying neurometabolic changes not only in WML but also in NAWM of RRMS patients. Our cohort of 16 RRMS patients were clinically stable while undergoing treatment with natalizumab. This supports findings in other studies in RRMS, showing that changes in neurometabolite profile, whole brain volume, lesion load and connectivity have been associated with alterations in cognitive and mood function.<sup>291, 292</sup> Despite their relatively short disease duration and low disability score, our RRMS cohort displayed impaired cognition as well as higher levels of mood and fatigue symptoms compared to age and sex-matched HCs.

Even though the whole brain lesion load was low in our patient group, our findings indicated a significant difference in mean whole brain volume and WM and GM volumes of the patient group compared to HCs (on average by -6%). In addition, CSF volume was consistently higher in MS patients than in HCs subjects (on average by 39%). These findings are likely to have significant clinical impacts. Others have shown that reduced brain volumes have been associated with an increased risk of disease progression and a decrease in treatment efficacy in MS patients.<sup>212</sup>

We used tissue segmentation of a large VOI (320 cm<sup>3</sup>) to measure the spectral voxel partial volumes of WM, GM and CSF. As expected, the partial volumes of the MRSI voxels correlated with the reduction in whole brain partial volumes described above. Compared to HCs, we found significantly reduced partial WM volume and increased

partial CSF volume of the RRMS group, but not GM, indicating that in the earlier phases of the disease white matter loss prevails.

Additionally, partial tissue volumes of each voxel within the VOI indicated that the partial CSF volume was significantly increased (on average by 22%) in WML voxels compared with NAWM and HCs voxels. Partial WM volume was significantly reduced (on average by -8%) in WML voxels compared to HCs voxels and there was no significant difference compared to NAWM voxels. This multi-voxel segmentation approach was validated by testing in vitro and in vivo and by summation of the total voxel volumes as described in the method. Hence, it is accurate and can be useful for disease monitoring of the whole brain. This is an important advancement in the segmentation technique as it allowed us to define tissue types per voxel. Our findings are in concordance with earlier studies that showed tissue types can be defined by their neurometabolite levels.<sup>71, 293</sup> The ability to segment individual voxel content within a large VOI into WML, NAWM, GM and CSF is unprecedented. This will further provide insights into the chemical characteristic of multiple brain region by virtue of tissue classification.

A significant increased CSF fraction, in WML and NAWM voxels, compared to HCs as shown in our cohort, reflects the development of atrophy which is prevalent particularly around the ventricular system, including the third and lateral ventricles, as well as adjacent to sulci.<sup>46, 294</sup> Changes in CSF fraction, are seen predominantly in RRMS and are associated with clinical disability and cognitive impairment.<sup>295</sup> Additionally, the progressive loss of WM atrophy in MS was confirmed by our findings with decreased volume in WM voxels.

We also evaluated the quality of fast <sup>1</sup>H MRSI in MS patients using LASER GOIA-W[16,4]sequence with spiral k-space sampling<sup>288</sup> covering a large tissue volume (320 cm<sup>3</sup>), yielding accelerated acquisition, extended spatial coverage, improved signal localization, wider spectral width, improved spatial resolution and clinically adequate SNR to reliably distinguish MRSI signal from noise.<sup>287</sup> Importantly, MRSI quality

assurance parameters (SNR and FWHM) were in line with other reliable 2D multi-voxel MRSI of MS patients.<sup>290</sup>

Several major neurometabolite ratios from three different tissue types within the large VOI was analyzed. These included NAA, m-Ins, GPC, Glx, tNAA and GSH. MRS data from WML, NAWM of RRMS patients and HCs were analyzed by using fast spiral MRSI technique coupled with tissue segmentation of the whole brain performed at short TE on the 3T system.

Previous studies have confirmed the role of MRS and tissue segmentation methods in MS patients and HCs.<sup>39, 293</sup> Based on these methods, several studies have compared spectral profiles of NAWM in MS patients and WM in HCs<sup>27, 46</sup>. However, few studies focussed on the comparison of metabolites in NAWM versus WML voxels in MS patients.<sup>285, 286</sup> Our observation confirmed the importance of NAA and m-Ins as indicators of axonal loss and gliosis in NAWM and WML using a spiral MRSI at short TE. We found a significant reduction in NAA and an increase in m-Ins in RRMS WML in comparison to RRMS NAWM and to age and sex-matched HCs, within VOI slice located at the cerebral cortex including frontal, parietal, occipital lobes as well as the superior aspect of the temporal lobe, which is consistent with findings of previous studies.<sup>38, 284</sup> These studies found reduced NAA (10-16%,  $p < 0.008$ ) and increased m-Ins (10%,  $p = 0.008$ ) in WMLs compared to NAWM in 25 RRMS patients, but used a different technique (PRESS 2D MRSI with single 15 mm slice). Two further MRSI studies found evidence of statistically significant lower NAA in WML relative to NAWM.<sup>144, 296</sup> The results from these cross-sectional analyses may suggest that early loss of neuronal integrity and microglial gliosis might not immediately impact on regional atrophy markers.<sup>48</sup> Furthermore, reduction in tNAA and GSH and increase in m-Ins in WML was also demonstrated in a study of 46 RRMS patients without significant difference compared to NAWM using PRESS 2D MRSI at 3T<sup>269</sup>, which partially agrees with our findings. Interestingly, other longitudinal studies demonstrated a treatment effect of natalizumab on neurometabolite levels in RRMSs,

showing higher levels of tNAA in WML post treatment, due to the anti-inflammatory and possibly neuroprotective effect of natalizumab.<sup>284</sup>

Fast MRSI measurements of neurometabolites within VOI volume showed not only significant differences in WML with HC but also a significant difference in NAA/tCr ratios between NAWM of RRMS and WM of HCs. This result was in line with previous studies<sup>285, 286</sup>, which also demonstrated a decrease of NAA in NAWM further supporting the importance of NAA as a more sensitive disease marker than conventional T2. Other studies have investigated metabolite alterations in different NAWM regions vs WM in HCs such as frontal-parietal NAWM of 27 RRMS patients<sup>43</sup> applying PRESS 2D MRSI with a single slice (15 mm) at 3T. These findings showed a reduction in NAA levels in NAWM but no significant difference relative to HCs, probably due to the early stages of the disease. Furthermore, absolute concentration of neurometabolites from the same NAWM regions have also been confirmed with significant reduction in tNAA level only in the parietal region (-7%,  $p < 0.043$ ) and increase in m-Ins level in parietal (19%,  $p < 0.01$ ) and frontal (23%,  $p < 0.01$ ) regions. The discrepancy in these results compared to ours is may be due to the difference in methodology applied and position of the VOI slice. Recently, a corresponding decreasing trend in NAA/Cr ratio within 7.5mm slice was observed in three NAWM regions (parietal, frontal and occipital)<sup>286</sup> in 17 RRMS patients, suggesting decreased NAA/Cr could be due to nerve fiber loss in NAWM regions. MRS on NAWM regions using PRESS 2D MRSI at 3T described that the highest degree of metabolic changes in NAWM were found in the parietal region. Alteration of neurometabolites in global NAWM and in individual NAWM regions can help identify disease progression in MS patients, which might not be apparent in routine assessment. Our findings of significant changes in NAWM and more so in WML of MS patients compared with healthy voxels using spiral 3D MRSI indicate that the metabolic abnormalities (reduced NAA and increased m-Ins) in RRMS is associated with a gradual loss of axonal integrity and astrogliosis in WM. These changes were associated with morphological changes within

the brain including increased CSF volume, total brain volume loss and T2 lesion volume. The use of NAA as a marker of neuronal integrity was further supported by the reduction in NAA levels associated with a 5% and 13% lower white matter content (NAWM and MS lesion voxels) compared to that seen in the same region in healthy controls.

In our study, we showed significantly lower levels of Glx/tCr ratios in RRMS in WML compared to NAWM ( $p=0.039$ ) and HCs ( $p=0.047$ ). However, no statistically significant differences were noticed in NAWM-Glx/tCr relative to WM in HCs. These results are consistent with other MRS studies in early as well as late stages<sup>27, 237</sup> that have shown lower Glx/tCr in NAWM relative to HCs. However, the lower levels of Glx/Cr ratio may well be due to higher creatine levels as evidenced in other studies.<sup>27</sup> Furthermore, reduced Glx in MS patients has been suggested to play a role in neuro-astrocyte exchanges and in excitotoxicity.<sup>48</sup> On the other hand, MRS (single-voxel TE-averaged) has reported a higher level of Glx in WML and NAWM relative to HCs.<sup>76</sup> The conflicting results may be due to the discrepancies in field strength, type of sequence (semi-LASER and PRESS), metabolic quantification (absolute vs creatine ratio) and spectral analysis. It could also result from a difference in treatment effects.

To our knowledge, only three fast MRSI studies have evaluated the metabolite alterations of MS patients and HCs. Even though different acquisition and quantitation methods were used (e.g. 3D fast EPSI at 3T), other findings have indicated a reduction in NAA and Glx in WM and increased m-Ins in WML, NAWM and GM regions in the RRMS group.<sup>48</sup> These results are in line with our study with spiral MRSI at 3T at short TE used, showing early loss of neuronal integrity and some levels of microglial gliosis before appearance as WML.

An important aspect of the spiral MRSI study was the full coverage of spectroscopic data within VOI of four contiguous slices (4x10mm). In order to evaluate the performance of our method, three different models (HCs vs NAWM, NAWM vs

WML, HCs vs WML) were built using RBF SVM method coupled with neurometabolites to tCr ratio with a significant difference between models.

The highest predictive performance was found in the HCs vs WML model (highest in measured of accuracy, sensitivity and specificity). This performance corresponded to a significant decrease in NAA/tCr and increased m-Ins/tCr with higher percentage change between WML and HCs voxels within VOI from one slice. However, the HCs vs NAWM model achieved the lowest predictive performance (lowest measured accuracy, sensitivity and specificity). In our cohort of well controlled patients no significant difference between NAWM and HC voxels were found apart from NAA/tCr. Although the RBF SVM model suggests that MRSI is less efficient in discriminating NAWM from HCs region voxels, it still reached a sensitivity of 0.76. The models (NAWM vs WML) clearly predicted MS lesions via neurometabolite levels with reasonable performance and also clearly identified healthy brain.

This is the first study to illustrate the performance of spiral MRSI sequence with LASER-GOIA-W[16,4] localization coupled with multi-voxel tissue segmentation of the whole brain covering a large VOI ( $320 \text{ cm}^3$ ) within individual and multiple slices. We used this approach to identify neurochemical differences in NAWM and WML in a cohort of stable RRMS on treatment with natalizumab and compared the results to age and sex-matched HCs. The multi-voxel and slice MRSI approach allowed the integration of the whole brain which enabled assessment of all tissue types and lesions at the same time.

Our novel analysis pipeline allowed individual small voxel analysis which demonstrated the true nature of NAWM and WML and distinguishes tissue types. The changes in the NAWM in the MS brain can lead to early detection of loss of neuronal integrity and allows for timely treatment adjustment. The limitations of our study are the relatively small cohort size, but it allowed us to gain expertise in post processing. Our findings need to be confirmed in a larger patient cohort over an extended treatment period. This will enable an investigation of long term impacts of treatment on disease

outcomes and metabolic changes. A larger patient cohort may also increase the sensitivity of the performance of the HCs vs NAWM model.

## **7.5 Conclusion**

This study confirmed that spiral MRSI of whole brain with adiabatic localization can be used to assess neurometabolites changes of the majority of brain in clinically relevant acquisition time at 3T. It revealed reliable metabolic information that could improve the diagnosis and clinical management of MS patients. This study confirmed the significant differences in MS neurometabolites between WML and NAWM voxels within small multi-voxel volumes ( $1 \text{ cm}^3$ ). It also confirmed the potential NAWM and WML damages which plays a critical role in MS pathology, which were confirmed by voxel segmentation within a larger VOI ( $320 \text{ cm}^3$ ). Spectroscopic SVM approach in the MS brain offers a sensitive clinical monitoring tool for MS disease progression. Longitudinal studies are required to assess the long-term impact of treatments on metabolic changes and disease outcomes to fully explore the potential of the spiral MRSI technique in monitoring disease progression.

## Chapter 8 : Summary and future work

### Future work and recommendations

Imaging techniques used in the medical management of MS are limited to detecting damaged tissue or brain lesions after it has occurred. Current imaging tools are incapable of predicting disease progression or have better indicators of changes in brain function and hence novel MRI techniques are needed to improve the long term clinical profile of this debilitating disease. Magnetic resonance spectroscopy (MRS) is a non-invasive technique enabling the metabolic profile of the brain in MS to be determined. This body of work was able to demonstrate the reliability of this technique in detecting metabolic differences in the MS brain. Indeed, the non-lesion containing parts of the brain previously termed “normal-appearing white ‘matter” are in fact seen to have an altered biochemical profile in MS suggesting it is in fact “ab-normal”.

In this thesis, we confirmed the validity of single voxel H-MRS technique by evaluating the diurnal stability and long-term repeatability and reliability of 1D H-MRS *in-vitro* and *in-vivo* at 3 Tesla. This study confirmed the stability of H-MRS in quantifying neurometabolite levels in longitudinal studies to quantify brain biochemical changes over extended periods of time. The findings of this study confirmed the reliable detection and distinction of neurometabolites between healthy controls (HCs) and relapsing-remitting multiple sclerosis (RRMS) patients with minimal diurnal variations.

A longitudinal study was designed using single voxel H-MRS to evaluate the impact of dimethyl fumarate (DMF) treatment longitudinally over 24 months on hippocampal neurometabolites in RRMS patients. This study showed that cross-sectional analysis identified a significant reduction in hippocampal N-acetylaspartate (NAA) and increase in myo-inositol (m-Ins) in the RRMS cohort at baseline, compared

to healthy controls. This study confirmed the importance of NAA and m-Ins as indicators of axonal loss and gliosis. This study also showed that treatment with DMF may impact on the hippocampal metabolism, specifically glutathione levels, which supports its assumed antioxidant mode of action, resulting in an anti-inflammatory effect in the MS brain following DMF treatment. This study is the first to illustrate a change in hippocampal metabolism associated with the onset of treatment with DMF in RRMS patients.

Another aspect of this study is an open-label longitudinal observational study designed to evaluate the impact of DMF treatment on the pre-frontal cortex (PFC) and posterior cingulate gyrus (PCG) metabolic profiles at pre- and post-treatment onset at four time points. This cross-sectional study showed significant reduction in NAA in PFC and PCG and increase in PFC tCho in the RRMS cohort compared to HCs. DMF treatment showed the mean NAA levels in PFC and PCG were altered significantly over the 24-month treatment period, but stabilised and didn't significantly change between 1st and 2nd year of treatment. This study demonstrated that MRS is a sensitive marker of disease activity with several metabolites correlated with clinical parameters, and capable to detect a treatment effect prior to volumetric change.

Additionally, in this thesis, the efficacy of different disease modulating therapies (fingolimod, interferon or glatiramer acetate) has also been evaluated using single voxel methods in a cross-sectional fashion. This study is the first *in-vivo* investigation of the impact of these treatments on the hippocampus, PFC and PCG metabolism in RRMS patients. This study also established the association between clinical symptoms in RRMS patients, especially cognitive functions and neurometabolites as well as volumetric changes. We also confirmed in this study the importance of NAA and m-Ins as indicators of axonal loss and gliosis. Our results demonstrated that hippocampal and PCG neurometabolite changes in RRMS were associated with severity of clinical and neuropsychological symptoms. Cross-sectional analysis suggested that H-MRS of

brain metabolites in these three regions are more sensitive markers than morphological changes.

In this thesis, the last study was designed to evaluate the performance of fast spiral three-dimensional magnetic resonance spectroscopic imaging (3D MRSI) technique coupled with tissue segmentation of the majority of the brain to identify neurometabolic differences in normal appearing white matter (NAWM) and white matter lesions (WML) of stable RRMS patients compared to age and sex-matched HCs. This study used a novel post-processing analysis pipeline that allowed individual small voxel analysis to inform true ingredients of NAWM and WML and distinguish tissue types. This includes a multi segmentation technique that was developed as part of this project. Our findings of significant changes in NAWM and more so in WML of RRMS patients compared with voxels without T2 MS lesions using spiral 3D MRSI indicate that the metabolic abnormalities (reduced NAA and increased m-Ins) in RRMS is associated with a gradual loss of axonal integrity and astrogliosis in WM. This study demonstrated the benefit of MRSI in evaluating RRMS neurometabolic changes in NAWM. Support vector machine (SVM) of MRSI data may be suited for clinical monitoring and progression of RRMS patients.

It will be vital to know if the biochemical differences seen in the MS brain are predictive of future lesion formation or are a consequence of existing lesions. This would be revealed by conducting further investigations of the biochemical changes associated with lesion development and re-myelination and as such increase our understanding of early disease processes and potentially factors associated with disease progression. Historically, conventional MRS is associated with long acquisition times, making the implementation of this technique in routine clinical scanning limited. Fast MRSI is novel in that it has the potential to evaluate the metabolic changes in the brain across a large region in a relatively short time period. This advancement takes this technique one step closer to utilisation in the routine clinic setting. However, more needs to be done to make these methods more clinically viable.

The findings of the impact of DMF treatment on three distinct RRMS brain regions using single voxel H-MRS techniques are preliminary and need to be confirmed in a larger patient cohort over an extended treatment period to enable longer term impact of DMF on disease outcomes and metabolic changes to be more fully explored. There was no difference between the impact of fingolimod and injectable treatments on RRMS neurometabolite profiles. A longitudinal study for fingolimod and injectable groups of patients as well as age and sex-matched HCs are warranted to evaluate at least at 2 years of treatment. Evaluation and comparison of the effects of fingolimod, DMF and injectable treatments on ARCS cognitive function will be valuable.

Multi-slice MRSI evaluations of whole brain will allow correlation of whole brain metabolic changes with clinical symptoms of disability (EDSS, cognitive function and fatigue/mood). Also, this will enable us to establish a relationship between clinical signs in RRMS cohort and volumetric MRI measures. Developing a multi-dimensional colour map presentation of data overlaying with structural image to help appreciate the neurochemical profiles, mainly major low/high concentration metabolites. This colour map can be extended to evaluate different tissue subtypes to understand their changes over time. Sample of colour map of single and multi-slice is shown in Figure 8-1 as a part of preliminary result to this future target using fast MRSI techniques.

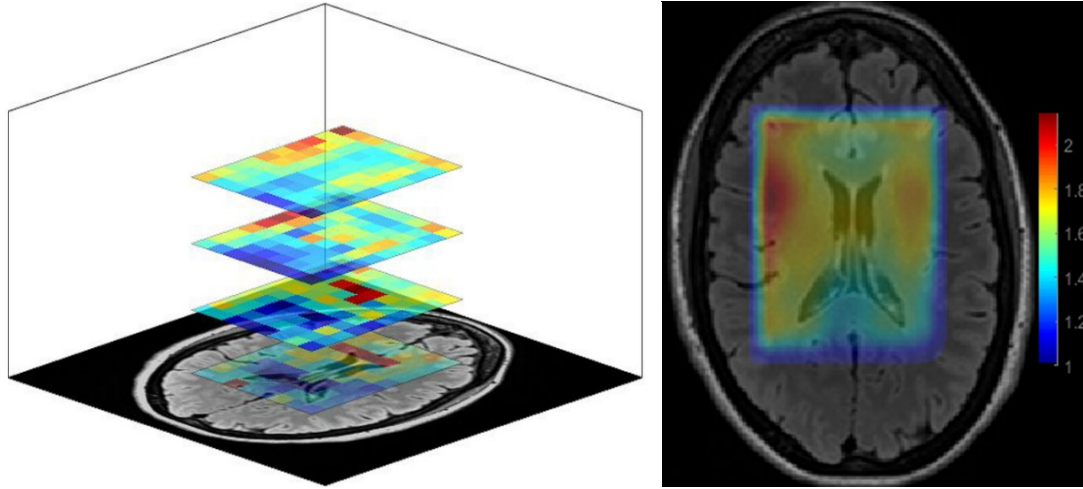


Figure 8-1. Mapping of NAA concentrations in single slice and multi-slice using fast MRSI based representation of data, overlaid with structural image.

The application of differential metabolic regions (DMR) to identify a cluster of 3 or more adjacent voxels all having statistically significant metabolic differences between RRMS and HCs may have the potential to enhance clinical monitoring and progression of MS patients. Sample of the mapping DMRs, located at deep cortical white matter in posterior parietal lobes at post-central gyrus, for neurometabolites in the RRMS brain using fast MRSI technique is shown in Figure 8-2 as a preliminary result to this future target.

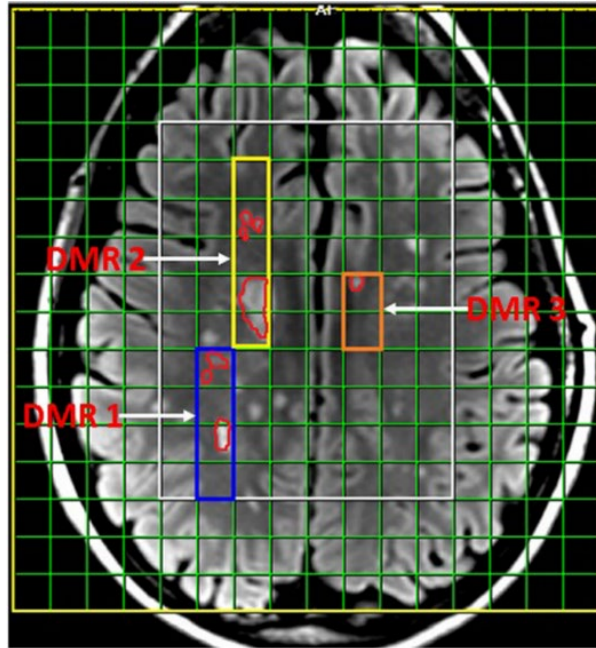


Figure 8-2. Sample of the mapping 3 DMRs, located at deep cortical white matter in posterior parietal lobes at post-central gyrus, for neurometabolites in the RRMS brain using fast MRSI technique. A DMR represents 3 or more adjacent voxels having statistically significant metabolic differences between RRMS and HCs.

## Bibliography

1. Kruger D. Multiple sclerosis. *JAAPA*. 2012;25: 54-55.
2. Koch-Henriksen N. The Danish Multiple Sclerosis Registry: a 50-year follow-up. *Mult Scler*. 1999;5: 293-296.
3. Tsang BK-T, Macdonel R. Multiple sclerosis Diagnosis, management and prognosis. *Australian Family Physician*. 2011;40.
4. Sedal L, Wilson IB, McDonald EA. Current management of relapsing-remitting multiple sclerosis. *Intern Med J*. 2014;44: 950-957.
5. DasGupta R, Fowler CJ. Bladder, bowel and sexual dysfunction in multiple sclerosis: management strategies. *Drugs*. 2003;63: 153-166.
6. Lublin FD, Reingold SC, Cohen JA, et al. Defining the clinical course of multiple sclerosis: the 2013 revisions. *Neurology*. 2014;83: 278-286.
7. Courtney SW. All About Multiple Sclerosis. In: Jack Burks MD, Borkowski A, Damiri P, Richman C, editors. New Jersey, US: Multiple Sclerosis Association of America, 2006.
8. Williams R, Rigby AS, Airey M, Robinson M, Ford H. Multiple sclerosis: it epidemiological, genetic, and health care impact. *J Epidemiol Community Health*. 1995;49: 563-569.
9. International Multiple Sclerosis Genetics C, Beecham AH, Patsopoulos NA, et al. Analysis of immune-related loci identifies 48 new susceptibility variants for multiple sclerosis. *Nat Genet*. 2013;45: 1353-1360.
10. Correale J, Gaitan MI. Multiple sclerosis and environmental factors: the role of vitamin D, parasites, and Epstein-Barr virus infection. *Acta Neurol Scand Suppl*. 2015;132: 46-55.
11. Damal K, Stoker E, Foley JF. Optimizing therapeutics in the management of patients with multiple sclerosis: a review of drug efficacy, dosing, and mechanisms of action. *Biologics*. 2013;7: 247-258.
12. Yeh EA, Weinstock-Guttman B. The management of pediatric multiple sclerosis. *J Child Neurol*. 2012;27: 1384-1393.
13. Lechner-Scott J, Kerr T, Spencer B, Agland S, Lydon A, Schofield PW. The Audio Recorded Cognitive Screen (ARCS) in patients with multiple sclerosis: a practical tool for multiple sclerosis clinics. *Mult Scler*. 2010;16: 1126-1133.
14. Gallo P, Van Wijmeersch B. Overview of the management of relapsing-remitting multiple sclerosis and practical recommendations. *Eur J Neurol*. 2015;22 Suppl 2: 14-21.
15. Tillema J-M, Pirko I. Neuroradiological evaluation of demyelinating disease. *Ther Adv Neurol Disord*. 2013;6: 249-268.
16. Rovira A, Wattjes MP, Tintore M, et al. Evidence-based guidelines: MAGNIMS consensus guidelines on the use of MRI in multiple sclerosis-clinical implementation in the diagnostic process. *Nat Rev Neurol*. 2015;11: 471-482.
17. Polman CH, Reingold SC, Banwell B, et al. Diagnostic criteria for multiple sclerosis: 2010 revisions to the McDonald criteria. *Ann Neurol*. 2011;69: 292-302.

18. Mike P. Wattjes, Àlex Rovira, David Miller, et al. Evidence-based guidelines: MAGNIMS consensus guidelines on the use of MRI in multiple sclerosis-establishing disease prognosis and monitoring patients. *Nat Rev Neurol*. 2015;11: 597-606.
19. Thompson AJ KA, MacManus DG et al. . Patterns of disease activity in multiple sclerosis: clinical and magnetic resonance imaging study., 1990.
20. Klawiter EC, Schmidt RE, Trinkaus K, et al. Radial diffusivity predicts demyelination in ex vivo multiple sclerosis spinal cords. *Neuroimage*. 2011;55: 1454-1460.
21. Sbardella E, Tona F, Petsas N, Pantano P. DTI Measurements in Multiple Sclerosis: Evaluation of Brain Damage and Clinical Implications. *Mult Scler Int*. 2013;2013: 671730.
22. Dutta R, Chang AS, Doud MK, et al. Demyelination Causes Synaptic Alterations in Hippocampi from Multiple Sclerosis Patients. *Ann Neurol*. 2011;69: 445-454.
23. Curran K, Emsell L, Leemans A. Quantitative DTI measures, 2016:65-87.
24. Rovira A, Leon A. MR in the diagnosis and monitoring of multiple sclerosis: an overview. *Eur J Radiol*. 2008;67: 409-414.
25. Rocca MA, Filippi M. Functional MRI in multiple sclerosis. *J Neuroimaging*. 2007;17 Suppl 1: 36s-41s.
26. Filippi M, Rocca MA. Functional MR imaging in multiple sclerosis. *Neuroimaging Clin N Am*. 2009;19: 59-70.
27. Marshall I, Thrippleton MJ, Bastin ME, et al. Characterisation of tissue-type metabolic content in secondary progressive multiple sclerosis: a magnetic resonance spectroscopic imaging study. *J Neurol*. 2018;265: 1795-1802.
28. Geurts JJG, Reuling IEW, Vrenken H, et al. MR spectroscopic evidence for thalamic and hippocampal, but not cortical, damage in multiple sclerosis. *Magnetic Resonance in Medicine*. 2006;55: 478-483.
29. Sarchielli P, Presciutti O, Tarducci R, et al. Localized H-1 magnetic resonance spectroscopy in mainly cortical gray matter of patients with multiple sclerosis. *J Neurol*. 2002;249: 902-910.
30. Rovira A, Alonso J. 1H magnetic resonance spectroscopy in multiple sclerosis and related disorders. *Neuroimaging Clin N Am*. 2013;23: 459-474.
31. Narayana PA. Magnetic resonance spectroscopy in the monitoring of multiple sclerosis. *J Neuroimaging*. 2005;15: 46S-57S.
32. Ramadan S, Lin A, Stanwell P. Glutamate and glutamine: a review of in vivo MRS in the human brain. *NMR Biomed*. 2013;26: 1630-1646.
33. Cao G, Edden RAE, Gao F, et al. Reduced GABA levels correlate with cognitive impairment in patients with relapsing-remitting multiple sclerosis. *Eur Radiol*. 2018;28: 1140-1148.
34. Cawley N, Solanky BS, Muhlert N, et al. Reduced gamma-aminobutyric acid concentration is associated with physical disability in progressive multiple sclerosis. *Brain*. 2015;138: 2584-2595.
35. Govindaraju V, Young K, Maudsley AA. Proton NMR chemical shifts and coupling constants for brain metabolites. *NMR Biomed*. 2000;13: 129-153.
36. Mountford C, Quadrelli S, Lin A, Ramadan S. Six fucose-alpha(1-2) sugars and alpha-fucose assigned in the human brain using in vivo two-dimensional MRS. *NMR Biomed*. 2015;28: 291-296.

37. Obert D, Helms G, Sattler MB, et al. Brain Metabolite Changes in Patients with Relapsing-Remitting and Secondary Progressive Multiple Sclerosis: A Two-Year Follow-Up Study. *PLoS One*. 2016;11: e0162583.
38. Kapeller P, McLean MA, Griffin CM, et al. Preliminary evidence for neuronal damage in cortical grey matter and normal appearing white matter in short duration relapsing-remitting multiple sclerosis: a quantitative MR spectroscopic imaging study. *J Neurol*. 2001;248: 131-138.
39. De Stefano N, Bartolozzi ML, Guidi L, Stromillo ML, Federico A. Magnetic resonance spectroscopy as a measure of brain damage in multiple sclerosis. *J Neurol Sci*. 2005;233: 203-208.
40. Muhlert N, Atzori M, De Vita E, et al. Memory in multiple sclerosis is linked to glutamate concentration in grey matter regions. *Journal of Neurology Neurosurgery and Psychiatry*. 2014;85: 834-840.
41. Mader I, Roser W, Kappos L, et al. Serial proton MR spectroscopy of contrast-enhancing multiple sclerosis plaques: absolute metabolic values over 2 years during a clinical pharmacological study. *AJNR Am J Neuroradiol*. 2000;21: 1220-1227.
42. Brief EE, Vavasour IM, Laule C, Li DK, Mackay AL. Proton MRS of large multiple sclerosis lesions reveals subtle changes in metabolite T(1) and area. *NMR Biomed*. 2010;23: 1033-1037.
43. Aboul-Enein F, Krssak M, Hoftberger R, Prayer D, Kristoferitsch W. Reduced NAA-levels in the NAWM of patients with MS is a feature of progression. A study with quantitative magnetic resonance spectroscopy at 3 Tesla. *PLoS One*. 2010;5: e11625.
44. Rahimian N, Saligheh Rad H, Firouznia K, et al. Magnetic resonance spectroscopic findings of chronic lesions in two subtypes of multiple sclerosis: primary progressive versus relapsing remitting. *Iran J Radiol*. 2013;10: 128-132.
45. Tiberio M, Chard DT, Altmann DR, et al. Metabolite changes in early relapsing-remitting multiple sclerosis. A two year follow-up study. *J Neurol*. 2006;253: 224-230.
46. Kirov, II, Tal A, Babb JS, Herbert J, Gonen O. Serial proton MR spectroscopy of gray and white matter in relapsing-remitting MS. *Neurology*. 2013;80: 39-46.
47. Mathiesen HK, Tscherning T, Sorensen PS, et al. Multi-slice echo-planar spectroscopic MR imaging provides both global and local metabolite measures in multiple sclerosis. *Magn Reson Med*. 2005;53: 750-759.
48. Donadieu M, Le Fur Y, Lecocq A, et al. Metabolic voxel-based analysis of the complete human brain using fast 3D-MRSI: Proof of concept in multiple sclerosis. *J Magn Reson Imaging*. 2016;44: 411-419.
49. Pelletier D, Nelson SJ, Grenier D, Lu Y, Genain C, Goodkin DE. 3-D echo planar (1)HMRS imaging in MS: metabolite comparison from supratentorial vs. central brain. *Magn Reson Imaging*. 2002;20: 599-606.
50. Mathiesen HK, Jonsson A, Tscherning T, et al. Correlation of global N-acetyl aspartate with cognitive impairment in multiple sclerosis. *Arch Neurol*. 2006;63: 533-536.
51. Al-iedani O, Arm J, Ribbons K, Lea R, Lechner-Scott J, Ramadan S. Diurnal stability and long-term repeatability of neurometabolites using single voxel 1H magnetic resonance spectroscopy. *European Journal of Radiology*. 2018;108: 107-113.
52. Al-iedani O, Ribbons KA, Lea R, Ramadan S, Lechner-Scott J. The effect of dimethyl fumarate treatment on hippocampal metabolite levels in RRMS using H-1-MR spectroscopy. *Multiple Sclerosis Journal*. 2017;23: 392-393.

53. Al-iedani O, Ribbons K, Lechner-Scott J, et al. Spiral-MRSI and tissue segmentation of normal-appearing white matter and white matter lesion load in relapsing remitting Multiple Sclerosis. ISMRM. Montreal, 2019.
54. Al-iedani O, Ribbons K, Golizadeh N, et al. Evaluation of metabolic alterations in the MS brain using fast Spiral MRSI and machine learning. *Multiple Sclerosis Journal: SAGE PUBLICATIONS LTD 1 OLIVERS YARD, 55 CITY ROAD, LONDON EC1Y 1SP, ENGLAND*, 2019:455-456.
55. Levin BE, Katzen HL, Maudsley A, et al. Whole-brain proton MR spectroscopic imaging in Parkinson's disease. *J Neuroimaging*. 2014;24: 39-44.
56. Mandal PK. Magnetic resonance spectroscopy (MRS) and its application in Alzheimer's disease. *Concepts in Magnetic Resonance Part A*. 2007;30A: 40-64.
57. Graham GD, Blamire AM, Howseman AM, et al. Proton magnetic resonance spectroscopy of cerebral lactate and other metabolites in stroke patients. *Stroke*. 1992;23: 333-340.
58. Adalsteinsson E, Langer-Gould A, Homer RJ, et al. Gray matter N-acetyl aspartate deficits in secondary progressive but not relapsing-remitting multiple sclerosis. *AJNR Am J Neuroradiol*. 2003;24: 1941-1945.
59. Heide AC, Kraft GH, Slimp JC, et al. Cerebral N-acetylaspartate is low in patients with multiple sclerosis and abnormal visual evoked potentials. *AJNR Am J Neuroradiol*. 1998;19: 1047-1054.
60. Bottomley PA, Edelstein WA, Foster TH, Adams WA. In vivo solvent-suppressed localized hydrogen nuclear magnetic resonance spectroscopy: a window to metabolism? *Proc Natl Acad Sci U S A*. 1985;82: 2148-2152.
61. Frahm J, Bruhn H, Gyngell ML, Merboldt KD, Hanicke W, Sauter R. Localized high-resolution proton NMR spectroscopy using stimulated echoes: initial applications to human brain in vivo. *Magn Reson Med*. 1989;9: 79-93.
62. Bertholdo D, Watcharakorn A, Castillo M. Brain proton magnetic resonance spectroscopy: introduction and overview. *Neuroimaging Clin N Am*. 2013;23: 359-380.
63. Ordidge RJ, Gordon RE. Methods and apparatus of obtaining NMR spectra: Google Patents, 1985.
64. Bottomley PA. Spatial localization in NMR spectroscopy in vivo. *Ann N Y Acad Sci*. 1987;508: 333-348.
65. Brown TR, Kincaid BM, Ugurbil K. NMR chemical shift imaging in three dimensions. *Proc Natl Acad Sci U S A*. 1982;79: 3523-3526.
66. Pykett IL, Rosen BR. Nuclear magnetic resonance: in vivo proton chemical shift imaging. *Work in progress. Radiology*. 1983;149: 197-201.
67. Rovira A, Auger C, Alonso J. Magnetic resonance monitoring of lesion evolution in multiple sclerosis. *Ther Adv Neurol Disord*. 2013;6: 298-310.
68. Sajja BR, Wolinsky JS, Narayana PA. Proton magnetic resonance spectroscopy in multiple sclerosis. *Neuroimaging Clin N Am*. 2009;19: 45-58.
69. Traboulsee A, Simon JH, Stone L, et al. Revised Recommendations of the Consortium of MS Centers Task Force for a Standardized MRI Protocol and Clinical Guidelines for the Diagnosis and Follow-Up of Multiple Sclerosis. *AJNR Am J Neuroradiol*. 2016;37: 394-401.
70. De Stefano N, Filippi M, Miller D, et al. Guidelines for using proton MR spectroscopy in multicenter clinical MS studies. *Neurology*. 2007;69: 1942-1952.

71. Caramanos Z, Narayanan S, Arnold DL. 1H-MRS quantification of tNA and tCr in patients with multiple sclerosis: a meta-analytic review. *Brain*. 2005;128: 2483-2506.
72. Duarte JM, Lei H, Mlynarik V, Gruetter R. The neurochemical profile quantified by in vivo 1H NMR spectroscopy. *Neuroimage*. 2012;61: 342-362.
73. Barkhof F. The clinico-radiological paradox in multiple sclerosis revisited. *Curr Opin Neurol*. 2002;15: 239-245.
74. Ontaneda D, Fox RJ. Imaging as an Outcome Measure in Multiple Sclerosis. *Neurotherapeutics*. 2016: 1-11.
75. Gonen O, Catalaa I, Babb JS, et al. Total brain N-acetylaspartate: a new measure of disease load in MS. *Neurology*. 2000;54: 15-19.
76. Srinivasan R, Sailasuta N, Hurd R, Nelson S, Pelletier D. Evidence of elevated glutamate in multiple sclerosis using magnetic resonance spectroscopy at 3 T. *Brain*. 2005;128: 1016-1025.
77. Gruber S, Pinker K, Riederer F, et al. Metabolic changes in the normal ageing brain: consistent findings from short and long echo time proton spectroscopy. *Eur J Radiol*. 2008;68: 320-327.
78. Drost DJ, Riddle WR, Clarke GD, Group AMT. Proton magnetic resonance spectroscopy in the brain: report of AAPM MR Task Group #9. *Med Phys*. 2002;29: 2177-2197.
79. Garwood M, DelaBarre L. The return of the frequency sweep: designing adiabatic pulses for contemporary NMR. *J Magn Reson*. 2001;153: 155-177.
80. Zhu H, Barker PB. MR spectroscopy and spectroscopic imaging of the brain. *Methods Mol Biol*. 2011;711: 203-226.
81. Bingolbali A, Fallone BG, Yahya A. Comparison of optimized long echo time STEAM and PRESS proton MR spectroscopy of lipid olefinic protons at 3 Tesla. *J Magn Reson Imaging*. 2013.
82. Duijn JH, Matson GB, Maudsley AA, Weiner MW. 3D phase encoding 1H spectroscopic imaging of human brain. *Magn Reson Imaging*. 1992;10: 315-319.
83. Li Y, Osorio JA, Ozturk-Isik E, et al. Considerations in applying 3D PRESS H-1 brain MRSI with an eight-channel phased-array coil at 3 T. *Magn Reson Imaging*. 2006;24: 1295-1302.
84. Ozhinsky E, Vigneron DB, Nelson SJ. Improved spatial coverage for brain 3D PRESS MRSI by automatic placement of outer-volume suppression saturation bands. *J Magn Reson Imaging*. 2011;33: 792-802.
85. Barker PB, Lin DDM. In vivo proton MR spectroscopy of the human brain. *Progress in Nuclear Magnetic Resonance Spectroscopy*. 2006;49: 99-128.
86. Zierhut ML, Ozturk-Isik E, Chen AP, Park I, Vigneron DB, Nelson SJ. (1)H spectroscopic imaging of human brain at 3 Tesla: comparison of fast three-dimensional magnetic resonance spectroscopic imaging techniques. *J Magn Reson Imaging*. 2009;30: 473-480.
87. Spielman DM, Adalsteinsson E, Lim KO. Quantitative assessment of improved homogeneity using higher-order shims for spectroscopic imaging of the brain. *Magn Reson Med*. 1998;40: 376-382.
88. Pruessmann KP, Weiger M, Scheidegger MB, Boesiger P. SENSE: Sensitivity encoding for fast MRI. *Magnetic Resonance in Medicine*. 1999;42: 952-962.
89. Sodickson DK, Manning WJ. Simultaneous acquisition of spatial harmonics (SMASH): fast imaging with radiofrequency coil arrays. *Magn Reson Med*. 1997;38: 591-603.

90. Griswold MA, Jakob PM, Heidemann RM, et al. Generalized autocalibrating partially parallel acquisitions (GRAPPA). *Magn Reson Med*. 2002;47: 1202-1210.
91. Dydak U, Weiger M, Pruessmann KP, Meier D, Boesiger P. Sensitivity-encoded spectroscopic imaging. *Magn Reson Med*. 2001;46: 713-722.
92. Banerjee S, Ozturk-Isik E, Nelson SJ, Majumdar S. Fast magnetic resonance spectroscopic imaging at 3 Tesla using autocalibrating parallel technique. *Conf Proc IEEE Eng Med Biol Soc*. 2006;1: 1866-1869.
93. Bonekamp D, Smith MA, Zhu H, Barker PB. Quantitative SENSE-MRSI of the human brain. *Magn Reson Imaging*. 2010;28: 305-313.
94. Posse S, Otazo R, Dager SR, Alger J. MR spectroscopic imaging: principles and recent advances. *J Magn Reson Imaging*. 2013;37: 1301-1325.
95. Otazo R, Tsai SY, Lin FH, Posse S. Accelerated short-TE 3D proton echo-planar spectroscopic imaging using 2D-SENSE with a 32-channel array coil. *Magn Reson Med*. 2007;58: 1107-1116.
96. Dydak U, Pruessmann KP, Weiger M, Tsao J, Meier D, Boesiger P. Parallel spectroscopic imaging with spin-echo trains. *Magn Reson Med*. 2003;50: 196-200.
97. Srinivasan R, Cunningham C, Chen A, et al. TE-averaged two-dimensional proton spectroscopic imaging of glutamate at 3 T. *Neuroimage*. 2006;30: 1171-1178.
98. Kim DH, Henry R, Spielman DM. Fast multivoxel two-dimensional spectroscopic imaging at 3 T. *Magn Reson Imaging*. 2007;25: 1155-1161.
99. Posse S, Otazo R, Caprihan A, et al. Proton echo-planar spectroscopic imaging of J-coupled resonances in human brain at 3 and 4 Tesla. *Magn Reson Med*. 2007;58: 236-244.
100. Dager SR, Corrigan NM, Richards TL, Posse S. Research applications of magnetic resonance spectroscopy to investigate psychiatric disorders. *Top Magn Reson Imaging*. 2008;19: 81-96.
101. Posse S, Tedeschi G, Risinger R, Ogg R, Le Bihan D. High speed 1H spectroscopic imaging in human brain by echo planar spatial-spectral encoding. *Magn Reson Med*. 1995;33: 34-40.
102. Adalsteinsson E, Irarrazabal P, Topp S, Meyer C, Macovski A, Spielman DM. Volumetric spectroscopic imaging with spiral-based k-space trajectories. *Magn Reson Med*. 1998;39: 889-898.
103. Paschal CB, Morris HD. K-space in the clinic. *J Magn Reson Imaging*. 2004;19: 145-159.
104. Gagoski AB. Spiral chemical shift imaging at 3T using 32 channel receive array and online reconstruction. *Prilozi*. 2010;31: 135-149.
105. Block KT, Frahm J. Spiral imaging: a critical appraisal. *J Magn Reson Imaging*. 2005;21: 657-668.
106. Pohmann R, von Kienlin M, Haase A. Theoretical evaluation and comparison of fast chemical shift imaging methods. *J Magn Reson*. 1997;129: 145-160.
107. Gu M, Kim DH, Mayer D, Sullivan EV, Pfefferbaum A, Spielman DM. Reproducibility study of whole-brain 1H spectroscopic imaging with automated quantification. *Magn Reson Med*. 2008;60: 542-547.
108. Delattre BM, Heidemann RM, Crowe LA, Vallee JP, Hyacinthe JN. Spiral demystified. *Magn Reson Imaging*. 2010;28: 862-881.
109. Mayer D, Kim DH, Spielman DM, Bammer R. Fast parallel spiral chemical shift imaging at 3T using iterative SENSE reconstruction. *Magn Reson Med*. 2008;59: 891-897.

110. Bogner W, Gagoski B, Hess AT, et al. 3D GABA imaging with real-time motion correction, shim update and reacquisition of adiabatic spiral MRSI. *Neuroimage*. 2014;103C: 290-302.
111. Bogner W, Hess AT, Gagoski B, et al. Real-time motion- and B-correction for LASER-localized spiral-accelerated 3D-MRSI of the brain at 3T. *Neuroimage*. 2013;88C: 22-31.
112. Andronesi OC, Gagoski BA, Sorensen AG. Neurologic 3D MR spectroscopic imaging with low-power adiabatic pulses and fast spiral acquisition. *Radiology*. 2012;262: 647-661.
113. Ozturk-Isik E, Chen AP, Crane JC, et al. 3D sensitivity encoded ellipsoidal MR spectroscopic imaging of gliomas at 3T. *Magn Reson Imaging*. 2009;27: 1249-1257.
114. Duyn JH, Moonen CTW. Fast Proton Spectroscopic Imaging of Human Brain Using Multiple Spin-Echoes. *Magnetic Resonance in Medicine*. 1993;30: 409-414.
115. Martin AJ, Liu H, Hall WA, Truwit CL. Preliminary assessment of turbo spectroscopic imaging for targeting in brain biopsy. *AJNR Am J Neuroradiol*. 2001;22: 959-968.
116. Stengel A, Neumann-Haefelin T, Singer OC, et al. Multiple spin-echo spectroscopic imaging for rapid quantitative assessment of N-acetylaspartate and lactate in acute stroke. *Magn Reson Med*. 2004;52: 228-238.
117. Yahya A, Fallone BG. Detection of glutamate and glutamine (Glx) by turbo spectroscopic imaging. *J Magn Reson*. 2009;196: 170-177.
118. Dydak U, Meier D, Lamerichs R, Boesiger P. Trading spectral separation at 3T for acquisition speed in multi spin-echo spectroscopic imaging. *AJNR Am J Neuroradiol*. 2006;27: 1441-1446.
119. Yang A, Xiao X, Wang Z. Evaluation of normal changes in pons metabolites due to aging using turbo spectroscopic imaging. *AJNR Am J Neuroradiol*. 2014;35: 2099-2105.
120. Mansfield P. Spatial mapping of the chemical shift in NMR. *Magn Reson Med*. 1984;1: 370-386.
121. Posse S, DeCarli C, Le Bihan D. Three-dimensional echo-planar MR spectroscopic imaging at short echo times in the human brain. *Radiology*. 1994;192: 733-738.
122. Ebel A, Soher BJ, Maudsley AA. Assessment of 3D proton MR echo-planar spectroscopic imaging using automated spectral analysis. *Magn Reson Med*. 2001;46: 1072-1078.
123. Otazo R, Mueller B, Ugurbil K, Wald L, Posse S. Signal-to-noise ratio and spectral linewidth improvements between 1.5 and 7 Tesla in proton echo-planar spectroscopic imaging. *Magn Reson Med*. 2006;56: 1200-1210.
124. Posse S, Dager SR, Richards TL, et al. In vivo measurement of regional brain metabolic response to hyperventilation using magnetic resonance: proton echo planar spectroscopic imaging (PEPSI). *Magn Reson Med*. 1997;37: 858-865.
125. Maudsley AA, Domenig C, Govind V, et al. Mapping of brain metabolite distributions by volumetric proton MR spectroscopic imaging (MRSI). *Magn Reson Med*. 2009;61: 548-559.
126. Maudsley AA, Darkazanli A, Alger JR, et al. Comprehensive processing, display and analysis for in vivo MR spectroscopic imaging. *NMR Biomed*. 2006;19: 492-503.
127. Rieseberg S, Frahm J, Finsterbusch J. Two-dimensional spatially-selective RF excitation pulses in echo-planar imaging. *Magn Reson Med*. 2002;47: 1186-1193.
128. Ding XQ, Maudsley AA, Sabati M, Sherif S, Dellani PR, Lanfermann H. Reproducibility and Reliability of Short-TE Whole-Brain MR Spectroscopic Imaging of Human Brain at 3T. *Magnetic Resonance in Medicine*. 2015;73: 921-928.

129. Lecocq A, Le Fur Y, Maudsley AA, et al. Whole-brain quantitative mapping of metabolites using short echo three-dimensional proton MRSI. *Journal of Magnetic Resonance Imaging*. 2015;42: 280-289.
130. Sabati M, Zhan J, Govind V, Arheart KL, Maudsley AA. Impact of reduced k-space acquisition on pathologic detectability for volumetric MR spectroscopic imaging. *J Magn Reson Imaging*. 2014;39: 224-234.
131. Kim DH, Gu M, Cunningham C, et al. Fast 3D (1)H MRSI of the corticospinal tract in pediatric brain. *J Magn Reson Imaging*. 2009;29: 1-6.
132. Lin FH, Tsai SY, Otazo R, et al. Sensitivity-encoded (SENSE) proton echo-planar spectroscopic imaging (PEPSI) in the human brain. *Magn Reson Med*. 2007;57: 249-257.
133. Zhu X, Ebel A, Ji JX, Schuff N. Spectral phase-corrected GRAPPA reconstruction of three-dimensional echo-planar spectroscopic imaging (3D-EPSI). *Magn Reson Med*. 2007;57: 815-820.
134. Tsai SY, Otazo R, Posse S, et al. Accelerated proton echo planar spectroscopic imaging (PEPSI) using GRAPPA with a 32-channel phased-array coil. *Magn Reson Med*. 2008;59: 989-998.
135. Wiggins GC, Triantafyllou C, Potthast A, Reykowski A, Nittka M, Wald LL. 32-channel 3 Tesla receive-only phased-array head coil with soccer-ball element geometry. *Magn Reson Med*. 2006;56: 216-223.
136. Mescher M, Merkle H, Kirsch J, Garwood M, Gruetter R. Simultaneous in vivo spectral editing and water suppression. *NMR Biomed*. 1998;11: 266-272.
137. Dydak U, Marjanska M, Posse S. High-Speed GABA Mapping in Human Brain with MEGA-PEPSI at 3 Tesla. *Proc. Intl. Soc. Mag. Reson. Med*. 2010; 18: 961.
138. Dydak U, J. S. Xu, Marjanska M, Posse S. 3D GABA Spectroscopic Imaging using MEGA-PEPSI. *Proc. Intl. Soc. Mag. Reson. Med*. 2011; 19: 1428.
139. Edden RA, Pomper MG, Barker PB. In vivo differentiation of N-acetyl aspartyl glutamate from N-acetyl aspartate at 3 Tesla. *Magn Reson Med*. 2007;57: 977-982.
140. Dong Z, Liu F, Kangarlu A, Peterson BS. Metabolite Mapping with Extended Brain Coverage Using a Fast Multisection MRSI Pulse Sequence and a Multichannel Coil. *Int J Biomed Imaging*. 2012;2012: 247161.
141. Sijens PE, Irwan R, Potze JH, Mostert JP, De Keyser J, Oudkerk M. Analysis of the human brain in primary progressive multiple sclerosis with mapping of the spatial distributions using 1H MR spectroscopy and diffusion tensor imaging. *Eur Radiol*. 2005;15: 1686-1693.
142. Arnold DL, Matthews PM, Francis GS, O'Connor J, Antel JP. Proton magnetic resonance spectroscopic imaging for metabolic characterization of demyelinating plaques. *Ann Neurol*. 1992;31: 235-241.
143. Rooney WD, Goodkin DE, Schuff N, Meyerhoff DJ, Norman D, Weiner MW. 1H MRSI of normal appearing white matter in multiple sclerosis. *Mult Scler*. 1997;3: 231-237.
144. Tedeschi G, Bonavita S, McFarland HF, Richert N, Duyn JH, Frank JA. Proton MR spectroscopic imaging in multiple sclerosis. *Neuroradiology*. 2002;44: 37-42.
145. Dominique Sappey-Marinier, Matthieu Bagory, Salem Hannoun, et al. Characterization of Neurodegenerative Processes in Multiple Sclerosis using Magnetic Resonance Spectroscopic Imaging and Diffusion Tensor Imaging. *MIAMS*. 2008: 60-70.

146. Husted CA, Goodin DS, Hugg JW, et al. Biochemical alterations in multiple sclerosis lesions and normal-appearing white matter detected by in vivo 31P and 1H spectroscopic imaging. *Ann Neurol*. 1994;36: 157-165.
147. Inglese M, Liu S, Babb JS, Mannon LJ, Grossman RI, Gonen O. Three-dimensional proton spectroscopy of deep gray matter nuclei in relapsing-remitting MS. *Neurology*. 2004;63: 170-172.
148. Chang L, Munsaka SM, Kraft-Terry S, Ernst T. Magnetic resonance spectroscopy to assess neuroinflammation and neuropathic pain. *J Neuroimmune Pharmacol*. 2013;8: 576-593.
149. Suhy J, Rooney WD, Goodkin DE, et al. 1H MRSI comparison of white matter and lesions in primary progressive and relapsing-remitting MS. *Mult Scler*. 2000;6: 148-155.
150. Chard DT, Griffin CM, McLean MA, et al. Brain metabolite changes in cortical grey and normal-appearing white matter in clinically early relapsing-remitting multiple sclerosis. *Brain*. 2002;125: 2342-2352.
151. Sharma R, Narayana PA, Wolinsky JS. Grey matter abnormalities in multiple sclerosis: proton magnetic resonance spectroscopic imaging. *Mult Scler*. 2001;7: 221-226.
152. Ratiney H, Okuda D, Graveron-Demilly D, Nelson SJ, Hauser S, Pelletier D. Estimation of myo-Inositol and macromolecule contents in Normal-appearing white and gray matter in MS using 3D-HMRSI at 3T. *Proc. Intl. Soc. Mag. Reson. Med*. 2006;14: 2635.
153. Khan O, Seraji-Bozorgzad N, Bao F, et al. The Relationship Between Brain MR Spectroscopy and Disability in Multiple Sclerosis: 20-Year Data from the U.S. Glatiramer Acetate Extension Study. *J Neuroimaging*. 2016.
154. De Stefano N, Filippi M. MR spectroscopy in multiple sclerosis. *J Neuroimaging*. 2007;17 Suppl 1: 31S-35S.
155. Donadieu M, Le Fur Y, Lecocq A, et al. Metabolic voxel-based analysis of the complete human brain using fast 3D-MRSI: Proof of concept in multiple sclerosis. *J Magn Reson Imaging*. 2016.
156. Mostert JP, Blaauw Y, Koch MW, Kuiper AJ, Hoogduin JM, De Keyser J. Reproducibility over a 1-month period of 1H-MR spectroscopic imaging NAA/Cr ratios in clinically stable multiple sclerosis patients. *Eur Radiol*. 2008;18: 1736-1740.
157. Vafaeyan H, Ebrahimzadeh SA, Rahimian N, et al. Quantification of diagnostic biomarkers to detect multiple sclerosis lesions employing (1)H-MRSI at 3T. *Australas Phys Eng Sci Med*. 2015;38: 611-618.
158. Y Choi , P Lee A, J Hughes , D.R Denney , Lynch SG. Longitudinal changes in metabolic neuroimaging markers linked to the clinical decline in patients with secondary progressive multiple sclerosis. *ECTRIMS Online Library*, Sep 16, 2016.
159. Katsavos S, Anagnostouli M. Biomarkers in Multiple Sclerosis: An Up-to-Date Overview. *Mult Scler Int*. 2013;2013: 340508.
160. Soreni N, Noseworthy MD, Konyer NB, Pullenayegum E, Schachar R. Interindividual, repositioning, and time-of-day effects on single voxel proton MR spectroscopy of the anterior cingulate cortex. *J Magn Reson Imaging*. 2010;32: 276-282.
161. Soreni N, Noseworthy MD, Cormier T, Oakden WK, Bells S, Schachar R. Intraindividual variability of striatal (1)H-MRS brain metabolite measurements at 3 T. *Magn Reson Imaging*. 2006;24: 187-194.
162. Evans CJ, McGonigle DJ, Edden RA. Diurnal stability of gamma-aminobutyric acid concentration in visual and sensorimotor cortex. *J Magn Reson Imaging*. 2010;31: 204-209.

163. Yasen AL, Smith J, Christie AD. Reliability of glutamate and GABA quantification using proton magnetic resonance spectroscopy. *Neurosci Lett*. 2017;643: 121-124.
164. Allaili N, Valabregue R, Auerbach EJ, et al. Single-voxel (1)H spectroscopy in the human hippocampus at 3 T using the LASER sequence: characterization of neurochemical profile and reproducibility. *NMR Biomed*. 2015;28: 1209-1217.
165. Schirmer T, Auer DP. On the reliability of quantitative clinical magnetic resonance spectroscopy of the human brain. *NMR Biomed*. 2000;13: 28-36.
166. Geurts JJ, Barkhof F, Castelijns JA, Uitdehaag BM, Polman CH, Pouwels PJ. Quantitative 1H-MRS of healthy human cortex, hippocampus, and thalamus: metabolite concentrations, quantification precision, and reproducibility. *J Magn Reson Imaging*. 2004;20: 366-371.
167. Terpstra M, Cheong I, Lyu T, et al. Test-retest reproducibility of neurochemical profiles with short-echo, single-voxel MR spectroscopy at 3T and 7T. *Magn Reson Med*. 2016;76: 1083-1091.
168. O'Gorman RL, Michels L, Edden RA, Murdoch JB, Martin E. In vivo detection of GABA and glutamate with MEGA-PRESS: reproducibility and gender effects. *J Magn Reson Imaging*. 2011;33: 1262-1267.
169. Hammen T, Stadlbauer A, Tomandl B, et al. Short TE single-voxel 1H-MR spectroscopy of hippocampal structures in healthy adults at 1.5 Tesla--how reproducible are the results? *NMR Biomed*. 2005;18: 195-201.
170. Brooks WM, Friedman SD, Stidley CA. Reproducibility of 1H-MRS in vivo. *Magn Reson Med*. 1999;41: 193-197.
171. Kojima S, Hirata M, Shinohara H, Ueno E. Reproducibility of scan prescription in follow-up brain MRI: manual versus automatic determination. *Radiol Phys Technol*. 2013;6: 375-384.
172. Quadrelli S, Mountford C, Ramadan S. Hitchhiker's Guide to Voxel Segmentation for Partial Volume Correction of In Vivo Magnetic Resonance Spectroscopy. *Magnetic Resonance Insights*. 2016;9: 1-8.
173. Ogg RJ, Kingsley PB, Taylor JS. WET, a T1- and B1-insensitive water-suppression method for in vivo localized 1H NMR spectroscopy. *J Magn Reson B*. 1994;104: 1-10.
174. Allen P, Bennett K, Heritage B. *SPSS Statistics Version 22: A Practical Guide*. Cengage Learning Australia, 2014.
175. Chard DT, McLean MA, Parker GJ, MacManus DG, Miller DH. Reproducibility of in vivo metabolite quantification with proton magnetic resonance spectroscopic imaging. *J Magn Reson Imaging*. 2002;15: 219-225.
176. Gasparovic C, Bedrick EJ, Mayer AR, et al. Test-Retest Reliability and Reproducibility of Short-Echo-Time Spectroscopic Imaging of Human Brain at 3T. *Magnetic Resonance in Medicine*. 2011;66: 324-332.
177. Zaki R, Bulgiba A, Nordin N, Ismail NA. A Systematic Review of Statistical Methods Used to Test for Reliability of Medical Instruments Measuring Continuous Variables. *Iranian Journal of Basic Medical Sciences*. 2013;16: 803-807.
178. Mlynárik V, Gruber S, Moser E. Proton T 1 and T 2 relaxation times of human brain metabolites at 3 Tesla. *NMR in Biomedicine: An International Journal Devoted to the Development and Application of Magnetic Resonance In Vivo*. 2001;14: 325-331.
179. Shannon BJ, Dosenbach RA, Su Y, et al. Morning-evening variation in human brain metabolism and memory circuits. *J Neurophysiol*. 2013;109: 1444-1456.

180. Baker EH, Basso G, Barker PB, Smith MA, Bonekamp D, Horska A. Regional apparent metabolite concentrations in young adult brain measured by H-1 MR spectroscopy at 3 tesla. *Journal of Magnetic Resonance Imaging*. 2008;27: 489-499.
181. Bladowska J, Zimny A, Koltowska A, et al. Evaluation of metabolic changes within the normal appearing gray and white matters in neurologically asymptomatic HIV-1-positive and HCV-positive patients: magnetic resonance spectroscopy and immunologic correlation. *Eur J Radiol*. 2013;82: 686-692.
182. Dou W, Speck O, Benner T, et al. Automatic voxel positioning for MRS at 7 T. *MAGMA*. 2015;28: 259-270.
183. Venkatraman TN, Hamer RM, Perkins DO, Song AW, Lieberman JA, Steen RG. Single-voxel 1H PRESS at 4.0 T: precision and variability of measurements in anterior cingulate and hippocampus. *NMR Biomed*. 2006;19: 484-491.
184. Kirov II, George IC, Jayawickrama N, Babb JS, Perry NN, Gonen O. Longitudinal inter- and intra-individual human brain metabolic quantification over 3 years with proton MR spectroscopy at 3 T. *Magn Reson Med*. 2012;67: 27-33.
185. Bartha R, Drost DJ, Menon RS, Williamson PC. Comparison of the quantification precision of human short echo time (1)H spectroscopy at 1.5 and 4.0 Tesla. *Magn Reson Med*. 2000;44: 185-192.
186. Mullins PG, Chen H, Xu J, Caprihan A, Gasparovic C. Comparative reliability of proton spectroscopy techniques designed to improve detection of J-coupled metabolites. *Magn Reson Med*. 2008;60: 964-969.
187. Wijtenburg SA, Gaston FE, Spieker EA, et al. Reproducibility of Phase Rotation STEAM at 3T: Focus on Glutathione. *Magnetic Resonance in Medicine*. 2014;72: 603-609.
188. Hoshino Y, Yoshikawa K, Inoue Y, et al. Reproducibility of short echo time proton magnetic resonance spectroscopy using point-resolved spatially localized spectroscopy sequence in normal human brains. *Radiat Med*. 1999;17: 115-120.
189. Gasparovic C, Bedrick EJ, Mayer AR, et al. Test-retest reliability and reproducibility of short-echo-time spectroscopic imaging of human brain at 3T. *Magn Reson Med*. 2011;66: 324-332.
190. Mountford CE, Stanwell P, Lin A, Ramadan S, Ross B. Neurospectroscopy: the past, present and future. *Chem Rev*. 2010;110: 3060-3086.
191. Rosen Y, Lenkinski RE. Recent advances in magnetic resonance neurospectroscopy. *Neurotherapeutics*. 2007;4: 330-345.
192. Weir JP. Quantifying test-retest reliability using the intraclass correlation coefficient and the SEM. *Journal of Strength and Conditioning Research*. 2005;19: 231-240.
193. Koo TK, Li MY. A Guideline of Selecting and Reporting Intraclass Correlation Coefficients for Reliability Research. *J Chiropr Med*. 2016;15: 155-163.
194. Bompreszi R. Dimethyl fumarate in the treatment of relapsing-remitting multiple sclerosis: an overview. *Therapeutic Advances in Neurological Disorders*. 2015;8: 20-30.
195. Ferreira B, Mendes F, Osorio N, Caseiro A, Gabriel A, Valado A. Glutathione in multiple sclerosis. *British Journal of Biomedical Science*. 2013;70: 75-79.
196. Srinivasan R, Ratiney H, Hammond-Rosenbluth KE, Pelletier D, Nelson SJ. MR spectroscopic imaging of glutathione in the white and gray matter at 7 T with an application to multiple sclerosis. *Magn Reson Imaging*. 2010;28: 163-170.

197. Henry R, Li Y, Zhu A, et al. 1-H MRSI in patients with relapsing multiple sclerosis at 7 Tesla (P6.121). *Neurology*. 2015;84.
198. Choi C, Ganji SK, DeBerardinis RJ, et al. Measurement of glycine in the human brain in vivo by 1H-MRS at 3 T: application in brain tumors. *Magn Reson Med*. 2011;66: 609-618.
199. Choi IY, Lee P, Hughes AJ, Denney DR, Lynch SG. Longitudinal changes of cerebral glutathione (GSH) levels associated with the clinical course of disease progression in patients with secondary progressive multiple sclerosis. *Mult Scler*. 2016.
200. Choi IY, Lee P, Adany P, et al. In vivo evidence of oxidative stress in brains of patients with progressive multiple sclerosis. *Mult Scler*. 2017: 1352458517711568.
201. Smith SM, De Stefano N, Jenkinson M, Matthews PM. Normalized accurate measurement of longitudinal brain change. *J Comput Assist Tomogr*. 2001;25: 466-475.
202. Ashburner J, Barnes G, Chen C , et al. SPM12 Available from URL: <http://www.fil.ion.ucl.ac.uk/spm/>.
203. Quadrelli S, Mountford C, Ramadan S. Hitchhiker's Guide to Voxel Segmentation for Partial Volume Correction of In Vivo Magnetic Resonance Spectroscopy. *Magnetic Resonance Insights*. 2016;9: 1-8.
204. Terpstra M, Henry PG, Gruetter R. Measurement of reduced glutathione (GSH) in human brain using LCmodel analysis of difference-edited spectra. *Magnetic Resonance in Medicine*. 2003;50: 19-23.
205. Duffy SL, Lagopoulos J, Hickie IB, et al. Glutathione relates to neuropsychological functioning in mild cognitive impairment. *Alzheimers & Dementia*. 2014;10: 67-75.
206. Provencher SW. Estimation of metabolite concentrations from localized in vivo proton NMR spectra. *Magn Reson Med*. 1993;30: 672-679.
207. Roxburgh RH, Seaman SR, Masterman T, et al. Multiple Sclerosis Severity Score: using disability and disease duration to rate disease severity. *Neurology*. 2005;64: 1144-1151.
208. Henry JD, Crawford JR. The short-form version of the Depression Anxiety Stress Scales (DASS-21): construct validity and normative data in a large non-clinical sample. *Br J Clin Psychol*. 2005;44: 227-239.
209. Fisk JD, Ritvo PG, Ross L, Haase DA, Marris TJ, Schlech WF. Measuring the functional impact of fatigue: initial validation of the fatigue impact scale. *Clin Infect Dis*. 1994;18 Suppl 1: S79-83.
210. Kim TW, Sung YH. Regular exercise promotes memory function and enhances hippocampal neuroplasticity in experimental autoimmune encephalomyelitis mice. *Neuroscience*. 2017;346: 173-181.
211. Roosendaal SD, Moraal B, Pouwels PJW, et al. Accumulation of cortical lesions in MS: relation with cognitive impairment. *Mult Scler*. 2009;15: 708-714.
212. Sormani MP, Kappos L, Radue EW, et al. Defining brain volume cutoffs to identify clinically relevant atrophy in RRMS. *Mult Scler*. 2017;23: 656-664.
213. Giorgio A, Battaglini M, Smith SM, De Stefano N. Brain Atrophy Assessment in Multiple Sclerosis: Importance and Limitations. *Neuroimaging Clin N Am*. 2008;18: 675-686.
214. Arnold DL, Gold R, Kappos L, et al. Effects of delayed-release dimethyl fumarate on MRI measures in the Phase 3 DEFINE study. *J Neurol*. 2014;261: 1794-1802.
215. De Stefano N, Stromillo ML, Giorgio A, et al. Establishing pathological cut-offs of brain atrophy rates in multiple sclerosis. *J Neurol Neurosurg Psychiatry*. 2016;87: 93-99.

216. Rovira À, Alonso J. 1H Magnetic Resonance Spectroscopy in Multiple Sclerosis and Related Disorders. *Neuroimaging Clinics*. 2013;23: 459-474.
217. Khan O, Seraji-Bozorgzad N, Bao F, et al. The Relationship Between Brain MR Spectroscopy and Disability in Multiple Sclerosis: 20-Year Data from the U.S. Glatiramer Acetate Extension Study. *J Neuroimaging*. 2017;27: 97-106.
218. Reinke SN, Broadhurst DL, Sykes BD, et al. Metabolomic profiling in multiple sclerosis: insights into biomarkers and pathogenesis. *Mult Scler*. 2014;20: 1396-1400.
219. Davitz MS, Wu WE, Soher BJ, et al. Quantifying global-brain metabolite level changes with whole-head proton MR spectroscopy at 3T. *Magn Reson Imaging*. 2017;35: 15-19.
220. Brennan MS, Matos MF, Li B, et al. Dimethyl Fumarate and Monoethyl Fumarate Exhibit Differential Effects on KEAP1, NRF2 Activation, and Glutathione Depletion In Vitro. *PLoS One*. 2015;10.
221. Ribbons K, Lea R, Schofield PW, Lechner-Scott J. Anxiety Levels Are Independently Associated With Cognitive Performance in an Australian Multiple Sclerosis Patient Cohort. *J Neuropsychiatry Clin Neurosci*. 2017;29: 128-134.
222. Colasanti A, Guo Q, Giannetti P, et al. Hippocampal Neuroinflammation, Functional Connectivity, and Depressive Symptoms in Multiple Sclerosis. *Biol Psychiatry*. 2016;80: 62-72.
223. Nigro S, Passamonti L, Riccelli R, et al. Structural 'connectomic' alterations in the limbic system of multiple sclerosis patients with major depression. *Mult Scler*. 2015;21: 1003-1012.
224. Choi IY, Lee SP, Denney DR, Lynch SG. Lower levels of glutathione in the brains of secondary progressive multiple sclerosis patients measured by 1H magnetic resonance chemical shift imaging at 3 T. *Mult Scler*. 2011;17: 289-296.
225. Gold R, Kappos L, Arnold DL, et al. Placebo-controlled phase 3 study of oral BG-12 for relapsing multiple sclerosis. *N Engl J Med*. 2012;367: 1098-1107.
226. Simpson D, Noble S, Perry C. Glatiramer Acetate. *CNS Drugs*. 2002;16: 825-850.
227. Hutchinson M. Natalizumab: A new treatment for relapsing remitting multiple sclerosis. *Therapeutics and Clinical Risk Management*. 2007;3: 259-268.
228. Sarchielli P, Presciutti O, Tarducci R, et al. 1H-MRS in patients with multiple sclerosis undergoing treatment with interferon beta-1a: results of a preliminary study. *J Neurol Neurosurg Psychiatry*. 1998;64: 204-212.
229. Toprak MK, Cakir B, Ulu EM, et al. The effects of interferon beta-1a on proton MR spectroscopic imaging in patients with multiple sclerosis, a controlled study, preliminary results. *Int J Neurosci*. 2008;118: 1645-1658.
230. Khan O, Shen Y, Caon C, et al. Axonal metabolic recovery and potential neuroprotective effect of glatiramer acetate in relapsing-remitting multiple sclerosis. *Mult Scler*. 2005;11: 646-651.
231. Schubert F, Seifert F, Elster C, et al. Serial 1H-MRS in relapsing-remitting multiple sclerosis: effects of interferon- $\beta$  therapy on absolute metabolite concentrations. *Magnetic Resonance Materials in Physics, Biology and Medicine*. 2002;14: 213.
232. Yetkin MF, Mirza M, Donmez H. Monitoring interferon beta treatment response with magnetic resonance spectroscopy in relapsing remitting multiple sclerosis. *Medicine (Baltimore)*. 2016;95: e4782.

233. Khan O, Shen Y, Bao F, et al. Long-term study of brain 1H-MRS study in multiple sclerosis: effect of glatiramer acetate therapy on axonal metabolic function and feasibility of long-Term H-MRS monitoring in multiple sclerosis. *J Neuroimaging*. 2008;18: 314-319.
234. Mills EA, Ogrodnik MA, Plave A, Mao-Draayer Y. Emerging Understanding of the Mechanism of Action for Dimethyl Fumarate in the Treatment of Multiple Sclerosis. *Frontiers in Neurology*. 2018;9: 5-5.
235. Fox RJ, Miller DH, Phillips JT, et al. Placebo-controlled phase 3 study of oral BG-12 or glatiramer in multiple sclerosis. *N Engl J Med*. 2012;367: 1087-1097.
236. Kresa-Reahl K, Repovic P, Robertson D, Okwuokenye M, Meltzer L, Mendoza JP. Effectiveness of Delayed-release Dimethyl Fumarate on Clinical and Patient-reported Outcomes in Patients With Relapsing Multiple Sclerosis Switching From Glatiramer Acetate: RESPOND, a Prospective Observational Study. *Clin Ther*. 2018;40: 2077-2087.
237. Wattjes MP, Harzheim M, Lutterbey GG, Klotz L, Schild HH, Traber F. Axonal damage but no increased glial cell activity in the normal-appearing white matter of patients with clinically isolated syndromes suggestive of multiple sclerosis using high-field magnetic resonance spectroscopy. *AJNR Am J Neuroradiol*. 2007;28: 1517-1522.
238. MacKay A, Laule C, Li DKB, Meyers SM, Russell-Schulz B, Vavasour IM. Magnetic Resonance Techniques for Investigation of Multiple Sclerosis. *AIP Conference Proceedings*. 2014;1626: 22-35.
239. Smith SM. Fast robust automated brain extraction. *Human Brain Mapping*. 2002;17: 143-155.
240. Jenkinson M, Bannister P, Brady M, Smith S. Improved Optimization for the Robust and Accurate Linear Registration and Motion Correction of Brain Images. *NeuroImage*. 2002;17: 825-841.
241. Jenkinson M, Smith S. A global optimisation method for robust affine registration of brain images. *Medical Image Analysis*. 2001;5: 143-156.
242. Smith SM, Jenkinson M, Woolrich MW, et al. Advances in functional and structural MR image analysis and implementation as FSL. *Neuroimage*. 2004;23 Suppl 1: S208-219.
243. Schmidt P, Gaser C, Arsic M, et al. An automated tool for detection of FLAIR-hyperintense white-matter lesions in Multiple Sclerosis. *NeuroImage*. 2012;59: 3774-3783.
244. Gelineau-Morel R, Tomassini V, Jenkinson M, Johansen-Berg H, Matthews PM, Palace J. The effect of hypointense white matter lesions on automated gray matter segmentation in multiple sclerosis. *Human Brain Mapping*. 2012;33: 2802-2814.
245. Drake AS, Weinstock-Guttman B, Morrow SA, Hojnacki D, Munschauer FE, Benedict RH. Psychometrics and normative data for the Multiple Sclerosis Functional Composite: replacing the PASAT with the Symbol Digit Modalities Test. *Mult Scler*. 2010;16: 228-237.
246. Parmenter BA, Weinstock-Guttman B, Garg N, Munschauer F, Benedict RH. Screening for cognitive impairment in multiple sclerosis using the Symbol digit Modalities Test. *Mult Scler*. 2007;13: 52-57.
247. Vingara LK, Yu HJ, Wagshul ME, et al. Metabolomic approach to human brain spectroscopy identifies associations between clinical features and the frontal lobe metabolome in multiple sclerosis. *Neuroimage*. 2013;82: 586-594.
248. Pokryszko-Dragan A, Bladowska J, Zimny A, et al. Magnetic resonance spectroscopy findings as related to fatigue and cognitive performance in multiple sclerosis patients with mild disability. *J Neurol Sci*. 2014;339: 35-40.

249. Leech R, Sharp DJ. The role of the posterior cingulate cortex in cognition and disease. *Brain*. 2014;137: 12-32.
250. Filippi M, Riccitelli G, Mattioli F, et al. Multiple sclerosis: effects of cognitive rehabilitation on structural and functional MR imaging measures—an explorative study. *Radiology*. 2012;262: 932-940.
251. Helms G, Stawiarz L, Kivisakk P, Link H. Regression analysis of metabolite concentrations estimated from localized proton MR spectra of active and chronic multiple sclerosis lesions. *Magn Reson Med*. 2000;43: 102-110.
252. Moffett JR, Ross B, Arun P, Madhavarao CN, Namboodiri AM. N-Acetylaspartate in the CNS: from neurodiagnostics to neurobiology. *Prog Neurobiol*. 2007;81: 89-131.
253. Narayanan S, De Stefano N, Francis GS, et al. Axonal metabolic recovery in multiple sclerosis patients treated with interferon beta-1b. *J Neurol*. 2001;248: 979-986.
254. De Stefano N, Narayanan S, Francis GS, et al. Evidence of axonal damage in the early stages of multiple sclerosis and its relevance to disability. *Arch Neurol*. 2001;58: 65-70.
255. De Stefano N, Matthews PM, Narayanan S, Francis GS, Antel JP, Arnold DL. Axonal dysfunction and disability in a relapse of multiple sclerosis: longitudinal study of a patient. *Neurology*. 1997;49: 1138-1141.
256. Gustafsson MC, Dahlqvist O, Jaworski J, Lundberg P, Landtblom AM. Low choline concentrations in normal-appearing white matter of patients with multiple sclerosis and normal MR imaging brain scans. *AJNR Am J Neuroradiol*. 2007;28: 1306-1312.
257. Londono AC, Mora CA. Nonconventional MRI biomarkers for in vivo monitoring of pathogenesis in multiple sclerosis. *Neurol Neuroimmunol Neuroinflamm*. 2014;1: e45.
258. Filippi M, Agosta F. Imaging biomarkers in multiple sclerosis. *J Magn Reson Imaging*. 2010;31: 770-788.
259. Healy BC, Buckle GJ, Ali EN, et al. Characterizing Clinical and MRI Dissociation in Patients with Multiple Sclerosis. *Journal of Neuroimaging*. 2017;27: 481-485.
260. Chard D, Trip SA. Resolving the clinico-radiological paradox in multiple sclerosis. *F1000Res*. 2017;6: 1828.
261. Bermel RA, Bakshi R. The measurement and clinical relevance of brain atrophy in multiple sclerosis. *Lancet Neurology*. 2006;5: 158-170.
262. Roosendaal SD, Bendfeldt K, Vrenken H, et al. Grey matter volume in a large cohort of MS patients: relation to MRI parameters and disability. *Multiple Sclerosis*. 2011;17: 1098-1106.
263. Miller DH, Lublin FD, Sormani MP, et al. Brain atrophy and disability worsening in primary progressive multiple sclerosis: insights from the INFORMS study. *Ann Clin Transl Neurol*. 2018;5: 346-356.
264. Shiee N, Bazin PL, Zackowski KM, et al. Revisiting brain atrophy and its relationship to disability in multiple sclerosis. *PLoS ONE*. 2012;7: e37049.
265. Castro-Borrero W, Graves D, Frohman TC, et al. Current and emerging therapies in multiple sclerosis: a systematic review. *Ther Adv Neurol Disord*. 2012;5: 205-220.
266. Ziemssen T, Hoffman J, Apfel R, Kern S. Effects of glatiramer acetate on fatigue and days of absence from work in first-time treated relapsing-remitting multiple sclerosis. *Health Qual Life Outcomes*. 2008;6: 67.

267. Radue EW, O'Connor P, Polman CH, et al. Impact of fingolimod therapy on magnetic resonance imaging outcomes in patients with multiple sclerosis. *Arch Neurol*. 2012;69: 1259-1269.
268. Smith PA, Schmid C, Zurbrugg S, et al. Fingolimod inhibits brain atrophy and promotes brain-derived neurotrophic factor in an animal model of multiple sclerosis. *J Neuroimmunol*. 2018;318: 103-113.
269. Fleischer V, Kolb R, Groppa S, Zipp F, Klose U, Gröger A. Metabolic Patterns in Chronic Multiple Sclerosis Lesions and Normal-appearing White Matter: Intraindividual Comparison by Using 2D MR Spectroscopic Imaging. *Radiology*. 2016;281: 536-543.
270. Steen C, D'Haeseleer M, Hoogduin JM, et al. Cerebral white matter blood flow and energy metabolism in multiple sclerosis. *Mult Scler*. 2013;19: 1282-1289.
271. Louapre C, Perlberg V, Garcia-Lorenzo D, et al. Brain networks disconnection in early multiple sclerosis cognitive deficits: an anatomofunctional study. *Hum Brain Mapp*. 2014;35: 4706-4717.
272. Rocca MA, Longoni G, Pagani E, et al. In vivo evidence of hippocampal dentate gyrus expansion in multiple sclerosis. *Hum Brain Mapp*. 2015;36: 4702-4713.
273. Koenig KA, Sakaie KE, Lowe MJ, et al. Hippocampal volume is related to cognitive decline and fornix diffusion measures in multiple sclerosis. *Magn Reson Imaging*. 2014;32: 354-358.
274. Anderson VM, Fisniku LK, Khaleeli Z, et al. Hippocampal atrophy in relapsing-remitting and primary progressive MS: a comparative study. *Multiple Sclerosis Journal*. 2010;16: 1083-1090.
275. Kiy G, Lehmann P, Hahn HK, Eling P, Kastrup A, Hildebrandt H. Decreased hippocampal volume, indirectly measured, is associated with depressive symptoms and consolidation deficits in multiple sclerosis. *Multiple Sclerosis Journal*. 2011;17: 1088-1097.
276. Sacco R, Bisecco A, Corbo D, et al. Cognitive impairment and memory disorders in relapsing-remitting multiple sclerosis: the role of white matter, gray matter and hippocampus. *J Neurol*. 2015;262: 1691-1697.
277. Roosendaal SD, Hulst HE, Vrenken H, et al. Structural and functional hippocampal changes in multiple sclerosis patients with intact memory function. *Radiology*. 2010;255: 595-604.
278. Efstathiopoulos P, Kourgiantaki A, Karali K, et al. Fingolimod induces neurogenesis in adult mouse hippocampus and improves contextual fear memory. *Transl Psychiatry*. 2015;5: e685.
279. Campbell HS, Hall AE, Sanson-Fisher RW, Barker D, Turner D, Taylor-Brown J. Development and validation of the Short-Form Survivor Unmet Needs Survey (SF-SUNS). *Support Care Cancer*. 2014;22: 1071-1079.
280. Al-iedani O, Ribbons K, Lea R, Ramadan S, Lechner-Scott J. A Longitudinal, Observational Study of the Effect of Dimethyl Fumarate on Hippocampal Metabolites in RRMS using 1H-MR Spectroscopy. *J Biomedical Sci*. 2018;7
281. Azevedo CJ, Kornak J, Chu P, et al. In vivo evidence of glutamate toxicity in multiple sclerosis. *Ann Neurol*. 2014;76: 269-278.
282. Kantorova E, Polacek H, Bittsanský M, et al. Hypothalamic damage in multiple sclerosis correlates with disease activity, disability, depression, and fatigue. *Neurol Res*. 2017;39: 323-330.
283. Bergsland N, Zivadinov R, Dwyer MG, Weinstock-Guttman B, Benedict RH. Localized atrophy of the thalamus and slowed cognitive processing speed in MS patients. *Multiple Sclerosis*. 2016;22: 1327-1336.

284. Wiebenga OT, Klauser AM, Schoonheim MM, et al. Enhanced axonal metabolism during early natalizumab treatment in relapsing-remitting multiple sclerosis. *AJNR Am J Neuroradiol.* 2015;36: 1116-1123.
285. Llufriu S, Kornak J, Ratiney H, et al. Magnetic resonance spectroscopy markers of disease progression in multiple sclerosis. *JAMA Neurol.* 2014;71: 840-847.
286. Sun J, Song H, Yang Y, et al. Metabolic changes in normal appearing white matter in multiple sclerosis patients using multivoxel magnetic resonance spectroscopy imaging. *Medicine (Baltimore).* 2017;96: e6534.
287. Andronesi OC, Gagoski BA, Sorensen AG. Neurologic 3D MR Spectroscopic Imaging with Low-Power Adiabatic Pulses and Fast Spiral Acquisition. *Radiology.* 2012;262: 647-661.
288. Andronesi OC, Ramadan S, Ratai EM, Jennings D, Mountford CE, Sorensen AG. Spectroscopic imaging with improved gradient modulated constant adiabaticity pulses on high-field clinical scanners. *J Magn Reson.* 2010;203: 283-293.
289. Quadrelli S, Mountford C, Ramadan S. Hitchhiker's Guide to Voxel Segmentation for Partial Volume Correction of In Vivo Magnetic Resonance Spectroscopy. *Magnetic Resonance Insights.* 2016;9: 1-8.
290. Wiebenga OT, Klauser AM, Nagtegaal GJ, et al. Longitudinal absolute metabolite quantification of white and gray matter regions in healthy controls using proton MR spectroscopic imaging. *NMR Biomed.* 2014;27: 304-311.
291. Giorgio A, De Stefano N. Cognition in multiple sclerosis: relevance of lesions, brain atrophy and proton MR spectroscopy. *Neurol Sci.* 2010;31: S245-248.
292. Vollmer T, Huynh L, Kelley C, et al. Relationship between brain volume loss and cognitive outcomes among patients with multiple sclerosis: a systematic literature review. *Neurol Sci.* 2016;37: 165-179.
293. Tal A, Kirov, II, Grossman RI, Gonen O. The role of gray and white matter segmentation in quantitative proton MR spectroscopic imaging. *NMR Biomed.* 2012;25: 1392-1400.
294. Turner B, Ramli N, Blumhardt LD, Jaspan T. Ventricular enlargement in multiple sclerosis: a comparison of three-dimensional and linear MRI estimates. *Neuroradiology.* 2001;43: 608-614.
295. Zivadinov R, Leist TP. Clinical–Magnetic Resonance Imaging Correlations in Multiple Sclerosis. *Journal of Neuroimaging.* 2005;15: 10S-21S.
296. He J, Inglese M, Li BS, Babb JS, Grossman RI, Gonen O. Relapsing-remitting multiple sclerosis: metabolic abnormality in nonenhancing lesions and normal-appearing white matter at MR imaging: initial experience. *Radiology.* 2005;234: 211-217.